Imperial College London

Department of Engineering and Earth Sciences

Sensitivities to Component Characterizations of Heavy Oil Viscosity in Numerical Reservoir Simulation of Steam-Injection Processes

Jacoba Johanna de la Porte

A thesis submitted in fulfilment of the requirements for the degree of Doctor of Philosophy of Imperial College London

Supervisors:

Prof. V. Vesovic (Imperial College)

Prof. C.A. Kossack (Schlumberger)

December 2012

DECLARATION OF ORIGINALITY

I hereby declare that this thesis is entirely my own work and that where any material could be construed as the work of others, it is fully referenced.

The copyright of this thesis rests with the author and is made available under a Creative Commons Attribution Non-Commercial No Derivatives licence. Researchers are free to copy, distribute or transmit the thesis on the condition that they attribute it, that they do not use it for commercial purposes and that they do not alter, transform or build upon it. For any reuse or redistribution, researchers must make clear to others the licence terms of this work.

Acknowledgements

My acknowledgements go to Professors Velisa Vesovic and Chuck Kossack for their technical advice and guidance. I would like to thank Chuck for his help over long distance and for each weekend meeting he fitted into a full travel and teaching schedule. I would also like to thank Dr Nico Riesco for his help during the research.

My deepest gratitude is towards my partner for his unequalled and loving support in all aspects of this undertaking.

I thank my two siblings for always being one step ahead of me. Thank you to our parents who believed in us and guided with love.

The work is dedicated to my children, the light and drive of my life.

S.D.G.

Abstract

This work examines heavy oil viscosity modelling during simulation of steam injection processes, such as steam-line-drive and SAGD, and the sensitivity of oil recovery predictions to the uncertainty in the oil viscosity. Analytical models to predict the sensitivity have been developed, confirmed by numerical simulation.

Heavy oil compositional component viscosities are modelled with the Free Volume model. The model is extended in this thesis to estimate the viscosities of long-chain *n*-alkanes from C_6H_{14} to $C_{45}H_{92}$ within an accuracy of 10% in the temperature range 27 to 300 °C (80 to 575 °F) and pressure range 0.1 to 120 MPa (14.5 to 17,400 psi). It estimates viscosities of long-chain *n*-alkanes up to $C_{64}H_{130}$ to within 30%. Extrapolated Free Volume molecular characteristic parameters, optimised based on available viscosity measurements for *n*-alkanes up to $C_{64}H_{130}$, are provided, and are the recommended values for use in heavy oil simulation.

A heavy pseudo-component, representing a combination of asphaltenes and resins, which are the compounds responsible for the high viscosities observed in heavy oil, is characterised in terms of molecular weight, shape and activation energy for viscous flow. A method to predict its viscosity as a function of its physical properties, pressure and temperature, using the Free Volume model, is demonstrated.

A density model based on the Tait model is extended, to predict the long-chain heavy oil compositional component densities within an accuracy of 3%, in the same temperature and pressure ranges as above.

A grouping procedure is demonstrated to achieve oil recovery results comparable to a 24-component simulation case, using two pseudo-components. Key is the mixing equation used to calculate the oil phase viscosity as components are grouped. The Arrhenius mixing equation is evaluated for accuracy in predicting hydrocarbon mixture viscosities. Guidelines for accurate use are provided, while mixtures with CO_2 are shown to require a different method.

Table of Contents

Abstract 4

List of Tables 9

List of Figures 14

1 Introduction 24

2 Evaluation of the Arrhenius Mixing Equation in Viscosity Modelling of Hydrocarbon Mixtures 29

2.1 Introduction 29

2.2 Theory 30

2.3 Results and Discussion 33

2.3.1 Benchmark data 33

2.3.2 Viscosity correlations 35

2.4 Results 37

2.4.1 Applicability of Arrhenius equation 38

2.4.2 Examples 40

2.5 Summary of Results 47

2.6 Conclusions 49

3 Thermal Oil Recovery Sensitivity to Component Grouping and Viscosity Modelling 52

3.1 Introduction 52

3.2 Component Grouping 54

3.3 Literature Review 56

3.4 Methodology 57

3.4.1 Splitting and characterisation 59

3.4.2 Grouping and characterisation 60

3.5 Simulation Results and Discussion 64

3.6 Steam Assited Gravity Drainage (SAGD) 67

3.7 Field Case 70

3.8 Limitations 80
3.9 Conclusions 81

4 Thermal Oil Recovery Sensitivity to Uncertainty in Viscosity, as a Function of Temperature Range 83
4.1 Introduction 83
4.2 Viscosity Ranges for Mobility of Heavy Oil 85
4.3 Effect of Viscosity Uncertainty as a Function of Temperature on Oil Recovery Predictions 90
4.3.1 Vertical producer combined with heater/ cyclic steam injection/steam line drive 90
4.3.2 Steam Assisted Gravity Drainage (SAGD) with horizontal wells 112
4.4 Chapter Conclusions 123

5 Viscosity Modelling of Individual Components 124
5.1 Introduction 124
5.2 Theory 125
5.2.1 Viscosity definition 125
5.2.2 Theory of flow in porous media as applied in simulator 126
5.3 Pure Component Density 128
5.4 Oil Viscosity Models: Theory and Equations 132
5.4.1 Pedersen Corresponding States method for heavy oil 133
5.4.2 Hard Sphere Model 135
5.4.3 Free Volume Model 137
5.5 Heavy Oil: Free Volume Model Extrapolation to Long-chain *n*-Alkanes 141
5.5.1 Polynomial fitting of Free Volume Model coefficients 143
5.5.2 Final Free Volume parameters for all pure *n*-alkanes up to C64 150
5.5.3 Free Volume model application to C16 at high pressures 154
5.6 Comparative Study on Oil Viscosity Models 157
5.7 Conclusions 167

6 Characterisation of a Heavy Pseudo-Component 170

6.1 Introduction 170
6.2 Resins and Asphaltenes Properties Review 175
6.2.1 Resin and asphaltene definitions 175
6.2.2 Resin-asphaltene grouping 175
6.2.3 Resin-asphaltene molecular weight 176
6.2.4 Resin-asphaltenes physical properties: size and shape 177
6.2.5 Resin-asphaltenes physical properties: energy of activation 178
6.2.6 Resin-asphaltenes physical properties: viscosity ranges 179
6.3 Viscosity Modelling per Pseudo-Component 181
6.3.1 Heavy pseudo-component viscosity with Free Volume Model 183
6.3.2 Viscosities of colloid systems 190
6.4 Conclusions 191

7 Thermal Simulation Sensitivities using Viscosities estimated by the Free Volume Model 193
7.1 Introduction 193
7.2 Case Descriptions 193
7.2.1 Reservoir models and development strategies 194
7.2.2 Component grouping/lumping 197
7.2.3 Component viscosities 201
7.3 Sensitivities 206
7.3.1 Steam-Line-Drive (SLD) 206
7.3.2 Steam-Assisted Gravity Drainage (SAGD) 223
7.4 Sensitivity Study Summary 227
7.5 Chapter Conclusions 230

8 Conclusions and Recommendations 232
8.1 Overall Summary 232
8.2 Specific Conclusions 232
8.2.1 Chapter 2: Evaluation of the Arrhenius Mixing Equation in Viscosity Modelling of Hydrocarbon Mixtures 232

8.2.2 Chapter 3: Thermal Recovery Sensitivity to Component Grouping and Viscosity Modelling. 233
8.2.3 Chapter 4: Thermal Recovery Sensitivity to Uncertainty in Viscosity, as a Function of Temperature Range 233
8.2.4 Chapter 5: Viscosity Modelling of Individual Components 234
8.2.5 Chapter 6: Characterisation of a Heavy Pseudo-Component 234
8.2.6 Chapter 7: Thermal Simulation Sensitivities using Viscosities estimated by the Free Volume Model 235
8.3 Recommendations 235

Appendix A: Viscosity Deviation Data for Arrhenius-Mixing Equation 237

Appendix B: Viscosity Modelling of Individual Components 272
B.1. Available Measured Data. 272
B.2. Viscosity Comparison Results: Hard Sphere *vs.* Free Volume 276
B.3. Matlab Codes 289

Appendix C: Heavy Pseudo-Component Viscosity using a Colloidal Systems Approach 302

Nomenclature 305

References 309

List of Tables

Table 2.1. Summary of results. 49

Table 3.1. Cumulative Field Oil Production (FOPT) and deviation from base case (24-components), per simulation case. 66

Table 3.2. Grouping of 10°API oil into 10, 5, 3 and 2 component cases. 73

Table 3.3. 10°API Oil: Cumulative oil production deviations. 74

Table 4.1. Viscosities for minimum and no-flow: sensitivity to different parameters. 87

Table 4.2. Critical viscosities for different permeabilities and flow rates. 88

Table 4.3. Oil viscosities per simulation case with errors introduced at discrete points: T=125, 250, 350 and 500°F, shown in red. 95

Table 4.4. Comparison of flow-rates per grid-cell (as distance from well) at time t = 408 days. Differences from base case are shown in red. 103

Table 4.5. Oil viscosities for cases with deviations (fraction). 104

Table 4.6. Butler model flow rates for simulation reservoir parameters. 113

Table 4.7. Simulation case properties. 115

Table 4.8. Sensitivity of production rate (full length of well) to error in oil viscosity at the steam-oil interface. 120

Table 4.9. SAGD Recovery sensitivity to temperature at which viscosity error occurs. 121

Table 4.10. SAGD viscosity-temperature sensitivity. 122

Table 5.1. Tait density coefficients (Ciotta, 2010). 128

Table 5.2. Density a_0' polynomial coefficients. 129

Table 5.3. Hard Sphere reduced viscosity coefficients. 137

Table 5.4. Viscosity and density measurements for *n*-alkanes C5 to C64, used in this study. 142

Table 5.5. Coefficients of fitted polynomials: first iteration. 145

Table 5.6. Evaluation of the 'first-guess' parameters (left) *vs.* the optimized values (right): Free Volume viscosity-deviations. 146

Table 5.7. Free Volume calculated viscosity deviations for control points. 148

Table 5.8. Coefficients of extrapolation polynomials: final iteration which included C17, C28, C36 and C44 parameters, optimised. 149

Table 5.9. Final Free Volume parameters for *n*-alkanes up to C64. 152

Table 5.10. C16 Free Volume parameters. 154

Table 5.11. Long-chain *n*-alkane viscosity deviation results for industry methods. 158

Table 5.12. Long-chain *n*-alkane viscosity deviation results for the Free Volume model (FV) and Hard Sphere method (HS). 160

Table 5.13. C60 viscosity comparisons. 163

Table 5.14. C64 viscosity comparisons. 164

Table 5.15. Calculated density, Hard Sphere and Free Volume viscosity deviation data for C6-C64, $P < 1400$ atm (20,000 psi). 165

Table 5.16. Calculated density, Hard Sphere and Free Volume viscosity deviation data for C6-C64, all pressures. 166

Table 5.17. Deviation Summary: all models, components C6-C44, $T = 10$-575 °F, $P = 15$ to 17,300 psi (LBC=Lohrenz-Bray-Clark; PED=Pedersen Corresponding States, AP=Aasberg-Petersen). 166

Table 6.1. SARA analysis ranges for Nigerian heavy oil and bitumen (after Lawal *et al.,* 2010). 172

Table 6.2. Molecular major axis diameters of asphaltenes and resins (from Groenzin and Mullins, 2000). 177

Table 6.3. Asphaltene volume fraction with associated activation energy (E_a). 178

Table 6.4. Maltene and asphaltene properties, as estimated from Lawal and Adenuga (2010). 182

Table 6.5. Lindbergh oil properties and SARA analysis (Jamaluddin *et al*., 1996). 185

Table 6.6. Composition (mole%) of Lindbergh Oil and de-asphalted sample A (Jamaluddin *et al*., 1996). 186

Table 6.7. Pseudo-component grouping, with heavy resin-asphaltene pseudo-component. 187

Table 6.8. Free Volume parameters for heavy pseudo-component (SPE4 case). 188

Table 6.9. Free Volume heavy pseudo-component viscosities for the SPE4 fluid, as a function of temperature. 189

Table 7.1. Detailed 24-component up-scaling to 15-components: 14 pure components plus 1 heavy pseudo-component. (Red components indicated the original SPE4 components). 198

Table 7.2. 15-component composition. 198

Table 7.3. 8-PC composition. 199

Table 7.4. 4-PC composition. 199

Table 7.5. 3-PC composition. 200

Table 7.6. 2-PC composition. 201

Table 7.7. 'Pure' component Free Volume viscosities: C1 to C16. 202

Table 7.8.'Pure' component Free Volume viscosities: C18 to C29, plus heavy resin-asphaltene component. 203

Table 7.9. 8-PC case component viscosities, with heavy resin-asphaltene component. 203

Table 7.10. 4-PC case component viscosities, with heavy resin-asphaltene component. 204

Table 7.11. 3-PC case component viscosities, with heavy resin-asphaltene component. 205

Table 7.12. 2-PC case component viscosities. 205

Table 7.13. SLD cumulative oil production (STB) for different heavy pseudo-component viscosity predictions. 209

Table 7.14. SLD cumulative oil production deviations for different heavy pseudo-component viscosity predictions from base case with 'measured' values. 209

Table 7.15. SLD-FV1 cumulative oil production (STB) as a function of number of pseudo-components. 211

Table 7.16. SLD-FV1 cumulative oil production deviation as a function of number of pseudo-components. 211

Table 7.17. SLD-FV2 cumulative oil production (STB) as a function of number of pseudo-components. 213

Table 7.18. SLD-FV2 cumulative oil production deviation as a function of number of pseudo-components. 213

Table 7.19. SLD-FV3 cumulative oil production (STB) as a function of number of pseudo-components. 214

Table 7.20. SLD-FV3 cumulative oil production deviation as a function of number of pseudo-components. 214

Table 7.21. Alternative 2-PC component-lumping scenario. 216

Table 7.22. 2-PC case component viscosities, using alternative component lumping scheme. 217

Table 7.23. 2-PC alternative grouping recovery results and deviations from 15 component cases. 221

Table 7.24. Field cumulative oil production: 10°API oil with Free Volume viscosities. 223

Table 7.25. SAGD cumulative oil production for each case (PC15 is the base case). 225

Table 7.26. SAGD cumulative oil production deviations per sensitivity case. 226

Table 7.27. SAGD cumulative oil (MSTB) produced per case: lumping strategy. 227

Table 7.28. SAGD Cumulative oil prediction deviations (%): lumping strategy. 227

Table 7.29. Summary of Sensitivity Results. 227

List of Figures

Figure 2.1. Relative deviations for binary mixtures containing *n*-octane measured by Aucejo *et al*. (1995) at 298.15 K and atmospheric pressure. 41

Figure 2.2. Relative deviations as a function of pressure for equimolar C8-C12 mixture at different temperatures, measured by Dymond *et al*. (1981). 42

Figure 2.3. RMS deviations for binary and ternary mixtures containing *n*-octane; measurements by Caudwell (2004). 43

Figure 2.4. Relative deviations as function of pressure for C1-C10 mixtures by Audonnet and Pádua (2004), at different temperatures. (Pressure and temperature ranges in field units: 1,450-10,878 psi and 85-247 °F.) 44

Figure 2.5. Relative deviation of CO2-C10 mixture. 45

Figure 2.6. Relative deviation of CO2-C5-C10 mixture. 46

Figure 2.7. Relative deviation of CO2-C4-C6-C10 mixture. 46

Figure 2.8. Relative deviation of CO2-C5-C6-C7-C10 mixture. 47

Figure 2.9. Summary of results: Maximum Absolute Deviation (MAX), Root Mean Square (RMS) error, and Bias. 48

Figure 3.1. Simulation model with one steam injector (I) and two oil producers (PNEAR and PFAR). 59

Figure 3.2. 24-Component composition. 60

Figure 3.3. 10-Component composition. 62

Figure 3.4. 5-Component composition. 62

Figure 3.5. 3-Component Composition. 63

Figure 3.6. 2-Component composition. 63

Figure 3.7. Heavy component viscosities of the 2-Comp cases. 63

Figure 3.8. Phase diagrams of the different groupings, overlain. 24-component bubble-point line: solid red+squares; 2-component bubble point line: solid green line. 64

Figure 3.9. Cumulative Production (FOPT) for groupings 10, 5 and 3, over a period of 5 years. (Black-dashed: 24-Comp base case, Dotted lines: method 1, Solid lines: method 2, Red: 10-Comp; Blue: 5-Comp; Green: 3-Comp). 65

Figure 3.10. FOPT comparison between 24-Comp case (base case) and 2-Comp cases with different viscosity mixing rules (Black: Base case, Green: 2-Comp with method 2 viscosity, Red: 2-Comp case with method 1 viscosity.) 65

Figure 3.11. Oil viscosity distribution after 4 months. 68

Figure 3.12. Cumulative oil production: 1000 cP oil with SAGD. (24-component base case: black dots; 10-PC: green; 5-PC: dark blue; 3-PC: light blue; 2-PC: red) 68

Figure 3.13. Clockwise from top left: (1) well steam production (STB/d CWE), (2) well GOR (MSCF/STB), (3) well gas production rates (MSCF/d) and cumulative gas procution(MSCF), (4) well oil production rates (STB/d) and cumulative oil production (STB). (24-component base case: black dots; 10-PC: green; 5-PC: dark blue; 3-PC: light blue; 2-PC: red). 69

Figure 3.14. Concentration of C18 in the gas-phase over time (24-component case). 70

Figure 3.15. Pseudo-component mole-fraction distributions for 10 API oil Base Case (30-Component) with 5-, 3- and 2-Component cases. 71

Figure 3.16. Pressure-Temperature phase diagrams for different groupings of 10ºAPI oil (Dark Green: 30-Comp Bubble-point line; Light green: 10-Comp; Light Blue: 5-Comp; Red-dashed: 3-Comp oil, Dark-blue: 2-Comp oil). 72

Figure 3.17. Cumulative production for each of the the groupings of the 10°API oil (Black solid: 30-Comp base case, Blue: 10-Comp; Green: 5-Comp; Black dotted: 3-Comp; Red: 2-Comp case). 74

Figure 3.18. 10-API 30-Comp case, water mole fraction in gas phase, *i.e.* steam movement (YMF31) at timestep 20 (~600 days). 75

Figure 3.19. 10-API 30 Comp case, mole fraction of Component 2 (C1) in gas phase (YMF2) at timestep 20 (~600 days). 75

Figure 3.20. 10-API 30 Comp case, mole fraction of Component 13 (C10) in gas phase (YMF13) at timestep 20 (~600 days). 76

Figure 3.21. 10-API 2 Comp case, steam movement (YMF3 water mole fraction in gas phase) at timestep 20 (~600 days). 77

Figure 3.22. 10-API 2 Comp case, mole fraction of Component 1 (C2 pseudo-component) in gas phase (YMF1) at timestep 20 (~600 days). 77

Figure 3.23. Cumulative oil production per well. PNEAR is on the left, with PFAR on the right. (Black dotted: base case, blue: 3- and 5-PC cases, green: 10-PC case and red: 2-PC case) 78

Figure 3.24. Steam production rates per well. PNEAR is on the left, with PFAR on the right. (Black dotted: base case, blue: 3- and 5-PC cases, green: 10-PC case and red: 2-PC case) 78

Figure 3.25. Cumulative oil production in PFAR in single production well cases. (Black dotted: 30-component base case, green: 2-PC case with gas viscosities determined with Arrhenius eq., red: 2-PC case with gas-viscosities determined by arithmetic average). 79

Figure 3.26. 10-API Oil cumulative prediction comparison, with initial reservoir pressure=200 psia. 80

Figure 3.27. Phase diagram of the 30-component case, 5-PC and 2-PC cases. 81

Figure 3.28. Phase diagram of alternative grouping of the 2-PC case. 81

Figure 4.1. Typical heavy oil viscosity *vs*. temperature relationships. (Attanasi and Meyer, 2007) 84

Figure 4.2. μ_{max} *vs* pressure drawdown (ΔP), area (A) and effective distance (L_e). 89

Figure 4.3. Linear-2D reservoir model. 91

Figure 4.4. (left) Areal view of base case temperature (°F). (right) cross-sectional view of oil viscosity (cP), at the end of the simulation period. 96

Figure 4.5. Linear dead oil model with heater in producer: cumulative oil production per case. 97

Figure 4.6. Base case (heat-source at producer): flow (red) *vs X*-distance from producer, with oil viscosity (green) 42 days after production started (t = 1.12 years). Temperature shown in blue. 98

Figure 4.7. Case VT125 (heat-source at producer, oil viscosity at T=125°F twice that of base case): flowrate (red), temperature (blue) and oil viscosity (green) profiles in reservoir at t = 1.12 years. 98

Figure 4.8. Case VT250 (heat-source at producer, oil viscosity at T=250°F twice that of base case): flowrate (red), temperature (blue) and oil viscosity (green) profiles in reservoir at t = 1.12 years. 99

Figure 4.9. Case-VT350 (heat-source at producer, oil viscosity at T=350°F twice that of base case): flowrate (red), temperature (blue) and viscosity (green) profiles in reservoir at t=1.12 years. 99

Figure 4.10. Viscosities and temperatures *vs.* distance from producer (heat source at producer). Solid lines represent temperature curves; dotted and dashed lines viscosity. 100

Figure 4.11. 2D-linear model: comparison of flow-rate vs distance from well. 101

Figure 4.12. Heat source some distance away from producer: cumulative oil production comparison. Base case: black dots, VT125: blue dashed. 102

Figure 4.13. Radial reservoir with production well at the centre. On the left is the oil viscosity distribution at the end of the simulation period (5 years) and on the right a vertical cross section showing the temperature distribution at the same time. 105

Figure 4.14. Oil Production rate (stb/d) at well. Black dotted line: base case; red dashed line: case VT125, and green dashed line: case VT500. Additional cases (VT250 and VT350) are in blue. 106

Figure 4.15. Block viscosities (cP) *vs*. time (a) near well (cell:1,1,1) at high temperature (T_w), (b) 22 ft into reservoir (3,1,1,), and (c) outer boundary at 450 ft (13,1,1,) at cold reservoir temperature (T_R). Black dotted line: base case; red dashed line: case VT125 and green dashed line: case VT500. Additional cases (VT250 and VT350) in blue. 106

Figure 4.16. Block temperatures (°F) vs time (a) near well (cell:1,1,1), (b) 22 ft into reservoir (3,1,1,) and (c) outer boundary at 450 ft (13,1,1,). Black dotted line: base case; red dashed line: case VT125 and green gashed line: case VT500. Additional cases (VT250 and VT350) in blue. Changes in temperatures in (a) are due to production, and later, drainage in the gridcells close to the well. 107

Figure 4.17. Rate sensitivities (S) to viscosity errors: error at T_R(cold)=red, and error at T_w(hot)=blue. 108

Figure 4.18. 4-Layer multi-phase model: cumulative oil production. Base case is shown in black dots, VT125 in blue, VT250 in green, VT350 in orange and VT500 in red. 109

Figure 4.19. Base case oil component oil viscosities (cP). 110

Figure 4.20. Heterogeneous reservoir with steam-line-drive. Steam injection with well in upper left corner(blue), oil production with well in lower right corner (green). 110

Figure 4.21. Heterogeneous reservoir with steam injection: oil recovery comparison. Base case in black, error at T_{Res}(cold) in blue. 111

Figure 4.22. Live oil, steam injection: deviations in oil recovery over time, for each viscosity-error case. 111

Figure 4.23. Oilrates in total well (WOPR, blue) and in the toe-segment (SOFR, green), in stb/d. 114

Figure 4.24. Oil viscosity as a function of temperature. 116

Figure 4.25. Oil flow vectors in the *YZ* plane (intersecting the horizontal producer at the centre-bottom perpendicularly). The lengths of the cell-arrows are an indication of the amount flowing in the cell. Red arrow indicates maximum flow towards well. 117

Figure 4.26. Oil saturation in *X*-section (*X*=3) at *t*=140 days. Green=S_{oi}, Red=S_{or}. 117

Figure 4.27. Temperature distribution in *X*-section (*X*=3) at time *t* -= 140 days. 118

Figure 4.28. Oil viscosity distribution in *X*-section (*X*=3) and *t* = 140 days. 118

Figure 4.29. Oil viscosity in some production-contributing blocks, at the steam-oil interface, with an average oil viscosity of 71.3 cP for the block shown (I=3, J=12-15, K=32-39). 118

Figure 4.30. Cumulative oil production per case. Base case (black dots); error at reservoir temperature (blue); error at highest temperature (dark blue +); error at temperature of steam-oil interface: red + triangles). 121

Figure 4.31. SAGD relative rate deviations based on a combination of cases VT300 and VT400. 122

Figure 5.1. Viscosity schematic. 126

Figure 5.2. Least-squares-fit of refined a_0-values as a function of carbon number (Cn). 130

Figure 5.3. C16 Calculated densities *vs.* Ciotta measured densities; 131

Figure 5.4. AAD in density per component for $P < 20{,}000$ psi (138 MPa). 131

Figure 5.5. Discrete fitting on left panel, with interpolation and extrapolation on the right. 144

Figure 5.6. C32 measured *vs.* calculated viscosities. Measured values in red, Free Volume, using first-guess coefficients in purple, Free Volume with optimized values in blue, Free Volume with further adjustments in *B* in green. 146

Figure 5.7. C36 measured *vs.* calculated viscosities. Measured values in red, Free Volume, using first-guess coefficients in purple, Free Volume with optimized values in blue, Free Volume with further adjustments in *B* in green. 147

Figure 5.8. Final Free Volume parameter polynomials, based on control points for C17, C28, C36 and C44. 150

Figure 5.9. Final range of l_m values as a function of Cn extrapolated to C64. 151

Figure 5.10. Final range of E_0 values as a function of Cn extrapolated to C64. 151

Figure 5.11. Final range of B values as a function of Cn extrapolated to C64. 151

Figure 5.12. C16 viscosities Free Volume fit (green) at low pressures (P<200 psi). 155

Figure 5.13. C16 viscosities Free Volume fit (green) at P = 3000 psi. 155

Figure 5.14. C16 Viscosity Free Volume fits at P = 6000 psi. 155

Figure 5.15. C16 viscosity Free Volume fits at P = 8700 psi. 156

Figure 5.16. C60 viscosity Free Volume fits at P = 2.98 atm. 156

Figure 5.17. C16 calculated viscosity relative deviations *vs.* temperature at P = 1500 psi. 164

Figure 5.18. C16 calculated viscosity relative deviations *vs.* temperature at P = 3000 psi. 165

Figure 5.19. Viscosity prediction deviations: AAD *vs.* Cn (P < 20,000 psi). 167

Figure 6.1. Separation of asphaltenes from heavy oil: influence of the precipitating alkane. (after Argillier *et al.*, 2002) 176

Figure 6.2. Lawal three-pseudo-component case with asphaltene pseudo-component viscosities (from Lawal, 2011). 180

Figure 6.3. Lawal four-pseudo-component case with resin-asphaltene pseudo-component viscosity (from Lawal, 2011). 180

Figure 6.4. Nigerian bitumen measured viscosities (from Lawal, 2011). 181

Figure 6.5. SPE4 Asphaltene+Resins pseudo-component viscosity (SPE4: black dots) modelled with the Free Volume Model (solid line). 190

Figure 7.1. Oil-water relative permeabilities. 194

Figure 7.2. Oil-gas relative permeabilities. 195

Figure 7.3. Steam-line-drive model: permeability distribution. 195

Figure 7.4. SAGD model: permeability distribution. 196

Figure 7.5. Phase envelope for 15 and 8-PC cases. Bubble-point line: pink, dew-point-line: green, 2-phase line: blue. 199

Figure 7.6. Phase envelope for 15 and 4 component cases. 200

Figure 7.7. Phase envelopes for 15 and 4 component cases, together with 3-PC case. 200

Figure 7.8. Phase envelope for 15, 4 and 3 component cases, compared with 2-PC case. 201

Figure 7.9. Dead-Oil mixture and component viscosities for 8-PC case. 204

Figure 7.10. Heavy pseudo-component (asphaltene + resin) viscosity vs. temperature: priority on fitting measured endpoints. 207

Figure 7.11. Heavy pseudo-component (asphaltene + resin) viscosity vs. temperature. 207

Figure 7.12. SLD Cumulative oil production (STB) for different heavy pseudo-component viscosity predictions. PC15 Experimental: black dots, PC15-FV1 case: red line, PC15-FV2 case: blue line, PC15-FV3 case: green line. 209

Figure 7.13. SLD-FV1 cumulative oil production (STB) as a function of number of pseudo-components. Case with ‘measured’ heavy oil viscosities shown in black dots, 15-PC base case in solid blue, 2-PC case in red. Other cases shown: 8-PC (dark green dotted), 4-PC (light green dotted), 3-PC (light blue dashed). 211

Figure 7.14. SLD-FV2 cumulative oil production (STB) as a function of number of pseudo-components. Case with 'measured' heavy oil viscosities shown in black dots, 15-PC base case in solid blue, 2-PC case in red. Other cases shown: 4-PC (dark green dotted), 3-PC (light green dashed). 213

Figure 7.15. SLD-FV3 cumulative oil production (STB) as a function of number of pseudo-components. Case with 'measured' heavy oil viscosities shown in black dots, 15-PC base case in solid blue, 2-PC case in red, 4-PC (dark green dotted), 3-PC (light green dashed). 214

Figure 7.16. Phase envelope of alternative 2-PC grouping case, overlaying original fifteen-component case with dew-line >1200 °F. 216

Figure 7.17. Cumulative oil production over time for the two 2-PC cases (FV1: heavy PC viscosity matched at endpoints), shown with the fifteen-component case (black dots). Original 2-PC case: green; new grouping: red. 218

Figure 7.18. Cumulative oil production over time for the two 2-PC cases (FV2: heavy PC viscosity matched at T_R and T_s), shown with the fifteen-component case (black dots). Original 2-PC case: green; new grouping: red. 218

Figure 7.19. Cumulative oil production over time for the two 2-PC cases (FV3: heavy PC viscosity minimum AAD), shown with the 15-component case (black dots). (Original 2-PC case: green; new grouping: red). 219

Figure 7.20. SLD-FV3: Steam production rates for 15-PC, 2-PC and alternative grouping 2-PC cases. Difference in steam-front arrival time at PFAR. (15-PC base case: black dotted line; 2-PC: green dashed line; 2-PC, alternative lumping: red line). 220

Figure 7.21. SLD-FV3: Oil production rates at PFAR. (15-PC base case: black dotted line; 2-PC: green dashed line; 2-PC, alternative lumping: red line). 220

Figure 7.22. Field cumulative oil production for 10°API oil, with Free Volume viscosities. (Base case: black dotted; 10-PC: green; 5-PC: dark blue; 3-PC: light blue; 2-PC: red) 222

Figure 7.23. Well cumulative oil production in 10°API cases. Left: PNEAR, Right: PFAR. (Base case: black dotted; 10-PC: green; 5-PC: dark blue; 3-PC: light blue; 2-PC: red) 223

Figure 7.24. Very heavy oil component viscosities for SAGD 8-PC case. 224

Figure 7.25. SAGD cumulative oil production sensitivity to number of pseudo-components. Base case (black dots), 8-PC case (red dotted line), 4-PC case (blue dashed line), 3-PC case (green dashed line), and 2-PC case (red). 225

Figure 7.26. SAGD Steam-Oil ratio (left) and daily oil production rates (right) for base case (black dots), 2-PC case (red), 8-PC case (red dotted line), 4-PC case (blue dashed line), and 3-PC case (green dashed line). 225

Figure 7.27. SAGD cumulative oil production sensitivity to lumping scenario. 15-component base case: black dotted line, 2-PC with original lumping: green, 2-PC with alternative lumping (grp2): red. 226

Figure 7.28. Oil recovery sensitivity to viscosity modelling and lumping results. (Deviations are relative to section-base case. Negative deviations indicate over-prediction). 229

Figure C.0.1. Relative viscosity parameters *vs* temperature. 304

1 Introduction

Exploitation of heavy oil (viscosity on the order of 1000 cP and higher) is gaining momentum in light of increased scarcity in conventional oil resources, combined with geopolitical factors affecting accessibility (Jaffe *et al*., 2011), but this resource remains challenging to produce. This is due to physical factors such as the high viscosities encountered, resulting in low mobility, and economic factors related to the expensive methods deployed to reduce the *in situ* viscosity, including thermal recovery methods.

In order to understand the significance of heavy oil production and usage in the global market, one would need to look at global crude oil reserves, resources and production, and compare the same numbers for heavy oil. However, detailed, exact numbers are not easily accessible for various reasons, such as (1) classifications of resources *vs*. reserves differ between countries, (2) definitions of heavy oil can differ, where some definitions include all oil with an API gravity between 10° and 20°, while others include oil up to 22°API, and (3) some numbers quoted in the public arena include bitumen, with API gravities less than 10°.

The U.S. Geological Survey (Meyer and Attanasi, 2003) estimated total worldwide technically recoverable heavy oil and bitumen to be on the order of two trillion barrels, based on recovery factors of 12 to 19% for heavy oil, and 9 to 32% for bitumen. In their estimate, heavy oil and bitumen reserves account for 57% of total oil reserves. In terms of resources, which include accumulations of which development plans have not been approved yet, heavy oil estimates are on the order of 3.4 trillion barrels, and for bitumen, 5.5 trillion barrels – a total of nearly 8 trillion barrels of oil (Meyer *et al*., 2007). The largest heavy oil deposits are the Lloydminster deposits in Canada, at 101.7 billion barrels of oil originally in place (OOIP), and the Orinoco belt in Venezuela, at 1.3 trillion barrels of oil originally in place, with 513 billion barrels of recoverable resources (Schenk *et al*., 2009). The Orinoco Belt recoverable oil is based on a median recovery factor of 45%. The maximum recovery factor for this area is estimated to be as high as 70%, using horizontal wells combined with thermal and other recovery processes. In terms of production, it was

reported in January 2012 that production from the Orinoco belt exceeded one million barrels per day (Marcano, 2012), whereas production projections for heavy oil and bitumen in Alberta in 2011 were on the order of 2.2 million barrels per day. To put these into perspective, the total non-OPEC production in 2010 was 47 million barrels of oil per day (Jaffe *et al*., 2011). With heavy oil and bitumen output predicted to increase in the coming years, this resource clearly plays a significant role in world energy supply.

Although heavy oil and bitumen resource estimates are huge, there are many challenges to the successful exploitation of these fields. One of the major issues is the high viscosity of the deposits, which makes production difficult and in some cases impossible. A number of technologies currently in use, namely cyclic steam simulation (CSS), steam-assisted gravity drainage (SAGD), vapour extraction (VAPEX), *in-situ* combustion, and combinations of these, are aimed at lowering the viscosity by either increasing the temperature or adding a solvent.

Reserves estimates are based on appropriate field development plans and production predictions, obtained with numerical simulation of these plans. In the light of the significance of this resource and the complexity of development methods, more accurate numerical simulation to predict ultimate recovery (reserves) and daily production rates is imperative. Thermal compositional simulation is used to model the thermally enhanced production methods and predict daily production rates of the oil, gas, water/steam and steam–injection rates required to reach economical oil rates and field recovery factors. Due to the sensitivity of the economic numbers to the recovery rates, as well as the amount of steam or heat required, and taking into account that the production rates are a directly inverse function of oil viscosity, a much higher level of accuracy is required in the oil viscosity predictions as a function of reservoir temperatures. A study, examining the sensitivity of numerical reservoir simulations to oil viscosity, confirmed that for highly viscous oils, the uncertainty in viscosity has a large effect on the calculation of production rates (Hernandez *et al*., 2002). In a more recent study, Mago *et al*. (2005) demonstrated the magnitude of error incurred in the recovery estimation of cyclic steam stimulation of extra-heavy oils. Knowledge of viscosity is thus essential for reliable reservoir exploitation and

development of new technologies, especially as management decisions and production strategies are frequently based on the results of these reservoir simulations.

There are a number of reasons why the prediction of viscosity of heavy oils is proving difficult. Firstly, heavy oils contain a large proportion of asphaltenes, waxes and other heavy components, and thus far no prediction scheme has been capable of successfully dealing with such mixtures. Secondly, the viscosity of heavy oil is a very strong function of temperature, and it is not uncommon for an increase of temperature of tens of degrees to reduce the viscosity by 2-3 orders of magnitude. Furthermore, the addition of light components can result in an order of magnitude decrease in viscosity. Thirdly, the current reliance on fitting sparse experimental data and using the resulting empirical correlation to estimate viscosity is highly problematic, because extrapolation, either in temperature or to similar mixtures, is highly unreliable. Finally, connate water is present in a large number of reservoirs, and when the heavy oil is extracted a heavy-oil/connate-water emulsion is formed. Laboratory measurements on such samples greatly overestimate the viscosity of heavy oil present in the reservoir. Added to this, viscosity measurements are highly sensitive to temperature, as well as the aging of the sample during which volatile components evaporate, causing compositional changes. Measurements can vary by as much as ±20% on an identical sample, measured at different laboratories (Chew *et al.,* 1959; Mago *et al*., 2005).

Current industry standard prediction methods involve, at best, a tuning of parameters in correlation models (Gabitto *et al.,* 2003) to fit the measured data, resulting in errors in the order of 50% in heavy oil (Hernandez, 2001). Hernandez also demonstrated that current industry standard correlation and modelling methods, such as Lohrenz-Bray-Clark, Pedersen's Corresponding States, and the STRAP method, are inadequate for heavy oil modelling, with a minimum error of above 70% in the heavy oil case he investigated.

The present research had four main objectives. Firstly, to investigate whether, in a heavy oil thermal simulation, one can obtain good oil recovery results while using a two-component characterisation, one light component (mostly methane), and one heavy pseudo-component.

The main focus was on recovery sensitivity to the oil viscosity modelling. Secondly, to determine techniques to estimate the component viscosities, as a function of pressure and temperature, of (1) intermediate molecular weight hydrocarbon components (C10 to C64) representing saturates and aromatics, and of (2) heavy hydrocarbon plus-fraction components consisting mostly of resins and asphaltenes. Thirdly, to determine the best technique of calculating an oil mixture viscosity, as a function of temperature, from component viscosities. The main questions were: (1) how can heavy oil viscosity be modelled more accurately on the component level as a function of temperature and pressure, honouring the complex molecular physics of hydrocarbon molecules? (2) How could accuracy be maintained while grouping into pseudo-components to obtain reasonable simulation time limits? (3) How does this affect the minimum number of pseudo-components required?

The current research considered steam injection only, and apply to Newtonian fluids only. Both the lumping procedures and viscosity modelling had been tested within these restrictions. When other EOR methods are considered, such as solvent or gas injection, VAPEX (vapour extraction), CHOPS (cold heavy oil production with sand), the applicability of the methods need to be evaluated.

The following brief thesis outline is provided to assist the reader in understanding the layout, since this thesis as a whole does not follow the normal outline of literature review, followed by theory, then results. A number of separate sections of research have been conducted in order to aid in heavy oil viscosity modelling during simulation, and each of these research-questions has been addressed and presented separately. Literature reviews and theory are shown within each chapter, as applicable to the subject matter.

In Chapter 2, results from the evaluation of the viscosity mixing method from Arrhenius are presented. This method is widely applied in petroleum reservoir simulation, and this work provides (a) deviation results for 1002 measured data points when this method is applied, and (b) new guidelines, derived from the analysis trends as to where and how it could be applied more accurately. Chapter 3 evaluates recovery prediction accuracy in using only

two pseudo-components during thermal simulation, from the perspective of pseudo-component viscosity mixing methods. The new guidelines, developed in Chapter 2, were applied, together with an equivalent carbon number (ECN) grouping method, presented in detail. Chapter 4 presents a new, simple, analytical model which was developed in the present work to establish the sensitivity of oil flow rate accuracy to the temperature range in which viscosity modelling accuracy is a priority, after establishing critical viscosities for oil- flow under various isothermal conditions. The sensitivity analysis included point-heating and well as Steam Assisted Gravity Drainage (SAGD). Chapter 5 presents extrapolated molecular characteristic Free Volume parameters to accurately model pure component viscosities for normal alkanes from CH4 to C64H130, based on the Free Volume viscosity model. Deviation results for 243 measured data points are provided. A density model, based on the Tait equation extended to accurately calculate long-chain *n*-alkane densities, is provided. Results are presented of a comparison of the Free Volume-calculated viscosity deviations from measured data, with those calculated by (1) Pedersen's Corresponding States method and (2) the Hard Sphere model. Chapter 6 contains a detailed literature review of some of the latest research in asphaltenes and resins with regard to heavy oil viscosity and lumping methods, providing an understanding and input into the characterisation of a complex, heavy pseudo-component, representative of the very complex molecules and compounds found in heavy oil. A method is demonstrated to model the heavy pseudo-component viscosity with the Free Volume model, and appropriate modelling parameters are provided. Chapter 7 presents simulation results from cases where the new component lumping method have been combined with the new viscosity models. Results from sensitivities of the total oil recovery towards the heavy pseudo-component viscosity as well as lumping scenarios are presented for steam line drive and SAGD processes.

2 Evaluation of the Arrhenius Mixing Equation in Viscosity Modelling of Hydrocarbon Mixtures

2.1 Introduction

In practice heavy oil viscosity is measured as a whole, *i.e*., as the viscosity of the mixture of pure hydrocarbon components. However, during simulation of thermal processes, it is necessary to capture various physical phenomena, such as distillation of lighter components into the steam phase, re-condensation of such components at the hot-steam-cold-oil interface, and the preferential first production of the lighter to intermediate components, leaving a very heavy dead-oil component for production at late times. These phenomena can often not accurately be simulated using the industry standard method of using one single dead-oil component with the measured oil viscosity as property. It is usually necessary to use a multi-component compositional model, in which case each component's viscosity variation with temperature will be required as input. Components could be 'pure' components, or pseudo-components, which are grouped 'pure' components, to reduce simulation times.

Viscosity mixing rules encompass all those methods used to determine the viscosity of (a) a pseudo-component and (b) the oil phase viscosity of a particular oil composition at the pressure and temperature within one simulation cell after a time-advance (time-step) during a simulation. Several different viscosity mixing rules exist, for example Arrhenius (1887), Grunberg and Nissan (1949) (discussed in more detail below), Teja and Rice (Reid *et al.,* 1987), mole-fraction-weighted arithmetic average, power-law and have been evaluated in the literature (Mago *et al.,* 2005). In the simulator used in this thesis, an Arrhenius-type equation (defaulted to the Arrhenius mole-fraction weighted geometric average, and shown later in this section) is used to determine the oil phase viscosity of any particular mixture at the prevailing temperature and pressure in each simulation grid cell, regardless of which mixing rule has been used to establish the pseudo-component liquid viscosities.

In the present work (also de la Porte *et al.*, 2009), the accuracy and applicability of the Arrhenius mixing rule is evaluated. The mole-fraction weighted average Arrhenius

equation is tested against a set of accurate benchmark data, consisting of the best available experimental data comprising compositionally well-defined hydrocarbon mixtures. Experimental data on real reservoir fluids had not been used here, as such data are not always sufficiently accurate to act as benchmark data. Furthermore, the issue of the heavy fraction, and how to properly estimate its viscosity, clouds the issue of the accuracy of the method. In a number of applications, the viscosity of heavy oil is reduced by introducing a light solvent. To test the accuracy of the method under such conditions, CO_2-hydrocarbon mixtures have been used as a further benchmark set, primarily because reasonably accurate data for CO_2-hydrocarbon mixtures are available.

2.2 Theory

Arrhenius-type equations for predicting the viscosity of a mixture stem from early work by Arrhenius (1887) who proposed the following expression:

$$\mu_{mix} = \prod_{i=1}^{n} \mu_i^{x_i} \tag{2.1}$$

where μ_{mix} is the mixture dynamic viscosity, and μ_i and x_i are the dynamic viscosity and mole fraction, respectively, of component *i*. The literature on predicting mixture viscosities is abundant, and multiple reviews are available (Touloukian *et al*., 1975; Irving, 1977a,b; Monnery *et al*., 1995; Poling *et al*., 2000). Although Irving's assessment (1977b) was particularly thorough, as the validation database consisted of over three hundred binary liquid mixtures at temperatures ranging from 0 to 180^{o}C, all the viscosities were measured at ambient pressure, and only one alkane-alkane mixture was used. The report evaluated not only the accuracy of the Arrhenius formula, but also similar formulae where the volume fraction is replaced by either the mass or the mole fraction. Irving concluded that the Arrhenius type equations should be used with mole fractions, and only with non-polar + non-polar mixtures. More recently, Poling *et al.* (2000) commented that the Arrhenius type equations are only accurate for liquid binary mixtures consisting of similar components of

comparable viscosity. For all the other mixtures the use of the Grunberg-Nissan equation (Grunberg and Nissan, 1949) was recommended (Poling *et al*., 2000):

$$\ln \mu_{mix} = \sum_{i=1}^{n} x_i \ln \mu_i + 2 \sum_{1 \le i < j \le n} x_i x_j G_{ij} \tag{2.2}$$

Here, x_i is the mole fraction of component *i*, and G_{ij} is an adjustable parameter that is obtained by fitting the equation to a particular binary mixture viscosity. These parameters are in general functions of both temperature and density, and for a limited number of mixtures, correlations based on group methods are available for their evaluation (Poling *et al*., 2000; Lemmon *et al*., 2007). This approach was recently used to correlate the compositional dependence of the viscosity of petroleum fluids with high asphaltene content (Werner *et al*., 1998). However, in a number of numerical thermal reservoir simulators (*e.g.,* ECLIPSE Reference Manual, 2008), the mole-average Arrhenius model is still the norm:

$$\ln \mu_{mix}(T, P) = \sum_{i=1}^{n} x_i \ln \mu_i(T, P) \tag{2.3}$$

where μ_i refers either to the viscosity of a pure component *i*, or more often to the viscosity of a given pseudo-component. In this model, both the viscosity of a mixture and the viscosity of the components are evaluated at the same temperature, *T*, and pressure, *P*. It is also customary to use x_i, the mole fraction of component *i*, as an adjustable parameter to match the measured viscosity, if available for the predictions of the above model. This simple model, sometimes matched to a measured viscosity, is used even for the simulation of steam injection in heavy oil reservoirs, where both the temperature and pressure change significantly over time.

Although eq. (2.3) is a simple mixing rule based on empirical evidence, it is possible to provide some physical foundation for it by means of Eyring's reaction rate theory (Glasstone *et al*., 1941), which states that μ

$$\mu_{mix} = \frac{h}{V} \exp\left(\frac{\Delta G^*}{RT} \right) \tag{2.4}$$

where ΔG^* is the activation energy, V is the molar volume, h is Planck's constant [6.626×10^{-34} J s], T is the absolute temperature (K), and R is the universal gas constant [8.3145 J/mol K]. Assuming that eq. (2.4) holds both for a mixture and for all the constituent pure components, one can derive

$$\ln \mu_{mix} = \sum_i x_i \ln \mu_i + \ln\left[\frac{\rho_{mix.}}{M_{w,mix}} \prod_i \frac{M_{w,i}^{x_i}}{\rho_i^{x_i}}\right] + \frac{1}{RT}\left[\Delta G^*_{mix} - \sum_i x_i \Delta G^*_i\right] \tag{2.5}$$

where ρ is the mass density, and M_w is the molecular weight. Depending on the mixture in question, one can make a number of further assumptions. In the context of this research, a mixture of alkanes has been assumed. Provided that the mixture is made up of components with similar numbers of carbon atoms, the mass densities of the pure components and the mixture, at the same temperature and pressure, will be approximately the same. Furthermore, the power law mixing rule for molecular weights will provide good estimates, to within a few percent, of the molecular weight of the mixture, as long as the difference in the number of carbon atoms between the components is not too large, or the mixture is not too rich in one component. Hence, the second term in eq. (2.5) will approach zero. If it is further assumed that alkane mixtures are nearly ideal, and that ideality extends to the activation energy in the Eyring theory, the third term in eq. (2.5) will approach zero, and one would recover the mole-average Arrhenius model.

One can also remove the assumptions of the equal mass densities from the above considerations, by calculating the pure component viscosity at the mixture density, in which case the mole-average Arrhenius model takes the following form:

$$\ln\mu_{mix}(T,\rho_{mix}) = \sum_{i=1}^{n} x_i \ln\mu_i(T,\rho_{mix}) \tag{2.6}$$

It is also possible to obtain the Arrhenius-type equation by making use of the fact that the density dependence of the viscosity of most pure liquid alkanes can be approximately described by a simple exponential (Kiran and Sen, 1992) or by the Assael and Dymond (1992) corresponding states expression. However, the simplifying assumptions are based on behaviour of the empirical parameters, and hence do not have the physical clarity obtained by the use of Eyring reaction rate theory.

2.3 Results and Discussion

In order to assess whether or not the mole-average Arrhenius equations are accurate enough to be used for predicting the viscosity of conventional and heavy crudes, an initial study was undertaken to investigate its accuracy by comparison with a compositionally well-defined benchmark dataset. The benchmark dataset consisted of 1002 data points measured for different alkane mixtures including binaries, ternaries and multi-component mixtures. The data set also included 46 CO_2-alkane binary mixtures data points.

2.3.1 Benchmark data

In this section, a brief description of the set of high-quality measurements chosen as the benchmark database is provided.

- Dymond *et al*. (1980, 1981): three binary systems C6-C12[1], C6-C16 and C8-C12; 220 measured viscosity data points were reported at temperatures of 25, 50, 75, and 100 ^{o}C (77-212 °F), and pressures up to the freezing pressure or 500 MPa (72,000 psi). The authors claimed 2% accuracy for their viscosity measurements.

- Wakefield and Marsh (1987, 1988): binary and quaternary mixtures consisting of components ranging from C6 to C16 at temperatures 303.16 and 308.16 K (85-95 °F) and atmospheric pressure. Wakefield and Marsh reported 45 data points and claimed an accuracy of 0.1%.

- Aucejo *et al*. (1995): 36 binary mixtures of various compositions, consisting of components ranging from C5 to C16. 392 measurements were reported at standard conditions, at the temperature of 298.15 K (77 °F) and atmospheric pressure. The authors claimed an accuracy of 0.2%.

[1] The notation used for mixture systems, for example C10-C12, is a shorthand notation for the binary system containing *n*-$C_{10}H_{22}$ and *n*-$C_{12}H_{26}$, or pseudo-components with similar characteristics. This notation will be used in the remainder of this thesis.

- Barrufet *et al*. (1996): 46 viscosity measurements of alkane mixtures with CO_2 were reported. Mixtures included CO_2 as part of a binary system with C10, up to a 5-component system with C5, C6, C7 and C10. Temperatures ranged between 310 K and 400 K (100-260 °F), and pressures between 0.2 and 12 MPa (30-1,700 psi). The accuracy of these measurements had been estimated to be of the order of 5-8% by comparing their measurements for pure components in previous work (Estrada-Baltaar *et al.,* 1998a,b; Barrufet *et al*., 1999) with the reference correlations described in the following section. Under normal circumstances these data would not comprise a primary data set. However, these measurements were performed for CO_2-alkane mixtures for which the data are scarce.

- Wu *et al*. (1998): Viscosities of five quaternary and one quinary *n*-alkane mixtures, with components ranging from C7 to C16, were reported. Seventy measurements are available at different temperatures ranging from 293.15 to 313.15 K (68-104°F), and at atmospheric pressure. The authors claimed an accuracy of 0.1%.

- Caudwell (2004): 126 viscosity measurements of a binary mixture, C8-C10, and ternary mixture, C3-C8-C10, at temperatures ranging from 323.15 to 473.15 K (122-392 °F) and pressures up to 201.9 MPa (29,000 psi), are reported. The author claimed an accuracy of 2%.

- Audonnet and Pádua (2004): 103 viscosity measurements of binary mixtures of C1 and C10, at pressures up to 75 MPa (11,000 psi) and temperatures ranging from 303 to 393 K (85-248 °F), were reported. The authors claimed an accuracy of 3%.

A further check on the reported accuracies of the mixture viscosity data, for each author, was performed by comparing their measured pure component viscosity, if available, against the relevant pure component correlations. In conclusion, the benchmark data set for alkane mixtures has reported accuracy better than 3%, which is more than adequate for testing purposes. The CO_2-alkane dataset has a much lower estimated accuracy of 5-8%.

2.3.2 Viscosity correlations

To obtain an accurate mixture prediction, it is essential to use pure viscosity correlations that are accurate and reliable. For this purpose, correlations (RefProp V8, NIST Standard Reference Data Base) that are based on a critical assessment of the available experimental data, with well-defined accuracy, had been chosen. The viscosity of carbon dioxide was determined with an uncertainty of ±2 to ±4% from the representation of Fenghour *et al*. (1998):

$$\mu(\rho,T) = \mu_0(T) + \Delta\mu(\rho,T) + \Delta\mu_c(\rho,T) \tag{2.7}$$

$$\mu_0(T) = \frac{1.00697T^{1/2}}{\sum_{i=0}^{4} a_i (\ln T^*)^i} \tag{2.8}$$

where the zero-density viscosity, μ_0, is in units of μPa s and the temperature, T, in Kelvin. An excess viscosity term, describing the density-dependency of viscosity behaviour outside the critical region, is defined as

$$\Delta\mu(\rho,T) = \sum_{i=1}^{n} b_i(T)\rho^i \tag{2.9}$$

The density coefficients $b_i(T)$ are represented by a functional relationship in the reduced temperature T^*.

The viscosity of pure methane was obtained from the representation of Vogel *et al*. (2000). The estimated uncertainty is of the order of ±1-2%, in the temperature and pressure range of interest to this work:

$$\mu(T,\rho) = \mu^{(0)}(T) + \mu^{(1)}(T)\rho + \mu^{(2)}(T)\rho^2 + \mu^{(3)}(T)\rho^3 + \mu^{(4)}(T)\rho^4 \tag{2.10}$$

The correlation of Vogel *et al*. (1998) was used for propane. The authors claimed an uncertainty of up to ±4%:

$$\mu(\rho,T) = \mu^{(0)}(T) + \mu^{(1)}(T)\rho + \Delta\mu_h(\rho,T) + \Delta\mu_c(\rho,T) \tag{2.11}$$

where $\mu^{(0)}$ is the viscosity in the zero-density limit, $\mu^{(1)}$ is a residual viscosity accounting for viscosity increase with density, $\Delta\mu_h$ represents higher density terms of the residual viscosity, and $\Delta\mu_c$ the critical enhancement representing the viscosity increase in near the critical point, in this case set to zero.

The viscosities of *n*-octane, *n*-nonane and *n*-decane were calculated from the representation by Huber *et al*. (2005) with an uncertainty of ±2 to ±5%:

$$\mu(\rho,T) = \mu^0(T)[1 + B_\mu(T)\rho] + \Delta_H\mu(\rho,T) + \Delta_c\mu(\rho,T) \tag{2.12}$$

$$\mu^0(T) = \frac{0.021357\sqrt{MT}}{\sigma^2 S^*_\mu(T^*)} \tag{2.13}$$

where

$$\ln S^*_\mu = \sum_{i=0}^{n} a_i (\ln T^*)^i \quad \text{and} \quad \sigma = 0.0809 V_c^{1/3},$$

where T^* is the reduced temperature is equal to Tk_B/ε, where k_B/ε is an energy scaling parameter in units of K. The higher density term $\Delta_H\mu(\rho,T)$ is represented in terms of the reduced density, $\delta = \rho/\rho_c$, and reduced temperature $\tau = T/T_c$:

$$\Delta_H\mu(\rho,T) = 1000\left(\sum_{j=2}^{3}\sum_{k=1}^{2}\alpha_{jk}\frac{\delta^j}{\tau^k} + c_1\delta\left(\frac{1}{\delta_0 - \delta} - \frac{1}{\delta_0}\right)\right) \tag{2.14}$$

where δ_0 is the reduced close-packed density, a function of the reduced temperature τ. Coefficients α_{jk} and c_i are specific to each individual component.

Another representation by Huber *et al*. (2004) was used to calculate the viscosity of *n*-dodecane. The authors claimed an uncertainty of up ±5%. The correlation is similar to eqs. (2.12) and (2.14), but without the third term representing the viscosity enhancement in the

critical region in eq.(2.12), and the reduced close-packed density, δ_0, calculated differently. Additionally, the component coefficients were specific to dodecane.

The viscosities of the remaining alkanes were obtained from the Hard Sphere-based corresponding states scheme of Assael *et al*. (1992), who claimed an uncertainty of ±6%.

2.4 Results

Results are categorized into three groups based on applicability and accuracy of the results after applying the Arrhenius rule to obtain multi-component mixture viscosities. All results are presented in terms of deviations and trends measured by eqs. (2.15) to (2.18), with full results, including the experimental and calculated viscosities for all mixtures, in Appendix A.

Relative deviation:

$$\Delta\mu \equiv 100(\mu_{\exp} - \mu_{calc}) / \mu_{\exp} \tag{2.15}$$

Maximum absolute deviation:

$$MAD = \left|\Delta\mu\right|_{\max} \tag{2.16}$$

Average deviation:

$$RMS = \Delta\mu_{rms} = \sqrt{\sum \frac{(\Delta\mu)^2}{n}} \tag{2.17}$$

Trend:

$$BIAS = \frac{\sum \Delta\mu}{n} \tag{2.18}$$

2.4.1 Applicability of Arrhenius equation

Within the context of the data evaluated, a summary of observations had been made about the use of the traditional mole-average Arrhenius equation, eq. (2.3). Findings were categorized into three groups, (A) where the method results are within the 10% uncertainty already inherent in reservoir simulation, (B) where the error is significant, but less than 30%, and (C) where the method can no longer be applied due to errors above 30%. Examples of each category are shown later.

2.4.1.1 Category A: MAD<10%

Mixtures where the mole-average Arrhenius equation, eq. (2.3), provides reasonable accuracy for use in petroleum engineering applications (<10% maximum absolute deviation):

- Binary mixtures made of pure components containing similar numbers of carbon atoms. To measure the similarity in a number of carbon atoms ΔC has been defined as the difference in the number of carbon atoms between the two components in the mixture. A good example of a mixture with low ΔC is the binary mixture of *n*-pentane and *n*-heptane (ΔC=2) from the Aucejo dataset.
- Binary mixtures with a higher ΔC, but a very low (<=20%) concentration of the lighter components, for example the C6-C12 mixture (ΔC=6) from the Aucejo dataset, with the mole fraction of the C6 component around 0.1, and the Wakefield C8-C14 mixture (ΔC=6) with the mole fraction of the C8 component around 0.15.[2] The binary mixture C10-C16, with a ΔC=6, exhibits deviations on the higher end of the range with a maximum deviation of 8.5% when x_{C10}=0.6095 and an average deviation (rms) of 6.4%, while for C9-C16 with a ΔC =7 the maximum deviation is above 10% when x_{C9} is around 0.5.
- Multi-component mixtures, even when ΔC between the lightest and heaviest components is large; for example the C7-C8-C11-C13 mixture from the Wu-dataset.

[2] Note that the deviations given in Table 2.1 for a given mixture might include points measured at different temperatures, pressures and composition.

It seems that one situation that helps improve the accuracy is when the intermediate components are symmetrically spaced. In this example, ΔC between adjacent components does not exceed 3. This is more evident when we compare the results for the Wu *et al*. mixtures C7-C10-C13-C16 with C7-C8-C12-C16, see Table 1. In both cases, ΔC between the lightest and the heaviest component is 9, but the former mixture, having components more equally spaced (*e.g.,* ΔC =3), exhibits an rms of 9%, compared with 19% for the latter.

- More symmetric 5-component mixtures with near-equally spaced number of carbon atoms, such as C7-C8-C11-C13-C15. Relative deviations for different compositions were between 6 and 9%.

2.4.1.2 Category B: RMS between 10 and 30%.

Mixtures where the traditional mole-average Arrhenius equation, eq. (2.3) is not sufficiently accurate to be used for petroleum engineering applications (rms error between 10-30%):

- Binary mixtures of heavier components, with a high ΔC, (of the order of ΔC >7), for example C6-C16 of Aucejo *et al*. and Dymond *et al*. and C7-C16 of Aucejo *et al*. Maximum absolute deviations in these cases are up to 33%.
- Asymmetrical mixtures, for example with more than one heavy component mixed with one light component, for example C3-C8-C10 from the Caudwell dataset. The maximum absolute deviations in these mixtures were found to be between 12 and 21%, with the maximum deviation associated with the mixture with the highest mole fraction of C3, in this case 0.425.
- Multicomponent mixtures with large ΔC between the lightest and heaviest component and the asymmetrical spacing of intermediate components. A good example is the mixture C7-C8-C12-C16 from the Wu dataset that exhibits maximum absolute deviation of around 21%.

2.4.1.3 Category C: RMS>40%

Mixtures where the traditional mole-average Arrhenius equation, eq. (2.3) should not be used for petroleum engineering applications, (rms error > 40%):

- Binary mixtures with large ΔC, for example C1-C10 from the Audonnet and Padua dataset, which are under-predicted by 49% with the maximum deviation of 63%.
- Mixtures with large differences in viscosity of the pure components, such as carbon dioxide (CO_2) and *n*-decane (n-$C_{10}H_{22}$). In these mixtures, the calculated viscosities were found to be, on average, nearly 50% smaller than the measured values.

2.4.2 Examples

2.4.2.1 Case 1

An example of the effect of mixture composition, as well as the effect of the increasing ΔC, on the binary-mixture viscosity deviation is illustrated in Figure 2.1. The relative deviation between the calculated and the measured mixture viscosity is plotted for C8-C9, C8-C10, C8-C11, C8-C12 and C8-C16 against the mole fraction of *n*-octane in each mixture. It can be observed that deviations are largest for the mixture with a highest ΔC, e.g., C8-C16 mixture; the deviation is at its maximum for equimolar composition; deviations for the mixtures C8-C9 to C8-C12 are <5%, within acceptable ranges, *i.e.,* <10%, at all mixture ratios.

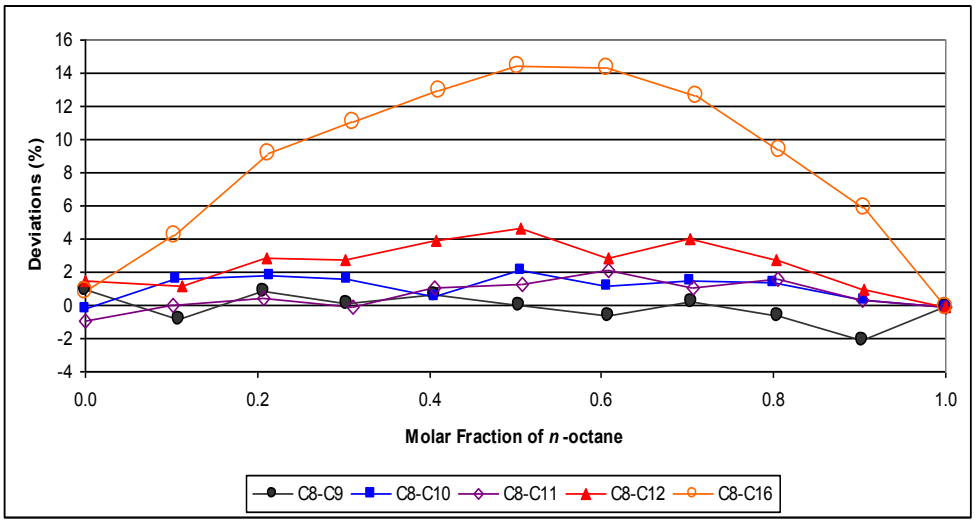


Figure 2.1. Relative deviations for binary mixtures containing *n*-octane measured by Aucejo *et al.* (1995) at 298.15 K and atmospheric pressure.

It is, however, instructive to observe whether or not similar behaviour occurs at higher pressures. Figure 2.2 shows the relative deviations between the calculated and measured viscosity of an equimolar C8-C12 mixture (Dymond *et al*., 1981) as a function of pressure. The deviations are within ±5% within the pressure range relevant to exploitable hydrocarbon reservoirs (P < 110 MPa / 15,000 psi / 1,100 bar), indicating that the accuracy of the method does not change with pressure, at least within the pressure range of interest. Higher deviations at pressures higher than 110 MPa indicate that the method may become less accurate above this limit, especially when combined with high temperatures. It was not possible to validate the method against the available data up to 500 MPa, as the pure correlations for *n*-octane and *n*-dodecane do not extend beyond 200 MPa.

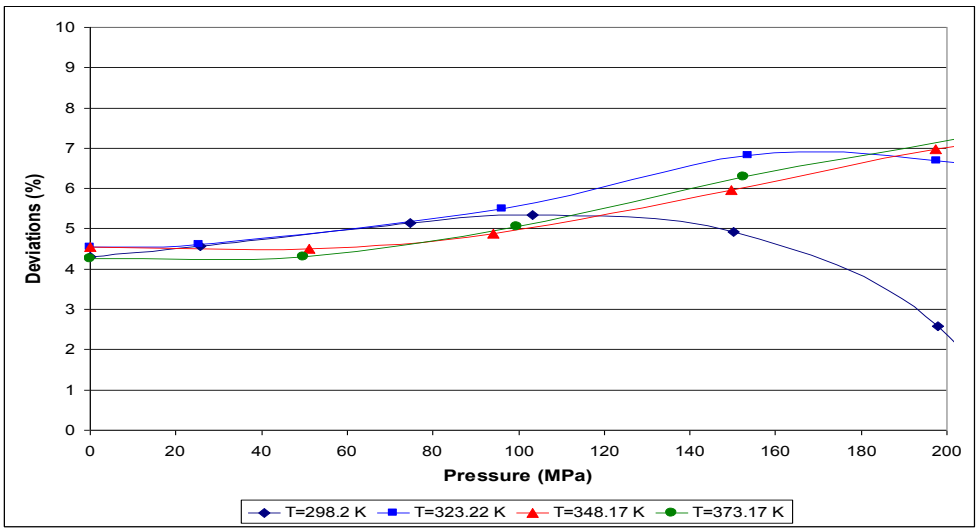


Figure 2.2. Relative deviations as a function of pressure for equimolar C8-C12 mixture at different temperatures, measured by Dymond *et al.* (1981).

2.4.2.2 Case 2

An example of a ternary system (C3-C8-C10), where the traditional mole-average Arrhenius equation, eq. (2.3), is within acceptable accuracy for one of the binary systems (C8-C10), but not for the ternary, is illustrated in Figure 2.3. In this example the Caudwell (2004) data had been analysed for two binary C8-C10 mixtures of different compositions (mix1: x_{C8}=0.743, x_{C10}=0.257; mix2: x_{C8}=0.434, x_{C10}=0.566) and three ternaries (mix3: x_{C8}=0.611, x_{C10}=0.211, x_{C3}=0.178; mix4: x_{C8}=0.312, x_{C10}=0.405, x_{C3}=0.283; mix5: x_{C8}=0.344, x_{C10}=0.231, x_{C3}=0.425), in terms of the maximum absolute deviation. For the C8-C10 binary mixtures the overall rms error, for both nearly equimolar and *n*-octane rich mixture, is around 4%, while the maximum absolute deviation is approximately 6%. However, if propane is added, the calculated mixture viscosity under-predicts the experimental viscosity with an average rms deviation of 17.5%. At low mole fractions of propane (mix3) the rms error is 13%, while the maximum absolute deviation is 14%. However for a mixture which contains 40% propane (mix5), the rms deviation increases to 19%, while the maximum absolute deviation increases to 21%.

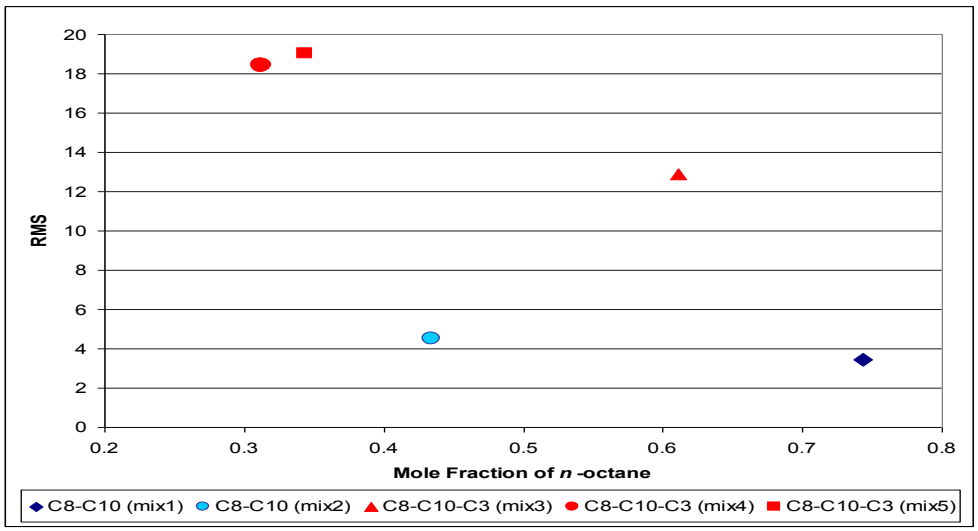


Figure 2.3. RMS deviations for binary and ternary mixtures containing *n*-octane; measurements by Caudwell (2004).

2.4.2.3 Case 3

In this example, the binary mixture of methane (C1) and *n*-decane (C10) is used to examine the effect of a large ΔC, and consequently, the high molecular-weight ratio. Figure 2.4 illustrates the relative deviations plotted against pressure for three binary C1-C10 mixtures of different compositions, along four different isotherms. In all cases, we observe unacceptably large relative deviations that increase with increasing concentration of the light component. In the worst case examined (x_{C1}=0.6), the maximum absolute deviation reached 63%, while the rms deviation was 49%. Figure 2.4 also illustrates that the sensitivity of the relative deviations to the changes in temperature and pressure remains low, even for large ΔC. It is instructive to observe that the measured viscosities of these mixtures ranged between 0.08 and 1.065 cP, while the calculated viscosities ranged between 0.043 and 0.715 cP. It is clear from the above example that the traditional mole-average Arrhenius equation, eq. (3), grossly under-predicts the viscosity of binary mixtures that consist of light and heavy components.

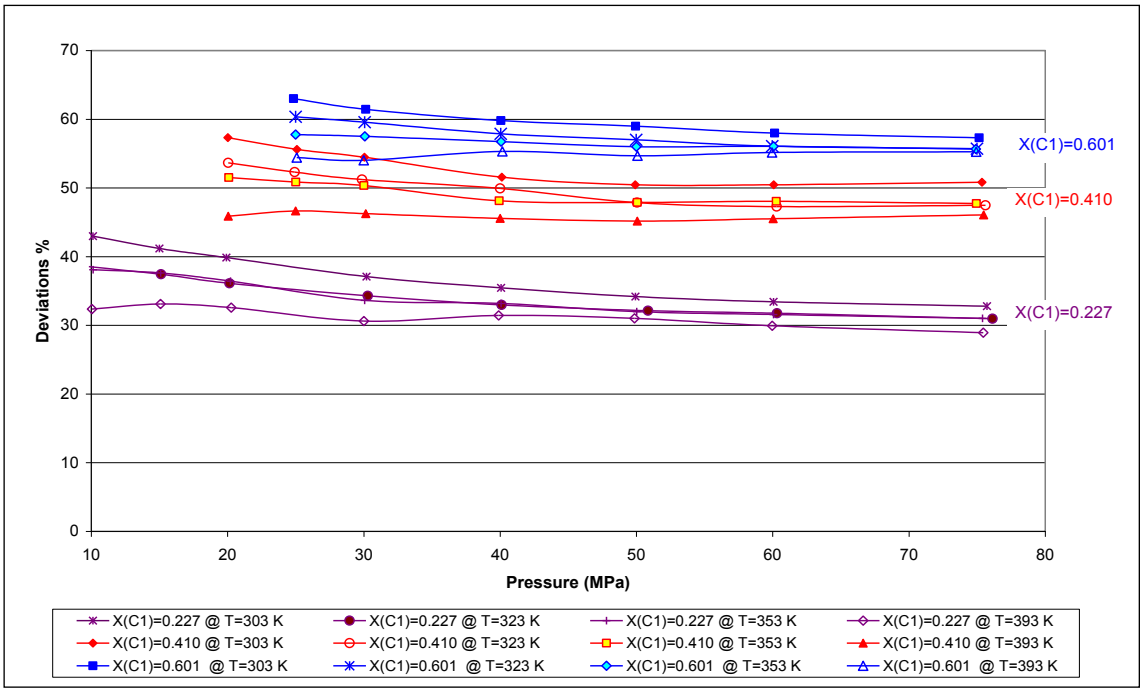


Figure 2.4. Relative deviations as function of pressure for C1-C10 mixtures by Audonnet and Pádua (2004), at different temperatures. (Pressure and temperature ranges in field units: 1,450-10,878 psi and 85-247 °F.)

2.4.2.4 CO_2 - alkane mixtures

In order to assess the suitability of the traditional mole-average Arrhenius equation to estimate the viscosity of CO_2-alkane mixtures, the relative deviations of eq. (2.3) from the viscosity data measured by Barrufet *et al*. (1996) are reported in Table 2.1. Figure 2.5 shows the relative deviations for three CO_2-C10 mixtures as a function of temperature. The deviations increase with the increase in concentration of the light component (CO_2), ranging from 20% for a mixture 15% rich in CO_2 to 80% for the equimolar mixture.

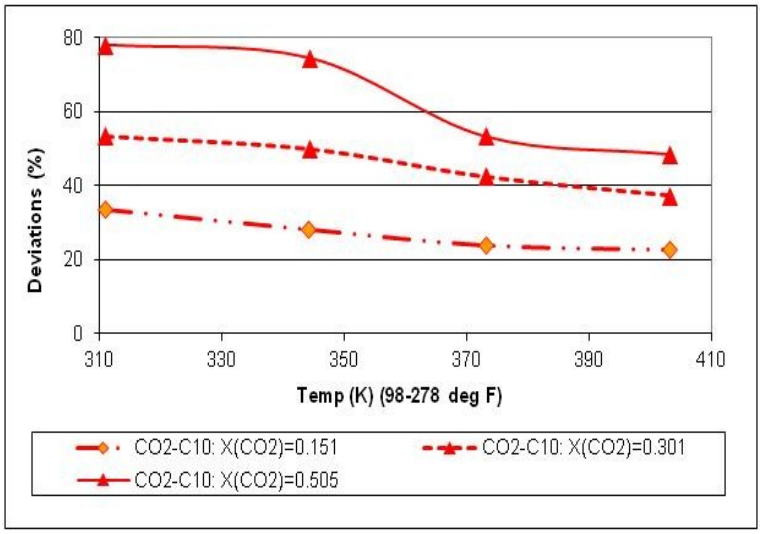


Figure 2.5. Relative deviation of CO2-C10 mixture.

Figure 2.6 to Figure 2.8 illustrate the deviations observed for multicomponent mixtures: CO_2-C5-C10, CO_2-C4-C6-C10 and CO_2-C5-C6-C7-C10 respectively. In all the cases the relative deviations are larger than 20%, increasing with an increase in CO_2 mole fraction. It is instructive to observe that in contrast to alkane mixtures, the addition of intermediate components does not decrease the deviations. The magnitude of the relative deviations seems mainly governed by the amount of CO_2 in the mixture. Both of these observations can be rationalized by the higher non-ideality of CO_2-alkane mixtures compared to the alkane mixtures.

It is clear that this method of calculating the mixture viscosities would be inappropriate in the simulation of CO_2 injection, combined with thermal stimulation.

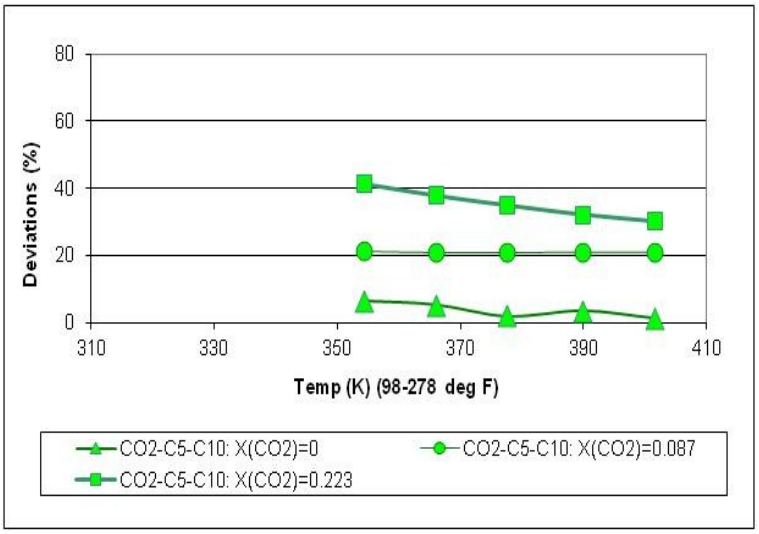


Figure 2.6. Relative deviation of CO2-C5-C10 mixture.

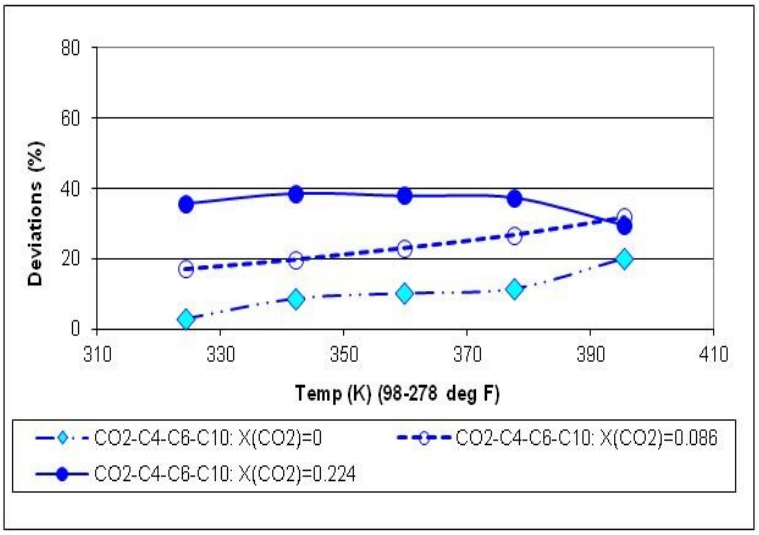


Figure 2.7. Relative deviation of CO2-C4-C6-C10 mixture.

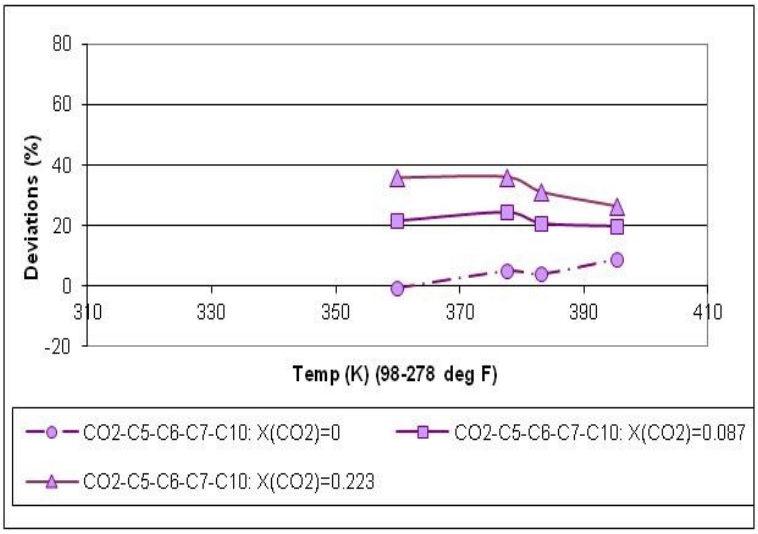


Figure 2.8. Relative deviation of CO2-C5-C6-C7-C10 mixture.

It is clear that high errors are introduced in CO_2-hydrocabon mixture viscosities when the Arrhenius mixing method is used. Deviations from measured data were above 20% at low concentrations of CO_2, and increased to nearly 80% at equimolar mixtures with decane.

2.5 Summary of Results

A summary of the results is presented in Figure 2.9 and Table 2.1**.** The full comprehensive study results are shown in Appendix A.

In general, the calculated viscosities were lower than the measured ones. Deviations decreased with increase in temperature, and, at the same time, slightly increased with increasing pressure. However, the results were less sensitive to the pressure and temperature conditions than to the compositional effect, at least within the ranges investigated (T = 298-423 K or 25-150 deg °C, and P = 0.1 to 200 MPa or 29,000 psi). Hence, the focus is mainly on ascertaining the influence of mixture composition. The largest deviations were in the CO_2 mixtures, seen to the right of the graph, and also prominent in Table 2.1 in the Barrufet section.

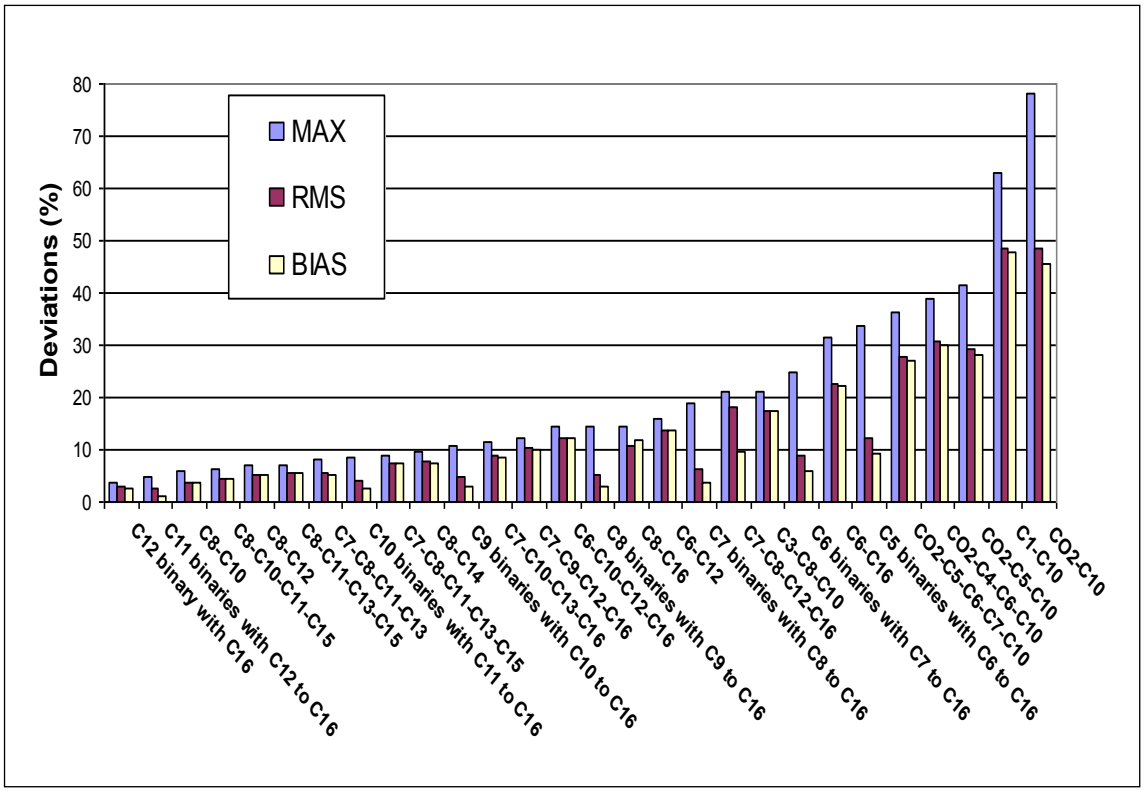


Figure 2.9. Summary of results: Maximum Absolute Deviation (MAX), Root Mean Square (RMS) error, and Bias.

Table 2.1. Summary of results.

Author	Year	Mixture	Temp (K)	Pressure (bar)	RMS	BIAS	MAD
Dymond *et al*	1981	C8-C12	298-373	1-2000	5	5	7
	1981	C6-C12	298-373	1-2000	14	14	16
	1980	C6-C16	298-373	1-2000	23	22	32
Wakefield *et al*	1988	C8-C14	303-308	1	8	7	10
	1988	C8-C16	318-338	1	11	12	15
	1988	C6-C10-C12-C16	303-308	1	12	12	14
	1988	C7-C9-C12-C16	303-308	1	10	10	12
Aucejo *et al*	1995	C5-binaries {C6 to C16}	298.15	1	12	9	34
		C6-binaries {C7 to C16}			9	6	25
		C7-binaries {C8 to C16}			6	4	19
		C8-binaries {C9 to C16}			5	3	14
		C9-binaries {C10 to C16}			5	3	11
		C10-binaries {C11 to C16}			4	3	8
		C11-binaries {C12 to C16}			2	1	5
		C12-binary {C16}			3	2	4
Barrufet *et al*	1996	CO2-C10	310-400	70-120	49	45	78
		CO2-C5-C10	354-400	25-50	29	28	41
		CO2-C4-C6-C10	325-395	3-50	31	30	39
		CO2-C5-C6-C7-C10	360-395	2.7-50	28	27	36
WU *et al*	1998	C7-C8-C11-C13	293-313	1	6	5	8
		C8-C10-C11-C15	308-313	1	5	4	6
		C8-C11-C13-C15	308-313	1	6	6	7
		C7-C10-C13-C16	308-313	1	9	9	12
		C7-C8-C12-C16	308-313	1	18	9	21
		C7-C8-C11-C13-C15	293-313	1	8	8	9
Audonnet *et al*	2004	C1-C10	303-393	1-750	49	48	63
Caudwell *et al*	2004	C3-C8-C10	323-373	200-700	17	17	21
		C8-C10	323-423	1-2000	4	4	6

2.6 Conclusions

The mole-average Arrhenius mixing rule had been tested against a set of accurate benchmark viscosity data that contained compositionally characterized alkane and CO_2-alkane mixtures.

The results show that the mole-average Arrhenius equation is of acceptable accuracy (error < 5-10%) for binary mixtures, providing the difference between the number of carbon atoms in the pure components, ΔC, is less than 3. For binary mixtures, the accuracy deteriorates rapidly with increasing ΔC. For methane (C1) and *n*-decane (C10) mixtures, the relative deviations between the experimental and the calculated viscosity as high as 60%, have been observed. For the CO_2–C10 mixture, the relative deviation was found to be nearly 80%. The temperature and pressure, at least in the range considered in this work, do not have much effect on the accuracy of the Arrhenius equation.

For the multi-component mixtures, the situation is more difficult to summarise, due, in part, to the scarcity of data on the multi-component alkane mixtures. In general, the addition of a light component to a mixture decreases the accuracy significantly. However, the addition of a component with a carbon number between the light and heavy components generally improves the accuracy, especially if the components in the resulting mixture are equally spaced in terms of their carbon numbers.

Overall, the mole-average Arrhenius mixing rule generally underestimates the mixture viscosities and may result in overestimating recovery factors. The largest deviations occur in mixtures with large ΔC. The most common application of this type of mixture is in the simulation of heavy-oil reservoirs where all the heavier components are grouped into one pseudo-component, say C20+, and mixed with a light pseudo-component, say C1. Therefore, care must be taken in choosing the pseudo-components for use in heavy-oil reservoir simulation. Using more than one heavy pseudo-component will reduce the error. The simulation of CO_2 injection into heavy-oil reservoirs, using the Arrhenius equation for viscosity calculation, is more than likely to result in overestimation of recovery factors. Hence, it is recommended that simulation of thermal recovery processes, in combination with CO_2 injection, should not use the default Arrhenius equation for calculation of the mixture viscosity.

The mole-average Arrhenius equation has been tested, where the viscosity of each pure component is calculated at the mixture density, rather than at the mixture pressure.

Although the relative deviations are significantly smaller, they are still unacceptably large for the mixtures of light and heavy components.

3 Thermal Oil Recovery Sensitivity to Component Grouping and Viscosity Modelling

3.1 Introduction

Hydrocarbon systems contain thousands of different pure components, from simple alkanes to complex asphaltenes. It is not possible to simulate the PVT behaviour of each component individually during a reservoir study, due to both lack of data, as well as the CPU power and time it would require. For compositional simulation, where a pressure-temperature flash calculation on each individual component in each simulation grid cell at each time step determines the composition of the oil mixture in the cell, and the equations are solved implicitly, a traditional maximum of four to five components and an absolute maximum of fourteen components are usually recommended.

When steam injection into a heavy oil (20°API and lower) reservoir is simulated, a fully compositional thermal simulation of this process is necessary in order to optimise the oil recovery or economics. In theory, to accurately simulate this process, a very fine numerical grid should be used, and the hydrocarbon system should be characterised by as many components as possible, in order to accurately account for the effects and processes that take place in the reservoir with the increasing temperatures. However, simulations of this nature of a full field with several injectors can take days, or even weeks, and are therefore neither economical nor feasible in terms of project delivery times. A partial solution to this problem is to characterize the heavy hydrocarbon components in as few pseudo-components as possible, while still maintaining overall accuracy. If a detailed laboratory component analysis of the oil is available, then these components should be grouped into a small number of pseudo-components with similar characteristics. The key questions to be addressed are: what is the minimum number of pseudo-components necessary to keep the errors in the simulation results to a minimum, and what is the best way of estimating the viscosity of each of these pseudo-components at various temperatures?

Simulation models of these thermal recovery processes in heavy oil fields began with a single component dead oil hydrocarbon system combined with water and steam. Recent advances in thermal simulators allow the use of multi-component characterisations with live hydrocarbon components that can exist in both the liquid and vapour phases. Yet many thermal steam flood or huff and puff simulations still characterize the oil with a single heavy hydrocarbon component. This simple approximation is used for two reasons. First, often the laboratory analysis of the heavy oil only provides a single heavy component molecular weight along with the mole fraction or weight fraction. Secondly, reservoir simulation engineers do not know the magnitude of the error created by using a single heavy component in their simulations. If the heavy oil mole fraction *vs.* molecular weight distribution is a simple unimodal distribution with a small standard deviation, one can postulate that characterizing the heavy fraction with a single component would be satisfactory. If the mole fraction *vs.* molecular weight distribution is a bimodal distribution, such as was described in the study 'Fourth SPE Comparative Solution Project: Comparison of Steam Injection Simulators'[3] by Aziz and co-workers (Aziz *et al.,* 1987), then a single component heavy oil characterisation might create significant errors in the predicted production.

Two different practical situations provided basis for this research. Case one is where the PVT laboratory makes a detailed analysis of the heavy oil, and provides a multi-component description of molecular weights and mole fractions. If the mole fraction *vs.* molecular weight distribution is bimodal, then what are the magnitudes of the reservoir simulation errors as the number of pseudo-components is decreased? And, can one accurately simulate this case with a single heavy pseudo-component? Also, as components are grouped into pseudo-components, what is the correct way to average the viscosities to obtain the pseudo-component viscosity? Case two is where the PVT laboratory makes a simple analysis resulting in a single pseudo-component for the entire heavy oil. What is the error in the simulation of a steam flood using this single heavy component, if the actual distribution of mole fractions vs. molecular weight is a bimodal one?

[3] Referred to as SPE4 in rest of this thesis

In this research, both cases were addressed. A base case, comprising of twenty-four detailed components (methane plus twenty-three components for the heavy oil) with a binomial distribution of mole fraction *vs.* molecular weight, was created and characterised to comply with the SPE4 fluid. This characterisation was grouped, step by step, into ten components, five components, three components, ending with two components: methane-group and one heavy component. Two methods to calculate the viscosity as a function of temperature and pressure of the lumped pseudo-components were used. The investigation compared the simulation results from the multi-component simulations and a single heavy component characterisation. The ECLIPSE Thermal simulator was used to run the cases and compare the results. The results quantify the errors involved, and propose a calculation of the pseudo-component viscosity as components are lumped together. The results are verified with a field case of which the 30-component fluid composition was determined in a laboratory.

Note: Different thermal simulators are available on the market, such as STARS (Computer Modelling Group Ltd), which is a leading thermal simulator. Other simulators tested during the Fourth SPE Benchmark study (Aziz, *et. al*., 1987) were from Arco Oil and Gas Co., Chevron Oil Field Research Co., Société Nationale Elf Aquitaine and Scientific Software-Intercomp (SSI). In the current research only ECLIPSE Thermal had been used, and results may differ from simulations performed with any other software.

3.2 Component Grouping

Two levels of grouping are found in compositional modelling: (1) single-carbon-fractions, and (2) pseudo-components for simulation purposes. The concept of single-carbon-number groups (SCNG), also called boiling point fractions, are used instead of pure components such as normal alkanes or paraffins and aromatics. These carbon number fractions are grouped based on a range of pure components that distil within a certain defined range of temperatures, normally 0.5 deg °C above that of the previous *n*-alkane boiling point, up to the current *n*-alkane boiling point +0.5 °C during a process called true boil point (TBP)

distillation (Pedersen *et al*., 2007). Katz and Firoozabadi (1978) compiled a library of the characteristics of these SCNG, generally used in the oil industry. An example of a SCNG would be C6 which include C_5H_{10}, Clyclopentane (C_5H_{10}), n-Hexane (C_6H_{14}), 2,2-Dimethylbutane (C_6H_{14}) amongst others. Benzene (C_6H_6), an aromatic, is grouped into the C7 SCNG based on its boiling point (80.2 °C) which is more than 0.5 °C higher than that of n-Hexane at 68.8 °C (Pedersen *et al.,* 2007).

Compositional analysis, as performed by PVT laboratories, normally provides SCNG components up to C6 with a characterised C7+ group, sometimes higher. In the case of heavy oil, however, the compositional analysis is more often in terms of SARA, which groups saturates, aromatics, resins and asphaltenes. Molecular weights and weight percentages of each SARA group are provided instead of the SCNG composition. In this section the former had been assumed, where a detailed composition is available. The second case of a SARA analysis is further explored in Chapter 7.

The main objective during grouping into pseudo-components for simulation purposes is to maintain the same flow behaviour of the oil and gas in the reservoir, while reducing CPU time. Crucial properties are the fluid phase-behaviour and the individual phase viscosities. Phase behaviour depends on the saturation pressure (P_{sat}) of the oil mixture at the prevailing conditions (PVT), and determines the amount of gas *vs.* oil in the grid cell, the composition of each phase, and consequently the phase viscosity. This in turn determines the mobility of the phase, where the mobility is defined as the ratio of the relative permeability, as a function of saturation, to the viscosity of the phase. In heavy oil, both the oil viscosity, as a function of composition, temperature and pressure, as well as the vapour to liquid ratios (K-values), are important during simulation. The question is, if the number of components is reduced by grouping into pseudo-components, essentially 'oil mixtures', which mixing rules should be used to maintain reasonable integrity, and what is the magnitude of the error incurred when the oil is characterised by one or two pseudo-components?

In this chapter, a grouping method based on equivalent carbon-number (ECN) lookup is applied to assess the sensitivity of simulation production predictions to the number of pseudo-components and the oil component viscosity mixing rule. A first attempt is made to answer the question of whether the oil industry standard method of using two components during thermal simulation, a live gas component and a dead oil component, could be applied to a 22°API oil with a bimodal distribution of the mole fractions. The accuracy is evaluated based on a 24-component base case. The same method is then applied to a 10°API oil to determine the sensitivity of the grouping and viscosity mixing methods used to the molefraction distribution and oil type.

3.3 Literature Review

In the fourth SPE thermal simulation benchmark study (SPE4; Aziz *et al*., 1987) three different cases were simulated with different industrial simulators. A three-component fluid description was used, which has been used as departure point in the present study. The (synthetic) fluid distribution was bi-modal, contrary to the log-normal distribution recommended by Whitson (Whitson *et al*., 1989). In a study based on a San Ardo oil of 12°API, Lolley and Richardson (1997) found that a gamma distribution with $\alpha = 1$ may not be correct for some medium-to-heavy oils. Gas chromatography (GC) analysis revealed a 'double hump', or bimodal compositional distribution in heavy oil, with an absence of significant C1-C6 composition. Lolley and Richardson (1998) recommended a minimum of four pseudo-components; however, they did not investigate the influence of the oil viscosity mixing rule on their findings.

Mago *et al*. (2005) assessed the impact of oil viscosity mixing rules in steam stimulation, and found that the common methods used at the time failed for thermal applications. They found that results were significantly affected, with possible over-prediction of recoveries.
A number of predictive mixture viscosity models have been evaluated by Hernandez *et al.* (2001), when they analyzed the sensitivity of simulation results to viscosity prediction. They found that heavy oil predictions were most sensitive, with deviations in cumulative production as large as two orders of magnitude difference, clearly illustrating the effect of

using incorrect viscosity predictions. De la Porte *et al*. (2009) published results from an investigation into the Arrhenius mixing rule, and provided guidelines of when the method would be accurate. The work also illustrated that grouping methods could adversely affect the mixture viscosity calculation. Wuttipittayamongkol (2009) evaluated three different grouping strategies for pseudo-components, wherein the pseudo-component viscosities were calculated with a correlation from Assael *et al*. (1992), and the mixture viscosities were calculated using two different methods: (1) the Vesovoc-Wakeham (VW) method (Royal *et al.,* 2003), and Arrhenius' equation (Arrhenius, 1887). It was found that the VW method was not sensitive to the grouping scheme, and results were within a 5% error-margin. The Arrhenius method was very accurate, with errors less than 2.5%, as long as the grouping scheme used the equal-mass-fraction that include C1-C3 rule (Joergense *et al.,* 1995).

In the present work, the method used to split the three components in the SPE4 benchmark model into twenty-three components with a bi-modal distribution, preserving the over-all character of the fluid, is briefly discussed. Methane in the amount of 10% is then added to the system. In order to quantify errors made in using only two or three components, the full composition is then grouped. A new grouping procedure is used to lump the components and define new 'pseudo-pure' components and their properties, creating four separate cases, each with a different number of pseudo-components. The final case contains one heavy pseudo-component, and methane. The pseudo-component viscosities are calculated using two different techniques for comparison. Simulations of all the cases are run with ECLIPSE Thermal, and comparisons are made. Findings were verified using a heavy oil reservoir fluid of 10°API (Krejbjerg and Pedersen, 2006; Pedersen and Christensen, 2007).

3.4 Methodology

The basis of this research was the SPE4 benchmark model in which the fluid component distribution followed a bimodal distribution – the worst case scenario. The original model, one-eighth of a nine-spot injection-production pattern, with dimensions of 9x5x4, was extended to 20×20×40 cells of dimensions 10×10×2 ft each, in order to limit numerical

dispersion. Porosity was 30%, permeabilities ranged between 500 mD and 2000 mD. The rock and fluid thermal conductivity was set to 24 Btu/ft/d/°F, with the rock heat capacity 35 Btu/ft^3/°F. The total thickness of the reservoir was 80ft. The initial reservoir pressure was 400 psi, with initial water saturation 45%, initial oil saturation 55%. The Peng Robinson Cubic equation of state was used to model the fluid. Closed boundaries were assumed, that is, that no energy loss to overburden or surrounding rock will occur. The extended model contained one steam injector and two oil producers, positioned on the corners of the grid (Figure 3.1). The original three-component fluid, with two live and one dead hydrocarbon (HC) components, were used as a guide for the creation of the twenty-four hydrocarbon components heavy oil used in this study.

The 24-component base case (synthetic fluid) was simulated for five years, by injecting steam at a temperature of 450 °F, a rate of 37.5 bls/d and steam-quality of 70%. The maximum bottom-hole injection pressure was set to 1000 psia. The two producers were bottom-hole pressure controlled (17 psia), with a steam production upper limit set to 2.5 and 1.25 CWE (cold water equivalent) stb/d. Viscosity data for simulation was provided in the form of a lookup table with component viscosities *vs*. temperatures. (SPE4).

Four new simulation cases were subsequently generated by grouping the twenty-four components, first into ten pseudo-components, then five, three and two pseudo-components. The grouping and characterisation is described in the section on Grouping. The production predictions from each of the simulation cases were compared and reported.

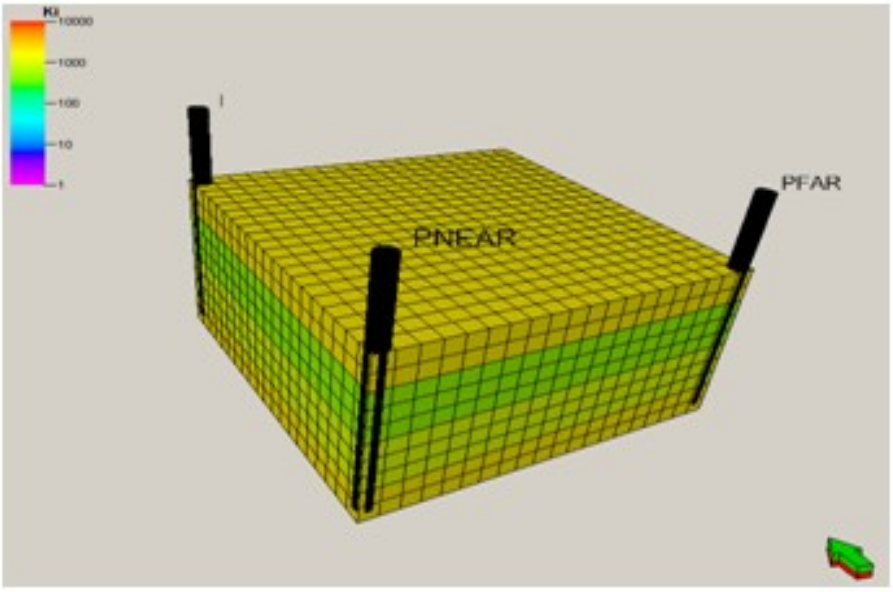


Figure 3.1. Simulation model with one steam injector (I) and two oil producers (PNEAR and PFAR).

3.4.1 Splitting and characterisation

The base case of twenty-four hydrocarbon components was created by first creating two normal distributions, frequency *vs.* molecular weight (MW). One distribution had a mean MW of 250 and a standard deviation of 50, whereas the other had a mean MW of 600 and a standard deviation of 100. Both distributions were created with 500 frequency values that had a small random element. The two distributions were merged together and normalised with a total mole fraction of 0.9; 10% methane was then added. The full composition consisted of methane and twenty-three heavier hydrocarbons. This created a bimodal distribution with peak MW values of 270 (C20) and 570 (C41) (Figure 3.2). Each new component was associated with an equivalent hydrocarbon number, based on its molecular weight.

The physical properties, such as the critical pressures and temperatures, of each of the twenty-four components were taken from the default single-carbon-number group (SCN) characteristics, as defined in the Schlumberger software, PVTi, (Katz and Firoozabadi, 1978). The Pedersen corresponding states method (Pedersen *et al*., 1987) was used to determine individual component viscosities and their temperature dependence. A Flash-

calculation method was used to calculate the temperature dependence of equilibrium coefficients (K-values). A brief investigation into sensitivity to the K-value method used, by applying both the Wilson method (Wilson, 1968) and the Crookston method with A, B and D coefficients (ECLIPSE Technical Manual, 2010), showed little sensitivity. The Peng-Robinson equation of state was used for the phase equilibrium calculations.

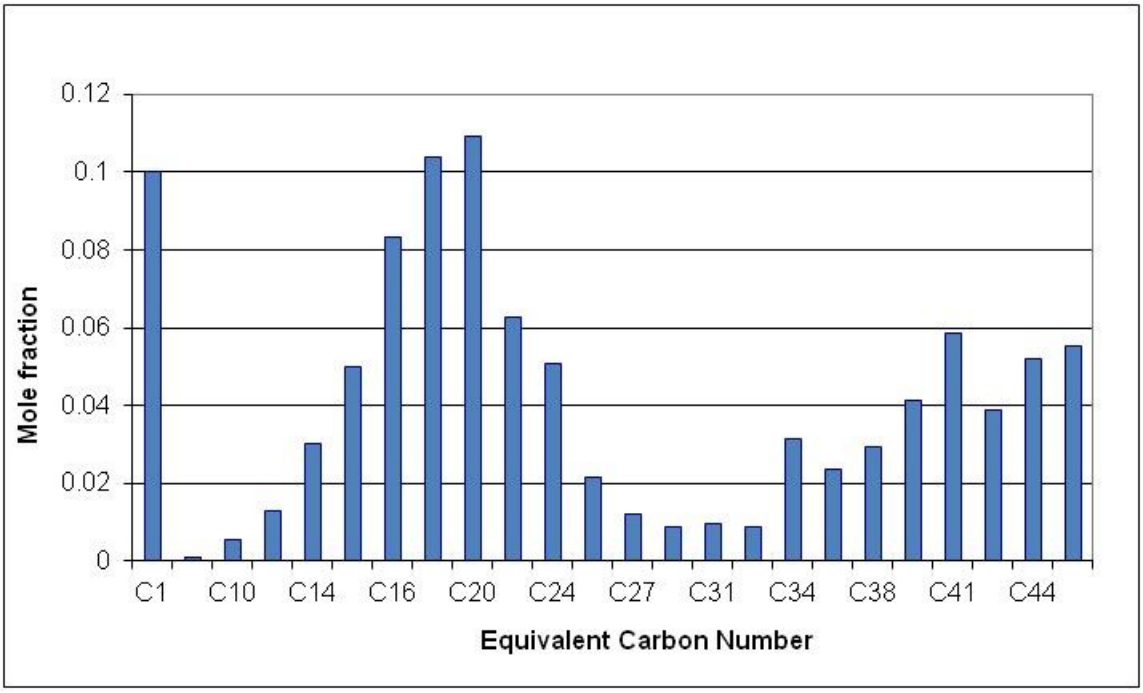


Figure 3.2. 24-Component composition.

3.4.2 Grouping and characterisation

In general, pseudisation of a multi-component system involves two steps: selection of the groups or pseudo-components, and associating physical properties to each group, such as molecular weight (MW), viscosity and K-values.

In this study, the components were grouped based on equality of molecular weights. The pseudo-component mole-weights were calculated as mole-fraction weighted averages of the pure component properties as follows:

$$MW_{pc} = \frac{\sum_{i=1}^{n} MW_i \times x_i}{x_{pc}} \tag{3.1}$$

where MW_{pc} is the molecular weight of the new pseudo-component (including n components), x_{pc} the mole fraction of the new pseudo-component (sum of 'pure' component mole fractions), MW_i the molecular weight of the pure component i, and x_i the mole fraction of pure component i.

The new pseudo-pure-component was then identified with one of the 24-component base case components, based on molecular weight, called the equivalent carbon number in this study. For example, if the molecular weight of the new pseudo-component was calculated to be 150, then new pseudo-component assumed the properties of C11H24 from the Katz-Firoozabadi library (Katz and Firoozabadi, 1978). This new component could be called a 'pseudo-pure' component. This method differed from classical grouping/lumping procedures, in which properties of the pseudo-component are usually taken as the mole-fraction weighted average of the pure components (Joergensen and Stenby, 1995).

The pseudo-component viscosity was calculated separately, using two methods which will provide the key comparison. The first method (method 1) was the simple arithmetic average with mole fraction as the weighting function:

$$\mu_{mix} = \frac{\sum_{i=1}^{n} x_i \mu_i}{\sum_{i=1}^{n} x_i} \tag{3.2}$$

This weighted average viscosity is the default calculation preformed in most PVT packages when components are grouped (PVTi Ref Manual, 2009).

The second method (method 2) is the Arrhenius method (Arrhenius, 1887), discussed in Chapter 2, for calculating mixture viscosities, expressed as follows:

$$\mu_{mix} = \prod_{i=1}^{n} \mu_i^{x_i} \tag{3.3}$$

where μ_{mix} is the mixture dynamic viscosity and μ_i and x_i are the dynamic viscosity and mole fraction of component i.

Figure 3.2 shows the base case composition, and Figure 3.3 to Figure 3.6 show the grouped-component compositions of each of the new cases.

Figure 3.8 shows the phase envelopes of the corresponding fluids, overlain. It can be observed that the binominal distribution was preserved, as well as the phase behaviour at each up the 'upscaling' steps. It was required that each of the groupings was done in such a way that the phase diagram of the new fluid remained very similar to that of the base case, preserving phase-behavior in the reservoir. Figure 3.7 shows the difference in the heavy component viscosities, as calculated by the two different methods.

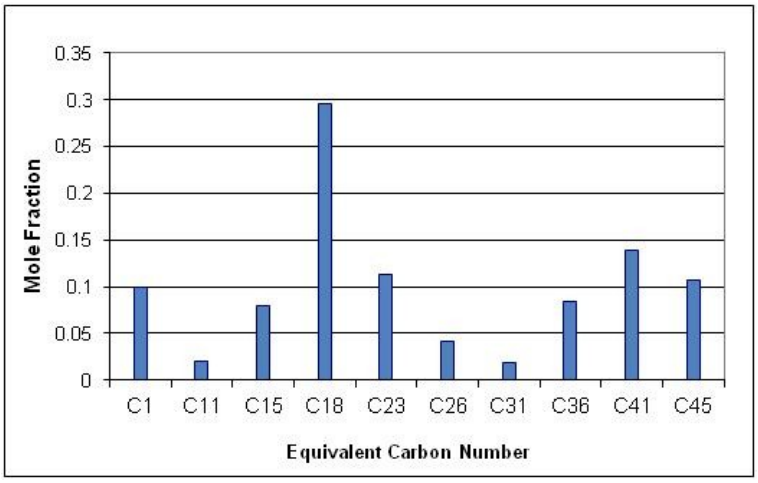


Figure 3.3. 10-Component composition.

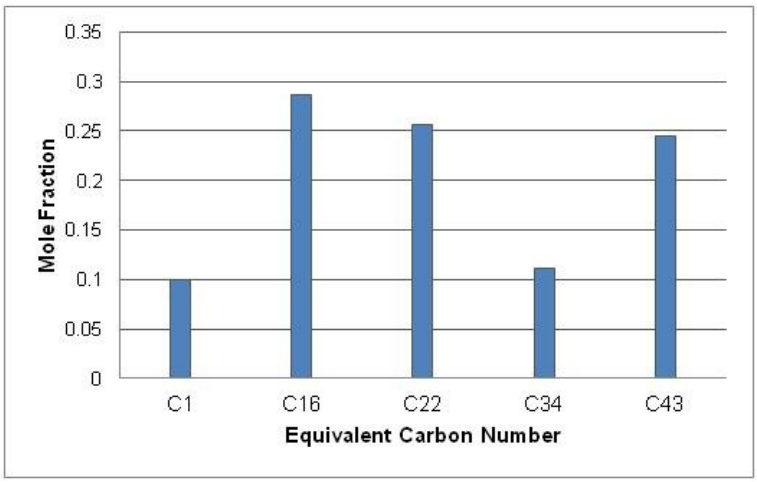


Figure 3.4. 5-Component composition.

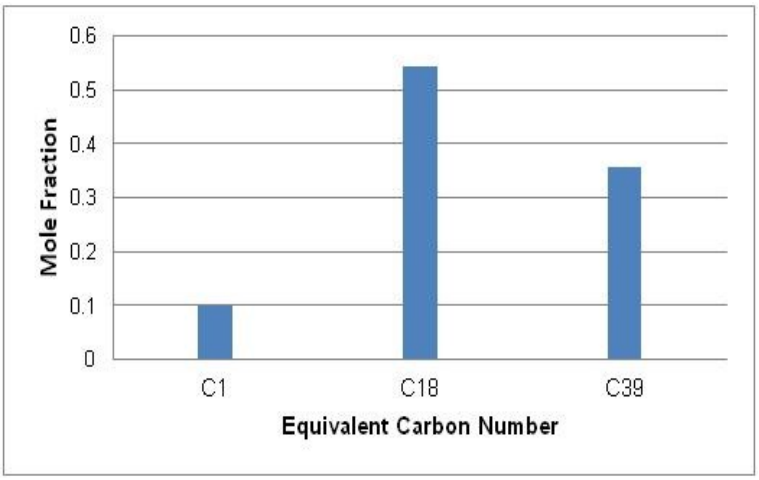


Figure 3.5. 3-Component Composition.

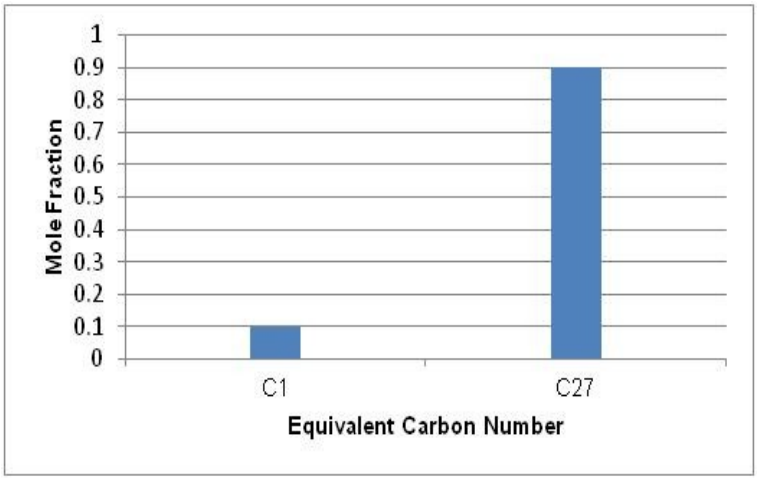


Figure 3.6. 2-Component composition.

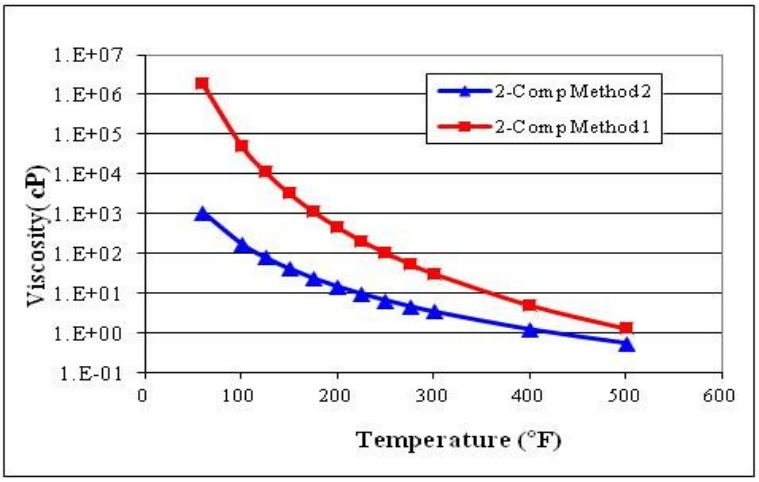


Figure 3.7. Heavy component viscosities of the 2-Comp cases.

(Red: method 1, Blue: method 2).

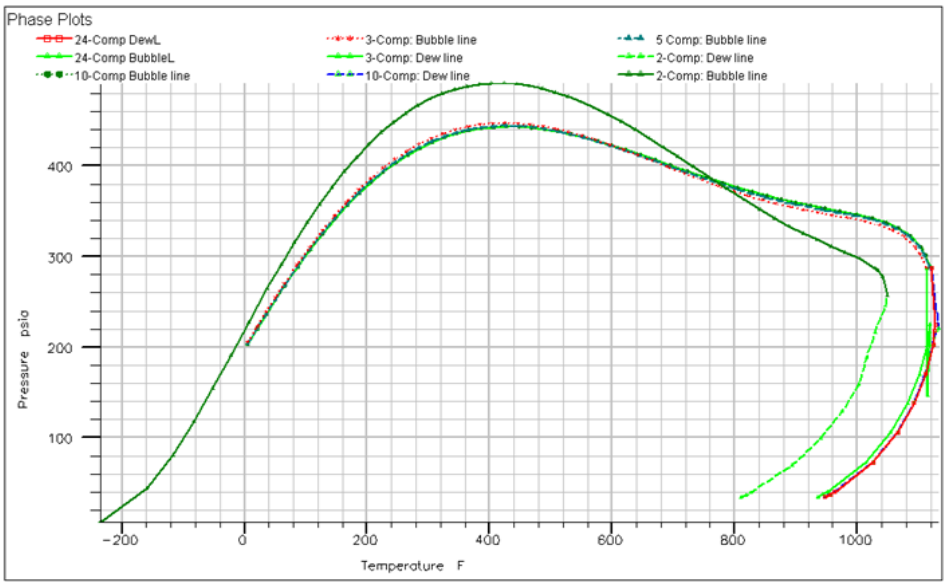


Figure 3.8. Phase diagrams of the different groupings, overlain. 24-component bubble-point line: solid red+squares; 2-component bubble point line: solid green line.

3.5 Simulation Results and Discussion

When heavy oil recovery is thermally enhanced, the intermediate components are distilled from the oil at the steam front, leaving behind a heavier oil. With an increase in temperature, the viscosity of this heavy oil is expected to decrease, enabling production. The main question addressed in this study is whether these physical phenomena are represented when fewer components are used, both in the case of an oil with a bi-modal component distribution, as well as in the case with low occurrence of the intermediates. If not, production results would differ significantly.

Nine different models, with four different groupings of the 24-component base case, and two different sets of pseudo-component viscosities, were simulated and compared. The most determining factor in the fluid behavior was the decrease in viscosity with the temperature increase in the reservoir. The resulting cumulative oil production over a period of five years for each of the cases, from twenty-four components down to three components, is shown in Figure 3.9. The 24-component base case is shown in a black dashed line and it can be observed that most of the grouped-component cases produced

similar results, with small deviations where viscosity method 1 was used. The only case with completely unacceptable results is the 2-component case (solid red line, legend key: 2-Comp Case: Visc method 1) with viscosities calculated with the mole-weighted average, seen on Figure 3.10. The two-component case with the default viscosity calculation, method 1, under-predicts significantly, whilst the two-component case, with Arrhenius-calculated viscosities (green line), slightly over-predicts.

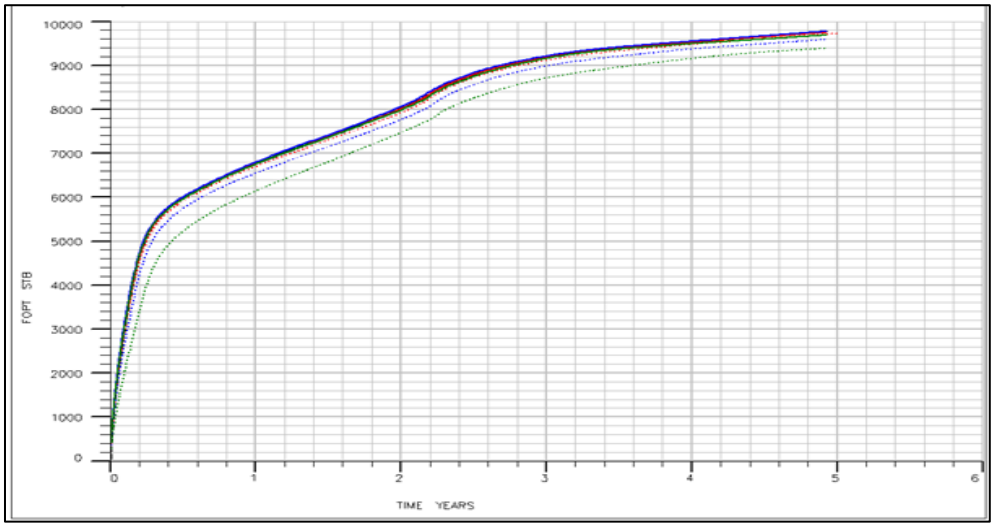


Figure 3.9. Cumulative Production (FOPT) for groupings 10, 5 and 3, over a period of 5 years. (Black-dashed: 24-Comp base case, Dotted lines: method 1, Solid lines: method 2, Red: 10-Comp; Blue: 5-Comp; Green: 3-Comp).

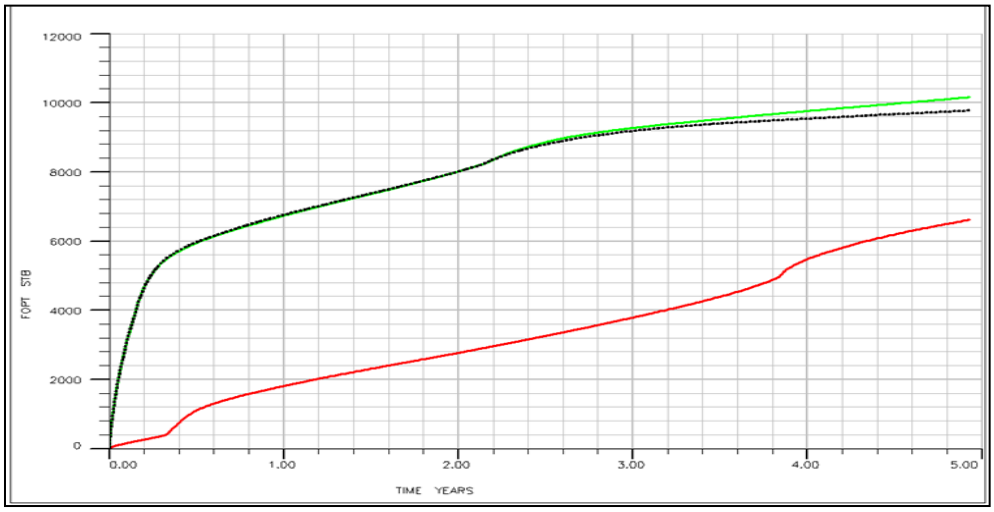


Figure 3.10. FOPT comparison between 24-Comp case (base case) and 2-Comp cases with different viscosity mixing rules (Black: Base case, Green: 2-Comp with method 2 viscosity, Red: 2-Comp case with method 1 viscosity.)

Table 3.1 shows a summary of the results of the study in terms of total cumulative oil (FOPT) and gas (FGPT) produced in each of the simulated cases, with the deviations in FOPT from the 24-component (base) case. It was found that the only case that resulted in a deviation of more than 5% from the base case was the case with two pseudo-components, using the molar-weighted average method to estimate the pseudo-component viscosities. In this case the cumulative oil production was calculated to be 32% lower than that of the 24-component base case. However, it is clearly possible to simulate heavy oil using only two pseudo-components, if the Arrhenius viscosity calculation is used.

In terms of CPU time, the 24-component cases ran in seven hours, while the two-component case with Arrhenius-calculated viscosities ran in thirty minutes on a single processor 2.53 GHz computer with 3 GB RAM.

Table 3.1. Cumulative Field Oil Production (FOPT) and deviation from base case (24-components), per simulation case.

Case	Viscosity Method*	FOPT	FGPT	End Cum Oil-Steam-Ratio	FOPT Deviation
		Mstb	Mscf		%
24 Comp		9.78	550.5	0.54	
10 Comp_1	1	9.71	544.6	0.54	0.66
10 Comp_2	2	9.75	531.9	0.54	0.29
5 Comp_1	1	9.60	534.9	0.53	1.85
5 Comp_2	2	9.78	541.4	0.54	0.02
3 Comp_1	1	9.39	554.3	0.52	3.95
3 Comp_2	2	9.69	543.5	0.54	0.90
2 Comp_1	1	6.61	974.2	0.37	32.35
2 Comp_2	2	10.16	534.3	0.56	-3.91

** 1 = MF-weighted arithmetic average*
2 = Arrhenius equation

3.6 Steam Assited Gravity Drainage (SAGD)

The case above was modified to test the method with a SAGD recovery process. The vertical resolution of the grid was refined to 20 cells of 2.5 ft each, with two horizontal wells completed in layers 14 and 20. The vertical distance between the two wells was 15 ft, with steam injection in the top well at a rate of 20 bls/d CWE, steam quality of 95%, injection temperature of 450°F, and a limiting bottomhole pressure of 1000 psi. The initial reservoir pressure was 400 psi. The bottom well was the oil producer, operated at a limiting liquid rate of 3000 stb/d, a bottomhole pressure of 100 psi, and maximum steam production limit of 300 bls/d CWE. The liquid rate target was set high enough not to become a limiting factor. Steam was circulated through both wells for three months, prior to the start of production. The dead oil viscosity at 60°F was 2,640 cP, as in the case above and five separate cases were run: the 24-component base case, a 10-pseudo-component (PC) case, a 5-, 3- and 2-pseudo-component cases.

The results from the simulations (Figure 3.11 to Figure 3.13), again, indicated that, for the cases ran, with the controls selected, the 2-PC results predictions were within an acceptable error margin, as long as the pseudo-component oil viscosities were determined with the Arrhenius mixing rule, also used in the simulator for the oil phase viscosity. The pseudo-component gas viscosity was calculated with the mole-fraction-weighted arithmetic average, as is done in the simulator for the gas phase.

Figure 3.11 shows the oil viscosity distribution after four months of simulation.

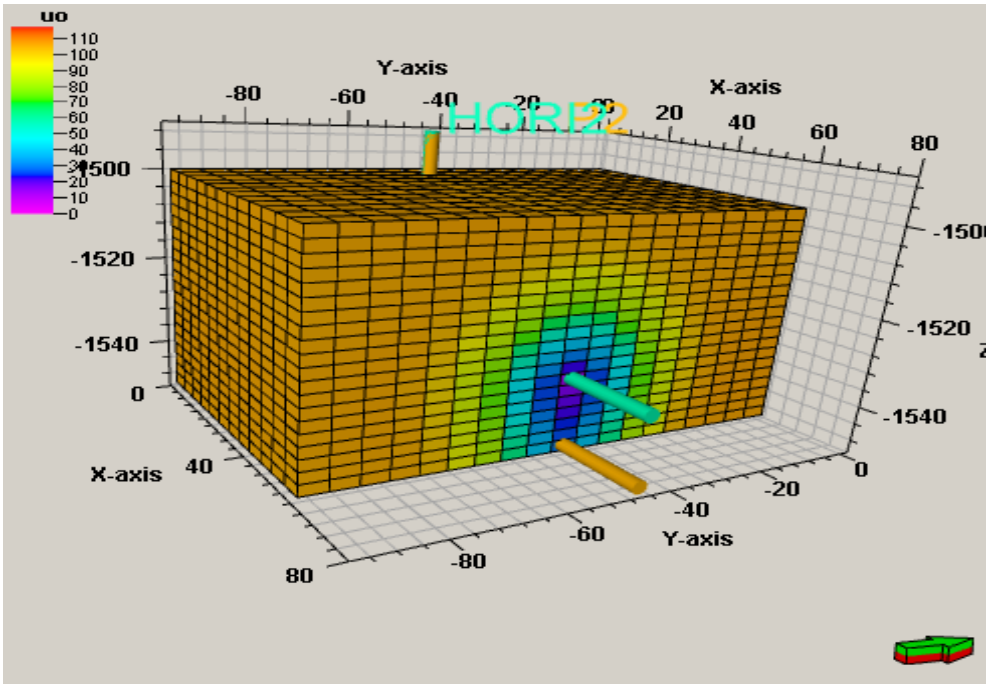


Figure 3.11. Oil viscosity distribution after 4 months.

Figure 3.12 shows virtually no difference in the culumative oil production predition.

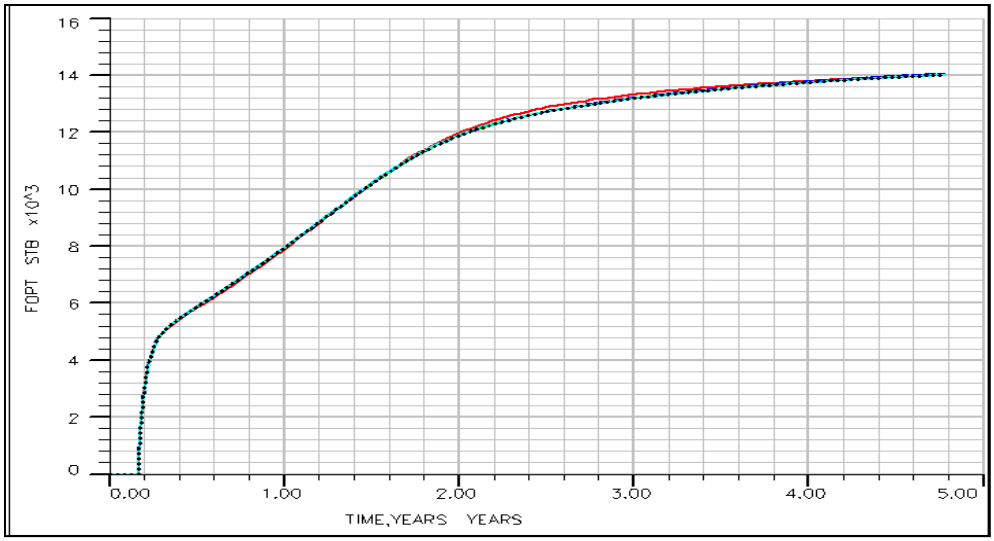


Figure 3.12. Cumulative oil production: 1000 cP oil with SAGD. (24-component base case: black dots; 10-PC: green; 5-PC: dark blue; 3-PC: light blue; 2-PC: red)

The only significant difference is in the GOR (Figure 3.13(2)).

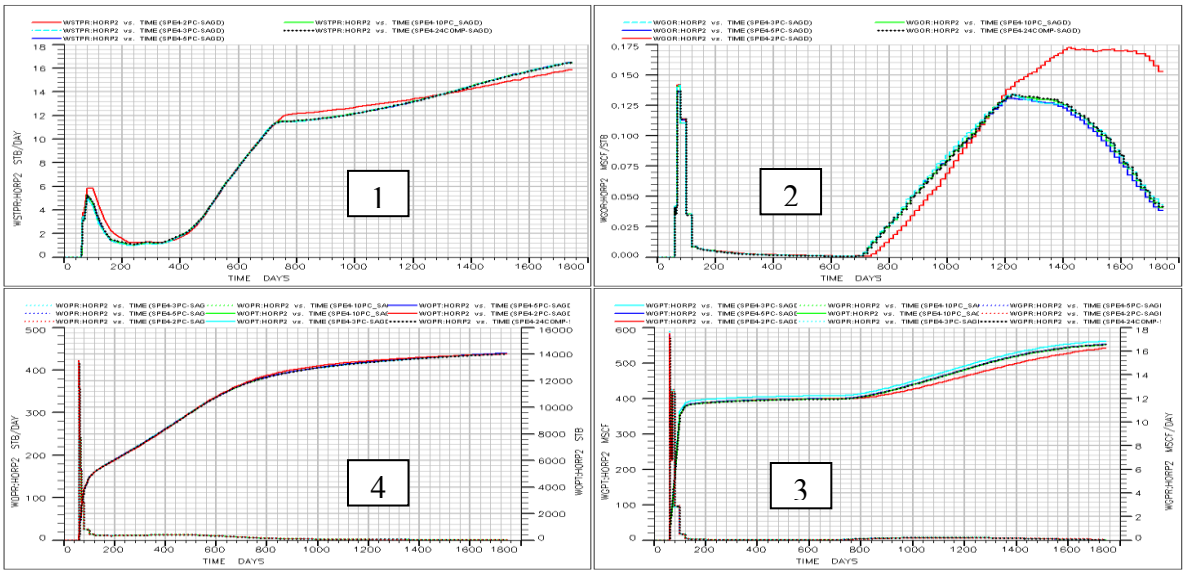


Figure 3.13. Clockwise from top left: (1) well steam production (STB/d CWE), (2) well GOR (MSCF/STB), (3) well gas production rates (MSCF/d) and cumulative gas procution(MSCF), (4) well oil production rates (STB/d) and cumulative oil production (STB). (24-component base case: black dots; 10-PC: green; 5-PC: dark blue; 3-PC: light blue; 2-PC: red).

In order to understand the results, one has to look at the composition of the gas phase in the 24-component case over time. The components of interest would be the lightest component mole fraction in the oil. If, for example, C18, the peak intermediate component at 10%, which, in the 2-PC case is lumped with the oil component, is found in the gas-phase in the 24-component case, the reservoir behaviour would differ. This component molefraction is found in the output as YMF8, since no C2-C6 components are present in the fluid system. As is shown Figure 3.14, the concentration of C18 in the gas phase is close to zero at all times. Even though it momentarily increases at the steam-oil interface, the molefraction in the gas phase is only 0.2% and too low to cause a difference between the 24-component case and the 2-PC case where this component will be lumped in oil phase.

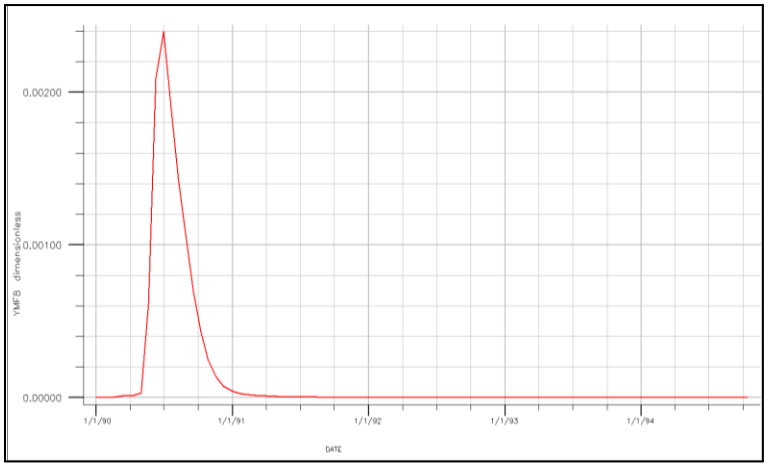


Figure 3.14. Concentration of C18 in the gas-phase over time (24-component case).

3.7 Field Case

The above methods of grouping and characterisation were then applied to a heavy oil of 10°API, described in Pedersen *et al.* (2007). The 30-component case has a fluid composition as shown in Figure 3.15 in blue, on a logarithmic scale (also in Table 3.2). The methane mole percentage is ~19%, the sum of the mole fractions of C2 to C11 is ~4%, and for C12 to C26 is ~38%. The heavy plus fraction content, with a molecular weight of 800, was ~39%. The same method of lumping the pure (SCN) components into pseudo-components had been followed and the pseudo-pure components in each of the cases are shown in Figure 3.15. Characterisation of the pseudo-pure components was performed as before. To ensure flow, the initial reservoir pressure was set to 2000 psia.

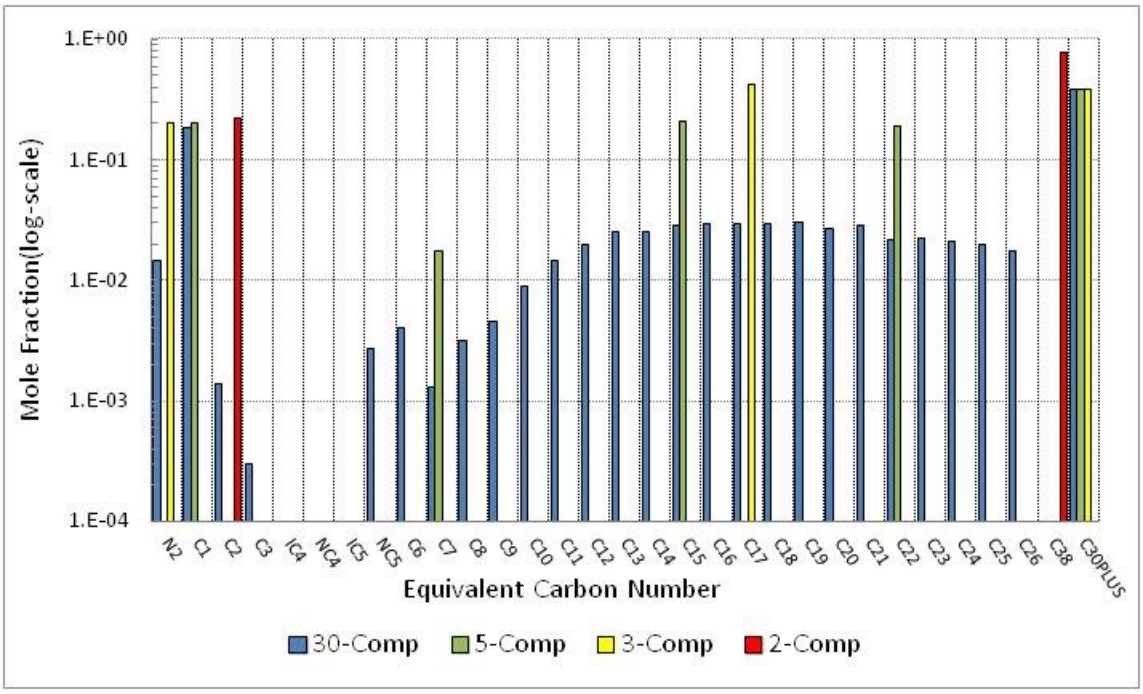


Figure 3.15. Pseudo-component mole-fraction distributions for 10 API oil Base Case (30-Component) with 5-, 3- and 2-Component cases.

In order to obtain the same cumulative oil production over five years in all the cases, two rules proved fundamental: preservation of the phase behaviour for the range of pressure and temperature conditions expected, and using the Arrhenius method in calculating the pseudo-component viscosity. Figure 3.16 shows the comparison of the pressure-temperature phase envelops of the five different fluids. In this figure the bubble-point line of the base case with thirty components is shown in dark green, with the 2-component case bubble-point line in dark blue. The initial reservoir pressure was set to 2000 psi and the temperature to 125°F, with the steam injection temperature set to 450°F. The 2-component case deviates from the base case, but phase behaviour is preserved sufficiently within the encountered reservoir temperature and pressure ranges to ensure acceptable simulation results.

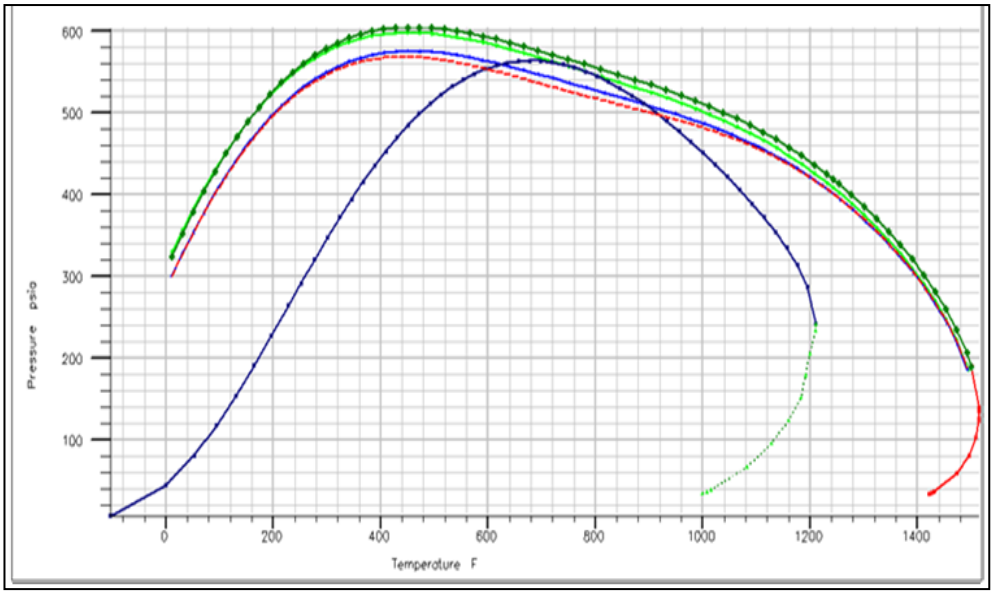


Figure 3.16. Pressure-Temperature phase diagrams for different groupings of 10ºAPI oil (Dark Green: 30-Comp Bubble-point line; Light green: 10-Comp; Light Blue: 5-Comp; Red-dashed: 3-Comp oil, Dark-blue: 2-Comp oil).

The initial 30-component composition, together with resulting equivalent carbon numbers during each lumping phase, is shown in Table 3.2. It can be observed that the methane concentration is higher in this fluid, at 19%; the intermediate components up to C26 have low concentrations and the C30+ fraction with MW of 831, at a high concentration of 38%. In order to obtain the 2-component case, consisting of 22% C2 and 78% C38, all components up to C12 were lumped into the light pseudo-component (C2), and all components above C12 into C38.

Table 3.2. Grouping of 10°API oil into 10, 5, 3 and 2 component cases.

30 Component case					10-Component case				5 Component case				3 Component case				2 Component case			
Cn	MW	Z_i	MF	wt%	Cn	Z_i	MW	wt%	Cn	Z_i	MW	wt%	Cn	Z_i	MW	wt%	Cn	Z_i	wt%	MW
N2	28.013	1.44	0.0144	0.10	N2	0.014	28.01	0.10	C1	0.2016	16.898	0.81	C1	0.2016	16.898	0.81	C2	0.2194	4.1	22.9
C1	16.043	18.72	0.1872	0.71	C1	0.187	16.043	0.71												
C2	30.07	0.14	0.0014	0.010	C4	0.005	57.2	0.06	C7	0.0178	91.30	0.39	C17	0.4191	244.22	24.31				
C3	44.097	0.03	0.0003	0.003																
IC4	58.124	0.01	0.0001	0.001																
NC4	58.124	0.01	0.0001	0.001																
IC5	72.151	0.01	0.0001	0.002																
NC5	72.151	0.27	0.0027	0.05																
C6	84	0.41	0.0041	0.08	C8	0.013	103.5	0.32												
C7	96	0.13	0.0013	0.03																
C8	107	0.32	0.0032	0.08																
C9	121	0.45	0.0045	0.13																
C10	134	0.9	0.009	0.29	C11	0.043	150.7	1.55	C15	0.2111	202.0	10.13								
C11	147	1.45	0.0145	0.51																
C12	161	1.97	0.0197	0.75																
C13	175	2.5	0.025	1.04	C14	0.079	191.0	3.60									C38	0.7806	95.9	532.9
C14	190	2.57	0.0257	1.16																
C15	206	2.86	0.0286	1.40																
C16	222	2.91	0.0291	1.53	C17	0.089	236.8	4.98												
C17	237	2.96	0.0296	1.67																
C18	251	2.99	0.0299	1.78																
C19	263	3.07	0.0307	1.92	C21	0.109	281.9	7.29	C22	0.1902	305.4	13.80								
C20	275	2.72	0.0272	1.78																
C21	291	2.9	0.029	2.00																
C22	305	2.2	0.022	1.59																
C23	318	2.26	0.0226	1.71	C24	0.081	336.9	6.50												
C24	331	2.14	0.0214	1.68																
C25	345	1.96	0.0196	1.61																
C26	359	1.77	0.0177	1.51																
C30PLUS	831.2	37.93	0.3793	74.88	C30+	0.379	831.2	74.88	C30+	0.3793	831.2	74.88	C30+	0.3793	831.2	74.88				

The comparison between the cumulative oil production, as predicted in the different cases, is shown in Figure 3.17, with base case in solid black and the two-component case in red. The deviations in cumulative oil production after five years are shown in Table 3.3. The 10-, 5- and 3-component cases over-predict by 3%, while the 2-component case over-predicts by 1%, all within the 10% error and uncertainty range assumed in most simulation studies. The deviation of the 2-component case at early time (around 200 days) is due to the early arrival of the steam at the nearest well, forcing the well into steam-rate control, instead of BHP control. This can be expected, due to the fact that the steam is 'lumped' with the intermediate components in the gaseous phase during simulation, adding up to a higher volume than in the 30-component case and thus arriving earlier. The well control masks the true, expected behaviour. Many of the intermediate components are either lumped with the

gas-component, or with the heavy oil component. In case of the oil component, they will have a decreasing effect on the oil density and oil viscosity, resulting in higher production rates. In the 30-component case, steam would have a distillation effect on the oil at the steam-front, stripping the oil of these intermediate components. The remaining oil has a high density and high viscosity, and subsequently lower mobility and lower production rates. Depending on the selection of the components to form part of the light pseudo-component, the behaviour of the intermediate components can still be captured in longer term predictions, even though early time deviations may occur.

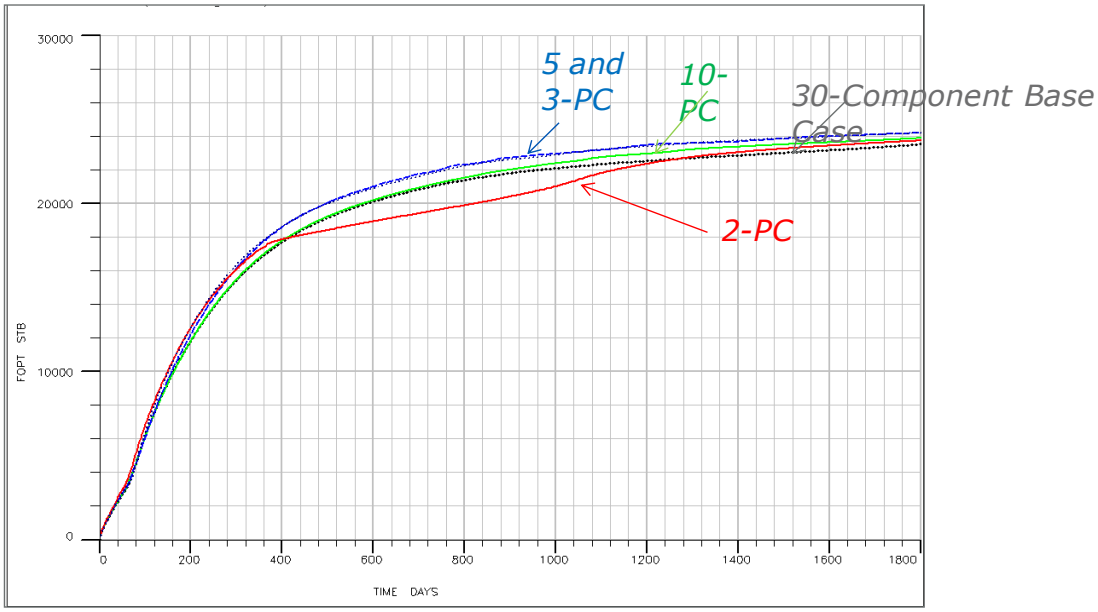


Figure 3.17. Cumulative production for each of the the groupings of the 10°API oil (Black solid: 30-Comp base case, Blue: 10-Comp; Green: 5-Comp; Black dotted: 3-Comp; Red: 2-Comp case).

Table 3.3. 10°API Oil: Cumulative oil production deviations.

Case	Cum Oil Production (STB)	Deviation (%)
30-COMP	2.352E+04	
10-COMP	2.388E+04	1.5
5-COMP	2.419E+04	2.9
3-COMP	2.419E+04	2.9
2-COMP	2.373E+04	0.9

Figure 3.18 to Figure 3.20 show the movement of steam through the reservoir, and the concentrations (mole fractions) of the C1 and C10 components in the vapour phase, at the

steam-front of the 30-component model. Behind the steam-front, hydrocarbon in liquid phase is left behind, consisting of the heavier components only, due to the distillation effect of the steam.

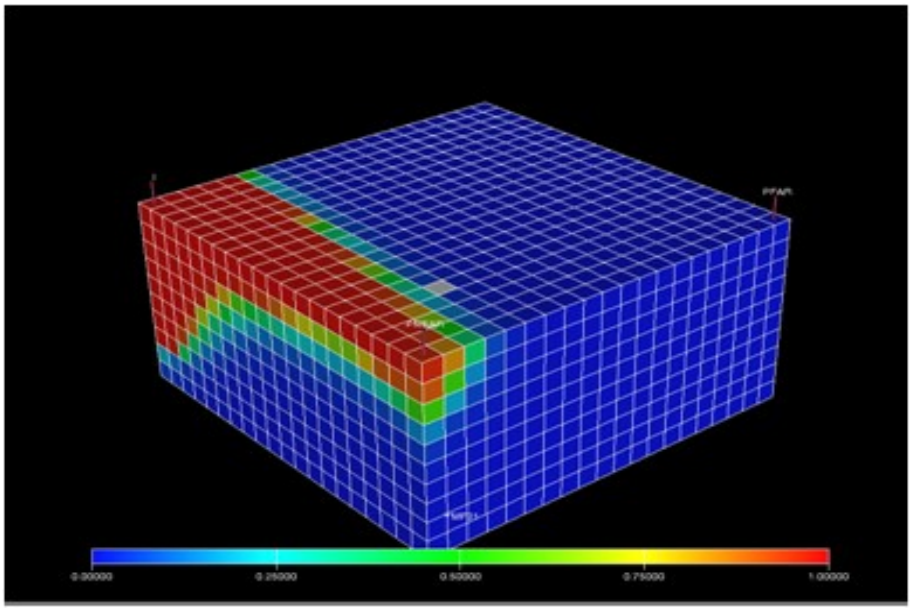


Figure 3.18. 10-API 30-Comp case, water mole fraction in gas phase, *i.e.* steam movement (YMF31) at timestep 20 (~600 days).

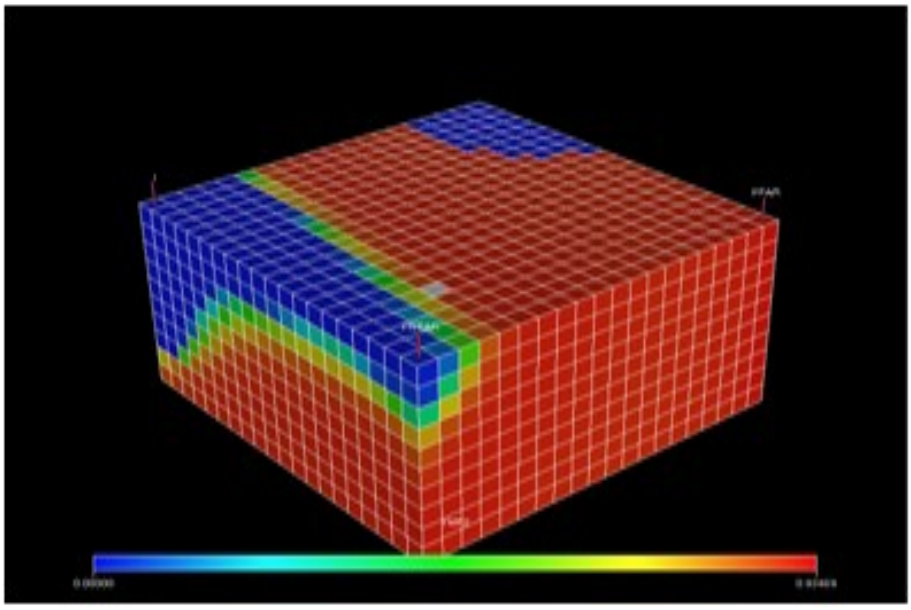


Figure 3.19. 10-API 30 Comp case, mole fraction of Component 2 (C1) in gas phase (YMF2) at timestep 20 (~600 days).

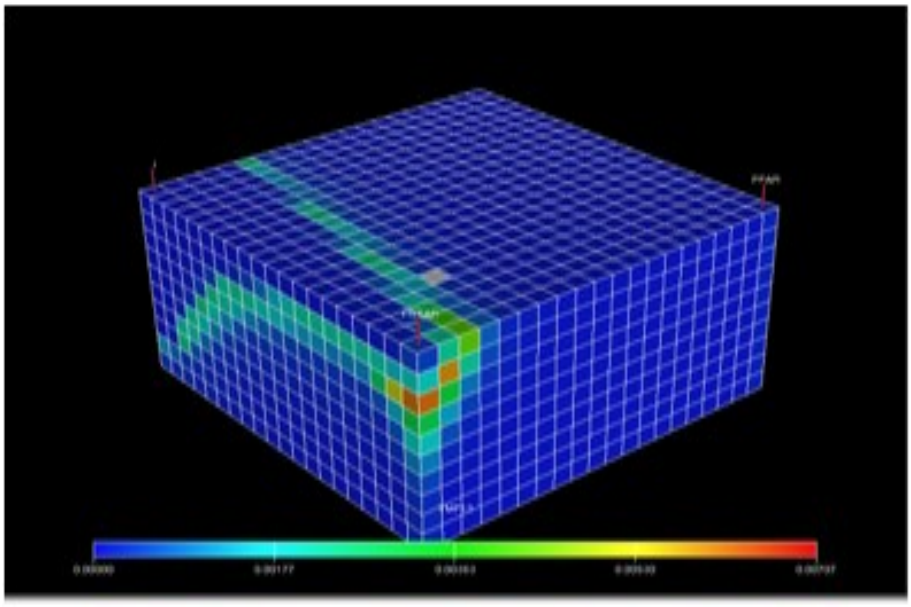


Figure 3.20. 10-API 30 Comp case, mole fraction of Component 13 (C10) in gas phase (YMF13) at timestep 20 (~600 days).

In order to be able to reproduce this behaviour with a two-component model, care has to be taken in the grouping of the components. The intermediate components, up to C12, were grouped with C1 in order to maintain the composition of the vapour in the presence of the steam-front. Figure 3.21 and Figure 3.22 show the steam-front movement in the two-component model, with the concentration of the light HC component in the vapour phase. The combination of C1 with the intermediate components lead to the combined effect as observed in the 30-component case, thus reproducing acceptable prediction results.

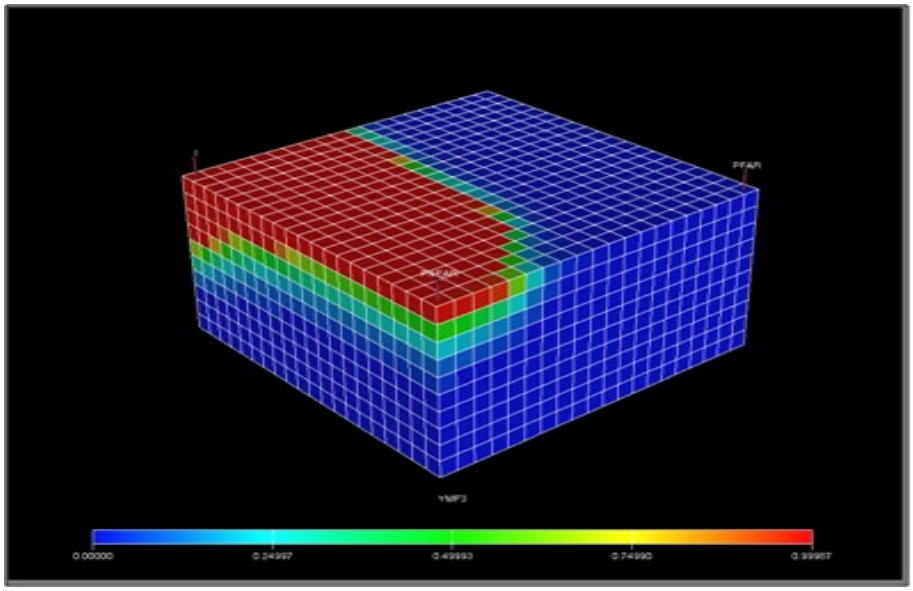


Figure 3.21. 10-API 2 Comp case, steam movement (YMF3 water mole fraction in gas phase) at timestep 20 (~600 days).

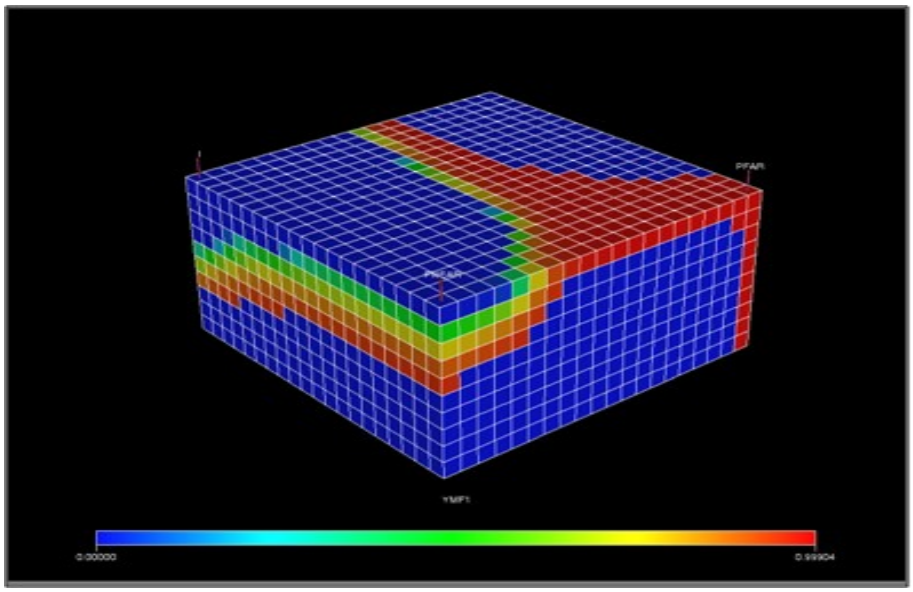


Figure 3.22. 10-API 2 Comp case, mole fraction of Component 1 (C2 pseudo-component) in gas phase (YMF1) at timestep 20 (~600 days).

Although the overall oil production prediction from the 2-component case appears to be accurate, the well-by-well production was different, as can be seen in Figure 3.23. On the left the cumulative production from the well, PNEAR can be seen, and on the right that of well PFAR. The results from the 2-component case are shown in red on both graphs. The fact that the steam arrives early at PNEAR in the 2-component case (Figure 3.24), forces the well to lower production, in order to maintain a constant steam production of 2.5 CWE.

The results is that the steam advance faster through the reservoir towards the second producer, PFAR, lowering the average oil viscosity more rapidly than in the other cases. This explains the higher production volume in the PFAR well. Steam arrival at PNEAR, in the other simulation cases, was more gradual, with no steam yet at PFAR during the simulation period.

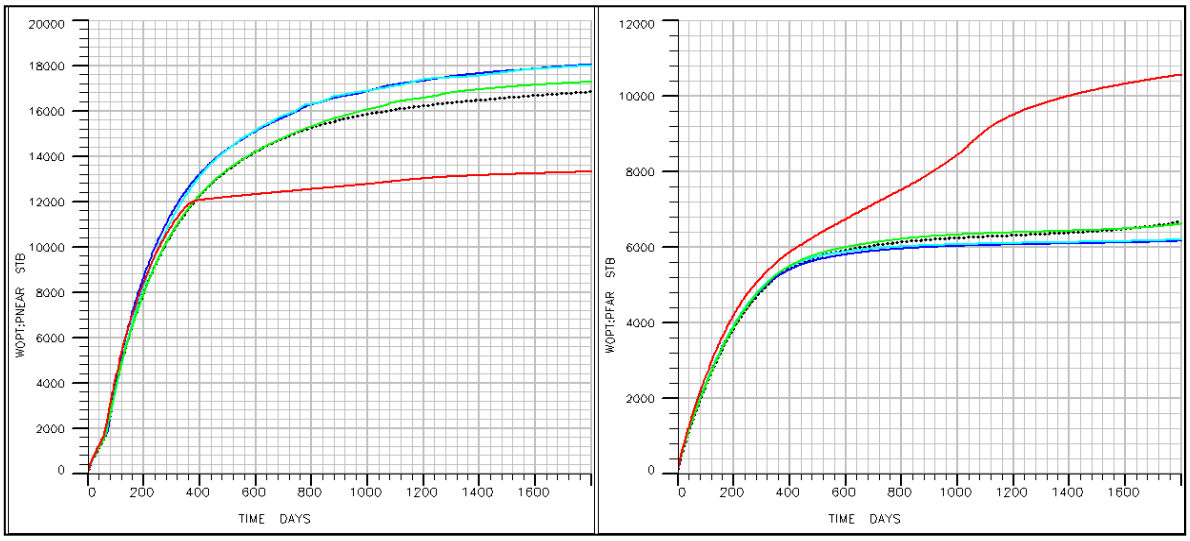


Figure 3.23. Cumulative oil production per well. PNEAR is on the left, with PFAR on the right. (Black dotted: base case, blue: 3- and 5-PC cases, green: 10-PC case and red: 2-PC case)

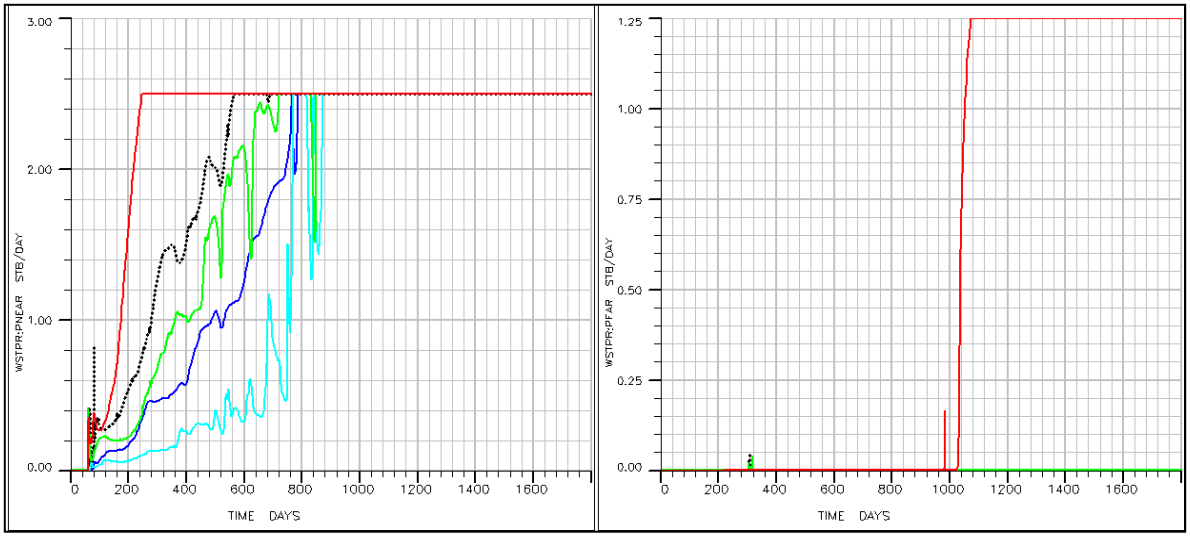


Figure 3.24. Steam production rates per well. PNEAR is on the left, with PFAR on the right. (Black dotted: base case, blue: 3- and 5-PC cases, green: 10-PC case and red: 2-PC case)

In the case of eliminating the interference of PNEAR, it was possible to achieve the same behaviour and results between the 30-component case and the 2-PC case, as is shown in Figure 3.25. In this figure, the black dotted line represents the 30-component base case, while the green and red lines represent 2-PC cases. It is clear that the case shown in green resulted in high inaccuracies, while the case shown in red produces acceptable results. The difference between the two cases is in the calculation of the pseudo-component gas viscosities. Accurate results were only possible if the pseudo-component gas viscosities were calculated using the mole-fraction weighted arithmetic average, and the Arrhenius equation was used for determining the pseudo-component oil viscosities. This is in agreement with the way the gas-phase and the oil-phase viscosities are determined in the simulator during simulation (as a default).

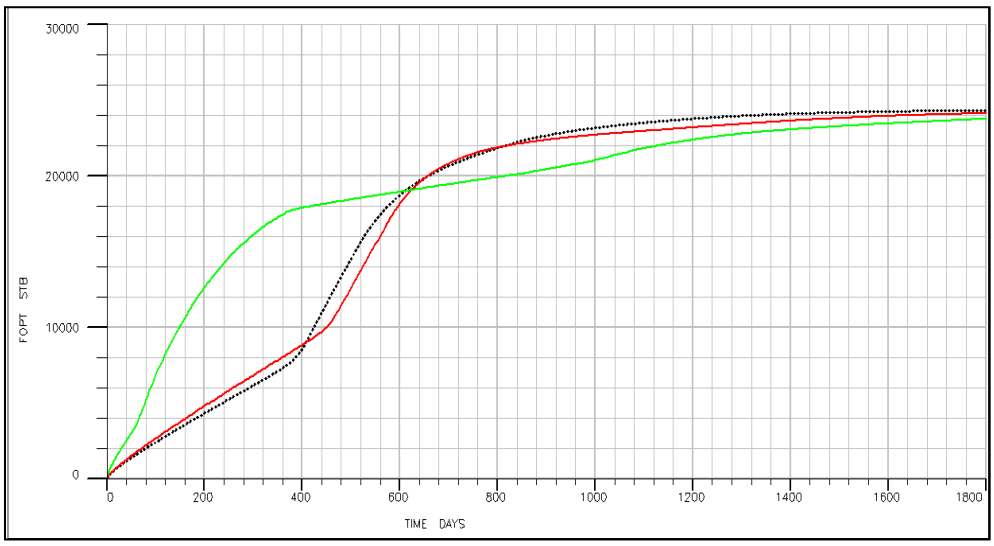


Figure 3.25. Cumulative oil production in PFAR in single production well cases. (Black dotted: 30-component base case, green: 2-PC case with gas viscosities determined with Arrhenius eq., red: 2-PC case with gas-viscosities determined by arithmetic average).

The fact that it is possible to predict field oil recovery of a complex heavy oil, using only two components, when the Arrhenius equation is used for the pseudo-component oil viscosities, and the arithmetic average for the gas viscosities, is an interesting finding. The explanation could be as simple as using the same mixing rule in the pseudoisation as is used in the simulator for calculating the phase viscosity, provided that the grouping is done correctly. However, the explanation is more likely that, in the long term, the effects of the

highly viscous heavy components overshadow those of the intermediate components in steam line drive. This will be investigated further in Chapter 7 after implementation of the Free Volume method in component viscosity modelling. Sensitivity to the recovery method is evaluated in the same chapter.

3.8 Limitations

The initial reservoir pressure has been found to have a profound effect on the results of the 10-API fluid case. If the pressure is set to 200 psia instead of the 2000 psia in the previous case, the 30-component oil recovery could not be matched using two pseudo-components, as grouped above. In this case the oil recovery was highly over-predicted due to the large percentage of the oil in the gas phase. (Figure 3.26).

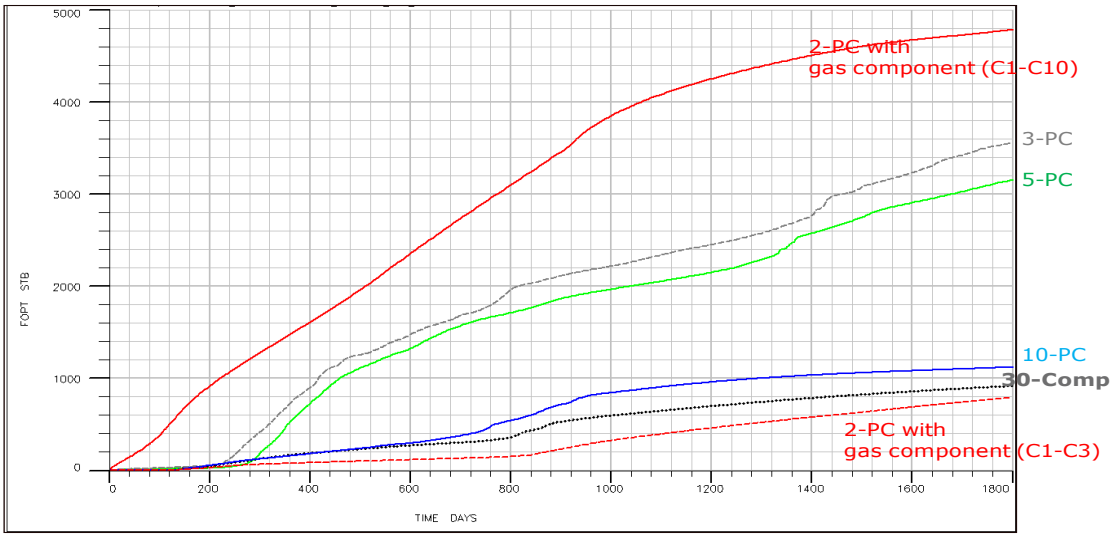


Figure 3.26. 10-API Oil cumulative prediction comparison, with initial reservoir pressure=200 psia.

It can be observed that the 2-PC case with all the light components, up to C10 grouped as one pseudo-component, highly over predicts the oil recovery, while the 2-PC case with N2, C1 and C2 lumped together, under-predicts the recovery, indicating the determining effect the lumping strategy has on the results. In this case, even the 3-PC and 5-PC cases would result in unacceptably large prediction errors. This is due to the fact that simulation starts in the 2-phase region of the phase-diagrams (P = 200 psia, T = 125°F), an area where the phase behaviour had not been matched (Figure 3.27). Figure 3.28 shows, additionally, the

phase diagram of the alternative 2-PC grouping. Although the phase diagram does not match that of the 30-component case, the fact that the initial reservoir conditions are within the 2-phase region, could aid in slightly better predictions than the original grouping.

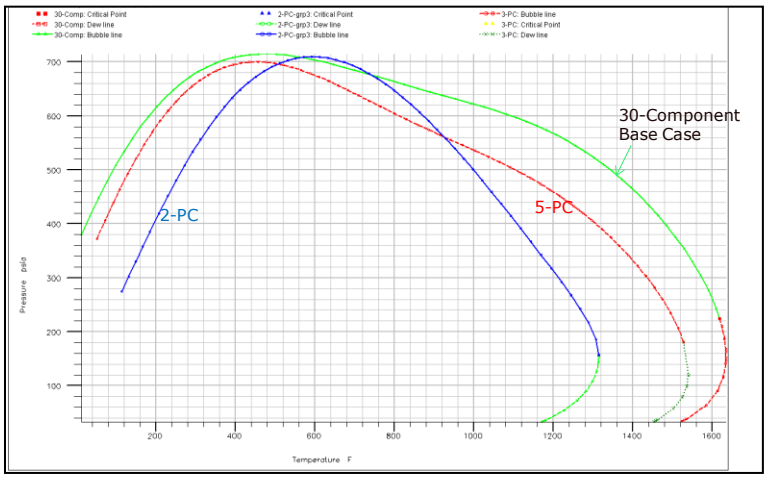


Figure 3.27. Phase diagram of the 30-component case, 5-PC and 2-PC cases.

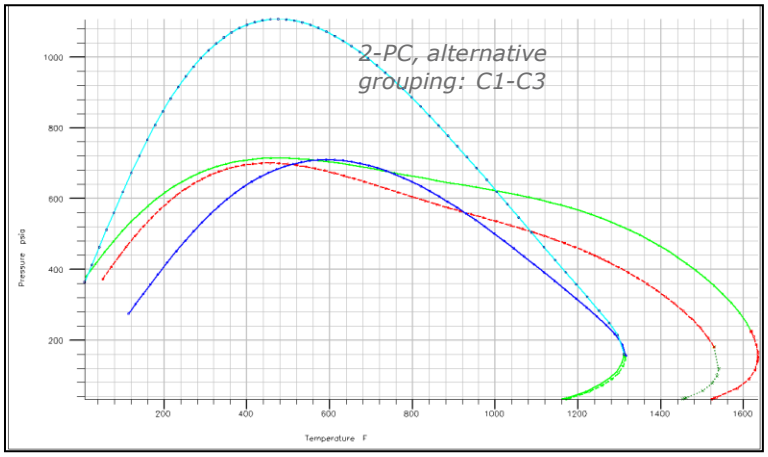


Figure 3.28. Phase diagram of alternative grouping of the 2-PC case.

3.9 Conclusions

In this study, a statistical method was used to generate a composition of multiple pure components with a bimodal distribution, based on SPE4. An ECN method to group and characterise each 'pseudo-pure'-component was used to test the predictions sensitivities to

the number of pseudo-pure components and the mixing method used in calculating the pseudo-pure-component viscosities.

It was found that it is possible to simulate this complex heavy oil using only two components, one gas component and one heavy oil component, and obtain results with less than 5% deviation from the 24-component base case, in some cases. The method used to approximate the viscosity of the heavy pseudo-component was crucial in obtaining accurate results. Incorrectly estimated pseudo-component viscosities resulted in a large error, wherein the cumulative oil production was calculated to be 32% less than that of the 24-component base case. The grouping calculations to create the pseudo-component molecular weights had been outside a PVT package, as explained in detail above, preserving phase behaviour within expected range of reservoir pressures and temperatures. ECN-components were based on the molecular weights. The ECN-component properties (T_c, P_c, *etc*.) are then the Katz-Firoozabadi library values of the 'pseudo-pure' component. Also, the pseudo-component oil viscosity during the grouping process must use the Arrhenius method, if that is the method used during simulation to determine the oil phase viscosity. Pseudo-component gas viscosities, on the other hand, were calculated with a molefraction-weighted arithmetic average, the same as is used for the gas-phase viscosity during simulation.

This process was demonstrated on two very different heavy oils. One was the 20ºAPI, bimodal molecular weight distribution oil from SPE4 and the other was a published, detailed-composition fluid of 10°API. It was also shown that the initial reservoir pressure is a determining factor in the choice in the number of pseudo-components, and that well controls may affect individual well predictions.

It has also been found that care should be taken in cases where intermediate components, such as C2 to C8, exist, and the initial reservoir pressure is below the bubble point pressure of the fluid system. Even a 10-pseudo-component grouping did not deliver acceptable results in this case. Results are thus highly dependent on fluid distribution as well as initial reservoir pressure.

4 Thermal Oil Recovery Sensitivity to Uncertainty in Viscosity, as a Function of Temperature Range

4.1 Introduction

Heavy oil viscosity is in the order of 1000-10,000 cP. However, extra heavy oil and bitumen reservoirs may have viscosities on the order of 5×10^5 cP (Khan *et al*., 1984). Among the questions that arise in modelling heavy oil viscosity are: how sensitive is the oil recovery to the uncertainty in viscosity; does the sensitivity depend on the magnitude of viscosity; what are the ranges of temperatures, if any, where higher accuracy in modelling the viscosity is required? Would the shape of the viscosity-temperature curve at the high end of the viscosity range, *i.e*., where the oil or tar is in near-solid stage, be of any importance during numerical simulation of the sub-surface recovery process? Or would it be sufficient to just accurately model the range where the *in-situ* oil is mobile? For numerical simulation of the subsurface processes only, the only temperature range relevant for the viscosity modelling is the minimum reservoir (initial) reservoir temperature, and the ultimate temperature expected to be reached during any thermal process in which heat is added. Flow in pipes at surface conditions had not been investigated in this study.

In order to answer these questions, firstly, an analytical investigation on the maximum or critical viscosity below which it is possible for oil to flow, as a function of reservoir quality and pressure draw-down, is performed. An effective length is defined to apply to both linear and radial models, together with a dimensionless number to determine the critical viscosity under specific reservoir conditions.

This is followed by an analytical investigation into the production rate sensitivity to viscosity errors at specific temperatures, first in a vertical well situation, which would be applicable to any of the following thermal recovery processes: down-hole heaters, cyclic steam injection, or steam-line drive. The analytical findings were tested with simulation. Since steam assisted gravity drainage (SAGD) is a different process (while still a drive process, it has a dominant gravitational component), and applied in extra-heavy oil

reservoirs with viscosities above 100,000 cP, it was analysed separately, analytically as well as with simulation.

A typical heavy oil–temperature relationship is shown in Figure 4.1, where the oil viscosity is plotted on a logarithmic scale and varies in a log-log fashion with temperature. Typical correlations used in the oil industry such as the Andrade formula, eq. (4.1), Vogel, eq. (4.2), ASTM, eq. (4.3), or a logarithmic formula, eq. (4.4) (Reid *et al*., 1987, ECLIPSE reference manual, 2010), often lack the flexibility to accurately fit all measured viscosity data for the full range of viscosities and temperatures. If the ranges of viscosities and temperatures for accurate fitting could be narrowed down, the influence on simulation recovery predictions could be limited.

$$\ln(\mu_o) = A + B/T \tag{4.1}$$

$$\ln(\mu_o) = A + \frac{B}{T + C} \tag{4.2}$$

$$\log_{10}(\mu_o + A) = BT^{-C} \tag{4.3}$$

$$\log_{10}(\mu_o) = A + B\log_{10}(T) \tag{4.4}$$

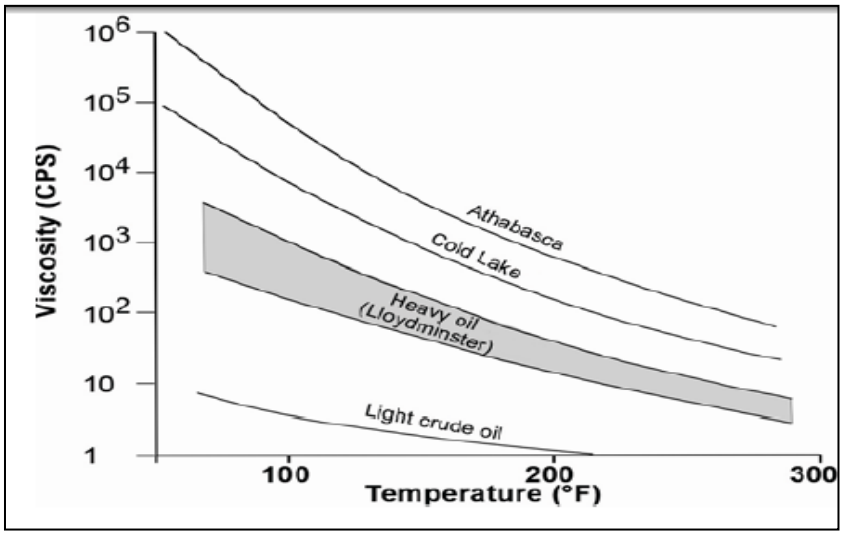


Figure 4.1. Typical heavy oil viscosity *vs*. temperature relationships. (Attanasi and Meyer, 2007)

4.2 Viscosity Ranges for Mobility of Heavy Oil

In order to determine the maximum or "critical" viscosity below which it is possible for oil to flow, as a function of reservoir quality and pressure draw-down, a simple steady-state analysis is first given. As is well known, the flowrate is given by Darcy law,

$$Q = -\frac{KA\Delta P}{\mu L} \tag{4.5}$$

where Q is the flow rate at the low-pressure end, A is the cross-sectional area through which flow occurs, L the flow distance, and ΔP is the total pressure drop, where flow will be in the direction of pressure decline. In radial terms (assuming steady-state flow) the flow velocity, q, is given (Archer and Wall, 1999) by:

$$Q = -\frac{2\pi kH\Delta P}{\mu \ln(r_o / r_w)} \tag{4.6}$$

where r_o is the outer boundary radius, r_w the wellbore radius, and H is the reservoir thickness. As the area normal to flow at the wellbore is $A=2\pi r_w H$, then

$$Q = -\frac{KA\Delta P}{\mu r_w \ln(r_o / r_w)}. \tag{4.7}$$

Setting eq. (4.5) and eq. (4.7) equal to each other, gives the effective length, L_e of the radial system,

$$L_e = r_w \ln(r_o / r_w), \tag{4.8}$$

so that the generalised Darcy's law can be written, for both the linear and radial case, as

$$Q = -\frac{KA\Delta P}{\mu L_e} \tag{4.9}$$

If the minimum flow rate that is acceptable, based on economic considerations, is $Q_{\min}$, then the maximum acceptable isothermal viscosity $\mu_{\max}$ for the reservoir will be

$$\mu_{\max} = -\frac{KA\Delta P}{Q_{\min} L_e}. \tag{4.10}$$

From this equation, it is possible to determine whether oil of a certain viscosity will be sufficiently mobile by inserting the observed reservoir ranges of the permeability, reservoir thickness (perforation height) and maximum pressure drawdown. For the purposes of this work, no-flow is defined as 0.001 bls/d, whereas a minimum flowrate of 1 bls/d was assumed as an acceptable 'mobile flow' rate. The viscosity value at which mobile flow is established, is termed the 'critical' or 'maximum' viscosity. Clearly, from eq. (4.10), it is possible to determine the ultimate critical viscosity, which would be the largest maximum value that could be obtained, by any choice of the other parameters. This would in effect be the highest viscosity value that might ever be of practical interest. This value can be obtained from eq. (4.10) by setting each of the variables to its most extreme limit. Based on ranges found in heavy oil reservoirs (Prats, 2005), one could set the permeability (K) to 10 Darcy, the thickness (H) to 500 ft, the drainage length (r_o) to, say, 50 ft, the maximum pressure drawdown (ΔP) to about 1000 psi, and the wellbore radius (r_w) to 6 inches. The calculation to determine the ultimate viscosity, is shown below.

Parameter	Field units		Metric Units	
r_w	6	inch	0.0254	m
r_o	50	ft	15.24	m
K_{max}	5	Darcy	4.93462E-12	m^2
H_{max}	500	ft	152.4	m
ΔP_{max}	1000	psi	6894757.28	Pa
Q_{min}	1	bls/d	1.84013E-06	m^3/s

Given the parameter values as above, the area A and the effective length L_e would be:

$$A = 2\times\pi\times r_w\times H = 24.322\,\text{m}^2, \text{ and } L_e = r_w\times\ln(r_o/r_w) = 0.1625\,\text{m},$$

which gives μ_{max}=2768 Pa s, or 2.77×10^6 cP, the ultimate critical viscosity in the most extreme case.

However, the likelihood of this combination occurring in reality is low, and if we assume ranges typical of heavy oil reservoirs, such as permeability, K, from 50 mD to 3 D, connection area, A, from 9 ft to 2500 ft^2, effective distance, L_e, from 3 to 2500 ft, and pressure drawdown, ΔP, on the order of 50 to 2000 psi, the calculated critical viscosities are

as shown in Table 4.1. For each parameter, the value applicable to the maximum, or critical viscosity, is shown in bold. The corresponding 'no-flow' viscosity is also given.

Table 4.1. Viscosities for minimum and no-flow: sensitivity to different parameters.

Parameter	Unit	Min	Max	μ_{crit} (cP) at Q=1bls/d	μ_{immob} (cP) at Q=0.001 bls/d
Permeability, K	mD	50	**3000**	700	700,000
Pressure draw-down, ΔP	psi	50	**2000**	2,300	2,300,000
Area, A	ft^2	9	**2500**	5,600	5,600,000
Flow distance, L_e	ft	**3**	2500	7,500	7,500,000

According to these calculations, oil with viscosities of up to 7,500 cP would be mobile under favourable reservoir conditions. Results can also be expressed in terms of a dimensionless quantity, say the H_c-number, where H_c is defined as the ratio between the actual mobility and the critical or maximum mobility for mobile flow:

$$H_c = \frac{K/\mu_{actual}}{K/\mu_{\max}} = \frac{\mu_{\max}}{\mu_{actual}}. \tag{4.11}$$

Oil will be mobile for $H_c \geq 1$, but immobile for $H_c < 1$.

Table 4.2 illustrates the critical viscosities for the two different flow rates at different permeabilities, for a reservoir area to effective length (A/L_e) ratio 1 ft, and a drawdown ΔP, of 200 psi. The second column in shows the viscosities for minimum flow (1 bls/day), and the third column the viscosities at which no-flow will occur. These are the maximum viscosities at which the oil will flow at 'base' conditions of a pressure drawdown of 200 psi and a contact area to distance-of-flow ratio of 1.

Table 4.2. Critical viscosities for different permeabilities and flow rates.

	Critical Oil Viscosity μ (cP)		
K **(mD)**	**Flow at 1 bls/d (mobile flow)**	**Flow at .001 bls/d (defined as no-flow)**	**Estimated API (Beggs, *et al.*, 1975; De Ghetto, *et al.*, 1995)**
50	11	11,270	18
80	18	18,032	17
100	23	22,540	16
180	41	40,572	15
250	56	56,350	14
500	113	112,700	13
800	180	180,320	12
1,000	225	225,400	12
2,000	451	450,800	11
3,000	676	676,200	10

For example, as illustrated in Table 4.2, in order to achieve a 1 bls/d flowrate, a reservoir with a permeability of 3000 mD could have a maximum viscosity of 676 cP (assuming a ΔP of 200 psi and a L_e/A ratio of 1ft). The critical mobility (λ) in this case is 4.44 mD/cP, while a mobility of 4.44×10^{-3} mD/cP would yield the 'non-flow' rate of 0.001 bls/d. If the connection area is 50 ft^2, this translates to the oil at an effective distance of 50 ft from the well flowing at a rate of, at least, 1 bls/d, provided that the maximum viscosity is no higher than 676 cP.

Further sensitivity results are given in Figure 4.2, which shows the critical viscosity ranges for minimum flow (1 bls/d) with variation of pressure draw-down (ΔP), area (A) and effective flow distance (L_e). If the pressure draw-down is increased from 200 psi to 2000 psi, the mobile oil viscosity increases linearly from 225 cP to 2250 cP (blue diamonds). The same applies to an increase in the area of flow: if the connection area increases from 100 ft^2 to 900 ft^2, the mobile oil viscosity increases from 225 cP to 2030 cP. This parameter will affect the selection of grid-block sizes during simulation, as flow is calculated between gridblock centres, but is also related to the perforation or well contact area. It can be observed from this figure that the maximum critical viscosity for the parameter ranges investigated is close to 10,000 cP. Having said this, it has to be understood that each

individual point on the graph represents the critical viscosity at the specific conditions represented by the parameter value on the *X*-axis.

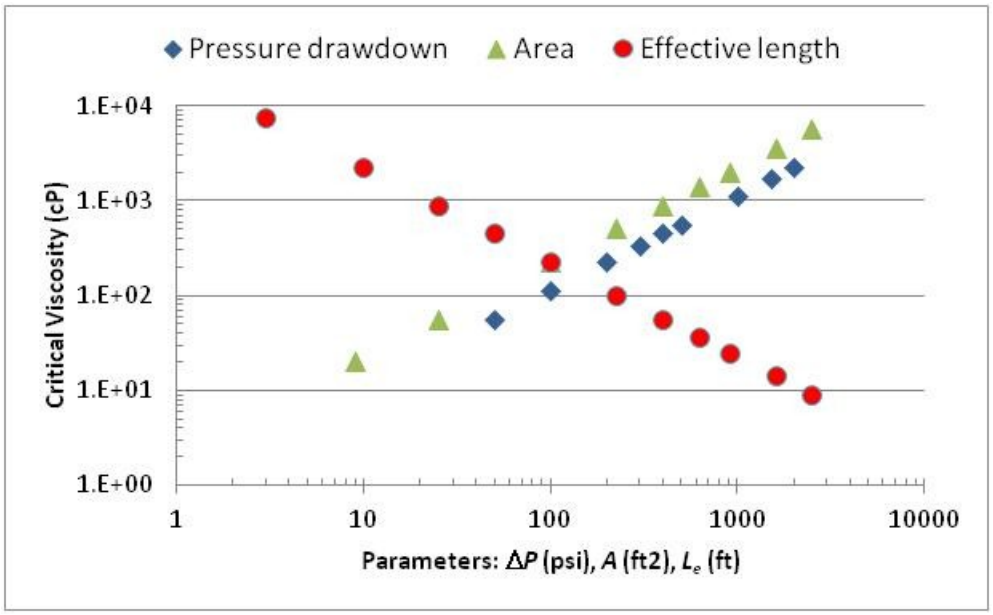


Figure 4.2. μ_{max} *vs* pressure drawdown (ΔP), area (A) and effective distance (L_e).

In conclusion, for the range of parameters used in this study, based on realistic field ranges, mobile oil viscosity is in the order of tens of thousands of cP. In field cases, recovery methods involving many different processes, such as *in-situ* temperature increases, solvent injection, polymer injection, *etc*., are employed to lower oil viscosity to a mobile range, or decrease the unfavourable mobility ratios. For the purpose of accurately modelling the oil rheology during reservoir simulation, it would be adequate to focus on the range of viscosities from, and below 10,000 cP. Clearly, in the case of extra-heavy oil (μ_o>10,000 cP), the path from initial *in-situ* viscosity *vs.* temperature to that of mobile viscosity oil is very steep, and highly dependent on the process used, as well as on the thermal properties of oil, injectives and rock. That modelling is not part of this work.

4.3 Effect of Viscosity Uncertainty as a Function of Temperature on Oil Recovery Predictions

The Schlumberger ECLIPSE Thermal simulator was used to simulate various cases in which errors were introduced in the viscosity-temperature relation to test the well flow-rate sensitivity to viscosity errors. Steam injection, down-hole heating and SAGD were simulated. To understand and support the simulation results, analytically determined sensitivities of oil production rates to the change in oil viscosity, for different production processes, steam-line-drive, cyclic steam injection and SAGD, were performed. The former was done with a simple model based on Darcy's law, in which viscosity was a function of temperature (T), and the latter was carried out with the LINDRAIN model (Butler *et al.,* 1994, 2004).

4.3.1 Vertical producer combined with heater/ cyclic steam injection/steam line drive

4.3.1.1 Analytical Model

In this section, a simple analytical model is developed to gain some insight into the effect of viscosity errors on oil production rates. Darcy's law is used, with oil viscosity a function of temperature, to establish a mathematical equation of the oil rate sensitivity to the oil viscosity at temperature T. The following situation is assumed in a linear 2D reservoir: the area around a well has been heated up and a temperature gradient in the reservoir exists, as can be seen in Figure 4.3, high at the producer, low at a distance L from the well. The producer is at a temperature T_w and pressure P_w, whereas at some boundary (L) in the reservoir, the oil is at initial temperature T_R, and the pressure is at the initial condition P_R.

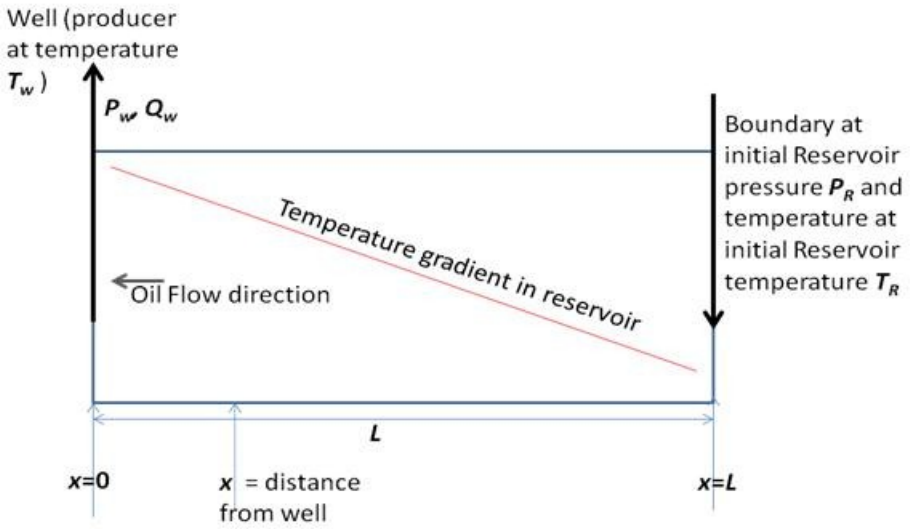


Figure 4.3. Linear-2D reservoir model.

At some distance, x, from the well, the temperature will be

$$T(x) = T_w - \frac{(T_R - T_w)x}{L}. \tag{4.12}$$

And the oil viscosity at x is given by

$$\mu = \mu(T) = \mu(x), \tag{4.13}$$

so that, according to Darcy's law,

$$\frac{dP}{dx} = \frac{q\mu(x)}{K} \tag{4.14}$$

where $q=Q/A$, in m/s. Taking the integral on both sides shows that the flux, q, depends on the average oil viscosity over the whole length L:

$$\int_0^L \frac{dP}{dx}dx = \int_0^L \frac{q\mu(x)}{K}dx \ , \tag{4.16}$$

$$\Delta P = \frac{qL}{K}\cdot\frac{1}{L}\int_0^L \mu(x)dx = \frac{qL}{K}\bar{\mu}, \tag{4.17}$$

where $\bar{\mu}$ is the spatially-averaged viscosity in the reservoir. Hence,

$$q = \frac{K\Delta P}{L\bar{\mu}} \ . \tag{4.18}$$

If it is assumed that

$$\ln \mu = a - bT \,, \tag{4.19}$$

which is a reasonable first-order model for the variation of viscosity with temperature, then

$$\mu = \mu_0 e^{-T/\hat{T}} \,, \tag{4.20}$$

where μ_0 and $\hat{T}$ are some reference viscosity and temperature, respectively, then the average viscosity in the area of interest would be

$$\bar{\mu} = \frac{1}{L}\int_0^L \mu_0 e^{-T(x)/\hat{T}}\, dx \,. \tag{4.21}$$

Then from eq. (4.12),

$$\bar{\mu} = \frac{\mu_0}{L}\int_0^L e^{-T_w/\hat{T}} . e^{-\frac{x}{L}\left(\frac{T_R - T_w}{\hat{T}}\right)} dx \,. \tag{4.22}$$

If new variables are temporarily defined as $\beta = (T_R - T_w)/\hat{T}$, and $s=x/L$ with $dx=Lds$, then

$$\bar{\mu} = \mu_0 e^{-T_w/\hat{T}} \int_0^1 e^{-\beta s} ds = \mu_0 e^{-T_w/\hat{T}} \left[\frac{-e^{-\beta s}}{\beta}\right]_0^1 = \mu_0 e^{-T_w/\hat{T}}\, \frac{(1-e^{-\beta})}{\beta} \,. \tag{4.23}$$

Replacing β and s with the original values, then, with some manipulation, it is found that

$$\bar{\mu} = \frac{\hat{T}}{T_R - T_w}(\mu_w(T_w) - \mu_R(T_R)) \,. \tag{4.24}$$

The rate, eq. (4.18), finally becomes a function of the endpoint viscosities only:

$$q = \frac{-K\Delta P \Delta T}{L\hat{T}(\mu_R - \mu_w)} \tag{4.25}$$

This expression can be used to find the sensitivities of the flowrate to the two endpoint viscosities. Using the chain rule, the derivative of the flowrate *vs*. viscosity, at any viscosity, μ, is given by

$$\frac{dq}{d\mu} = \frac{d\left(\dfrac{-K\Delta P \Delta T}{\hat{L}T(\mu - \mu_w)}\right)}{d\mu} = \frac{-K\Delta P \Delta T}{\hat{L}T}(\mu - \mu_w)^{-2} \cdot 1 \tag{4.26}$$

The sensitivity S of the fractional flow rate with respect to fractional changes in viscosity is given by

$$S = \frac{(\delta q / q)}{(\delta \mu / \mu)} = \frac{\mu}{q}\frac{\delta q}{\delta \mu}. \tag{4.27}$$

Inserting the derivative equation (eq. (4.26)) into the rate equation (eq. (4.25)), the equation for the rate sensitivity with respect to errors in the viscosity at the low reservoir temperature, T_R, becomes, with $\mu(T_R) = \mu_R$:

$$S = \frac{\mu_R}{q}\frac{dq}{d\mu_R} = \mu_R \times \left[\frac{K\Delta P\Delta T}{L\hat{T}}(\mu_R - \mu_w)^{-2}\right] \times \left[\frac{-L\hat{T}(\mu_R - \mu_w)}{K\Delta P\Delta T}\right] \tag{4.28}$$

Resulting in

$$S = \frac{\mu_R}{q}\frac{dq}{d\mu_R} = -\frac{\mu_R}{\mu_R - \mu_w} \tag{4.29}$$

On the other hand, for an error in the viscosity at the high well temperature, $\mu(T_w) = \mu_w$, the sensitivity S will be

$$S = \frac{\mu_w}{\mu_R - \mu_w} \tag{4.30}$$

In the cases of recovery processes, cyclic steam injection (huff-n-puff) and a downhole heater, the cold reservoir viscosity at the boundary is much higher than the viscosities in the heated well region, *i.e.,* $\mu_R >> \mu_w$. So, if the viscosity error is at the low temperature end, (T_R or μ_R), eq. (4.29) shows that $S \rightarrow$ -1 , and the error in flowrate will be equal in magnitude to the viscosity error, but in an opposite direction.

On the other hand, for errors at the high temperature end of the viscosity curve (T_w or μ_w), eq. (4.30) shows that there will be a negligibly small error in flowrate, since $S \rightarrow 0$ as $\mu_w/\mu_R \rightarrow 0$.

This shows clearly that the flow rate at the well is highly sensitive to the viscosity at the initial reservoir temperatures in heavy oil reservoirs, while much less sensitive to the viscosity at high temperatures. The question then arises as to whether this finding applies to all recovery processes used in heavy oil reservoirs.

In production scenarios where the steam is injected a distance L away from the producer, the viscosity at the injector temperature, T_R, will be much lower than the viscosity at the cold producer, *i.e.,* $\mu_R << \mu_w$. In this case, for a viscosity error at low temperatures (μ_w), the error in the predicted flowrate will be of the same magnitude, but opposite sign, since $S \rightarrow -1$. If the error in viscosity is at the high temperature, T_R, the error in the predicted flowrate will be relatively small, since in this case $|S| << 1$.

This supports the previous finding: the recovery prediction is most sensitive to a viscosity error at cold temperatures for line-drive, cyclic steam injection and heater recovery processes.

4.3.1.2 Numerical Simulation

Thermal simulation with the ECLIPSE simulator was used to test the findings of the simple analytical model. The main objective was to determine the viscosity or temperature at which any error has negligible influence on production predictions and recovery factors: would this be in the high viscosity range at low temperatures, or the low viscosity range at high temperatures, or would errors at both ends have equal effects? The analysis starts off with a linear two-dimensional model, heated by a down-hole heater, and builds up to a ten-layered heterogeneous steam-injection model.

4.3.1.2.1 Linear 2-Dimensional Model with Heater

This was done first with a very simple two-dimensional, linear reservoir simulation case. The reservoir of 500×50×50 ft (grid: 13×1×1) was filled 100% with dead oil, with no relative permeability or capillary pressure effects or phase changes, and a producer located in the first cell. Production was controlled by rate, and minimum bottomhole pressure of 20 psi, with the rate target of 500 stb/d, and minimum rate of 1 stb/d. Oil viscosity as a function of temperature was provided via a lookup table. Five separate cases were simulated: a base case, plus four cases where errors were introduced in the viscosities at discreet temperatures: 125, 250, 350 and 500°F, as shown in Table 4.3. In each case, the viscosity at the temperature specified is twice that of the base case. The simulator interpolates linearly between the specified temperatures, which results in further, smaller errors at temperatures around the point where the viscosity is assumed to be imprecisely known.

Table 4.3. Oil viscosities per simulation case with errors introduced at discrete points: *T*=125, 250, 350 and 500°F, shown in red.

Temp (°F)	Viscosity (cP)				
	Base Case	VT125	VT250	VT350	VT500
75	57,800	57,800	57,800	57,800	57,800
80	37,408	37,408	37,408	37,408	37,408
85	28,056	28,056	28,056	28,056	28,056
90	18,704	18,704	18,704	18,704	18,704
95	15,000	15,000	15,000	15,000	15,000
100	11,040	11,040	11,040	11,040	11,040
105	8,678	8,678	8,678	8,678	8,678
110	7,439	7,439	7,439	7,439	7,439
120	6,198	6,198	6,198	6,198	6,198
125	4,959	**9,918**	4,959	4,959	4,959
130	3,719	3,719	3,719	3,719	3,719
135	2,479	2,479	2,479	2,479	2,479
140	1,239	1,239	1,239	1,239	1,239
150	1,122	1,122	1,122	1,122	1,122
200	165	165	165	165	165
250	43.5	43.5	**87**	43.5	43.5
300	12.8	12.8	12.8	12.8	12.8
350	5.2	5.2	5.2	**10.4**	5.2
500	1.65	1.65	1.65	1.65	**3.3**

The reservoir temperature was set at 125°F, and the initial reservoir pressure at 525 psi. In the first instance, the heater was placed in the producer, transmitting heat for one year prior to production, at a rate ensuring the reservoir temperature reached temperatures above 300°F. Figure 4.4 shows the base case temperature and oil viscosity (VOIL, in cP) in the reservoir at the end of the simulation period. On the left is an areal view of the reservoir (*X-Y*) and on the right a cross-section through the reservoir at the position of the well (*X-Z* direction).

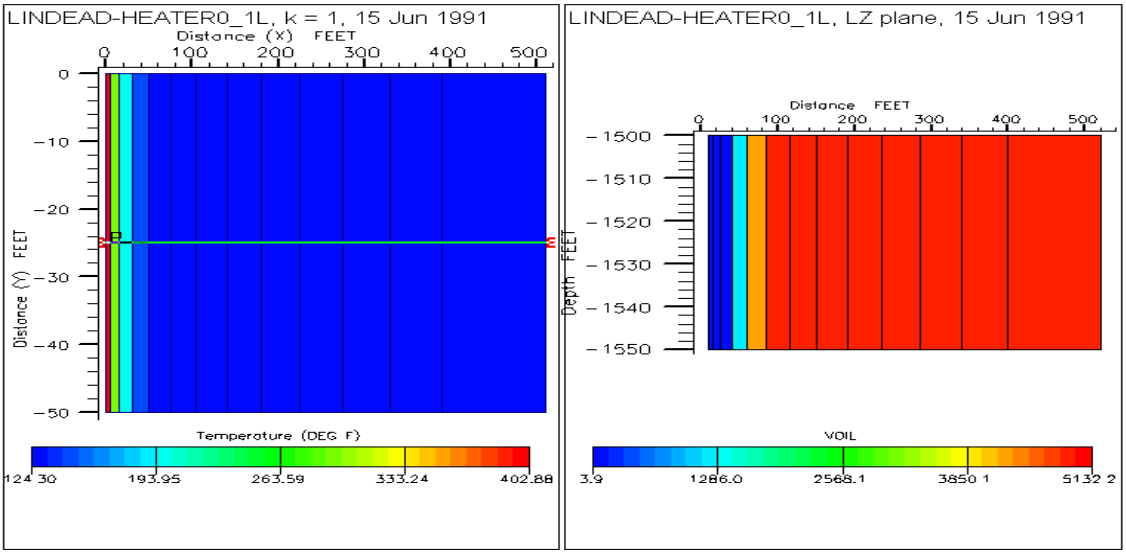


Figure 4.4. (left) Areal view of base case temperature (°F). (right) cross-sectional view of oil viscosity (cP), at the end of the simulation period.

This experimental case clearly showed that viscosity errors at cold end of the temperature range have the greatest effect on the recovery prediction, as shown in Figure 4.5, where the cumulative oil production of the five cases are compared. The base case recovery is shown as black dots, indicating a recovery of 440 stb over 1.45 years. The cases with the viscosity error at temperatures 250°F and above show the exact same recovery, but the case, VT125, with the viscosity error at the reservoir temperature of 125°F, shows a recovery of 380 stb at the same point in time, and a total recovery of 407 STB after 1.52 years, a deviation of 9% in the recovery after 1.52 years. The deviation at 1.45 years is 15%, with a maximum deviation at 1.18 years of 19.4%. All three other cases had 0% deviation at the end of the simulation, with a maximum of 1.1% deviation in the case of the error at 350°F at early times.

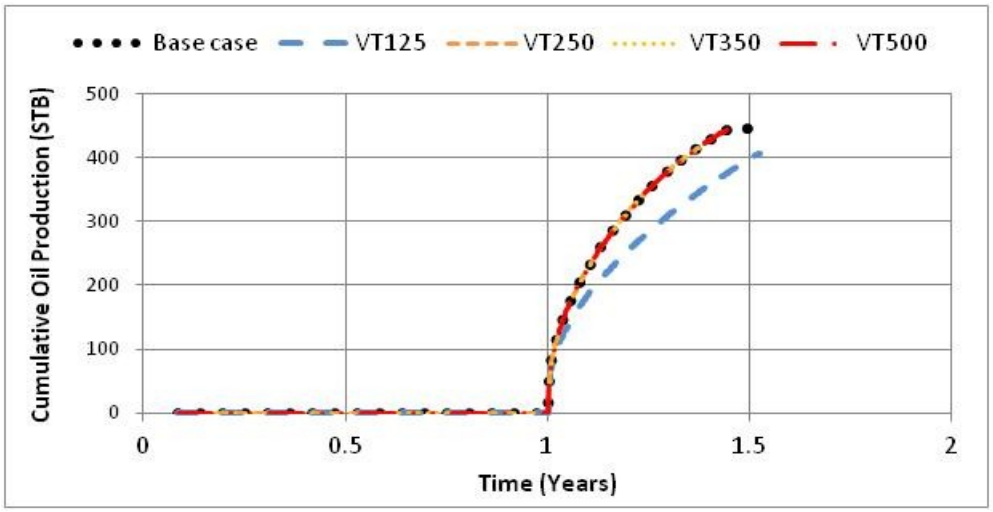


Figure 4.5. Linear dead oil model with heater in producer: cumulative oil production per case.

In order to understand this behaviour on a more detailed level, the temperature and viscosity distributions in the reservoir for the different cases were compared. In each of Figure 4.6 to Figure 4.9, the temperature, viscosity and flow-rate, as a function of distance from the well, for each of the sensitivity cases, are shown at a time t = 367 days after the heating started, and after 1 day of production. In each graph, flow-rate is shown in red, with oil viscosity in green and temperature in blue, where the flow rate is the rate in the positive direction, ie. negative in the direction of the well. It is very clear that the main differences in reservoir behaviour are associated with case VT125 (Figure 4.7), where the flowrate per gridcell (red line) is less than the other cases, for the full distance, 0 to 450 ft away from the production well, where the production well is at x = 0 ft.

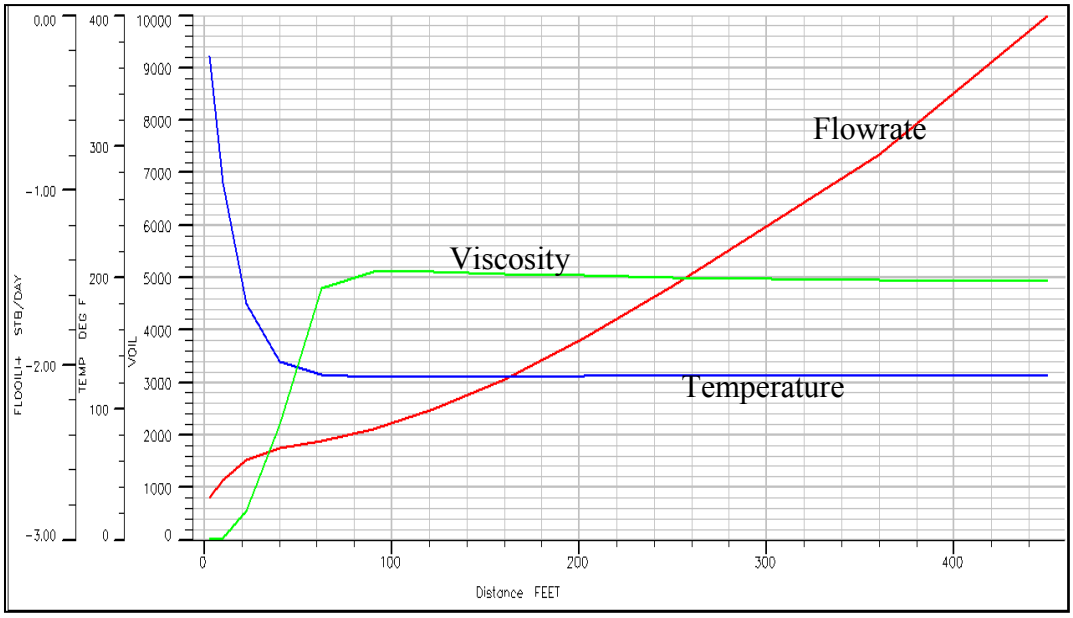


Figure 4.6. Base case (heat-source at producer): flow (red) *vs X*-distance from producer, with oil viscosity (green) 42 days after production started (*t* = 1.12 years). Temperature shown in blue.

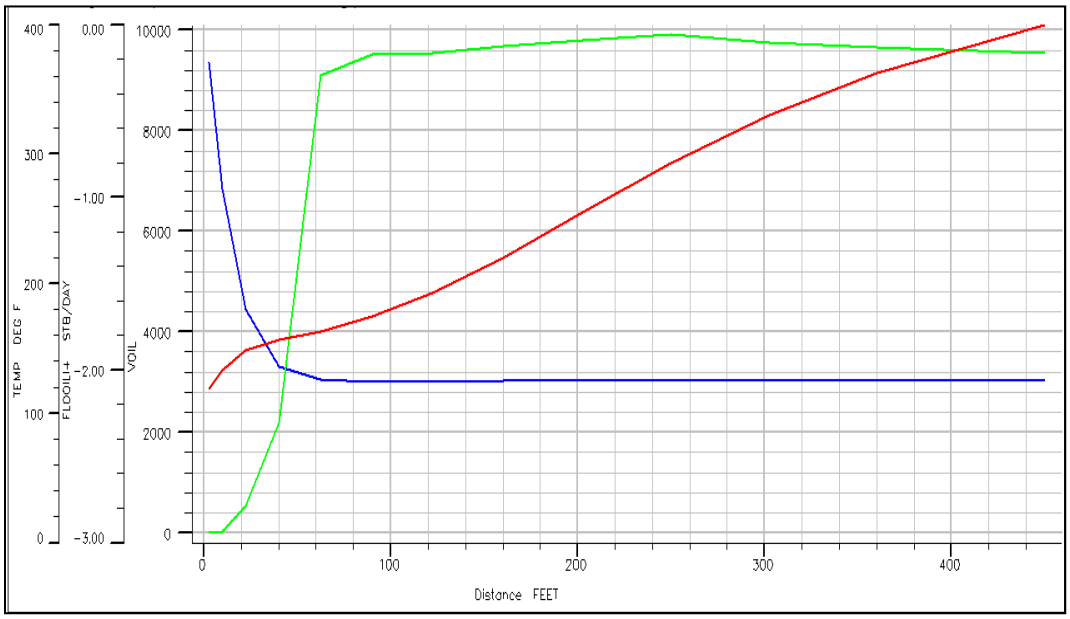


Figure 4.7. Case VT125 (heat-source at producer, oil viscosity at *T*=125°F twice that of base case): flowrate (red), temperature (blue) and oil viscosity (green) profiles in reservoir at *t* = 1.12 years.

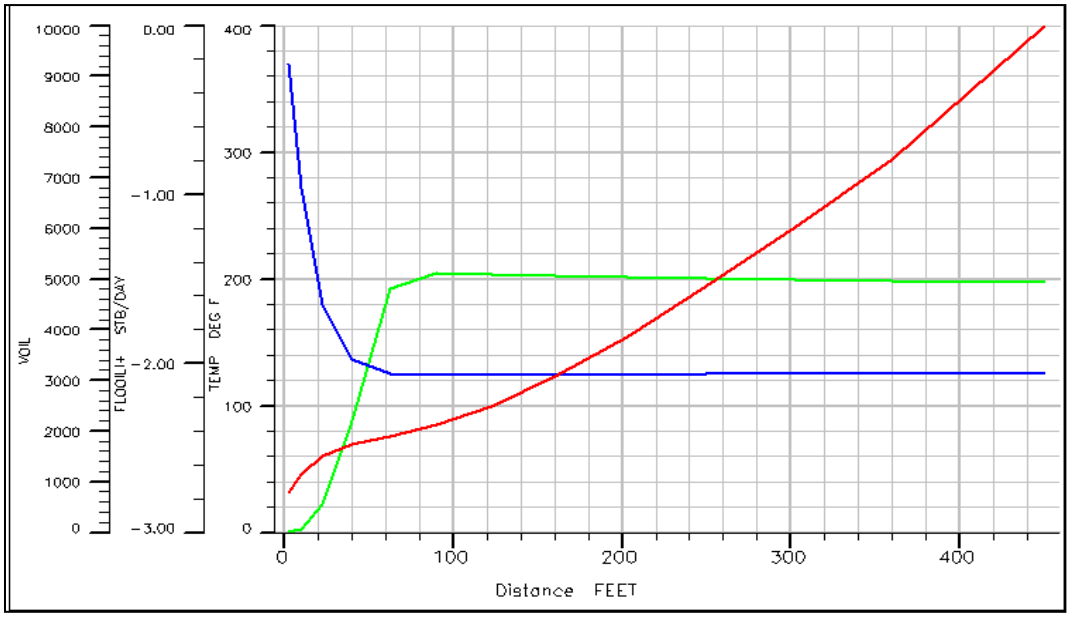


Figure 4.8. Case VT250 (heat-source at producer, oil viscosity at *T*=250°F twice that of base case): flowrate (red), temperature (blue) and oil viscosity (green) profiles in reservoir at *t* = 1.12 years.

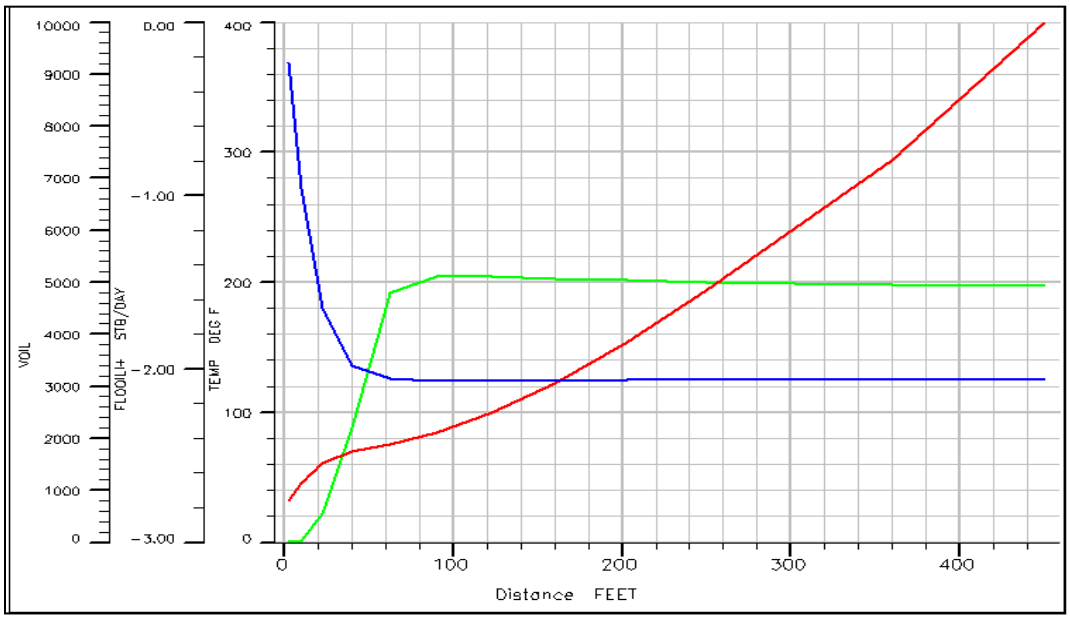


Figure 4.9. Case-VT350 (heat-source at producer, oil viscosity at *T*=350°F twice that of base case): flowrate (red), temperature (blue) and viscosity (green) profiles in reservoir at t=1.12 years.

The following general observations can be made from these graphs. The temperature increase did not penetrate into the reservoir very far, with the temperature at the initial reservoir temperature ~60 ft from the well. The heat penetration from the heater prior to

production, dependent on conduction only, was not influenced by the difference in viscosities between the different cases, with all the cases having the same temperature-*vs*-distance distribution at the start of production. This is expected, since heat diffusion is a function of the thermal conductivity of the rock and fluid, and depends also on the fluid density (Prats, 1982; Somerton, 1992). In the present work the density of the fluids has not been adjusted. The maximum temperature reached in the reservoir during simulation was not above 400°F, rendering the case VT500 irrelevant. The highest flowrate is in the vicinity of the well, with a zero flow at 500 ft from the well. The highest deviation in flowrate from the base case is in the VT125 case, with the maximum flowrate at 2.1 bbls/d, as opposed to 2.8 bls/d in the base case. The other cases did not exhibit this.

Figure 4.10 shows a comparison of the viscosity profiles and temperature profiles at t = 1.12 years. The temperature curves of all four cases overlay each other, again illustrating that the viscosity increases at specific temperatures did not affect the temperature distribution significantly, even after production started. This is mainly due to the fact that the oil flow was in the opposite direction to the heat conduction or diffusion. Slight variations in the high temperature viscosities (VT 250, VT350) in the oil within 20 ft from the well can be observed, but it is the VT125 case, with the viscosity deviation at reservoir temperature, which dominates. The majority of the reservoir is at reservoir temperature, with the very high viscosity of case VT125, at nearly 10,000 cP, shown in yellow.

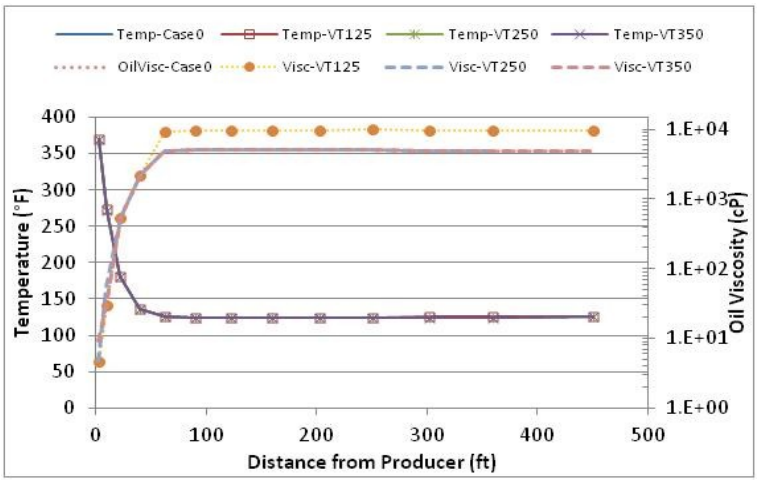


Figure 4.10. Viscosities and temperatures *vs.* distance from producer (heat source at producer). Solid lines represent temperature curves; dotted and dashed lines viscosity.

If the absolute flow rates are compared, at the same time step, as a function of the distance from the well, as in Figure 4.11, it is very clear that the VT125 case is the only case where there is a significant difference.

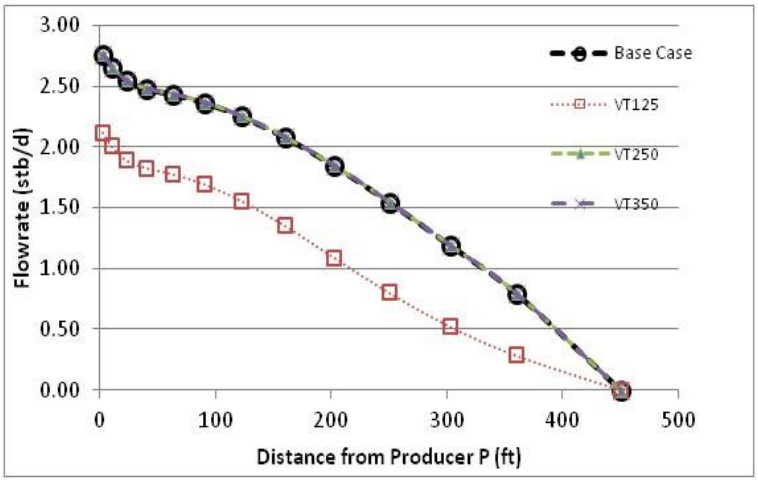


Figure 4.11. 2D-linear model: comparison of flow-rate vs distance from well.

Two questions arise: (a) why is the flow rate at the well not affected by the viscosity errors at the higher temperatures, even though the temperature at the well is in that range, and the viscosity difference is visible in the comparison (Table 4.4); and (b) why is the rate difference between the base case and the VT125 case at the cold temperatures not exactly two-fold, similar to the viscosity difference. The answer to these questions lies in the influence of assumed boundary conditions, the small volume of the first gridcell in which the temperature is high and the steep temperature variation curve (low heat penetration into the reservoir). The fluctuation in the viscosity is too brief to have a permanent influence in the high temperature cases (VT250, VT350). Furthermore, a change in viscosity at a specific temperature leads to a linear interpolation by the simulator at all temperatures between the two specified values, thus decreasing (smoothing) the effect of one single point.

For the case with the heat source (downhole heater) on the opposite side than the producer, the cumulative rates are shown in Figure 4.12, with the base case in black dots and the case with viscosity error at T_R, 125°F (VT125), in blue. The cases with the error at 250°F and

350°F are shown in green and red, respectively, overlaying the base-case. The highest deviation in the cumulative rate was in the VT125 case at early times, at 22%, with a 9% deviation at the end of the Base Case run (Figure 4.12). The deviations in the VT250 and VT350 cases were less than 0.001%.

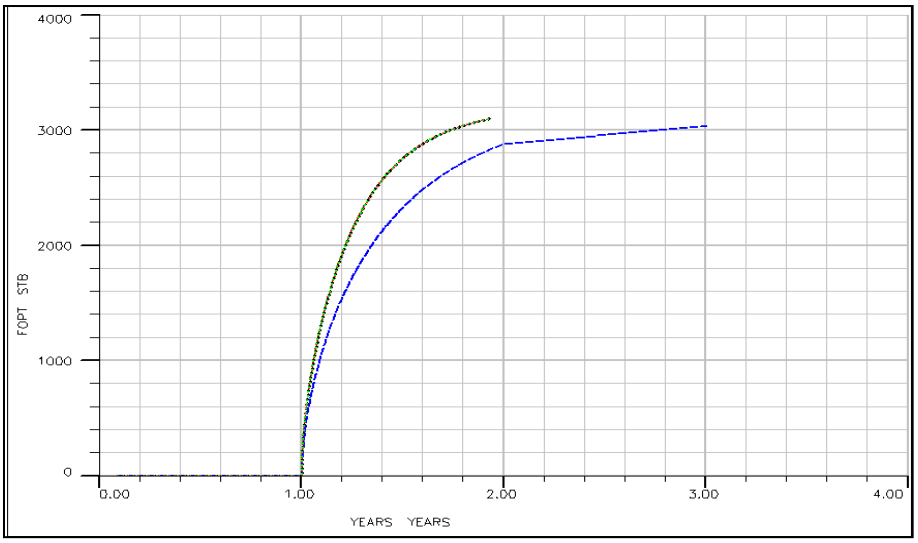


Figure 4.12. Heat source some distance away from producer: cumulative oil production comparison. Base case: black dots, VT125: blue dashed.

Table 4.4 shows the temperature and viscosity values at t = 408 days, as a function of the distance from the well, for each of the cases (with the heat source at the producer). The base case values are shown on the left-hand side of the table. Each of the sensitivity cases contains a column indicating the ratio of the flowrate at the specific distance from the well, to the base-case flowrate. The cases VT250 and VT350 show no significant differences, but the VT125 case shows flowrate differences at the cold reservoir temperature (125°F), as well as in the vicinity of the well where the temperatures are higher. This is due to low support (low mobility) from the high-viscosity regions, affecting the pressure-differential and thus volume-drainage rates of the simulation grid cells as a function of distance from well. The expectation of a flowrate-deviation only dependent on the viscosity deviation is thus not possible.

Table 4.4. Comparison of flow-rates per grid-cell (as distance from well) at time t = 408 days. Differences from base case are shown in red.

Base Case (J=1, K=1) at t=408 days				VT125 (J=1, K=1) at t=408 days				VT250 (J=1, K=1) at t=408 days				VT350 (J=1, K=1) at t=408 days			
Distance x	TEMP	Oil Visc	Flow at x ft, towards Producer	TEMP	Oil Visc	Flow at x ft, towards Producer	Q_0 / Q_{125}	TEMP	Oil Visc	Flow at x ft, towards Producer	Q_0 / Q_{250}	TEMP	Oil Visc	Flow at x ft, towards Producer	Q_0 / Q_{350}
(ft)	(° F)	cP	(stb/D)	(° F)	cP	(stb/D)		(° F)	cP	(stb/D)		(° F)	cP	(stb/D)	
2.5	369	4.7	2.76	370	4.7	2.11	1.31	369	4.7	2.76	1.0	369	9.3	2.76	1.0
10	272	30	2.66	273	29	2.00	1.33	272	54	2.66	1.0	272	30	2.66	1.0
22.5	180	545	2.54	180	540	1.89	1.35	180	545	2.54	1.0	180	545	2.54	1.0
40	136	2203	2.48	136	2195	1.82	1.36	136	2202	2.48	1.0	136	2203	2.48	1.0
62.5	126	4796	2.43	126	9092	1.77	1.37	126	4796	2.43	1.0	126	4796	2.43	1.0
90	124	5106	2.36	124	9511	1.69	1.40	124	5106	2.36	1.0	124	5106	2.37	1.0
122.5	124	5102	2.25	125	9551	1.55	1.45	124	5102	2.25	1.0	124	5102	2.25	1.0
160	125	5073	2.08	125	9672	1.35	1.54	125	5073	2.08	1.0	125	5073	2.08	1.0
202.5	125	5040	1.84	125	9799	1.09	1.70	125	5040	1.84	1.0	125	5040	1.84	1.0
250	125	5008	1.55	125	9916	0.80	1.93	125	5008	1.55	1.0	125	5008	1.55	1.0
302.5	125	4978	1.19	125	9764	0.52	2.28	125	4978	1.19	1.0	125	4978	1.19	1.0
360	125	4952	0.79	125	9650	0.28	2.79	125	4952	0.79	1.0	125	4952	0.79	1.0
450	125	4926	0.00	125	9552	0.00		125	4926	0.00		125	4926	0.00	

A small change in the base case viscosity at the 'cold' end of the reservoir can be observed in Table 4.4. This is due to the effect of energy loss through production prior to thermal enhancement penetrating the full distance, causing the temperature to drop very slightly. The viscosity-temperature gradient at these temperatures is very high, and a very slight change in temperature has a noticeable effect on the oil viscosity.

The conclusion of the simple analytical model, that the priority should be to model the low temperature viscosity more accurately, has thus been confirmed. In the case where the heat-source is some distance away from the well, the same conclusion applies. The next step was to investigate a more complex four-layered radial model.

4.3.1.2.2 4-Layer Radial Model, 100% filled with Dead Oil

This situation was studied with a simplified experimental simulation case: a four-layer (homogeneous) dead oil radial model, with a downhole heater. The reservoir was 100% oil-saturated, to eliminate any additional flow effects, and establish a straight-forward relationship between the oil rate and the viscosity. The well was produced at a target rate of 500 stb/d, with a minimum rate of 1 stb/d and a bottomhole pressure of 20 psi. As no steam was injected, and water saturation was 0, no relative permeability effects needed to be taken into account. The initial reservoir temperature (T_R) was 125 °F, initial reservoir pressure 525 psia, with a reservoir permeability of 2D and a porosity of 30%. The outer radius of the reservoir was 510 ft. The reservoir was first heated up to a temperature of >500°F in the well region, after which production started.

Oil viscosity 'errors' were introduced, one at a time, at temperatures 125, 250, 350 and 500°F, with the base case containing the 'accurate' viscosities (Table 4.5).

Table 4.5. Oil viscosities for cases with deviations (fraction).

T	Base Case	μ-VT125	$\Delta\mu/\mu_0$	μ-VT250	$\Delta\mu/\mu_0$	μ-VT350	$\Delta\mu/\mu_0$	μ-VT500	$\Delta\mu/\mu_0$
°F	cP	cP		cP		cP		cP	
125	4,959	**12,398**	2.5	4,959	0	4,959	0	4,959	0
130	3,719	3,719	0	3,719	0	3,719	0	3,719	0
135	2,480	2,480	0	2,479	0	2,479	0	2,480	0
140	1,240	1,240	0	1,239	0	1,239	0	1,240	0
150	1,122	1,122	0	1,122	0	1,122	0	1,122	0
200	165	165	0	165	0	165	0	165	0
250	44	44	0	**161**	2.7	44	0	44	0
300	13	13	0	13	0	13	0	13	0
350	5.2	5.2	0	5.2	0	**10.0**	1.9	5.2	0
500	1.65	1.65	0	1.65	0	1.65	0	**4.0**	1.4

The top view of the radial reservoir is shown on the left of Figure 4.13, showing the base case viscosity distribution after five years, and on the right, a vertical cross section through the well, showing the temperature distribution at the same time. If our estimates according to the analytical model are correct, the error at the 'cold' reservoir temperature (T_R) would introduce the highest error in the production rate. Figure 4.14 shows the well production

rates from each the simulation cases compared to the base case rate in black dots. It is clear that the rate most affected by the error in the oil viscosity is case VT125, where the error was made at the low temperature end (T_R) of the viscosity range. The error in the viscosity at the high temperature had no effect in this case. Figure 4.15 and Figure 4.16 show the variation in block viscosities and corresponding block temperatures over time at three different distances from the well: (a) block (1,1,1), 2.5 ft from the well; (b) block (3,1,1), 22.5 ft from the well and in the outer circle; and (c) block (13,1,1), 450 ft from the well. The temperature in case (c) is the reservoir temperature T_R=125°F, while the temperature in (a) is T_w > 500°F, with the viscosity difference in the VT125 clear at (c) and in case VT500 at (a). The deviations in the viscosities at intermediate temperatures 250 and 350°F are visible in (b). It is clear that errors in viscosities in the intermediate temperatures have not had the same effect as at the low temperature.

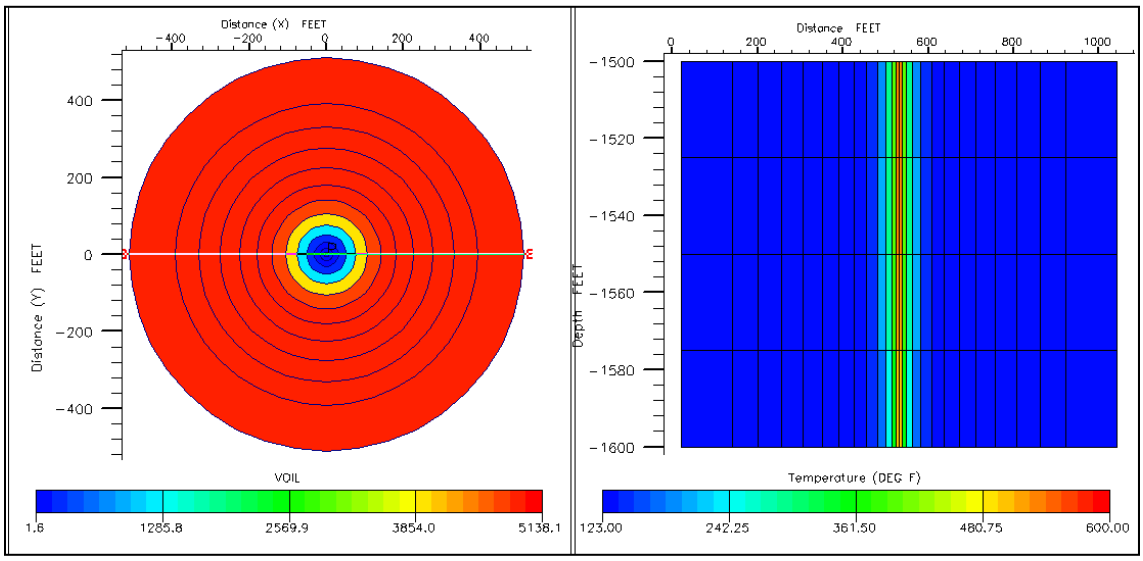


Figure 4.13. Radial reservoir with production well at the centre. On the left is the oil viscosity distribution at the end of the simulation period (5 years) and on the right a vertical cross section showing the temperature distribution at the same time.

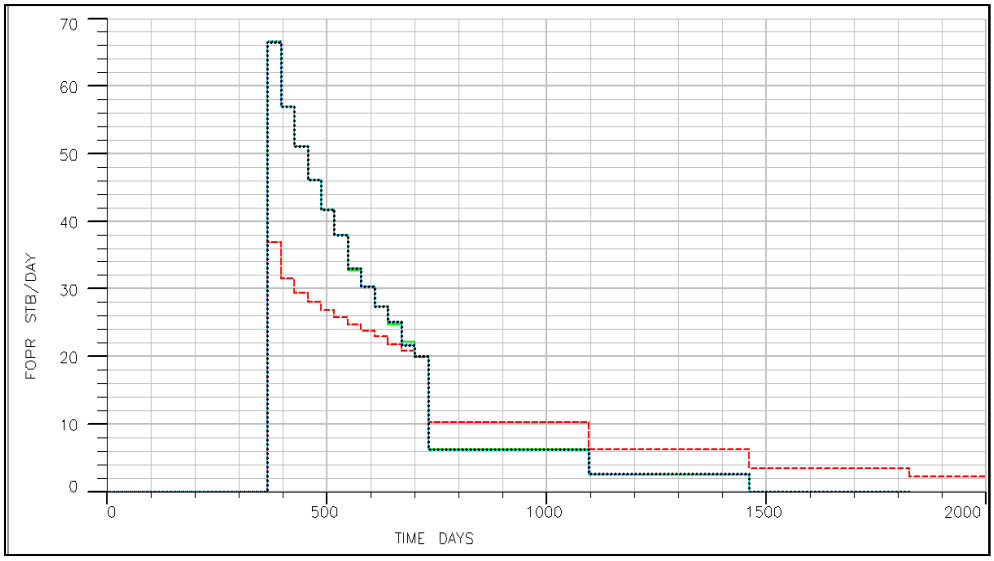


Figure 4.14. Oil Production rate (stb/d) at well. Black dotted line: base case; red dashed line: case VT125, and green dashed line: case VT500. Additional cases (VT250 and VT350) are in blue.

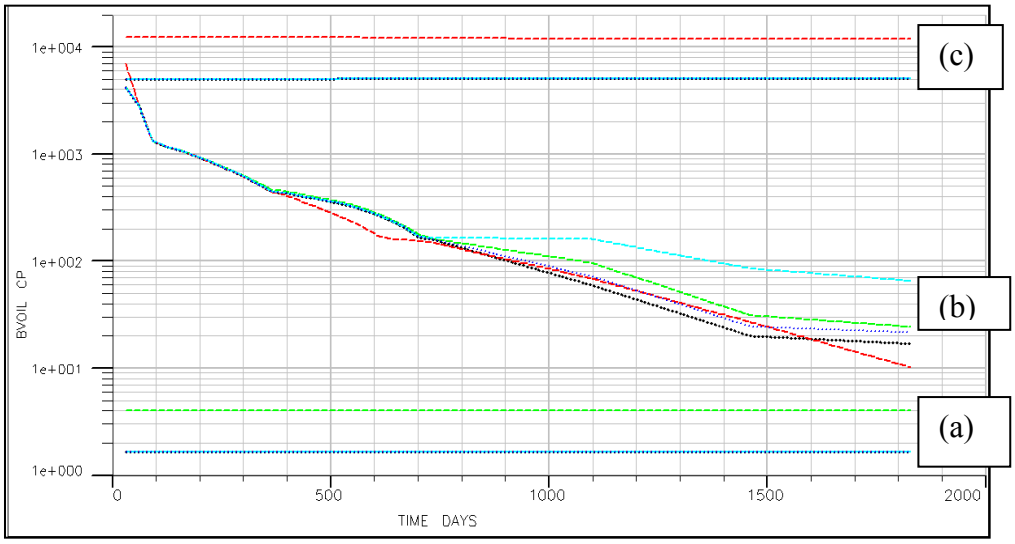


Figure 4.15. Block viscosities (cP) *vs.* time (a) near well (cell:1,1,1) at high temperature (T_w), (b) 22 ft into reservoir (3,1,1,), and (c) outer boundary at 450 ft (13,1,1,) at cold reservoir temperature (T_R). Black dotted line: base case; red dashed line: case VT125 and green dashed line: case VT500. Additional cases (VT250 and VT350) in blue.

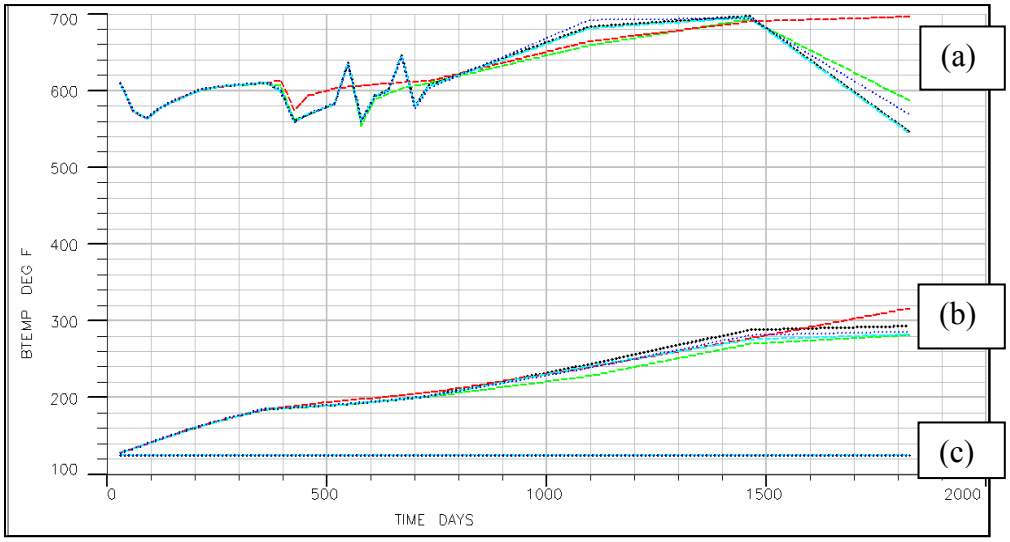


Figure 4.16. Block temperatures (°F) vs time (a) near well (cell:1,1,1), (b) 22 ft into reservoir (3,1,1,) and (c) outer boundary at 450 ft (13,1,1,). Black dotted line: base case; red dashed line: case VT125 and green gashed line: case VT500. Additional cases (VT250 and VT350) in blue. Changes in temperatures in (a) are due to production, and later, drainage in the gridcells close to the well.

The rate sensitivity expressed as a ratio of the rate deviation to viscosity deviation, is given by

$$QDEV = \frac{\Delta q / q_0}{\Delta \mu / \mu_0} = \frac{(q_0 - q_{VTn}) / q_0}{(\mu_0 - \mu_{VTn}) / \mu_0}$$

where q_0 is the base-case flowrate, μ_0 the base-case viscosity, and q_{VTn} and μ_{VTn} the flowrate and oil viscosity of the sensitivity case, either VT125 or VT500. *QDEV* is plotted for the two cases VT125 and VT500 in Figure 4.17, with the red line representing case VT125 where the viscosity error is at the cold reservoir temperature (T_R=125°F), and the blue line case VT500, where the error is at the hot well temperature (T_w=500°F).

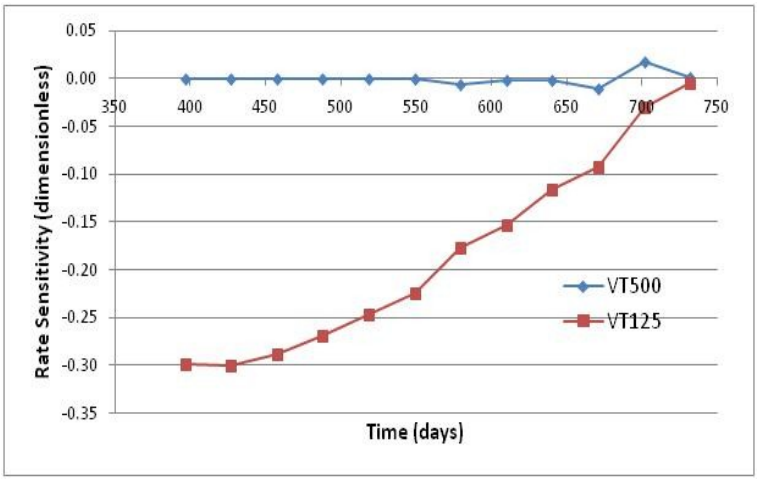


Figure 4.17. Rate sensitivities (*S*) to viscosity errors: error at T_R(cold)=red, and error at T_w(hot)=blue.

In terms of sensitivity *S*, defined in eq. (4.29) for the error at reservoir temperature (S_{cold}), and eq. (4.30) for the error at hot temperatures (S_{hot}), the sensitivity approaches zero:

$$S_{hot} = 1.65/(4962\text{-}1.65) \rightarrow 0$$

and for the error at the lower temperatures, the sensitivity approaches 1:

$$S_{cold}=12364/(12364\text{-}1.65)\rightarrow 1$$

This confirms the earlier findings that the well production rate is most sensitive to the error in the viscosity at the cold reservoir temperature T_R, and much less sensitive to viscosity errors at the highest temperature. The next section investigates the effect of multiple phases.

4.3.1.2.3 4-Layer Radial Model, S_{wi} = 45%

The investigation was extended to a 4-layer radial model with dead oil, and initial water saturation of 45%. The temperature was increased by a heater in the producer, to a maximum of 600°F. The results again showed the highest deviation in the VT125 case, where the viscosity error was at the 'cold' end of the temperature range, even though the initial water was vapourised and phase and relative permeability effects were introduced. Figure 4.18 shows the cumulative oil production comparison to the base case (black dotted

line). The highest deviation is in VT125 (blue), with the smallest deviation in VT500. The effect of the steam was to increase the deviations in the VT250 and VT350 cases.

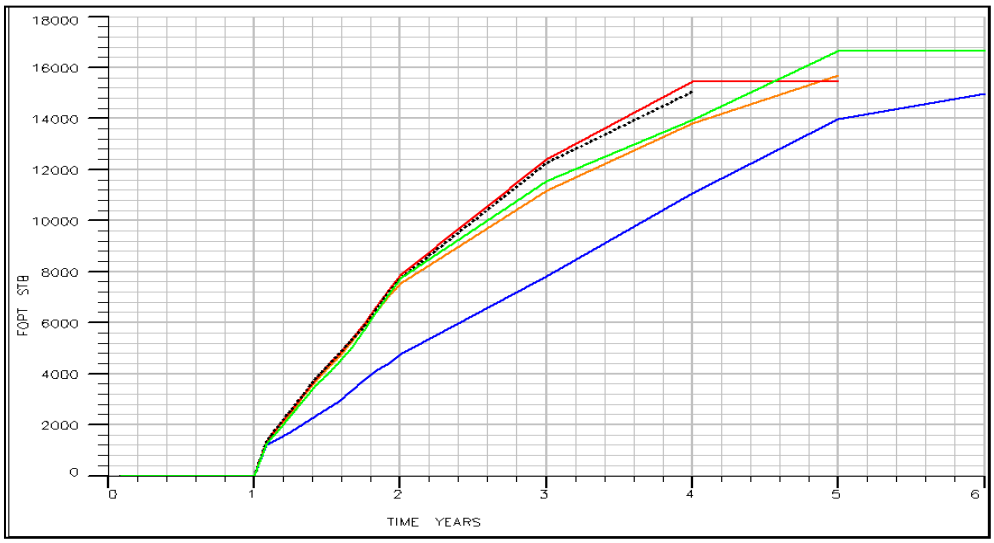


Figure 4.18. 4-Layer multi-phase model: cumulative oil production. Base case is shown in black dots, VT125 in blue, VT250 in green, VT350 in orange and VT500 in red.

4.3.1.2.4 10-Layered, Heterogeneous Steam Injection Case with Live Oil

The study was extended to a 'real' case, where the reservoir was heterogeneous with live oil; initial reservoir pressure was set to 400 psi and temperature to 125°F. The oil was simulated with three pseudo-components: 10% gaseous, 54% C17-ECN and 36% heavy-pseudo-component, with molecular weights of 16, 260 and 556 respectively. The oil viscosity as a function of temperature (Figure 4.19) was modelled with the Free Volume model (Chapter 5), with errors introduced at discreet temperatures as before. Steam was injected at a constant rate at the upper left corner, with the oil producer in the lower right corner (Figure 4.20).

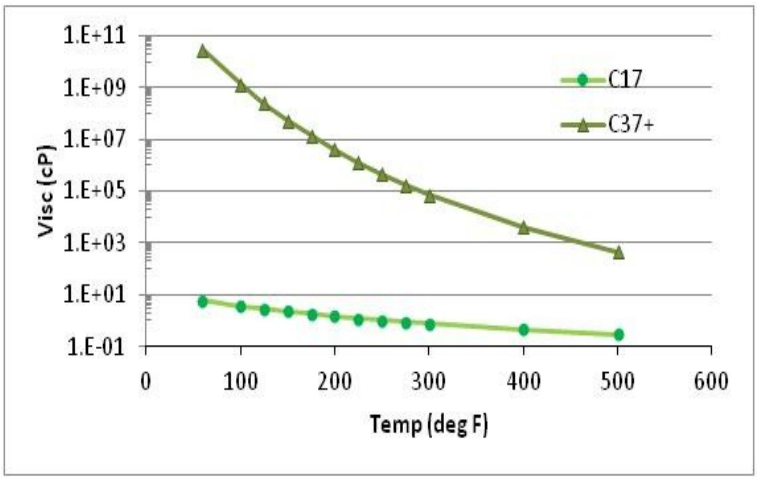


Figure 4.19. Base case oil component oil viscosities (cP).

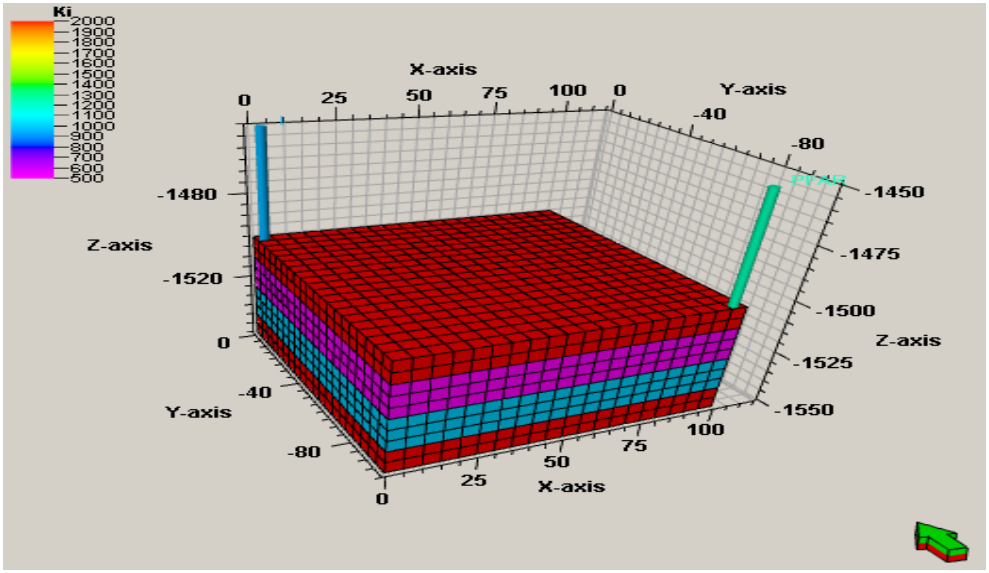


Figure 4.20. Heterogeneous reservoir with steam-line-drive. Steam injection with well in upper left corner(blue), oil production with well in lower right corner (green).

The results again confirmed the analytical model finding: the case with the error in the viscosity at low temperature had the most significant deviation in cumulative oil produced (Figure 4.21 and Figure 4.22). Although the large deviation (max nearly 50%) is only at early times before the whole drainage area is heated, it will have an impact on economics and planning.

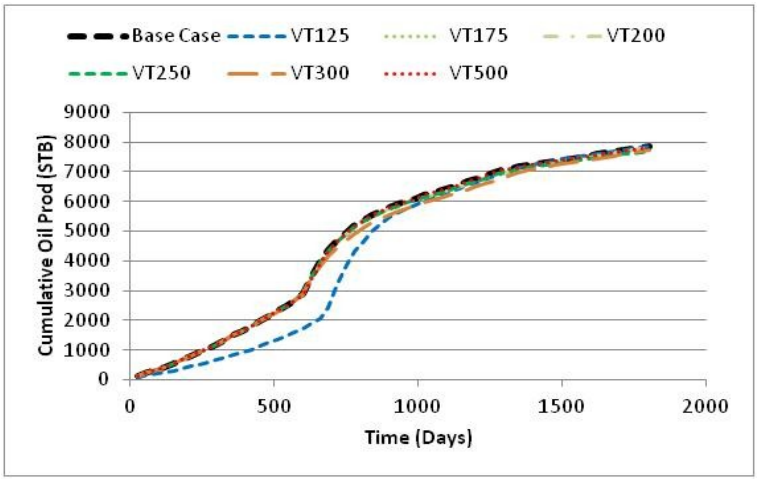


Figure 4.21. Heterogeneous reservoir with steam injection: oil recovery comparison. Base case in black, error at T_{Res}(cold) in blue.

Figure 4.22 shows the relative percentage deviation of the cumulative oil production over time, for each case, as compared to the base case. The disappearance of the low-temperature viscosity error case deviation at 800 days is due to the fact that the temperature change thorough out the reservoir is relatively quick. The distribution in a steam line drive is a function of the vapour flow through the reservoir, which is very mobile in comparison to the heavy oil, with the steam reaching the producer after 600 days. The average temperature in the reservoir at that time is around 250°F. The average temperature in the reservoir at the end of the run is around 300°F, which explains the deviation in the VT300 case being more visible at that time, even still below 5%.

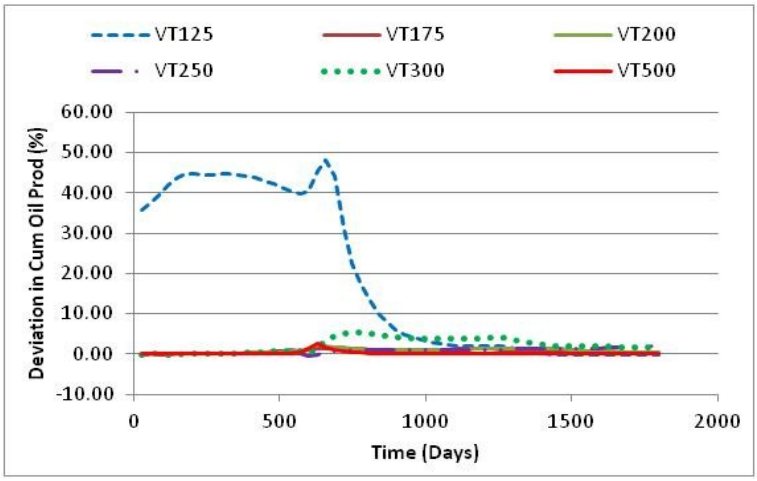


Figure 4.22. Live oil, steam injection: deviations in oil recovery over time, for each viscosity-error case.

It is clear that viscosity errors at low temperatures will results in large errors in oil production predictions in the early times of steam line-drive cases, but, once the production well drainage area had been heated up, the errors will have little influence. Errors at high temperatures result in recovery deviations at late time of less than 5%. The low deviations are due to much lower volumes recovered at these temperatures, with flowrates in the order of less than two barrels a day.

4.3.1.3 Conclusions for Vertical Producer + Heater or Steam Line Drive

In conclusion, for all cases where the majority of the production is from unheated zones, errors in viscosity predictions at lower temperatures have the largest effects on production rate predictions. This would include the use of down-hole heaters and cyclic steam injection (huff-n-puff) where heat is injected but produced with the oil, resulting in low reservoir penetration, and steam-line-drive, where there is a time-delay at the producer in the viscosity-lowering effects of the heat. The magnitude of the sensitivity depends on the difference between the viscosities at the initial and steam temperatures, i.e. a function of the viscosity-temperature relationship.

4.3.2 Steam Assisted Gravity Drainage (SAGD) with horizontal wells

4.3.2.1 Analytical Investigation

An existing analytical model (Butler, 1994) was exploited to verify oil rate *vs*. viscosity sensitivity for the SAGD process. The model is formulated as in eq. (4.31). The simulation model properties were inserted into the equation to verify that the model and the simulation give the same results. In order to establish the rate sensitivity to the temperature range in which the oil viscosity had been inaccurately predicted, firstly the sensistivity of flowrate to viscosity coefficient was mathematically determined, then, secondly, this finding was verified with further simulations.

Butler's analytical model states that

$$Q = 2L\sqrt{\frac{2k\phi g\alpha\Delta S_o H}{m\nu_s}} \tag{4.31}$$

where Q is the flowrate (m^3/s), L is the length of the horizontal well (m), k is the effective permeability to oil (m^2) (k_i is the permeability per layer in layered system), ϕ is the porosity, α is the thermal diffusivity ($K/\rho C_p$) in (m^2/s), g is the gravitational acceleration constant (m/s^2), ΔS_o is the initial oil saturation (S_{oi}) minus the residual oil saturation (S_{or}), H is the thickness of the reservoir (or H_i of layer, if layered system), m is a dimensionless parameter related to the variation of oil viscosity with temperature (usually on the order of 3-4), and ν_s is the oil kinematic viscosity at the steam-oil interface temperature (m^2/s). Specifically, the factor m is defined as follows (Butler 1994):

$$\frac{1}{m} = \int_{T_R}^{T_s} \left(\frac{\nu_s}{\nu} - \frac{\nu_s}{\nu_R} \right) \frac{dT}{T - T_R} \ . \tag{4.32}$$

4.3.2.1.1 Numerical Simulation: Model Verification

Assuming a dynamic viscosity (μ_s) of 75 cP in the reservoir at the steam-oil interface, a density of the very heavy oil equal to that of water, 1000 kg/m^3 at standard conditions, and a Butler viscosity parameter of m = 4, it was possible to replicate the results from the simulations (Figure 4.23). (Note that although Butler verified his model against simple laboratory experiments, it is difficult to find verification of this model for realistic field cases, in the open literature.) The results from the analytical model are shown in Table 4.6, with the property values used in the simulation model shown in Table 4.7. The vertical distance between the steam injector and the oil producer was 15 ft (5 m).

Table 4.6. Butler model flow rates for simulation reservoir parameters.

q (1 segment)	7.41E-05	m^3/s	40.28	bls/d
Q (full well)	3.71E-04	m^3/s	201.42	bls/d

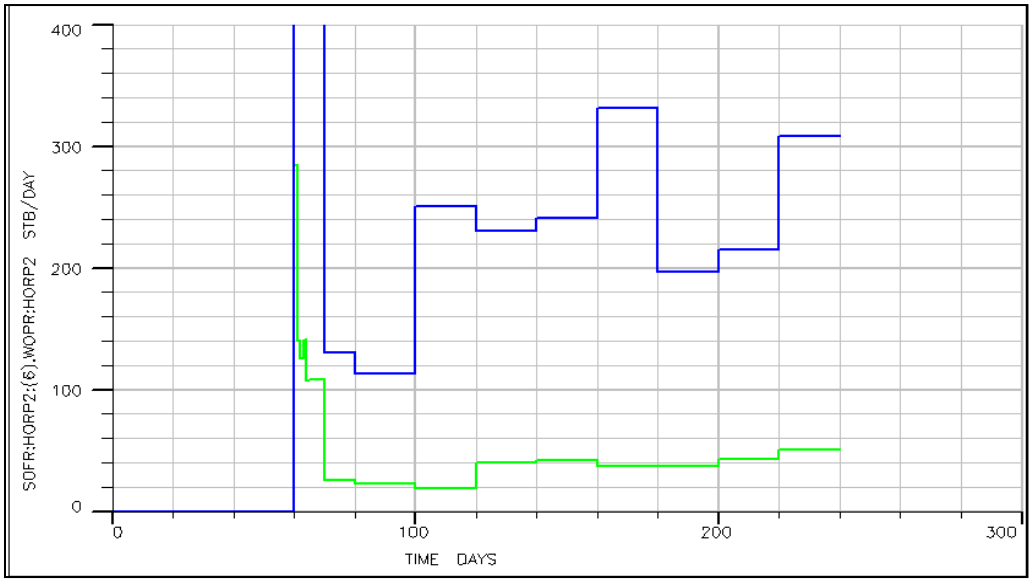


Figure 4.23. Oilrates in total well (WOPR, blue) and in the toe-segment (SOFR, green), in stb/d.

It can be observed that, in the toe-segment (segment-length L=300 ft), where the flow consists of only the flow from the reservoir into the well, the rate is as predicted with the analytical model, i.e. around 40 bls/d. The total rate of the well (full length L=1500 ft), is around 200 bls/d, as predicted by the Butler model. The variations in rate in the numerical model are due to boundary conditions affecting initial and late-time rates.

Table 4.7. Simulation case properties.

E300 Model		Field-units		Absolute units	
Parameter	Symbol	Value	Unit	Value	Unit
Reservoir thickness	H	100	ft	30.48	M
Length of one segment of horizontal well	L	300	ft	91.44	M
Length of full horizontal well	L	1500	ft	457.2	M
Oil viscosity at T_{res}	μ	100,000	cP	1.00E-01	m^2/s
Oil viscosity* at T_{steam}	μ_s	75	cP	7.50E-05	m^2/s
Permeability	k_1	2	D	1.97E-12	m^2
	k_2	0.5	D	4.93E-13	m^2
	k_3	1	D	9.87E-13	m^2
	k_4	2	D	1.97E-12	m^2
Layer-height	h_1	20	ft	6.10	m
	h_2	30	ft	9.14	m
	h_3	30	ft	9.14	m
	h_4	20	ft	6.10	m
Avg K*h	$k_{avg}h$	125	D.m	3.76E-11	m^3
Soi – Sor	ΔS_o	0.4			
Gravitational acceleration	g			9.87	m/s^2
Porosity	ϕ	0.3			
Viscosity-temperature ratio parameter	m	4	(assume)		
Thermal conductivity rock	K	24	BTU/ft/day/°F	1.73E+00	watt/m-K
Heat capacity rock	$C_{p\text{-}rock}$	35	$BTU/ft^3/°F$	1.020E-06	J/Kg/K
Heat capacity rock (volumetric)	$C_{p\text{-}rock}$	35	$BTU/ft^3/°F$	2,345,700	$J/m^3/K$
Rock+oil thermal diffusivity	α	7.378E-03	cm^2/s	7.38E-07	m^2/s

**Kinematic viscosity assumes 10 API oil with oil specific gravity =1*

The oil viscosity as a function of temperature was calculated with the Free Volume model (Chapter 5), which takes into account the oil density as a function of pressure and temperature. The values used in the simulation model are shown in Figure 4.24.

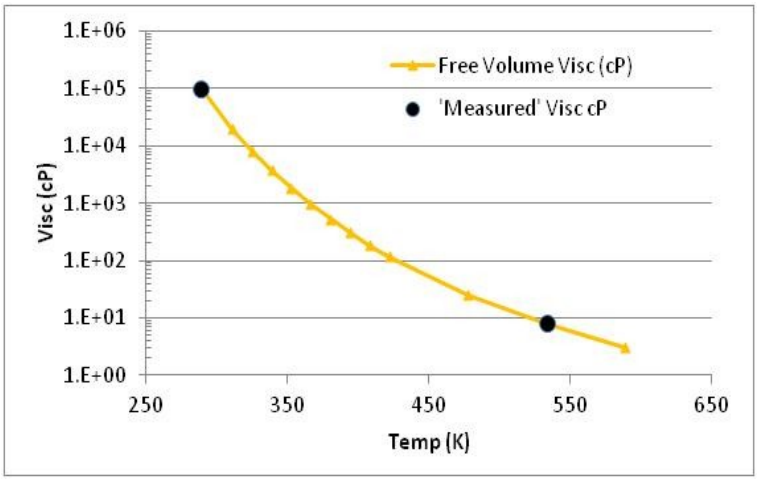


Figure 4.24. Oil viscosity as a function of temperature.

At the initial reservoir temperature of 125°F (325 K), the oil viscosity is 8,300 cP, whereas at the highest temperature (steam-injection temperature) of 500°F (507 K), it is 7.8 cP. Within the steam chamber itself, the reservoir temperature is 500°F, but cools down rapidly across the oil-steam interface due to the hot steam being in contact with the cold oil and rock, and, additionally due to the energy lost in condensation of the steam and/or vaporization of the lighter HC components. Within the high temperature zone inside the steam chamber, the oil saturation is at residual (S_{or}) and thus immobile, and the oil produced at the well is from the oil flowing tangentially/diagonally at the interface towards the producer mainly under gravitational forces. Figure 4.25, a vertical cross-section (*YZ*) through the reservoir, perpendicularly crossing the oil producer located at the bottom centre, illustrates the flow-directions of the oil in the reservoir at 140 days. The cell-arrow directions indicate the flow direction of the oil in each of the cells and the lengths of the arrows are the relative flow-rates. The production at the well is clearly dominated by the diagonal flow in the bottom layers of the reservoir (red arrow), following the edge of the steam chamber.

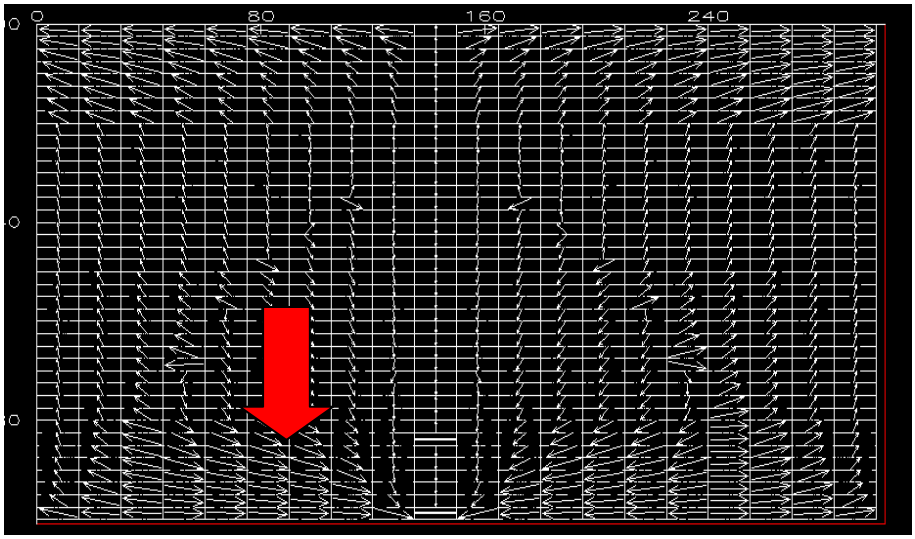


Figure 4.25. Oil flow vectors in the *YZ* plane (intersecting the horizontal producer at the centre-bottom perpendicularly). The lengths of the cell-arrows are an indication of the amount flowing in the cell. Red arrow indicates maximum flow towards well.

Figure 4.26 to Figure 4.28 show the oil saturation, temperature and oil viscosity distributions in the same cross-section, at the same point in time. It is clear that the mobile oil (favourable saturation and oil viscosity) is in the same area as indicated by the arrows: four cells to the left and right of the producer, and up to eight cells vertically. The oil viscosities in this area range between 211 cP and 3 cP, with the average of the flowing cells shown in Figure 4.29, around 72 cP.

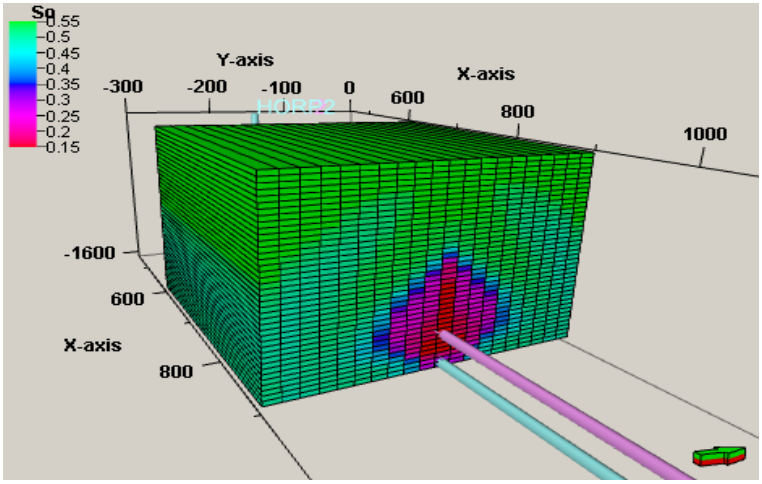


Figure 4.26. Oil saturation in *X*-section (*X*=3) at *t*=140 days. Green=S_{oi}, Red=S_{or}.

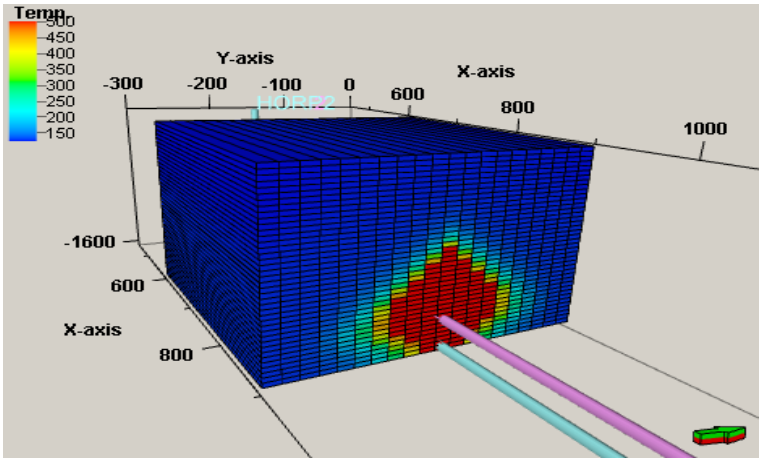


Figure 4.27. Temperature distribution in *X*-section (*X*=3) at time *t* -= 140 days.

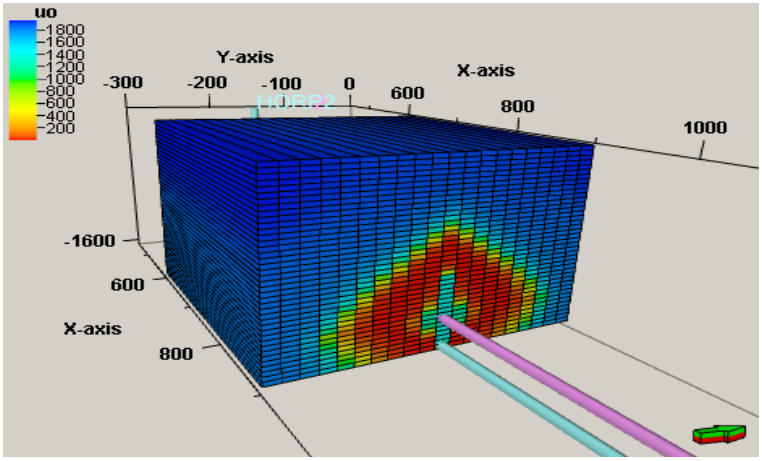


Figure 4.28. Oil viscosity distribution in *X*-section (*X*=3) and *t* = 140 days.

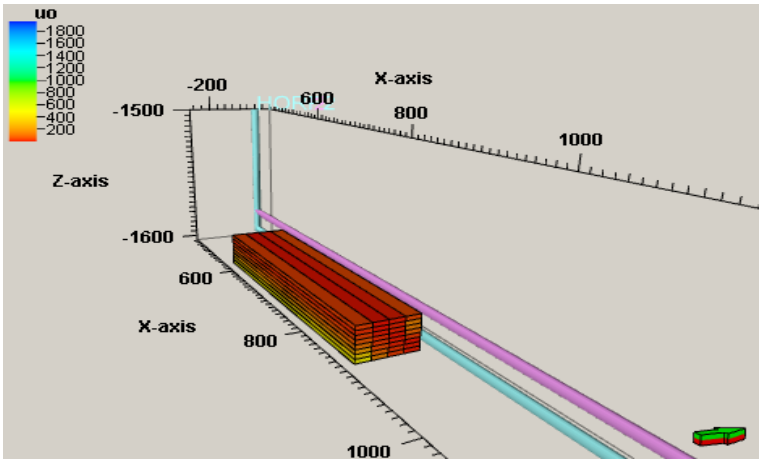


Figure 4.29. Oil viscosity in some production-contributing blocks, at the steam-oil interface, with an average oil viscosity of 71.3 cP for the block shown (I=3, J=12-15, K=32-39).

In order to answer the question of which viscosity range should be prioritised in modelling the oil viscosity as a function of temperature, the initial high viscosity at the low temperature, or the mid-to-low range of viscosities at the temperatures at the steam-oil interface, the dimensionless sensitivity derivative of the Butler model is calculated as follows:

$$S=\frac{dq/q}{d\nu_s/\nu_s}=-0.5c\nu_s^{-3/2}.\frac{\nu_s}{c\nu_s^{-1/2}}=-0.5 \quad . \tag{4.33}$$

Where $c=2L\sqrt{\frac{1.5\Delta S_o khg\alpha\phi}{m}}=3.2136\times10^{-6}$.

From eq. (4.33) it can be determined that for a 20% error in the viscosity prediction, the error in the flow rate prediction will be 10%. Or in terms of flow rate, an over-prediction of 15 cP on the estimation of the oil viscosity at the steam-oil interface (ν_s), say μ_s = 80 cP ($\Delta\mu/\mu$=0.18), the equivalent of a kinematic viscosity of 8×10^{-5} m^2/s (for a 10 API oil), will result in an error of $\Delta q/q = -2.9\times10^{-5}$ m^3/s, or -16 bls/d over the full length of the 1500 ft well. This is further explored in Table 4.8. Note that the change in the effective permeability, as a function of the oil saturation, had not been taken into account for this quick analytical evaluation. Clearly, as the oil saturation decreases, so would the effective permeability.

Table 4.8 shows examples of the errors in predicted production rates for errors made in the viscosity prediction at the steam-oil interface temperature, based on eq. (4.31) and eq. (4.33). The table shows the actual error in the rate prediction, based on the parameters provided in Table 4.7, for each of the viscosity predictions as shown on the left.

Table 4.8. Sensitivity of production rate (full length of well) to error in oil viscosity at the steam-oil interface.

	Steam-Oil Interface Viscosity		Well flow rate		Error in Viscosity Prediction	Result Error in Rate Prediction			Sensi-tivity S
	μ_s (cP)	V_s (m^2/s)	q (m^3/s)	q (bls/d)	$\Delta\mu_s$ (cP)	Δq (bls/d)	$\Delta v_s/v_s$ (%)	$\Delta q/q$ (%)	$\Delta q/q$ / $\Delta v_s/v_s$
Base case	**75**	**7.5E-05**	**3.71E-04**	**201.42**					
Prediction 1	80	8.0E-05	3.59E-04	195.02	5	-6.40	6.67	-3.18	-0.5
Prediction 2	85	8.5E-05	3.48E-04	189.20	10	-12.22	12.50	-6.27	-0.5
Prediction 3	90	9.0E-05	3.38E-04	183.87	15	-17.55	17.65	-9.28	-0.5
Prediction 4	95	9.5E-05	3.29E-04	178.97	20	-22.45	22.22	-12.21	-0.5
Prediction 5	100	1.0E-04	3.21E-04	174.43	25	-26.99	26.32	-15.08	-0.5

It can be observed that an overestimation of 20 cP can under-estimate the well production rate by nearly 2,000 bls/d. From these results it is clear that a relatively small error in the viscosity estimation at the steam-oil interface temperature can result in significant errors in rate predictions. The next sections will use numerical simulation to confirm these predictions.

4.3.2.1.2 Numerical Simulation: Sensitivity to Viscosity Error Temperature

A series of live-oil (four pseudo-components) simulations has been run, each with a 100% error in the oil viscosity at one specific temperature; for example, in the case VT125, the viscosity at a temperature of 125°F is twice that of the viscosity in the base case at the same temperature. This has been done for each of the discreet temperature values of 125, 150, 175, 200, 225, 250, 275, 300, 400 and 500°F.

The cumulative oil production results are shown in Figure 4.30, with the base case results indicated by black dots. The highest deviation is in the case where the error is at a temperature of 400 °F, shown in red.

Table 4.9 shows the relative error in cumulative production, as compared to the base case, for each of the cases.

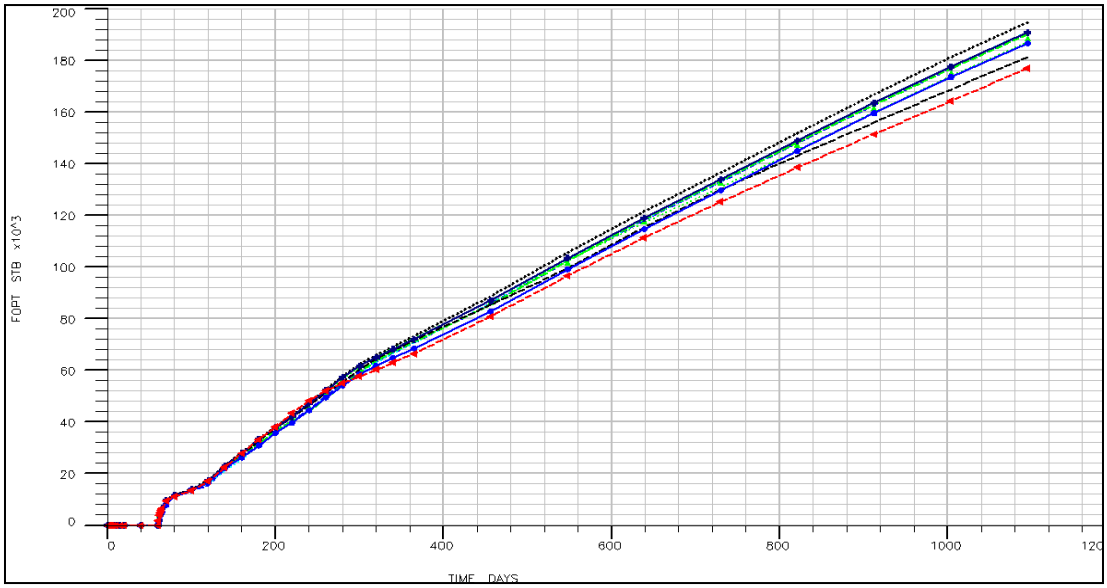


Figure 4.30. Cumulative oil production per case. Base case (black dots); error at reservoir temperature (blue); error at highest temperature (dark blue +); error at temperature of steam-oil interface: red + triangles).

Table 4.9. SAGD Recovery sensitivity to temperature at which viscosity error occurs.

Case	Cumulative Oil Production (STB)	% Error in Recovery Prediction
Base Case	1.95E+05	
VT125	1.87E+05	4.14
VT150	1.90E+05	2.32
VT175	1.91E+05	1.91
VT225	1.90E+05	2.41
VT250	1.88E+05	3.43
VT275	1.87E+05	3.93
VT300	1.81E+05	6.87
VT400	1.77E+05	9.12
VT500	1.91E+05	2.03

The results of the sensitivity indicated that the highest sensitivity was in the case of VT400, where the viscosity error was at T = 400°F, the temperature at the steam-oil interface, with 9.12% under-prediction in the cumulative production over three years production. However, an increase in deviation is also observed with the viscosity error at T=300 °F, leading to the conclusion that the steam-oil interface temperature in this case is somewhere between these two temperatures. Since the simulator linearly interpolates viscosities

between the temperatures, an estimate of the relative viscosity error, based on a combination of the two cases is calculated, as shown in Table 4.9. This leads to the conclusion that the relative error in the viscosity, as simulated, is closer to 50%, in which case, based on the analytical study, results in a rate deviation of around 25%. This is the result from the simulation during the period 200 to 400 days, as shown in Figure 4.31. Note that the simulation results include noise effects as a result of the simulator switching well controls due to convergence issues during thermal multi-segmented simulation. At late times boundary effects influence results.

Table 4.10. SAGD viscosity-temperature sensitivity.

	Oil mixture viscosity (cP)				Calculated	Predicted (Anal)
T (°F)	Base Case	VT300	VT400	VT300-400 avg	$\Delta v_s/v_s$ (%)	$\Delta q/q$ (%)
300	34.8	**69.5***	34.8	**52.1**	-50	-25
350-interpolation	21.7	**39.1**	**26.0**	**32.5**	-50	-25
400	8.63	8.63	**17.26**	**12.9**	-50	-25
450-interpolation	5.8	5.8	**10.1**	**7.9**	-37	-19
500	2.95	2.95	2.95	2.95		

**Viscosities with 'errors' are shown in red.*

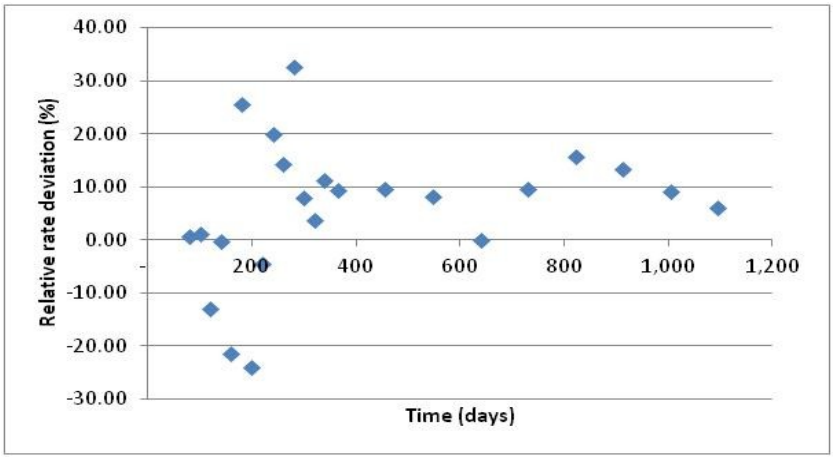


Figure 4.31. SAGD relative rate deviations based on a combination of cases VT300 and VT400.

It is clear that a relatively small error (in absolute values the difference was only between 2 and 11 cP), in the estimated viscosity at the steam-oil interface temperature, in this case between 300 and 400 °F, yields a cumulative oil production prediction error that approaches 10%.

4.4 Chapter Conclusions

Depending on reservoir conditions (pressure drawdown, distance from well, well-contact area and reservoir permeability) the oil can be mobile at very high viscosities, of the order of 10^4 cP. It would therefore be important to include this range in viscosity modelling evaluations.

The temperature ranges at which recovery predictions are most sensitive to uncertainty in viscosity are found to be dependent on the thermal recovery method used. For down-hole heaters, cyclic steam injection and line-drive steam-flooding, accuracy of the oil viscosity at the initial reservoir temperatures is essential, whereas in the case of SAGD, accuracy of oil viscosity at the oil-steam interface, *i.e.* in the mid-to-high temperature ranges achieved in the reservoir, is crucial to accurate recovery predictions.

5 Viscosity Modelling of Individual Components

5.1 Introduction

Oil consists of a mixture of individual hydrocarbon pure components, and in the case of heavy oil, thousands of components, some of which form very complex compounds. In order to perform numerical simulation of the flow of these complex fluids through a subsurface reservoir, the individual components are indentified and characterised. At each advance in time during simulation, a flash calculation in each grid cell determines the status of each individual component at the prevailing pressure and temperature. This is done for each individual simulation grid cell, to establish the components present in each of the phases, liquid and vapour, depending on the saturation or bubble point/dew point pressure of each component, and component K-values (equilibrium values) as a function of pressure and temperature. Thus, the composition of the oil in each cell, at each timestep, changes due to the changes in pressure and temperature. Therefore, the viscosity of the liquid mixture in each simulation cell, at each timestep, is a function of the viscosity of each individual component comprising the oil phase, the pressure and the temperature. This requires viscosity modelling on an individual component basis, as a function of pressure and temperature.

Current industry practice in the modelling of hydrocarbon component viscosities in liquid phase is based on grouping individual pure components into single carbon number groups (SCNG) based on true boiling points (Pedersen and Christensen, 2007). Each of these components' viscosities are modelled with one of a range of models or correlations, currently Lohrenz-Bray-Clark (Lohrenz *et al.*, 1964), Pedersen's Corresponding States (Pedersen and Christensen, 2007), or Aasberg-Petersen (Aasberg-Petersen *et al*., 1991). However, although these models are established and have been proven to be accurate for black oil systems over many years, the new focus on unconventional oil, such as heavy oil, has necessitated an evaluation of the applicability of these methods to the very complex components that constitute heavy oil, extra heavy oil and bitumen. Many different such evaluations (Hernandez, 2001; Lindeloff *et al.*, 2004; Zéberg-Mikkelsen *et al.,* 2006) have

pointed out that these models are not appropriate for use with heavy oil, and may under-predict heavy oil viscosities by as much as a factor of two.

This section reviews and then compares three methods, Pedersen's Corresponding States method (Pedersen and Christensen, 2007), Assael and Dymond's Hard Sphere model (Dymond *et al.,* 1989, Assael *et al*., 1990) and Allal, Boned and co-workers's Free Volume model (Allal *et al*., 2001), based on long alkane viscosity measurements. The models are tested for accuracy in heavy oil applications, and for ease of use. The Free Volume model parameters are then extrapolated to long normal alkanes, up to C64. Included in this study was an extrapolation of the modified Tait equation (Ciotta, 2010) to C64 components in order to calculate the density. It is acknowledged that only limited experimental data exist for long-chain *n*-alkane viscosities, and the present work was limited by this factor.

5.2 Theory

5.2.1 Viscosity definition

If a shear stress, τ, (pressure-differential) is applied to a confined fluid, the fluid will move. A velocity gradient within the moving fluid, perpendicular to the flow direction, is created, with the highest velocity at the point where the stress is applied. This gradient is caused by inter-molecular forces attractive or repulsive, and friction. The ratio between the stress applied and the velocity gradient is called the viscosity coefficient of the fluid.

$$\tau = \mu \frac{\partial u}{\partial y} \tag{5.1}$$

The higher the gradient, the higher the viscosity, which is an indication of the internal friction between the layers of fluid, causing a resistance to flow. Factors affecting this property include available free space for molecules to move into, molecular shape and entropy, all connected to fluid density, pressure and temperature.

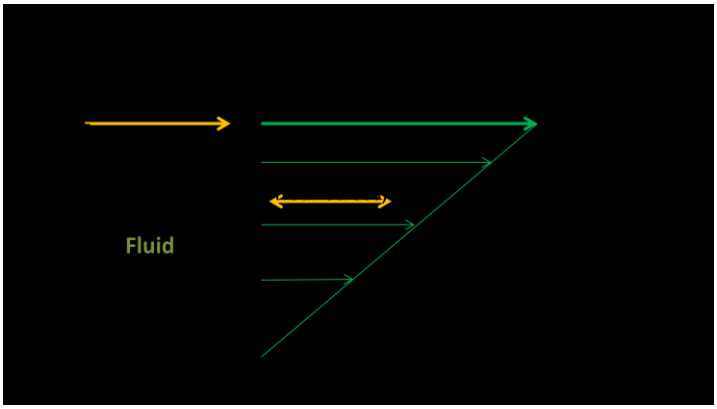


Figure 5.1. Viscosity schematic.

5.2.2 Theory of flow in porous media as applied in simulator

Flow is simulated per component per phase, where a phase could be oil, water and vapour. Vapour could contain gas and steam. At each point in time, a flash calculation determines the phase-status of each component in each cell, determining the composition of the phase. The net flow rate F_{ci} of a hydrocarbon component (Eclipse Technical Description, 2010), or water component, c, from cell i into neighbouring cells, is the sum of the component flow in each of the phases, p, and into (negative) and from (positive) all neighbouring cells, n:

$$F_{ci} = \sum_{n} \mathrm{Y}_{ni} \sum_{p} M_{p}^{c} \cdot dP_{pni} \tag{5.2}$$

and the net flow rate of energy from cell i into/from neighbouring cells n:

$$F_{ei} = \sum_{n} \mathrm{Y}_{ni} \sum_{p} M_{p}^{e} \cdot dP_{pni} \tag{5.3}$$

where, in both equations, Y_{ni} is the transmissibility between neighbouring cells n and i, M^{c}_{p} the generalized mobility of the component c in phase p, M^{e}_{p} the generalized mobility of enthalpy e in phase p, dP_{pni} the pressure difference in phase p between neighbouring cells n and i, and p the phase, which could be any one of gas, oil or water. The assumption is that there is no water in the oil phase, and no hydrocarbon in the water phase. The gas phase can

contain water in vaporised state, as well as hydrocarbon. *C* is the hydrocarbon or water component, where *c* ranges from 1 to *N+1,* (*N* is the total number of hydrocarbon components, or pseudo/grouped components, in the system).

The component mobilities, per component in a phase, and energy mobilities per phase are calculated as follows:

$$M_p^c = x_p^c \cdot k_{rp}(S_p) \cdot \frac{b_p}{\mu_p} \tag{5.4}$$

$$M_p^e = H \cdot k_{rp}(S_p) \cdot \frac{b_p}{\mu_p} \tag{5.5}$$

where k_{rp} the relative permeability of phase p at saturation S_p; b_p is the molar density and μ_p the viscosity of phase p, and x^c_p the molar fraction of component c in the phase p; H_p is the molar enthalpy in phase p.

The gas phase (including the steam vapour) viscosity is determined by the arithmetic average of the component gas-phase viscosities

$$\mu_g = \sum_{c=1}^{N_c+1} y^c \cdot \mu_g^c \tag{5.6}$$

and the oil phase viscosity by a mole-fraction weighted geometric average of the component liquid viscosities

$$\log \mu_o = \sum_{c=1}^{N_c} x^c \cdot \log(\mu_o^c) \tag{5.7}$$

5.3 Pure Component Density

Accuracy in pure component density estimation forms a fundamental part of the accuracy of the component viscosity estimation at any given pressure and temperature. The densities in this work are calculated with the modified Tait Equation, eq. (5.8), as described by Ciotta (2010). He suggested simplified forms for calculating parameters B (MPa) and ρ_0 (density at P_0 = 0.1MPa, in kg/m^3) as functions of temperature, as in eq. (5.9) and eq. (5.10). Based on his experimental research on hexadecane (n-$C_{16}H_{24}$), Ciotta determined the a_i and b_i coefficients for n-$C_{16}H_{24}$, as listed in Table 5.1:

$$\rho = \rho_0 / \left[1 - C log_{10}\left(\frac{B+P}{B+P_0}\right)\right] \tag{5.8}$$

with temperature T in K, C = 0.198 (dimensionless),

$$B = \sum_{i=0}^{2} b_i T^i \tag{5.9}$$

and density at atmospheric pressure (kg/m^3):

$$\rho_0 = \sum_{i=0}^{2} a_i T^i \tag{5.10}$$

Table 5.1. Tait density coefficients (Ciotta, 2010).

a_0	981
a_1	-0.711
a_2	0
b_0	410
b_1	-1.42
b_2	0.0013

During the current research, it was determined that the modified Tait Equation with the Ciotta coefficients resulted in higher accuracy for long alkanes than did the original equation with the Assael coefficients (Assael *et al.,* 2009). Based on our database of long alkane densities, calculated values were sensitive only to the a_0 coefficient. The main goal of this section was to improve accuracy of heavier component density by extrapolating the density coefficients to long alkanes, up to $C_{64}H_{130}$. Using a database consisting of 452 measured data points for long alkane densities (Appendix B.1.), a relationship between the

a_0 coefficient and the number of carbon atoms in the molecule (Cn) has been established by the method described below.

The optimal values of parameter a_0 were obtained by a least-squares fit of the calculated densities to experimentally measured densities for the following long *n*-alkane components, [C17, C20, C22, C24, C28, C30, C32, C40, C44]. The value of a_0 was extended to short-chain *n*-alkanes by incorporating experimental density data of shorter *n*-alkanes [C5-C14]. The a_0 coefficient of C16, as estimated by Ciotta (2010), was assumed fixed. A 6th-order polynomial was fitted to the discrete a_0 values, extrapolating this parameter to produce the full range required from C1 to C64:

$$a0 = \sum_{i=0}^{7} a'_{0i} Cn^{i} \tag{5.11}$$

where the $a_0'_i$ are the coefficients of the polynomial as listed in Table 5.2.

Table 5.2. Density a_0' polynomial coefficients.

i	$a_0'_i$
0	5.45E+02
1	9.44E+01
2	-9.18E+00
3	5.05E-01
4	-1.61E-02
5	2.93E-04
6	-2.82E-06
7	1.12E-08

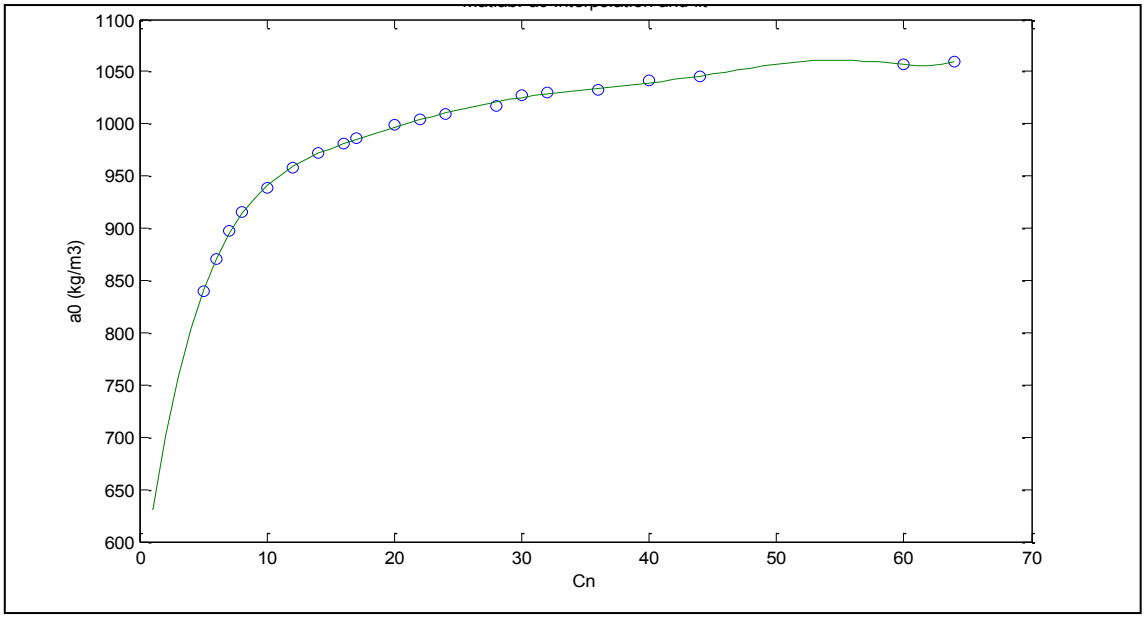


Figure 5.2. Least-squares-fit of refined a_0-values as a function of carbon number (Cn).

Figure 5.2 shows the extrapolated a_0 coefficients *vs*. carbon number (Cn). The green curve in Figure 1 represents (5.4), and the blue circles are the discrete data. A rapid increase in the value of a_0 with Cn can be observed at low Cn values, but at higher values it seems that a plateau is reached.

Figure 5.3 shows the newly calculated densities *vs*. the measured data by Ciotta (2010). The data in the figure follow the two trends of increasing densities with pressure increase, and decreasing densities with increasing temperatures. Each group on the figure represents a number of measurements made at different temperatures at the same pressure (e.g., points 41 to 47 represent densities at P = 80.4 MPa, with increasing temperature). It is clear that the modifications to a_0 had no effect on the C16 densities.

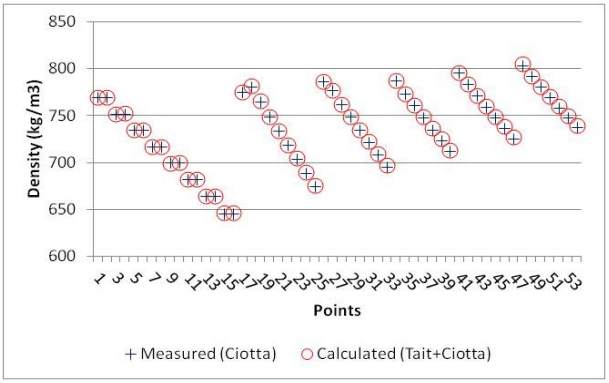


Figure 5.3. C16 Calculated densities *vs.* Ciotta measured densities; (a_0 calculated with (5.4).

Figure 5.4 shows a summary of the AAD (average absolute deviations) between the calculated densities and available measured densities for components C6 to C64 in the pressure range of 1-3 bar and temperature range of 20-200 °C. The newly modified equation predicts with acceptable accuracy (AAD < 3%) the densities of *n*-alkanes up to C64 at pressures < 20,000 psi. For C6, C8 and C16 the deviations to densities of measured at pressures up to 140 MPa (~1400 bar or ~20,000 psi) are also included. The maximum deviation (-3.2%) in this pressure range is in the C6 density measured at 1009 atm and 20 °C (Dymond *et al.,* 1980a).

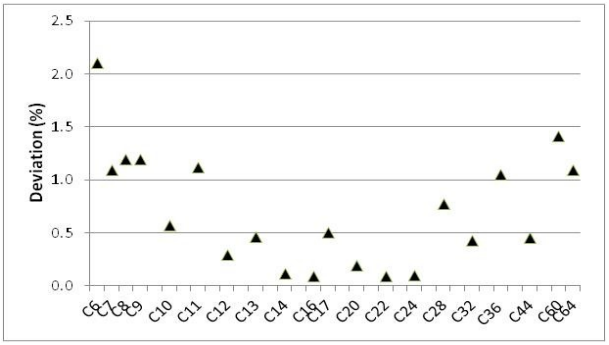


Figure 5.4. AAD[4] in density per component for *P* < 20,000 psi (138 MPa).

[4] Average Absolute Deviation:

$$AAD = \frac{\sum_{i=1}^{N} \left| \frac{(\rho_{i,meas} - \rho_{i,calc})}{\rho_{i,meas}} \right|}{N} \qquad (5.12)$$

Higher deviations, of up to -4.6%, have been observed at very high pressures above 186 MPa (27,000 psi), such as the pressures used by Dymond *et al.* (1981) and Ciotta (2010). A single-point -5.5% deviation was observed for one of the C60 measurements (Assen *et al.,* 1990) at 0.3 MPa and 90 °C, but a suspiciously high deviation in both the viscosity calculations for the same measurement leads to the conclusion that this is an erroneous data point, and has been removed from the dataset. Detailed calculated values and deviation data per component are tabulated in the Appendix B.2.

Overall, low deviations observed on long alkanes validated the new a_0-polynomal as being acceptable for use in all density calculations for the purpose of the viscosity modelling research.

5.4 Oil Viscosity Models: Theory and Equations

Gas viscosity theory is well developed, and mostly incorporates the Chapman-Enskog theory and its assumptions; however, oil viscosity theory is less developed (Reid *et al.,* 1987). Discontinuities between vapour and liquid viscosities of the same pure component exist (for example, Reid *et al.,* (1987)) show that the benzene liquid viscosity near the boiling point (353.4 K) is 36 times that of the benzene vapour viscosity at the same temperature, and it is only at the critical point that all the properties converge. Currently, very few models are capable of modelling complex heavy component viscosities over the full range of required pressures and temperatures for thermal reservoir simulation, and no corresponding states model fully captures the physics of the thermodynamic inter-molecular behaviour at the saturation pressures of complex fluids (Reid *et al.,* 1987). Component liquid viscosities are therefore modelled separately from the component gas viscosities in this study.

Oil viscosity models currently commonly used in the oil industry (PVTi Reference manual, 2010) include the Lohrenz-Bray-Clark Correlation (Lohrenz *et al.,* 1964), the Pedersen Corresponding States Method (Pedersen *et al.,* 1984), the Aasberg-Petersen Model

(Aasberg-Petersen *et al.,* 1991). New available oil viscosity models (Zéberg-Mikkelsen *et al.,* 2006) include:

1. Assael-Dymond Hard Sphere method: (Dymond, 1989; Assael and Dymond *et al.,* 1992) a corresponding states correlation of viscosity of dense fluids as a function of the reduced molar volume and a roughness factor.

2. Free Volume Model (Allal *et al.,* 2001): a free-volume-fraction (where free-volume is the difference between the hard-sphere volume and the molecular volume) based approach to model the viscosity of dense Newtonian fluids. It is connected to the molecular structure of the fluid and takes into account, on a molecular level, friction, potential energy of interaction, and energy barriers to be crossed during diffusion.

3. Frictional Model: (Zéberg-Mikkelsen *et al.,* 2001 This model is based on basic principles of mechanics and thermodynamics, wherein a frictional term is coupled to the van der Waals forces in an EOS model of the fluid.

4. Molecular dynamics viscosity model (Galliero and Boned, 2005): a correlation based on corresponding states principal, using the Lennard-Jones fluid as the reference and based on molecular dynamics simulations.

Three models or methods are evaluated in the current work: the Pedersen Corresponding States method, Assael-Dymond's Hard Sphere model, and Allal and Boned's Free Volume model.

5.4.1 Pedersen Corresponding States method for heavy oil

The Corresponding States method is based on the assumption that if the correct 'reduced' quantities are used, the viscosity of all components for all conditions (P,T) of interest can be generated using the same correlation. In the Pedersen correlation for pure components,

each of the critical properties of the new component, critical temperature (T_{cx}), critical pressure (P_{cx}) and the molecular weight of the component (MW_x) is 'reduced' by taking the ratio of the property to the same critical property of a reference component, usually methane, of which the properties are well defined. A correction factor, α, a function of the reduced density (ρ_r) and the molecular weight of the new component, is introduced when the viscosity of a mixture with heavy components are computed.

$$\frac{\mu_x(P,T)}{\mu_0(P_0,T_0)} = \left(\frac{T_{cx}}{T_{c0}}\right)^{-1/6} \left(\frac{P_{cx}}{P_{c0}}\right)^{2/3} \left(\frac{MW_x}{MW_0}\right)^{1/2} \tag{5.13}$$

In the Pedersen implementation of corresponding states with regard to calculating the viscosity of a pure component, methane is used as a reference fluid, and reduced quantities are defined in terms of the methane critical properties (T_c,P_c) and the viscosity at a 'reduced' (P,T). Equations used during this study were from (Pedersen *et al.,* 2007)[5]:

$$\mu_x(P,T) = \frac{(P_c^*)^{2/3}(MW^*)^{1/2}}{(T_c^*)^{1/6}} \mu_o(P/P_c^*, T/T_c^*) \tag{5.14}$$

where 'o' refers to the reference component (methane) and 'x' to the component under investigation, T_c is the critical temperature, P_c the critical pressure, and P and T the conditions at which component x viscosity is required. The reduced values P_c*, T_c* and MW* are defined as follows:

$$P_c^* = \frac{P_{cx}}{P_{co}}, \quad T_c^* = \frac{T_{cx}}{T_{co}}, \quad MW^* = \frac{MW_x}{MW_o}.$$

Methane viscosity (μ_o) at the adjusted (P',T') = (P/P_c^*,T/T_c^*) was calculated as per Pedersen's extended method[6], shown in eq. (5.15). This extension provides continuity at and below the methane freezing point:

$$\mu_o(\rho', T') = \mu_{o0}(T') + \mu_{o1}(T') + F_1 \Delta\mu_o'(\rho', T') + F_2 \Delta\mu_o''(\rho', T'), \tag{5.15}$$

where

[5] Pedersen, K.S. and Christensen, P.L., 2007. Phase Behaviour of Petroleum Fluids, eq. (10.5), p 199.
[6] Ditto, eqs. (10.29) to (10.32), p. 205.

$$F_1 = \frac{HTAN + 1}{2} \quad \text{and} \quad F_2 = \frac{1 - HTAN}{2},$$

with

$$HTAN = \frac{e^{(\Delta T')} - e^{(-\Delta T')}}{e^{(\Delta T')} + e^{(-\Delta T')}} \quad \text{and} \quad \Delta T' = T' - T_F .$$

In these equations, T_F is the freezing point of methane (91 K). The rest of the terms, μ_o, μ_1 and $\Delta\mu'$, were calculated as described by Pedersen, with the associated constants[7]. No mixture modelling was incorporated.

In order to adapt the Corresponding States model for use with heavy oil mixtures, the reference fluid could be modified. Instead of using methane as the reference fluid, the stabilized crude viscosity could be used (Rønningsen, 1993; Lindeloff *et al*., 2004; Pedersen and Christensen, 2007). In their method, crude oil viscosity is calculated using a semi-log correlation in MW and $1/T$. This procedure was not tested in the present work, since the prediction of the crude oil mixture viscosity, starting from pure components, was the objective here.

5.4.2 Hard Sphere Model

The Assael-Dymond Hard Sphere viscosity model, used to predict the viscosity of fluids with changes in temperature and density, is based on a corresponding states method, assuming the viscosity to be proportional to the smooth hard-sphere viscosity of the fluid. In this method, the reduced viscosity overlays a known universal curve in reduced molar volume, log μ^* *vs*. log V^*. The reduced volume (V^*) is expressed as the ratio between the actual volume (V) and the hard-sphere or core-volume (V_0), as measured at 'zero' density when no inter-molecular forces are involved. The assumption is that smooth-hard-sphere (SHS) behaviour is followed at zero-density when the fluid is highly diluted, and that the

[7] Ditto. Eqs. (10.7) to (10.10); Tables 10.1 and 10.2, pp 199-202.

viscosity (μ_{SHS}) can be calculated based on the Enskog theory. The ratio between experimental viscosities and the SHS viscosities provides the roughness factor, an indication of the non-spherical nature of the molecule.

Once the roughness factor R_μ and V_0 (the volume at zero-density, or the hard-sphere volume with no molecular interaction) had been determined, the coefficients, used to overlay the curve with the universal one, can be calculated. With these known, the viscosity at the conditions of interest can be determined.

This model was first published in 1989 (Dymond and Awan, 1989). Several additional publications followed (Assael *et al.*, 1992a; Assael *et al*., 1992b; Assael *et al*., 1994), which included extensions to different component groups and different associated constants.

Sun and Teja (2009) published a simplification of the model and coefficients in 2009, reducing the number of coefficients required. Assael and co-workers (Assael *et al.,* 2009) responded to the Sun and Teja (2009) paper and verified the simplifications as valid.

The model evaluated was in the form as expressed by Sun and Teja (2009), originally from Assael *et al*. (1992b):

$$\mu^* = C(MRT)^{-0.5}\,\mu(V)^{2/3}, \tag{5.16}$$

with $C = 16(2N_A)^{1/3}\pi^{1/2}/5 = 6.035\times10^8$, where N_A is Avodrago's number (6.02214×10^{23}/mole). In (5.16) μ^* is the reduced viscosity, M is the molecular weight (kg/mole), V is the molar volume (m^3/mole) at the required pressure and temperature (P,T), μ is the viscosity (Pa s), T is the temperature in K, R_μ is the roughness factor, depending on molecular chain-length, and R the universal gas constant, equal to 8.31451 (J/mole K). The following equation was used for the universal curve fit:

$$\log_{10}\frac{\mu^*}{R_\mu} = \sum a_{\mu,i}\left(\frac{1}{V^*}\right)^i \tag{5.17}$$

where V^* is the reduced molar volume, (V/V_0), $V_0$is the zero-density molar-volume (dilute gas or hard-sphere volume),and $a_{\mu,i}$ are the reduced viscosity coefficients as tabulated in Table 5.3 (Ciotta, 2010). These coefficients are independent of chemical structure, and valid for conditions where the reduced volumes are within the range $1.5 \leq V^* \leq 5$.

Table 5.3. Hard Sphere reduced viscosity coefficients.

i	$a_{\mu,i}$
0	1.095
1	-9.26
2	71.04
3	-301.90
4	797.69
5	-1221.98
6	987.56
7	−319.46

In the present work, the above reduced viscosity coefficients have been used, together with expressions for V_0 and R_μ from Sun and Teja (2009), as below. The density was determined as described in eqs. (5.8) to (5.10) as input for the volume at the required conditions.

To calculate the molar volume at zero-density as a function of the hydrocarbon length (C_n) and the temperature (T), the following correlation was used from Sun and Teja (2009):

$$10^5 V_0 = (0.85501 + 0.39526 C_n) + (3.162 C_n^{1.17694}) / T^{0.3} . \quad (5.18)$$

The roughness factor for non-smooth spheres was determined from the Sun and Teja (2009) as follows:

$$R_\mu = 1.0055 + 0.0472 C_n . \quad (5.19)$$

5.4.3 Free Volume Model

The Free Volume theory is now reviewed in more detail, as this model was selected for further research, applying it to heavy oil viscosity modelling. It becomes clear that many

different physical phenomena are incorporated into this model, when the history and theory thereof is further explored.

The Free Volume model applied in this work, and as described by Allal *et al*. (2001), has its origins in the Eyring theory (Glasstone *et al*., 1941) and the Andrade/Arrhenius type equation, $\mu = Ae^{B/T}$. The concept of a liquid's resistance to flow being dependent on the free, available space for molecules to move into, was used by Doolittle (1951) to develop an empirical relationship to determine liquid viscosity as $\mu = Ae^{B/f_v}$, where f_v, the free volume fraction, is defined by $f_v = v_f/v_0 = (v\text{-}v_0)/v_0$, with v_f being the specific volume of free-space defined per mass of liquid at any temperature, v_0 the specific volume of liquid extrapolated to absolute zero without change of phase, and v the specific volume of liquid at any temperature. Doolittle (1951) defined the 'free space' concept as 'that space seemingly arising from the total thermal expansion of the liquid without change of phase. Relative free-space is therefore the fractional increase in volume resulting from expansion'. This concept also leads to the idea that resistance to flow depends on the relative number of molecules available for flow, compared to the space available to flow into. The theory, which forms the basis of the free volume model used in this work, was originally developed by Cohen and Turnbull (1959) and assumes molecular hard spheres (cores), with some 'free volume' for movement associated with it. They defined the free volume to be the 'cage' volume of a molecule minus the hard-sphere volume, and expanded the free-volume concept to incorporate diffusion, pressure, and temperature, justifying Doolittle's formula at constant temperature, with B the characteristic of the free-volume overlap.

Allal *et al*. (2000) developed a free-volume based model for Newtonian fluids that incorporated the pressure-temperature effects on viscosity, and, additionally, connected the molecular structure to the viscosity via the free-volume. The theory of diffusion of molecules provided further basis to their model. In their approach the viscosity is the product of the fluid modulus and the mean relaxation time, which in turn becomes a function of density, molecular weight, temperature and average time for a molecule to change its configuration (τ_H), when a combination of the dumbbell model (molecular structure), Stokes's Law and the spring force (friction) is applied. This stabilization time

(τ_H), called the characteristic relaxation time, is related to friction and the process of molecular diffusion, as well as the size of the molecule (the average quadratic length b^2, in the spring).

Allal *et al*. (2000) showed that in a generalised dumbbell model, and with integration of the relaxation function, the viscosity becomes

$$\mu = \frac{\rho N_a L^2 \xi}{M}, \tag{5.20}$$

where L represents an average quadratic length, which, in the case of a linear molecule, is $L^2 = b^2/12$, and for a spherical molecule $L^2 = 3\langle r^2\rangle/5$. For a Gaussian molecule, $L^2 = \langle r^2\rangle N/36$, where $\langle r^2\rangle$ is the mean quadratic end-to-end distance of the molecule, and b^2 the average quadratic length of the spring as before. The friction coefficient ξ represents mobility and diffusion in the equation. Allal *et al.* (1996) used Nechitailo's (1991) expression of the free volume v_f,

$$v_f = \left(\frac{4k_B T}{k_s}\right)^{3/2},$$

where k_s is the stiffness of the background in the dumbbell model, defined by $k_s = 2E/(N_a b_d^2)$, and assumed that the molecule is in such a state that the molecular potential energy of interaction with its neighbours is E/N_a, with the mean displacement of the molecule, b_d, defined such that the hard-core-volume is given by $v_0 = b_d^3$. In this case, the stiffness becomes $k_s = (1/2)k_s b_d^2 = (E/N_a)$, which gives the free volume as a function of the hard-core volume, temperature and energy: $v_f = b_d^3(2RT/E)^{3/2}$. They then wrote the free volume fraction f_v as a function of internal energy E, which was then expanded to eq. (5.21) by Allal *et al.* (2000):

$$f_v = \frac{v_f}{v_0} = \left(\frac{2RT}{E}\right)^{3/2} = \left(\frac{2RT}{E_0 + PM/\rho}\right)^{3/2}. \tag{5.21}$$

Eq. (5.21) takes into account that the total internal energy could be expressed as $E=E_0 + PN_a v$ (where v is the total volume occupied by one molecule, hard-core plus free volume $(1/\rho)$) or $E = E_0 + PV$, where E_0 is associated with a barrier energy the molecule needs to

overcome in order to diffuse, and PV is the additional thermodynamic energy provided by pressure and temperature. To include friction, they combined the Doolittle equation and eq. (5.20), and, with the friction coefficient written as $\xi = \xi_0 \exp(B/f_v)$, the viscosity was expressed as

$$\mu = N_a \rho \frac{L^2}{M} \xi_0 \exp(B/f_v), \tag{5.22}$$

where ξ_0 is friction at zero density, *i.e.,* at very high free volume (as at very high temperatures). Allal (Allal *et al*., 1996) has shown that the total energy per molecule is equal to the product of the friction at zero density (ξ_0), the average molecular volume ($\bar{v}$) and the dissipation length b_f. Based on their assumption that all thermal energy of activation is transformed into kinetic energy and the average molecular volume is $\bar{v}^2 = 3RT/M$, they developed the following equation for friction at zero density:

$$\xi_0 = \frac{E}{N_a b_f} \sqrt{\frac{M}{3RT}}. \tag{5.23}$$

Again assuming that the total energy E is given by an internal energy term E_0 (in this case connected to the reaction barrier energy) plus a mechanical energy term, PV or PM/ρ, and the ratio of L^2 (average quadratic length of molecule) to b_f (dissipation length of order $v^{1/3}$) is defined as the characteristic length l_m, their final equation was obtained:

$$\mu = \frac{\rho l_m [(E_0 + (PM/\rho)]}{\sqrt{3RTM}} \exp\left[B \left(\frac{E_0 + (PM/\rho)}{2RT} \right)^{3/2} \right], \tag{5.24}$$

where μ is the viscosity (Pa s), ρ is the density (kg/m^3), P is the pressure (MPa), M is the molecular weight (kg/mole), R is the universal gas constant (8.31451 J/mole K), T is the temperature (K), E_0 is the the energy associated with the molecular activation energy barrier (J/mole), l_m is associated with a molecular characteristic length, where $l_m = L^2/b_f$ (Å), and B is associated with the free volume overlap (dimensionless). The parameters l_m, E_0 and B are characteristic of a molecule.

The parameter l_m decreases with increase of chain length of molecule, representative of the decrease in available volume for molecule to move into, while E_0 increases with chain length, representing the increased barrier energy associated with longer molecules and/or increase in internal energy associated with the heavier molecules. The parameter B decreases with chain length, as free volume overlap decreases.

The model has been tested during various comparison studies (Boned *et al.,* 2003; Zéberg-Mikkelsen *et al.,* 2004, Zéberg-Mikkelsen *et al.,* 2006) and provided the most accurate results (AAD < 10%) plus continuity between gas, liquid and dense liquids. In the present study the model in eq. (5.24) has been applied to long-chain alkanes up to C64. Coefficients (l_m, E_0 and B) for C1 to C10, C12, C14 and C16 from Allal *et al*. (2000) had been assumed fixed, and used as basis for extrapolations to C64. Density was calculated with the aforementioned modifications to the Tait equation, as specified in eqs. (5.8) to (5.10).

5.5 Heavy Oil: Free Volume Model Extrapolation to Long-chain *n*-Alkanes

This section of the research was focused on the Free Volume viscosity model for prediction of viscosity of long-chain *n*-alkanes. The aim was to find the most accurate way of predicting the viscosity of pure and pseudo-pure components to represent the heavy oil in simulations. The Free Volume model, as presented by Allal *et al.* (2000) contained relevant parameter estimations (l_m, E_0 and B) for components up to C16. The present contribution is to extend this up to C64, through optimisation in cases where measured data exist, and fitting polynomials, using a least-squares method, to discrete available data for long-chain *n*-alkanes C17, C20, C22, C24, C28, C32, C44, C60, C64. The viscosity data measurements used in this study are listed in Table 5.4, with a total of 264 data points. The complete list of available data and references is detailed in Appendix B.1., including reasons for exclusion.

Table 5.4. Viscosity and density measurements for *n*-alkanes C5 to C64, used in this study.

Cn	Reference	# Data points	*P* Range (MPa)	*T* range (K)
6	Dymond *et al.,* 1980 (II)	37	0.1 - 419	298 – 373
7	Doolittle *et al.,* 1951	4	0.1	263.15 - 373.15
8	Dymond *et al.,* 1981 (III)	41	0.1 - 505	298.15 -373.15
8	Doolittle *et al.,* 1951	4	0.1	263.15 -373.15
9	Doolittle *et al.,* 1951	5	0.1	263.15 -423.15
10	Quiemada *et al.,* 2005	6	0.1	293 – 343
11	Doolittle *et al.,* 1951	6	0.1	263.15 - 473.15
12	Giller *et al.,* 1949	11	0.1	262.15 - 293.15
12	Dymond *et al.,* 1981 (III)	32	0.1 - 501.6	298-373
14	Giller *et al.,* 1949	10	1	277.65 - 293.15
16	Ciotta, 2010	54	1 - 101	298 – 473
17	Doolittle *et al.,* 1951	7	0.1	293.15 - 573.15
20	Quiemada *et al.,* 2005	4	0.1	313 – 343
22	Quiemada *et al.,* 2005	3	0.1	323 – 343
24	Wakefield *et al.,* 1988a	3	0.1	318 – 338
24	Quiemada *et al.,* 2005	2	0.1	333 – 343
28	Doolittle *et al.,* 1951	7	0.1	293.15 - 573.15
32	Aasen *et al.,* 1990	8	0.3	353.15 - 473.15
36	Doolittle *et al.,* 1951	5	0.1	323.15 -573.15
44	Aasen *et al.,* 1990	5	0.3	369.15 - 473.15
60	Aasen *et al.,* 1990	5	0.3	407.15 -466.15
64	Doolittle *et al.,* 1951	5	0.1	323.15 - 573.15

5.5.1 Polynomial fitting[8] of Free Volume Model coefficients

5.5.1.1 Methodology

The objective of this part of the study was to use existing, published, values of the three molecular characteristic parameters (l_m, E_0 and B) to find a first-pass least-squares polynomial fit for interpolation and extrapolation to cover the full range of *n*-alkanes from C1 to C64. Published values existed for the following pure *n*-alkanes: C1-C10, C12, C14, C16 (Allal *et al.,* 2000). Refinement of the parameter extrapolations were done by optimisation of a least-squares fit to additional 'control' points, where the new control-points were obtained in the following manner: The first-pass extrapolated values were used as first-guess-input to optimise l_m, E_0 and B values for C22, C32 and C44, individually, in matching the measured viscosity data for these components, after which the new optimised parameters were used as control points in refining the extrapolation polynomial. The method is analogous to history matching production data in oil reservoirs in order to refine the numerical model, using certain uncertainty parameters. In this instance the uncertainty parameters consisted of the three parameters l_m, E_0 and B. A few iterations, plus extending the 'training' data to include C17, C20, C28, C36 and C44 led to the final polynomials and coefficients for each of the three parameters, l_m, E_0 and B.

Figure 5.5 shows the discrete data values (open circles) for each of the three parameters on the left as a function of the molecular weight (*MW*), an indication of carbon number or chain length, Cn, in *n*-alkanes. A polynomial was fitted (solid line) to obtain the Free Volume fitting coefficients as a function of molecular weight. These coefficients were applied to a refined and extrapolated dataset of the molecular weights (*MW*) of *n*-alkanes up to C64, as seen on the right panel in Figure 5.5.

[8] Matlab V 7.12.0.635 (R2011a)

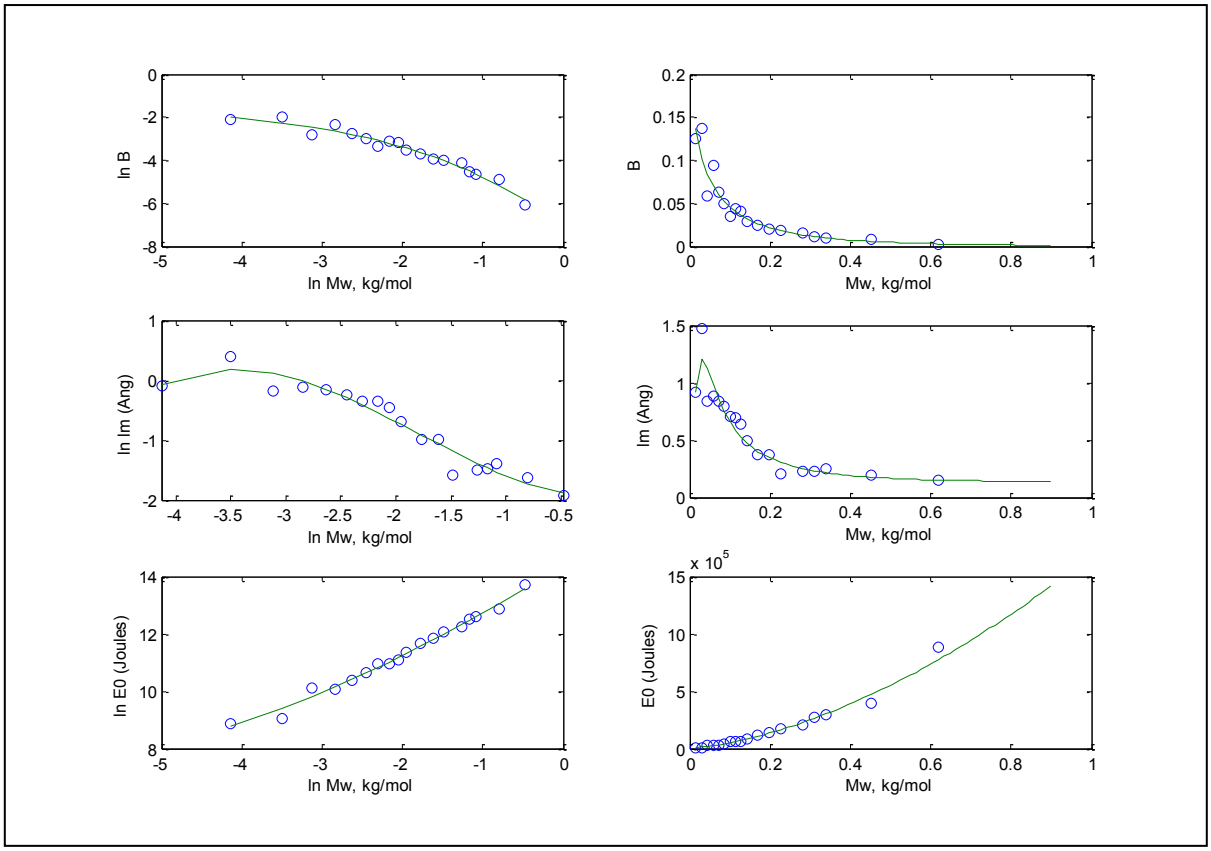


Figure 5.5. Discrete fitting on left panel, with interpolation and extrapolation on the right.

It can be observed that l_m and B decreases with increase in molecular weight (Mw), while E_0 increases, as more energy is required for a molecule to break intermolecular bonds.

A 3rd-order polynomial used in the refined and extrapolated fitting and was of the form

$$\ln y = \sum_{i=0}^{3} a_i (\ln(MW))^i \,, \tag{5.25}$$

where y represents either l_m, E_0 or B, and MW is the molecular weight of the pure component in kg/mol. Table 5.5 shows the corresponding coefficients of the refined and extrapolated polynomial (eq. (5.25)).

Table 5.5. Coefficients of fitted polynomials: first iteration.

	l_m Coeff	E_0 Coeff	B Coeff
a0	-1.94563	14.33364	-7.07178
a1	0.15397	1.629365	-2.83202
a2	0.61720	0.021786	-0.58952
a3	0.11393	-0.011391	-0.0489

A high number of decimal places has been maintained, due to the high sensitivity of the computed parameters to these coefficients.

5.5.1.2 Accuracy in Viscosity Predictions, using the 'first-guess' Values

Table 5.6 shows the deviations in the calculated viscosities from the measured published values, using the first-guess extrapolation of the Free Volume parameters. All of the measurements are at 1 bar, except those for C32 and C44, which were at a pressure of 3 bar. Temperatures varied between 300 K and 573 K (25 to 400 °C). It can be observed that the optimized values gave better results in most cases, except C28 and C36 where maximum absolute deviations were above 20%.

Table 5.6. Evaluation of the 'first-guess' parameters (left) *vs.* the optimized values (right): Free Volume viscosity-deviations.

Comp	'First guess' Free Volume parameters		Optimized Free Volume parameters	
	AAD (%)	MAD[9] (%)	AAD (%)	MAD (%)
C17	4.26	8.21	4.73	8.82
C20	10.56	15.57	2.89	6.52
C22	6.52	7.84	1.57	3.31
C24	1.48	1.87	0.43	0.82
C28	6.22	12.84	11.85	26.55
C32	12.81	18.38	6.47	8.60
C36	7.37	14.34	14.87	31.68
C44	5.56	9.47	4.43	8.20
Average	14.06	17.60	5.91	9.15

Further adjustment of the *B* parameter was performed for C28, C32 and C36. Figure 5.6 and Figure 5.7 show the measured *vs.* calculated viscosities for C32 and C36, compared to the values computed with *B* adjusted manually.

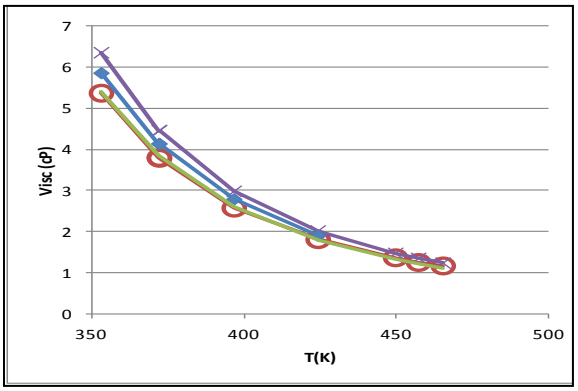


Figure 5.6. C32 measured *vs.* calculated viscosities. Measured values in red, Free Volume, using first-guess coefficients in purple, Free Volume with optimized values in blue, Free Volume with further adjustments in *B* in green.

[9] $MAD = \max\left|\frac{100\times(measured - calculated)}{measured}\right|$

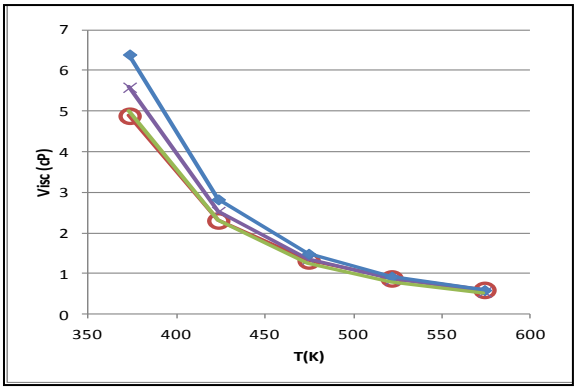


Figure 5.7. C36 measured *vs.* calculated viscosities. Measured values in red, Free Volume, using first-guess coefficients in purple, Free Volume with optimized values in blue, Free Volume with further adjustments in *B* in green.

It is clear from these figures that it is possible to obtain very accurate viscosity values relatively easily, by adjusting one or all three parameters in the Free Volume Model. During fitting to measured data, one would optimise E_0 first to get the energy at low temperatures correct, as the viscosities are most sensitive to this parameter. Parameter E_0 is linked to different types of energy in different publications, but appears to be related to either the internal energy of the molecule, or the 'barrier' energy of activation, which is the energy necessary to break the initial bonds with neighbouring molecules. However, the actual physical meaning of this parameter gets lost when linked to the dimensionless B parameter, which is associated with the free volume overlap, but in reality basically used as a fitting coefficient. The parameter B was used to control the slope of the curve *vs*. temperature, and l_m was used to control the vertical position of the curve. The parameter E_0 influenced both the slope and the position, with a stronger influence on the position. Freedom of variation of all three parameters were limited by imposing rules for E_0 to increase monotonically, and l_m and B to decrease monotonically with increase in molecular weight.

Once a good fit was obtained for the selected long-chain *n*-alkanes, where measured viscosity data existed, the newly determined Free Volume parameters for these components were added to the 'control' data in the extrapolation polynomial. A fit was acceptable when it resulted in an AAD of 5% and less, a MAD of less than 15%. Table 5.7 shows the Free Volume calculated viscosity deviation data for these components.

Table 5.7. Free Volume calculated viscosity deviations for control points.

Comp	Temp(K):	Ref *P* (atm):	Calculated Density (kg/m^3):	Measured Viscosity (cP)	Free Volume Viscosity Deviations		
					Rel Dev (%)	AAD (%)	Max Abs Dev (%)
C17	300.15	0.987	772.0	3.526	4.31	4.73	8.82
	323.15	0.987	755.7	2.170	8.82		
	372.86	0.987	720.3	1.022	8.69		
	423.12	0.987	684.6	0.599	4.65		
	474.41	0.987	648.1	0.390	1.61		
	521.61	0.987	614.6	0.281	-0.30		
C20	313.2	0.987	774.2	4.01	-6.52	2.89	6.52
	323.2	0.987	767.1	3.2	-3.58		
	333.2	0.987	760.0	2.61	-1.43		
	343.2	0.987	752.9	2.17	0.03		
C22	323.2	0.987	774.1	4.128	-3.31	1.57	3.31
	333.2	0.987	767.0	3.342	-1.41		
	343.2	0.987	759.9	2.754	0.00		
C24	333.2	0.987	773.4	4.48	-0.82	0.43	0.82
	343.2	0.987	766.3	3.67	0.05		
C28	372.58	0.987	756.2	2.898	4.34	5.41	9.79
	423.07	0.987	720.3	1.4615	0.99		
	474.57	0.987	683.6	0.8743	-4.10		
	521.47	0.987	650.3	0.5994	-7.80		
	573.81	0.987	613.1	0.4156	-9.79		
C32	353.11	2.96	777.8	5.368	0.65	2.11	4.79
	372.1	2.96	764.3	3.805	0.93		
	372.16	2.96	764.3	3.785	1.36		
	396.69	2.96	746.9	2.574	1.19		
	424.25	2.96	727.4	1.808	-1.20		
	449.69	2.96	709.3	1.366	-3.55		
	457.22	2.96	704.0	1.252	-3.18		
	465.3	2.96	698.3	1.168	-4.79		
C36	373.06	0.987	768.9	4.892	2.37	6.01	12.75
	423.16	0.987	733.3	2.315	-0.07		
	474.19	0.987	697.0	1.3309	-5.28		

Comp	Temp(K):	Ref *P* (atm):	Calculated Density (kg/m^3):	Measured Viscosity (cP)	Free Volume Viscosity Deviations		
					Rel Dev (%)	AAD (%)	Max Abs Dev (%)
	521.09	0.987	663.7	0.8889	-9.56		
	573.54	0.987	626.4	0.6068	-12.75		
C44	368.37	2.96	784.1	8.338	4.80	4.43	8.20
	398.88	2.96	762.5	4.696	8.20		
	424.96	2.96	744.0	3.232	5.87		
	447.5	2.96	728.0	2.452	3.24		
	473.1	2.96	709.9	1.865	0.03		
Average						3.45	6.87

It can be observed that the average AAD in the Free Volume calculated viscosities for these components was 3.45%, and average MAD 6.87%. The three Free Volume parameters of these components were added to the parameter extrapolation procedure as control points.

5.5.1.3 Final Iteration Equations Coefficients

Once all the control data have been determined, a final extrapolation of each of the three parameters has been performed by a least-squares-fitting procedure to the 'known' parameters, or 'control' points. The final extrapolation polynomial consisted of eq. (5.25), with the coefficients as listed in Table 5.8, for each of the Free Volume parameters.

Table 5.8. Coefficients of extrapolation polynomials: final iteration which included C17, C28, C36 and C44 parameters, optimised.

	l_m Coeff	E_0 Coeff	B Coeff
a0	-1.8796	14.3927	-7.0877
a1	0.2527	1.7095	-2.8359
a2	0.6607	0.05586	-0.58557
a3	0.1197	-0.00698	-0.0479

Figure 5.8 shows the final polynomial-fittings for each of the three Free Volume parameters.

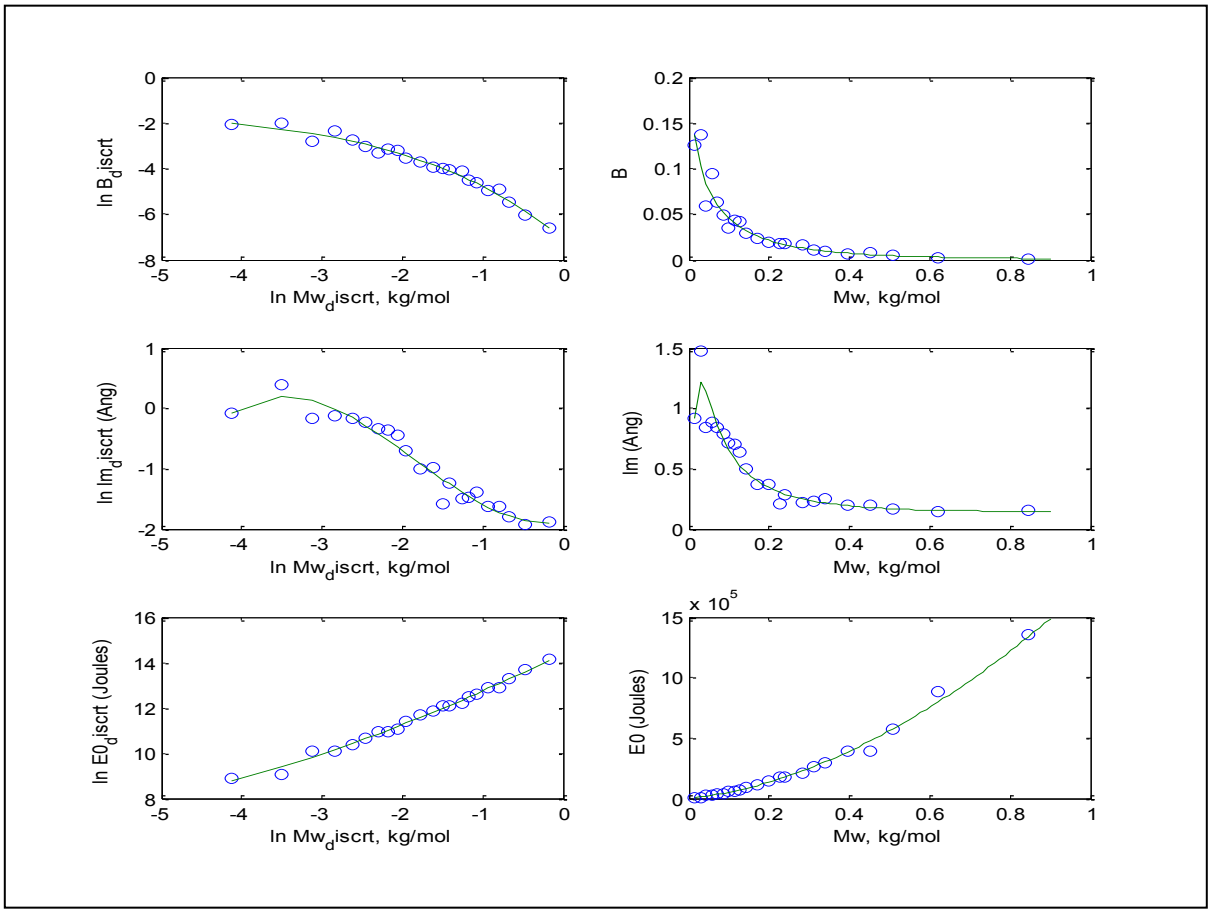


Figure 5.8. Final Free Volume parameter polynomials, based on control points for C17, C28, C36 and C44.

5.5.2 Final Free Volume parameters for all pure *n*-alkanes up to C64

The final values for the three parameters for C1 to C64 are shown below in Figure 5.9 to Figure 5.11, and Table 5.9. Some deviations from the smooth curves can be observed where previously published component-specific parameters (Allal *et al*., 2000) were honoured.

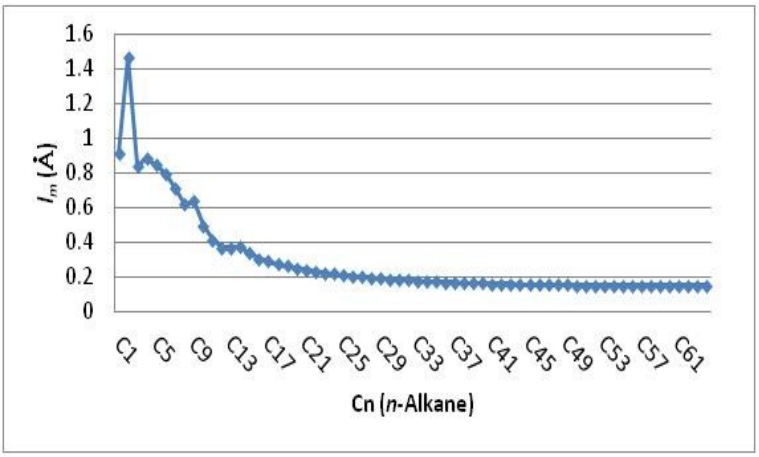


Figure 5.9. Final range of l_m values as a function of Cn extrapolated to C64.

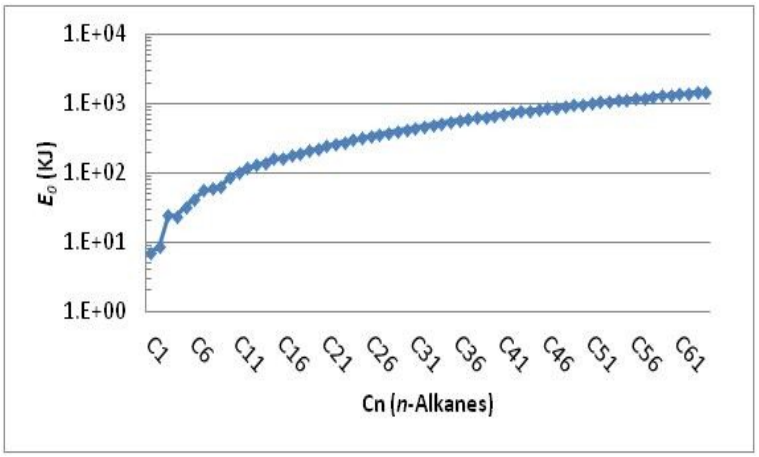


Figure 5.10. Final range of E_0 values as a function of Cn extrapolated to C64.

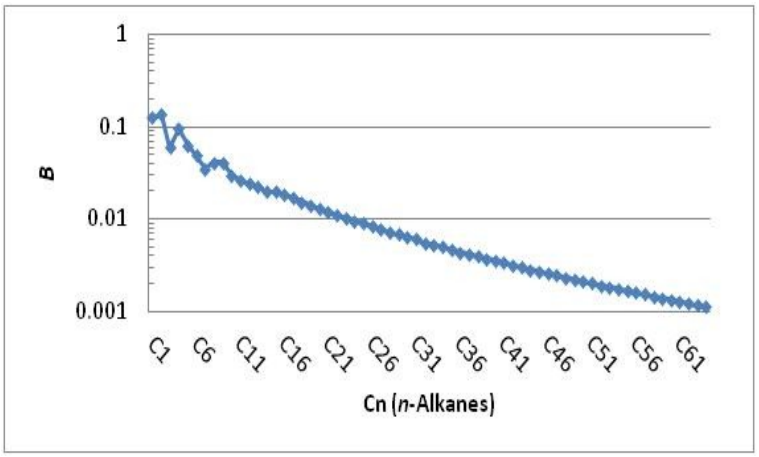


Figure 5.11. Final range of B values as a function of Cn extrapolated to C64.

Table 5.9 contains the values of l_m (Å), E_0 (J/mole) and B for all *n*-alkanes from C1 to C64. Parameter values for lighter components, C2, C3, C4, C5, C7, C9 and C14, are from Allal

et al., 2001a. The parameter numbers are shown with a high order of significant numbers due to the very high sensitivity the viscosities exhibited towards each of these parameters.

Table 5.9. Final Free Volume parameters for *n*-alkanes up to C64.

Comp data		Final Free Volume Parameters		
Cn	***MW***			
	(x10^{-3} kg/mole)	**l_m (Å)**	**E_0 (J/mole)**	***B* (dimless)**
C1	16.04	0.912704	7075.999	0.1255726
C2	30.07	1.469586	8623.474	0.1364979
C3	44.10	0.842437	24577.727	0.0589878
C4	58.12	0.882164	23615.299	0.0944296
C5	72.15	0.844084	32747.847	0.0627691
C6	86.18	0.790793	41979.528	0.0492035
C7	100.21	0.710398	56508.036	0.0352772
C8	114.23	0.616968	59565.1464	0.040578507
C9	128.30	0.636363	64586.668	0.0412388
C10	142.28	0.495906	86965.542	0.0295993
C11	156.31	0.411637	103967.678	0.026763934
C12	170.34	0.369264	116003.825	0.0239963
C13	184.37	0.369757	131164.625	0.022636616
C14	198.39	0.372467	141885.634	0.01958
C15	212.42	0.337235	160153.953	0.019602257
C16	226.00	0.304272	165980.3	0.018124
C17	240.50	0.288085	178304.395	0.017195
C18	254.50	0.273875	194050.768	0.015287
C19	268.50	0.261336	210559.569	0.014087
C20	282.56	0.250217	227725.838	0.012748
C21	296.57	0.240315	245244.967	0.012035
C22	310.60	0.231463	263512.658	0.010905
C23	324.60	0.223522	282124.894	0.010356
C24	338.65	0.216375	301577.902	0.00957
C25	352.68	0.209925	321168.136	0.008969
C26	366.71	0.204089	341492.248	0.008364
C27	380.73	0.198797	362347.076	0.007811
C28	394.76	0.192988	384429.621	0.007130786
C29	408.79	0.189612	405637.04	0.006838
C30	422.81	0.185623	428066.625	0.00641
C31	436.84	0.181982	451015.799	0.006015
C32	450.87	0.179656	473982.101	0.0054292
C33	464.89	0.175616	498463.18	0.005313
C34	478.92	0.172835	522956.784	0.005001

Comp data		Final Free Volume Parameters		
Cn	***MW***			
	(x10^{-3} kg/mole)	***l_m* (Å)**	***E_0* (J/mole)**	***B* (dimless)**
C35	492.95	0.17029	547960.756	0.004711
C36	506.97	0.166962	574073.027	0.00431648
C37	521.00	0.165832	599491.605	0.004193
C38	535.03	0.163885	626014.579	0.00396
C39	549.00	0.162106	653040.104	0.003744
C40	563.08	0.160483	680566.405	0.003542
C41	577.00	0.159004	708591.767	0.003353
C42	591.13	0.157659	737114.535	0.003177
C43	605.16	0.156438	766133.108	0.003012
C44	619.19	0.155334	797445.937	0.002838
C45	633.21	0.154338	825651.524	0.002713
C46	647.22	0.153445	856148.414	0.002577
C47	661.24	0.152647	887135.2	0.00245
C48	675.27	0.151939	918610.513	0.00233
C49	689.30	0.151317	950573.025	0.002218
C50	703.32	0.150774	983021.447	0.002112
C51	717.35	0.150307	1015954.52	0.002012
C52	731.38	0.149912	1049371.03	0.001918
C53	745.40	0.149585	1083269.78	0.001829
C54	759.43	0.149324	1117649.62	0.001745
C55	773.46	0.149124	1152509.42	0.001666
C56	787.49	0.148983	1187848.08	0.001591
C57	801.51	0.148899	1223664.52	0.001521
C58	815.54	0.148868	1259957.7	0.001454
C59	829.57	0.14889	1296726.59	0.00139
C60	843.61	0.148961	1333970.2	0.00133
C61	857.62	0.14908	1371687.54	0.001274
C62	871.65	0.149246	1409877.67	0.00122
C63	885.67	0.149455	1448539.65	0.001168
C64	899.70	0.149708	1487672.56	0.00112

5.5.3 Free Volume model application to C16 at high pressures

The results of the application of the Free Volume Model to obtain the viscosity of C16 at high pressures (Ciotta, 2010), matched well with the measured values. Both the published values for the three fitting parameters (l_m, E_0 and B) as well as the optimised values, based on the polynomial fit as described above, gave good results, with the original published values resulting in an AAD of 9.5% and the optimised values from the present work resulting in an AAD of 4.7%. In the former case the MAD is 26%, and in the latter it is 11%. The final optimisation was achieved by adjusting E_0 only. Table 5.10 shows the original values from Allal *et al.* (2000), with the values predicted by the polynomial and the final optimised values. The viscosities are very sensitive to the value of E_0.

Table 5.10. C16 Free Volume parameters.

l_m (Å)	E_o (J/mole)	B	Origin
0.204931	177467.853	0.01781	Original Published Values
0.304272	162725.8076	0.018124	Polynomial Prediction
0.304272	165980.3237	0.018124	Predicted E_0 Optimized

Figure 5.12 to Figure 5.15 show the comparison between the calculated viscosities using the parameters of Table 5.10, compared with the C16 Ciotta-measured values. Different pressure ranges are shown separately. It is clear that the match is slightly less accurate at higher pressures, and the optimised parameters were selected such that a slight over-prediction of the viscosity values occurs. This is a conservative approach and preferable in terms of ultimate recovery predictions of heavy oil. Care has also been taken that the higher viscosities at the lower temperatures are most accurate, as simulation recovery results are more sensitive to errors in these values. It has also been assumed that heavy oil reservoirs would not experience pressures above 9000 psi.

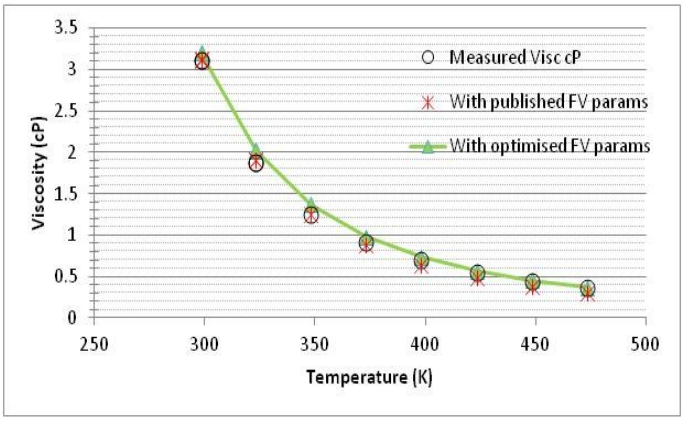


Figure 5.12. C16 viscosities Free Volume fit (green) at low pressures (*P*<200 psi).

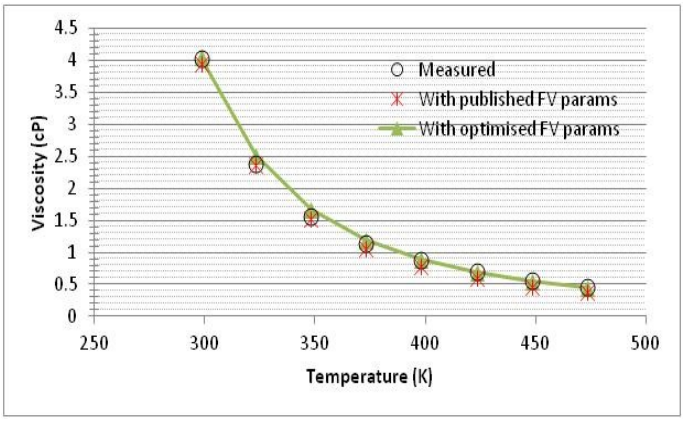


Figure 5.13. C16 viscosities Free Volume fit (green) at *P* = 3000 psi.

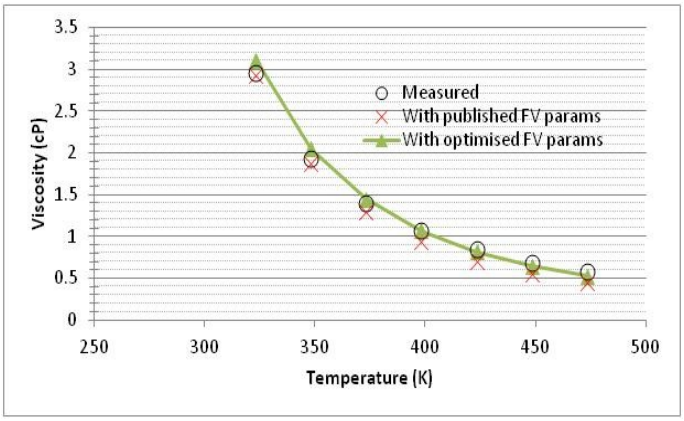


Figure 5.14. C16 Viscosity Free Volume fits at *P* = 6000 psi.

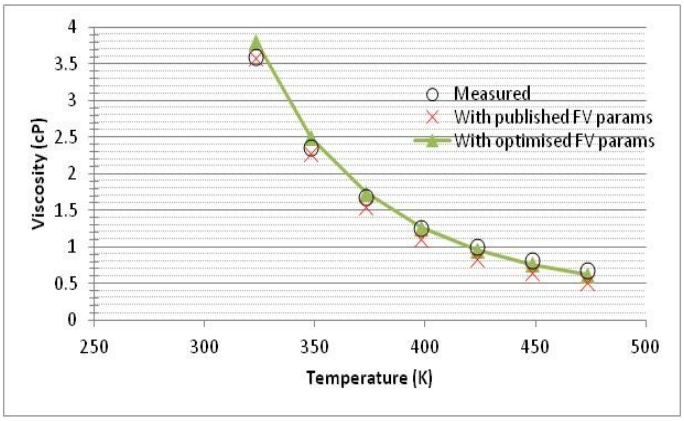


Figure 5.15. C16 viscosity Free Volume fits at *P* = 8700 psi.

Figure 5.16 shows the fit obtained for the very long-chain *n*-alkanes, C60, using the Free Volume model with the parameters listed in Table 5.10.

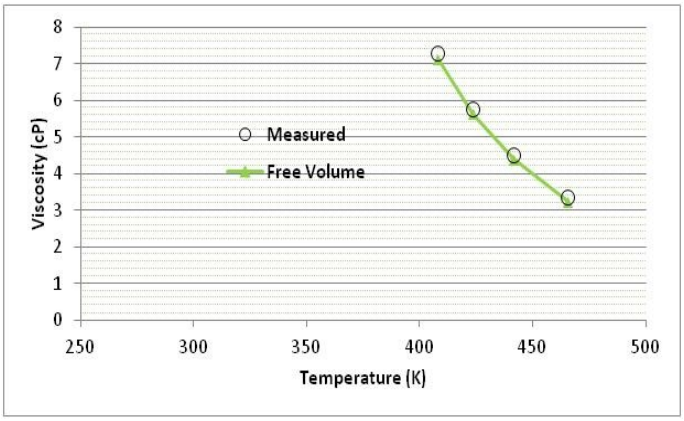


Figure 5.16. C60 viscosity Free Volume fits at *P* = 2.98 atm.

It is clear that the Free Volume model with the extrapolated parameters give accurate results for C60, with an AAD of 2.4%. The parameter extrapolations to C60 are, however, based on very limited measured viscosity data, and only available at higher temperatures, above 100 °C.

5.6 Comparative Study on Oil Viscosity Models

In order to find the most accurate viscosity model for heavy oil, currently available, three models were applied to the data in Table 5.4: Corresponding States, Hard Sphere and Free Volume. The modified Tait Equation with the newly extrapolated coefficients (a_0 only) has been used in all calculations of densities.

In general both the Sun and Teja version of the Hard Sphere model, as well as the Free Volume model were easily extrapolated to a maximum of C64 within the pressure and temperature ranges that can be expected in petroleum heavy oil reservoirs exploited using steam injection. It was not possible to extrapolate the Pedersen Corresponding States model, with liquid methane as reference, due to the transformed conditions (eq. (5.7)) required, which translated into methane being in a gas phase. Instead, the predicted viscosity values from three popular viscosity models, Pedersen Corresponding States, Lohrenz-Bray-Clark correlation (Lohrenz *et al*., 1964) and Aasberg-Petersen Corresponding States (Aasberg-Petersen *et al*., 1991), as implemented in industry standard software (SIS PVTi V2010.1; CMG WinProp V2010.10), have been included in the comparisons. The results from some of the long-chain alkanes, C10 (Wakefield, 1988b), C16 (Ciotta, 2010) measurements at pressures between 150 and 10,000 psi, C24 (Wakefield *et al*., 1988a; Queimada *et al*., 2005), C28 (Doolittle, 1951), C32 and C44 (Assen *et al*., 1990), are shown in Table 5.11 and Table 5.12. Table 5.11 shows the results for the un-tuned industry methods, Pedersen (PED), Lohrenz-Bray-Clark (LBC) and Aasberg-Petersen (AP). The data were limited to components up to C44 due to the limitation of available library components in the software. More detailed results are available in Appendix B.2.

Table 5.11. Long-chain *n*-alkane viscosity deviation results for industry methods.

Cn	*MW* (kg/mole)	Conditions		Measured data		Industry Software			Deviations from Measured data (%)		
		P (psi)	*T* (°C)	ρ (kg/m^3)	μ (cP)	μ LBC (cP)	μ PED (cP)	μ AP (cP)	$\Delta\mu$ LBC	$\Delta\mu$ PED	$\Delta\mu$ AP
Wakefield, 1988b											
C10	0.142	14.7	20	728.8	0.899	0.701	1.078	0.810	-22.0	19.9	-9.9
		14.7	30	722.4	0.766	0.650	0.922	0.715	-15.2	20.4	-6.7
		14.7	40	714.9	0.666	0.601	0.803	0.639	-9.8	20.5	-4.0
		14.7	50	707.1	0.587	0.555	0.709	0.578	-5.5	20.7	-1.6
		14.7	60	699.4	0.522	0.511	0.633	0.527	-2.0	21.3	0.9
		14.7	70	691.6	0.472	0.471	0.572	0.484	-0.3	21.1	2.6
Ciotta, 2010											
C16	0.226	154	25	769.2	3.107	0.775	6.95	2.158	-75.1	124	-30.5
		157	25	769.2	3.109	0.775	6.96	2.159	-75.1	124	-30.6
		158	50	751.5	1.874	0.678	3.413	1.388	-63.8	82	-25.9
		181	50	751.7	1.872	0.680	3.427	1.392	-63.7	83	-25.7
		146	75	734.4	1.255	0.588	1.995	0.988	-53.1	59	-21.2
		175	100	717.2	0.911	0.508	1.335	0.763	-44.2	47	-16.2
		178	125	700.1	0.693	0.434	0.969	0.617	-37.4	40	-10.9
		197	150	682.2	0.542	0.368	0.753	0.520	-32.0	39	-4.1
		160	175	664	0.437	0.308	0.604	0.444	-29.5	38	1.7
		181	200	645.4	0.359	0.258	0.506	0.391	-28.3	41	8.8
		1452	25	775	3.497	0.834	8.44	2.457	-76.1	141	-29.7
		3059	25	781.2	4.032	0.901	10.31	2.802	-77.7	156	-30.5
		3060	50	765.2	2.387	0.811	5.21	1.842	-66.0	118	-22.8
		2908	75	749.2	1.57	0.720	3.08	1.328	-54.1	96	-15.4
		2912	100	733.9	1.136	0.642	2.11	1.046	-43.5	86	-8.0
		2966	125	719.1	0.872	0.571	1.59	0.870	-34.5	82	-0.3
		3015	150	704.2	0.691	0.507	1.27	0.751	-26.6	84	8.6
		2933	175	688.7	0.559	0.443	1.038	0.656	-20.7	86	17.3
		3012	200	674.2	0.469	0.392	0.895	0.592	-16.4	91	26.3
		4424	25	786.4	4.534	0.952	11.90	3.072	-79.0	162	-32.2
		5945	50	776.9	2.957	0.920	7.002	2.230	-68.9	137	-24.6
		5877	75	762.5	1.939	0.838	4.260	1.640	-56.8	120	-15.4
		5903	100	748.6	1.397	0.764	2.963	1.306	-45.3	112	-6.5
		5910	125	735.1	1.066	0.694	2.237	1.091	-34.9	110	2.4

Cn	*MW* (kg/mole)	Conditions		Measured data		Industry Software			Deviations from Measured data (%)		
		P (psi)	*T* (°C)	ρ (kg/m^3)	μ (cP)	μ LBC (cP)	μ PED (cP)	μ AP (cP)	$\Delta\mu$ LBC	$\Delta\mu$ PED	$\Delta\mu$ AP
		5932	150	721.5	0.845	0.629	1.794	0.946	-25.5	112	11.9
		5874	175	708.1	0.689	0.567	1.489	0.836	-17.7	116	21.4
		5944	200	695.3	0.579	0.514	1.286	0.758	-11.3	122	30.8
		8773	50	787.1	3.598	1.011	8.779	2.576	-71.9	144	-28.4
		8801	75	773.7	2.356	0.936	5.420	1.913	-60.3	130	-18.8
		8812	100	760.8	1.678	0.865	3.780	1.528	-48.4	125	-9.0
		8783	125	748.2	1.265	0.797	2.850	1.277	-37.0	125	1.0
		8708	150	735.2	0.998	0.730	2.271	1.103	-26.8	128	10.6
		8769	175	723.5	0.82	0.673	1.905	0.984	-17.9	132	19.9
		8814	200	711.8	0.688	0.619	1.641	0.891	-10.1	138	29.4
Wakefield *et al*., 1988a											
C24	0.339	14.5	45	782	5.729	0.528	44.89	2.598	-90.8	684	-54.7
		14.5	55	776	4.787	0.509	28.55	2.165	-89.4	496	-54.8
		14.5	65	770	3.849	0.491	19.06	1.838	-87.3	395	-52.3
Queimada *et al*., 2005											
C24	0.339	14.7	60	772.7	4.477	0.500	23.16	1.989	-88.8	417	-55.6
		14.7	70	766.2	3.666	0.481	15.81	1.703	-86.9	331	-53.6
Doolittle *et al.*, 1951											
C28	0.395	14.5	100	755.5	2.898	0.367	15.46	1.154	-87.3	434	-60.2
		14.5	150	723.5	1.4615	0.307	4.153	0.759	-79.0	184	-48.1
		14.5	200	691	0.8743	0.252	1.799	0.563	-71.2	106	-35.6
		14.5	250	657.8	0.5994	0.203	1.024	0.447	-66.2	71	-25.4
		14.5	300	622.6	0.4156	0.160	0.682	0.366	-61.6	64	-11.8
Aasen *et al.*, 1990											
C32	0.451	43.5	80	773.9	5.368	0.301	96.23	1.087	-94.4	1693	-79.8
		43.5	99	762	3.805	0.285	40.70	0.925	-92.5	970	-75.7
		43.5	99	762	3.785	0.285	40.60	0.925	-92.5	973	-75.6
		43.5	124	746.6	2.574	0.264	16.62	0.776	-89.8	546	-69.9

Cn	*MW* (kg/mole)	Conditions		Measured data		Industry Software			Deviations from Measured data (%)		
		P (psi)	*T* (°C)	ρ (kg/m^3)	μ (cP)	μ LBC (cP)	μ PED (cP)	μ AP (cP)	$\Delta\mu$ LBC	$\Delta\mu$ PED	$\Delta\mu$ AP
		43.5	151	729.4	1.808	0.241	7.596	0.658	-86.7	320	-63.6
		43.5	177	713.4	1.366	0.221	4.300	0.578	-83.9	215	-57.7
		43.5	184	708.7	1.252	0.215	3.717	0.558	-82.9	197	-55.4
		43.5	192	703.7	1.168	0.208	3.210	0.539	-82.2	175	-53.9
Aasen *et al.*, 1990											
C44	0.619	43.5	95	776.5	8.338	0.157	1143	0.135	-98.1	13609	-98.4
		43.5	126	757.8	4.696	0.147	193.6	0.174	-96.9	4023	-96.3
		43.5	152	741.9	3.232	0.139	60.61	0.203	-95.7	1775	-93.7
		43.5	174	728.1	2.452	0.133	27.03	0.223	-94.6	1002	-90.9
		43.5	200	712.4	1.865	0.125	12.79	0.241	-93.3	586	-87.1

It is clear that the methods usually used in the oil and gas industry, if un-tuned, will result in high viscosity deviations from measured data, even with the components characterised as pure *n*-alkanes. The deviations increase with chain length, and are at their highest at the lower values of the temperature range. The average absolute deviation for all the data, C6 to C44, is shown later in Table 5.17.

Table 5.12 shows the results from the Free Volume model (FV) and the Hard Sphere method (HS) for the same components.

Table 5.12. Long-chain *n*-alkane viscosity deviation results for the Free Volume model (FV) and Hard Sphere method (HS).

Cn	*MW* (kg/mole)	Conditions		Measured data		Calculated data			Deviations from Measured data (%)		
		P (psi)	*T* (°C)	ρ (kg/m^3)	μ (cP)	ρ (kg/m^3)	μ FV (cP)	μ HS (cP)	$\Delta\rho$	$\Delta\mu$ FV	$\Delta\mu$ HS
Wakefield *et al.*, 1988a											
C10	0.142	14.7	20	728.8	0.899	732.5	0.911	0.946	0.5	1.4	5.3
		14.7	30	722.4	0.766	725.4	0.796	0.817	0.4	3.9	6.7

Cn	*MW* (kg/mole)	Conditions		Measured data		Calculated data			Deviations from Measured data (%)		
		P (psi)	*T* (°C)	ρ (kg/m^3)	μ (cP)	ρ (kg/m^3)	μ FV (cP)	μ HS (cP)	$\Delta\rho$	$\Delta\mu$ FV	$\Delta\mu$ HS
		14.7	40	714.9	0.666	718.3	0.701	0.715	0.5	5.2	7.3
		14.7	50	707.1	0.587	711.2	0.622	0.633	0.6	6.0	7.8
		14.7	60	699.4	0.522	704.1	0.557	0.566	0.7	6.7	8.4
		14.7	70	691.6	0.472	697.0	0.501	0.511	0.8	6.2	8.2
Ciotta 2010											
C16	0.226	154	25	769.2	3.107	769.7	3.198	3.183	0.1	2.9	2.5
		157	25	769.2	3.109	769.7	3.199	3.184	0.1	2.9	2.4
		158	50	751.5	1.874	752.1	2.018	1.870	0.1	7.7	-0.2
		181	50	751.7	1.872	752.2	2.022	1.874	0.1	8.0	0.1
		146	75	734.4	1.255	734.4	1.365	1.219	0.0	8.7	-2.9
		175	100	717.2	0.911	717.0	0.980	0.868	0.0	7.6	-4.7
		178	125	700.1	0.693	699.4	0.732	0.656	-0.1	5.7	-5.3
		197	150	682.2	0.542	682.0	0.568	0.522	0.0	4.8	-3.8
		160	175	664	0.437	664.1	0.452	0.428	0.0	3.4	-2.1
		181	200	645.4	0.359	646.6	0.369	0.361	0.2	2.7	0.7
		1452	25	775	3.497	775.2	3.555	3.587	0.0	1.6	2.6
		3059	25	781.2	4.032	781.6	4.044	4.131	0.1	0.3	2.5
		3060	50	765.2	2.387	765.6	2.515	2.403	0.1	5.4	0.7
		2908	75	749.2	1.57	749.1	1.666	1.537	0.0	6.1	-2.1
		2912	100	733.9	1.136	733.7	1.185	1.088	0.0	4.3	-4.2
		2966	125	719.1	0.872	718.9	0.884	0.825	0.0	1.4	-5.4
		3015	150	704.2	0.691	704.5	0.685	0.658	0.0	-0.9	-4.8
		2933	175	688.7	0.559	689.5	0.543	0.540	0.1	-2.9	-3.4
		3012	200	674.2	0.469	675.6	0.444	0.460	0.2	-5.3	-1.9
		4424	25	786.4	4.534	786.7	4.506	4.634	0.0	-0.6	2.2
		5945	50	776.9	2.957	777.1	3.109	3.017	0.0	5.1	2.0
		5877	75	762.5	1.939	762.4	2.046	1.926	0.0	5.5	-0.7
		5903	100	748.6	1.397	748.6	1.443	1.354	0.0	3.3	-3.1
		5910	125	735.1	1.066	735.2	1.065	1.017	0.0	-0.1	-4.6
		5932	150	721.5	0.845	722.4	0.819	0.806	0.1	-3.1	-4.6
		5874	175	708.1	0.689	709.5	0.647	0.661	0.2	-6.1	-4.0
		5944	200	695.3	0.579	697.0	0.527	0.560	0.2	-9.0	-3.4
		8773	50	787.1	3.598	787.1	3.807	3.712	0.0	5.8	3.2
		8801	75	773.7	2.356	773.7	2.490	2.362	0.0	5.7	0.2

Cn	*MW* (kg/mole)	Conditions		Measured data		Calculated data			Deviations from Measured data (%)		
		P (psi)	*T* (°C)	ρ (kg/m^3)	μ (cP)	ρ (kg/m^3)	μ FV (cP)	μ HS (cP)	$\Delta\rho$	$\Delta\mu$ FV	$\Delta\mu$ HS
		8812	100	760.8	1.678	760.9	1.736	1.644	0.0	3.4	-2.0
		8783	125	748.2	1.265	748.5	1.267	1.222	0.0	0.1	-3.4
		8708	150	735.2	0.998	736.4	0.961	0.957	0.2	-3.7	-4.1
		8769	175	723.5	0.82	725.2	0.760	0.786	0.2	-7.3	-4.2
		8814	200	711.8	0.688	713.5	0.615	0.659	0.2	-11	-4.2
Wakefield *et al.*, 1988a											
C24	0.339	14.5	45	782	5.729	784.1	6.073	7.969	0.3	6.0	39.1
		14.5	55	776	4.787	777.0	4.916	6.029	0.1	2.7	25.9
		14.5	65	770	3.849	769.9	4.036	4.662	0.0	4.8	21.1
Queimada *et al.*, 2005											
C24	0.339	14.7	60	772.7	4.477	773.4	4.443	0.282	0.1	-0.8	-94
		14.7	70	766.2	3.666	766.3	3.671	4.128	0.0	0.1	12.6
Doolittle 1951											
C28	0.395	14.5	100	755.5	2.898	755.7	2.997	3.582	0.0	3.4	23.6
		14.5	150	723.5	1.461	720.2	1.475	1.483	-0.5	0.9	1.5
		14.5	200	691	0.874	684.6	0.850	0.819	-0.9	-2.7	-6.4
		14.5	250	657.8	0.599	649.1	0.545	0.537	-1.3	-9.0	-10
		14.5	300	622.6	0.415	613.5	0.377	0.390	-1.5	-9.4	-6.3
Aasen *et al.*, 1990											
C32	0.451	43.5	80	773.9	5.368	777.8	5.404	9.531	0.5	0.7	78
		43.5	99	762	3.805	764.3	3.842	5.777	0.3	1.0	52
		43.5	99	762	3.785	764.3	3.838	5.769	0.3	1.4	52
		43.5	124	746.6	2.574	746.9	2.605	3.344	0.0	1.2	30
		43.5	151	729.4	1.808	727.4	1.787	2.033	-0.3	-1.2	12
		43.5	177	713.4	1.366	709.3	1.318	1.401	-0.6	-3.5	2.6
		43.5	184	708.7	1.252	704.0	1.212	1.272	-0.7	-3.2	1.6
		43.5	192	703.7	1.168	698.3	1.112	1.153	-0.8	-4.8	-1.3
Assen *et al.*, 1990											

Cn	*MW* (kg/mole)	Conditions		Measured data		Calculated data			Deviations from Measured data (%)		
		P (psi)	*T* (°C)	ρ (kg/m^3)	μ (cP)	ρ (kg/m^3)	μ FV (cP)	μ HS (cP)	$\Delta\rho$	$\Delta\mu$ FV	$\Delta\mu$ HS
C44	0.619	43.5	95	776.5	8.338	784.1	8.740	23.69	1.0	4.8	184
		43.5	126	757.8	4.696	762.5	5.082	9.663	0.6	8.2	106
		43.5	152	741.9	3.232	744.0	3.422	5.166	0.3	5.9	60
		43.5	174	728.1	2.452	728.0	2.532	3.294	0.0	3.3	34
		43.5	200	712.4	1.865	709.9	1.866	2.153	-0.4	0.0	15

It can be observed that these two models produce more accurate results for the long-chain *n*-alkanes. The Hard Sphere method shows higher deviations for the very long alkanes, C32 and C44, whereas the Free Volume model, as extrapolated in this work, results in deviations of less than 10%. The highest deviations in the Hard Sphere model are at the lower end of the temperature ranges (T < 150 °C), but shows very high accuracy for all the viscosity measurements of C16, even at pressures as high as 15,000 psi. Overall, the Free Volume model gave the best results, with all deviations being less than 10% for pressures less than 10,000 psi. At the higher pressures, for example at 15,000 psi and a temperature of 50 °C, the Free Volume model resulted in a maximum deviation of 15%.

The Free Volume and Hard Sphere models were applied to C60 (Aasen *et al*., 1990) and C64 (Doolittle, 1951) additionally, and then compared with the published measurements. Table 5.13 and Table 5.14 show the results.

Table 5.13. C60 viscosity comparisons.

Conditions		Measured data		Calculated data			Deviations from Measured data (%)		
P (atm)	*T* (K)	ρ (kg/m^3)	μ (cP)	ρ (kg/m^3)	μ FV (cP)	μ HS (cP)	$\Delta\rho$	$\Delta\mu$ FV	$\Delta\mu$ HS
3.0	407.9	762	7.31	767.2	7.14	24.9	0.7	-2	241
3.0	423.5	752.6	5.76	756.1	5.63	15.7	0.5	-2	172
3.0	441.5	741.7	4.51	743.4	4.39	9.8	0.2	-3	116
3.0	465.5	727.3	3.38	726.3	3.24	5.6	-0.1	-4	67

One spurious data point at T = 462 K from the C60 data set has been omitted, as it did not follow the decreasing trend with increasing temperature. Without this point, the Free

Volume model provides very accurate results for C60, with an AAD of 2.8% and an MAD of 4%. The Hard Sphere deviations are higher, with AAD = 149% and MAD = 241%.

Table 5.14. C64 viscosity comparisons.

Conditions		Measured data		Calculated data			Deviations from Measured data (%)		
P (atm)	T (K)	ρ (kg/m^3)	μ (cP)	ρ (kg/m^3)	μ FV (cP)	μ HS (cP)	$\Delta\rho$	$\Delta\mu$ FV	$\Delta\mu$ HS
1.0	383.2	781.8	14.35	786.6	10.3	76.2	0.6	-28	431
1.0	423.2	757.9	7.14	758.2	5.4	20.3	0.0	-24	184
1.0	474.4	728.3	3.71	721.7	2.8	5.7	-0.9	-24	53
1.0	521.4	698.1	2.33	688.3	1.8	2.5	-1.4	-24	8
1.0	573.8	668	1.52	651.1	1.1	1.3	-2.5	-26	-13

The Free Volume model provides less accurate results for C64, with AAD = 25% and MAD = 28%, whereas the Hard Sphere model resulted in AAD = 138% and MAD = 431%. Figure 5.17 and Figure 5.18 show the relative deviations in viscosity predictions for $C_{16}H_{34}$ as a function of temperature, at two different pressures. The extensive database of measured data points, taken from the Ciotta (2010) database, includes viscosities at multiple temperatures (25-200°C), at each pressure.

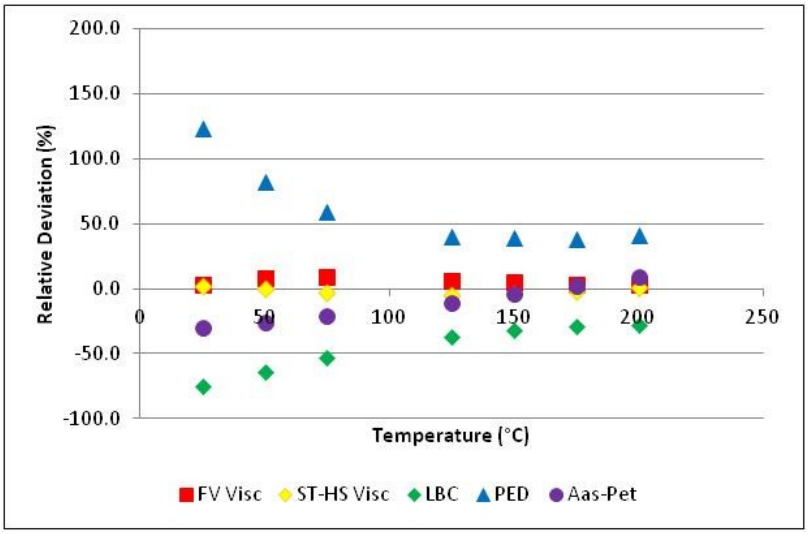


Figure 5.17. C16 calculated viscosity relative deviations *vs.* temperature at P = 1500 psi.

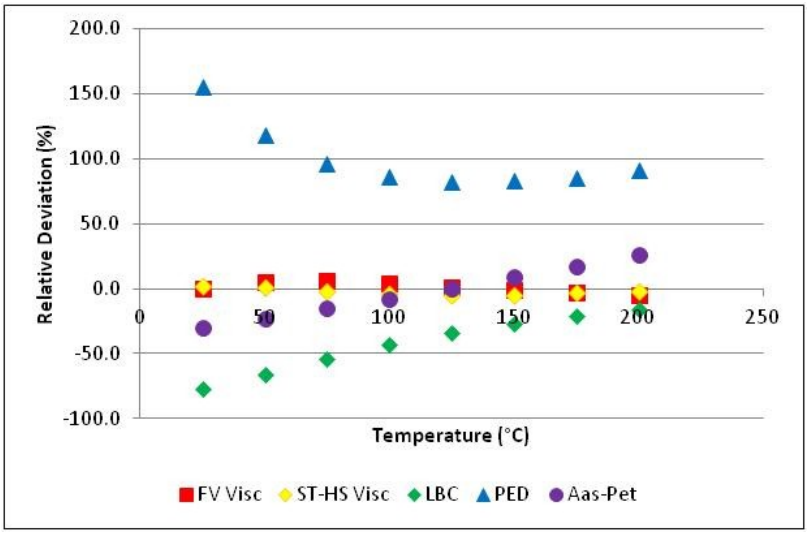


Figure 5.18. C16 calculated viscosity relative deviations *vs.* temperature at *P* = 3000 psi.

It was found that the untuned Pedersen Corresponding States method, as implemented in Computer Modelling Group (CMG) and Schlumberger (SLB) PVT packages, resulted in deviations higher than 50% for pressures of ~3000 psi. LBC and Aasberg-Petersen under-predicted, and both the Hard Sphere and Free Volume models were very accurate. In general, absolute deviations increased with pressure, and decreased with temperature.

A summary of the deviations of the calculated Free Volume and Hard Sphere viscosities from all the available measured viscosity data listed in Appendix B.2., are shown in Table 5.15 and Table 5.16. Table 5.15 shows the average absolute deviation (AAD) for all the components C6-C64, at pressures of interest in heavy oil reservoirs, whereas Table 5.16 shows the same data, but with the high-pressure data (> 20,000 psi) from the Dymond and co-workers (1980, 1981) and Ciotta (2010) datasets now included.

Table 5.15. Calculated density, Hard Sphere and Free Volume viscosity deviation data for C6-C64, *P* < 1400 atm (20,000 psi).

Total AAD %			Total MAD %		
Density	Free Volume Viscosity	Hard Sphere Viscosity	Density	Free Volume Viscosity	Hard Sphere Viscosity
0.6	5.3	16.4	4.3	30.6	431.0

Table 5.16. Calculated density, Hard Sphere and Free Volume viscosity deviation data for C6-C64, all pressures.

Total AAD %			Total MAD %		
Density	Free Volume Viscosity	Hard Sphere Viscosity	Density	Free Volume Viscosity	Hard Sphere Viscosity
0.9	19.8	20.5	5.5	317.4	431.0

It is clear that the models decrease in accuracy at the very high pressure ranges, with density being under-predicted by 4.6%, the Free Volume model over-predicting the viscosity by 300%, and the Hard Sphere viscosity under-predicted by 55% in the case of C8 at a pressure of 4989 atm and temperature of 323 K (50 °C). The measured density and viscosity at these conditions were 859 kg/m^3 and 6.5 mPa s (6.5 cP), respectively. The highest deviation (430%) of the Hard Sphere model was for the C64 viscosity at P = 1 atm and T = 383 K (110 °C). The measured value was 14 mPa s (14 cP), whereas the Hard Sphere model predicted 76 mPa s (76 cP). Detailed deviation data are provided in Appendix B.2.).

A summary of the comparative results, including industry software models, for components C6-C44, is shown in Table 5.17. The results include the average and maximum absolute deviations between the 185 measured viscosities, measured over a temperature range of 10-575 °F and a pressure range of 15 to 17,300 psi for components from C6 to C44, for each of the prediction methods.

Table 5.17. Deviation Summary: all models, components C6-C44, T = 10-575 °F, P = 15 to 17,300 psi (LBC=Lohrenz-Bray-Clark; PED=Pedersen Corresponding States, AP=Aasberg-Petersen).

AAD (%)					MAD (%)				
Free Volume	Hard Sphere	LBC	PED	AP	Free Volume	Hard Sphere	LBC	PED	AP
5	10	50	245	30	30	185	100	13600	100

It is apparent that the models currently available in the industry break down in predicting the viscosities of long *n*-alkanes. Both the Free Volume model and the Hard Sphere method

show promise in the prediction of heavy oil component viscosities, with average absolute deviations of less than 10% for components C6-C44.

Figure 5.19 shows a comparison of the absolute average deviation (AAD) in viscosity predictions on the full database of available measured data. It is clear that the Free Volume Model (in red) as extended in the present work, produces the lowest deviations for the full range C6-C44, with Pedersen Corresponding States method over-predicting.

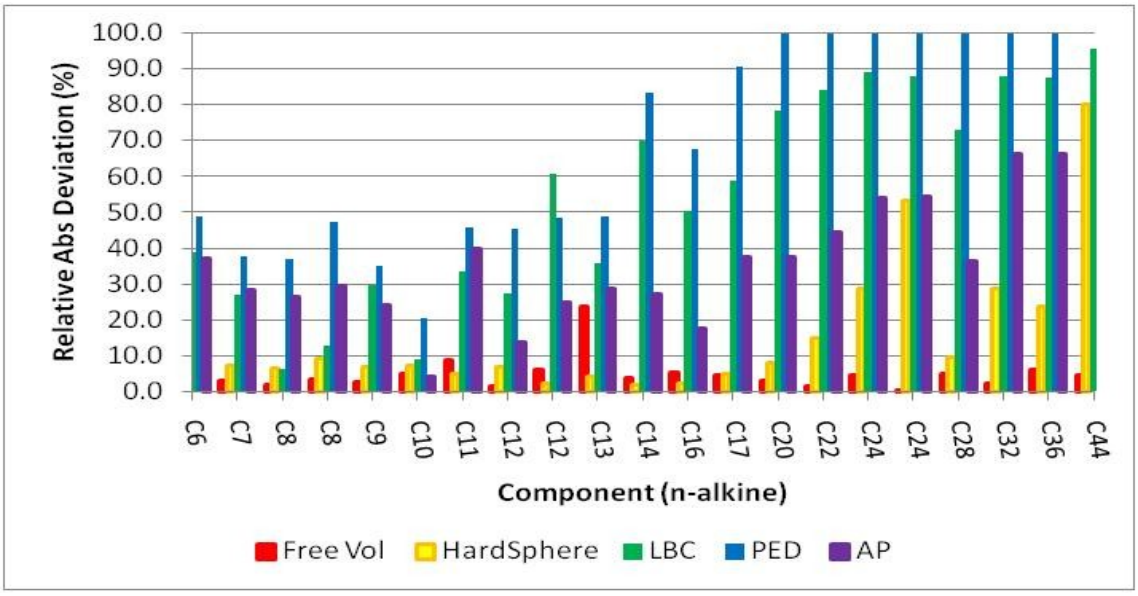


Figure 5.19. Viscosity prediction deviations: AAD *vs.* Cn ($P < 20{,}000$ psi).

5.7 Conclusions

A new extension of the Tait density model has successfully been developed to accurately predict densities of long-chain *n*-alkanes up to C64. The average absolute deviations of the calculated data were less than 3% for measurements at pressures lower than 20,000 psi, well within the pressure limits applicable in heavy oil reservoirs, and less than 5% for pressures above that.

Various viscosity models were evaluated for accuracy in predicting long-chain *n*-alkane viscosities as a function of pressure and temperature. Methods from the industry included Pedersen's Corresponding States method, the Lohrenz-Bray-Clark correlation and the Aasberg-Petersen Corresponding States method. Two new models were implemented, the Hard Sphere model and the Free Volume model, of which the Free Volume model parameters were extrapolated by a least-squares fit to be able to predict viscosities of pure *n*-alkanes up to C64.

In total, good estimates for the fitting parameters (l_m, E_0 and B) for all *n*-alkanes from C6 to C64 have been provided, delivering suitable liquid viscosity models that adequately predict viscosities of long-chain *n*-alkanes from C6 up to C64, with total AAD of 6% and MAD of 30.6% for all the available measured data at pressures less than 10,000 psi.

The industry models, and in particular the Pedersen model in its un-tuned form, was found to be unsuitable to model heavy oil viscosity-temperature relationships, resulting in absolute average deviations (AAD) of up to 245% in modelling heavier components up to C44. The Hard Sphere model delivered results with an AAD of 11%, whereas for the Free Volume model the AAD was 5%, for the same data. This study found that the Hard Sphere and Free Volume models were both more accurate in predicting the viscosities of a large range of *n*-alkanes up to C45, with errors less than 5% in the temperature and pressure ranges of T = 0-600 °F, P = 14.5-17,000 psi. The LBC and Aasberg-Petersen methods under-predicted viscosities of components longer than C10 ($C_{10}H_{22}$) and Pedersen over-predicted up to two to three orders of magnitude in the case of *n*-alkanes longer than C20. The Hard Sphere and Free Volume-calculated viscosities for C60 and C64 resulted in an AAD of 15% for the Free Volume model, and 143% for the Hard Sphere model. The respective MAD results were 28% and 431%. Of all the models evaluated, the Free Volume model deviations were the lowest, based on the parameter extrapolations in this work.

For more accurate heavy oil simulation predictions, involving heavy oil pseudo-components based on an equivalent pure-components (molecular weights in the same order as those of C25 to C80), the Free Volume Model could be used. In the case of *n*-alkanes

heavier than C45, for which critical property data are lacking, the Free Volume Model proved easy to tune, and provided accuracy within the acceptable range of reservoir uncertainties inherent in simulation. Again, it is acknowledged that limited data exist for long-chain *n*-alkane viscosity measurements, and the present conclusions might be limited to the ranges of pressure and temperatures included in this study.

6 Characterisation of a Heavy Pseudo-Component

6.1 Introduction

In this section some of the latest research on asphaltenes and resins is reviewed in order to justify and derive properties for a newly introduced heavy pseudo-component.

It was illustrated in Chapter 3 and in de la Porte *et al.* (2011) that it is possible to perform a compositional simulation of steam-drive of heavy oil, using only two pseudo-components. Applying the Equivalent Carbon Number (ECN)-grouping method to two different oils with different compositions, it was found that a two-component model could yield cumulative oil production that were within 5% of that predicted by a 24 to 30-component model. The accuracy of agreement depended to on the viscosity mixing rule used during lumping/grouping of the components into pseudo-components. The question remained as to whether or not this finding would hold when the component viscosities are predicted with the Free Volume model; this question will be addressed in this section and the next.

For the prediction of the individual component viscosities as a function of temperature, various different methods (Pedersen's Corresponding States (Pedersen *et al.,* 1984, Pedersen and Christensen, 2007), Aasberg-Petersen (Aasberg-Petersen *et al*., 1991), Lohrenz-Bray-Clark (Lohrenz *et al*., 1964), Hard Sphere (Dymond and Awan, 1989; Assael *et al*., 1992; Sun and Teja, 2009), and Free Volume (Allal *et al*., 2001)) were compared in Chapter 5. The computations were for *n*-alkanes only, where laboratory measurements exist, and showed the Free Volume model to be promising in predicting viscosities for components in the liquid phase, ranging from C_2H_6 to long chains up to $C_{64}H_{130}$. The model is based on Eyring's and other physical theories, giving it a sound physical base. It is also relatively easy to implement, and only knowledge of the component density is required. It was shown in Chapter 5, how the parameters l_m, E_0 and B for long chain *n*-alkanes up to C64 were computed to predict viscosities of all *n*-alkanes from C1 to C64, at relevant pressures and temperatures. However, it was clear that the viscosity of a true heavy oil (μ_o

> 1,000 cP at standard conditions) was not represented, and that an additional heavy pseudo-component would be required during viscosity modelling for field simulations to represent the true nature of heavy oil, consisting of more complex molecules such as aromatics, resins and asphaltenes. The question arose: what was the exact cause for the large increase in viscosities in heavy oil, and how can it be represented, based on sound physics?

Luo and Gu (2007) extensively reviewed research on heavy oil viscosities in terms of asphaltene content. They refer to studies (Sheu *et al*., 1995; Yen *et al*., 1994) which show heavy oil viscosity is a strong function of its asphaltene characteristics, and orders of magnitude increases in viscosity were observed with a relatively small increase in asphaltene concentration (Mack, 1932). Their research is further discussed in the viscosity review later in this chapter.

In order to define, and incorporate, one such heavy pseudo-component into the viscosity modelling scheme, for thermal compositional simulation with two or three pseudo-components, the SARA (saturates, aromatics, resins, asphaltenes) compositional classification is further explored. The SARA analysis, commonly used in heavy oil analysis, consists of a fractionation method separating the crude oil into four main classes, based on polarity and solubility. Ranges of molecular weights (MW), mole percentages and associated relative weight percentages (wt.%) per SARA compound of Nigerian bitumen and heavy oils are shown in Table 6.1 (Lawal *et al.,* 2010). It can be observed that even though the weight-percentages of the asphaltenes are high, on the order of 25%, the associated mole-percentage is very low, at 3%. The resins mole-percentage is much higher, in the order of 40%, with a very similar weight percentage. Aromatics contribute the least in terms of weight-percentage (11%), with saturates accounting for up to 45% of the mole-fraction (25 wt%). In the same table, the equivalent carbon numbers are shown, firstly based on boiling-point fractions (SCNG) (Katz and Firoozabadi, 1978), then on pure chain-

molecules or *n*-alkanes with a fomula of C_nH_{2n+2} (ECN)[10]. It is of interest to note the overlap in ECNs representing Saturates and Aromatics, providing some basis for reasoning that it would sufficiently accurate to combine these in viscosity modelling. Molecular weights of resins fall in the long-chain groups range, with asphaltenes above C300. It is recognised that these molecules are not chain molecules with single bonds, and it is only for the purpose of viewing them from the perspective of the grouping scheme used in Chapter 3 that the ECN reference is made.

Table 6.1. SARA analysis ranges for Nigerian heavy oil and bitumen (after Lawal *et al.*, 2010).

	Saturates	Aromatics	Resins	Asphaltenes	Whole Bitumen
MW (g/mole)	352-389	375-420	634-731	4436-6173	588-748
Mole%	39.2-44.9	20.7-25.2	34.4-42	2.6-3.3	
wt%	20.4-26.9	11.6-16.1	37.1-41	19.9-27	
SCNG	C26	C27-C30			
ECN (Cn)	C25-C28	C27-C30	C45-C52	C316-C440	C42-C53

The SARA method of grouping of molecules-types, and, in particular, the contribution the resins and asphaltenes would make towards the mixture viscosity, will be incorporated into the viscosity modelling described in Chapter 5 via a heavy pseudo-component. Lawal and his collaborator (Lawal and Adenuga, 2010; Lawal, 2011) introduced numerical simulation with pseudo-components based on the SARA analysis, investigating different combinations of the four groups with a gas component included. However, their pseudo-component mixture viscosities were obtained by tuning the Pedersen Corresponding States correlation (Pedersen *et al*., 1987) to match the measured viscosities of the Nigerian bitumen. In the present research, the Free Volume model is used. Chapter 5 described the viscosity modelling of saturates (alkanes) without taking the contributions of the other SARA groups into account, resulting in viscosities up to 75 cP for C45 at 60 °F. As a consequence, in

[10] Hydrocarbons with C_nH_{2n+2} will be called Cn in this research.

order for the Arrhenius mixture rule (Chapter 2; Arrhenius, 1887) to result in an oil viscosity of heavy oil proportions (say 5,000 cP), the proposed single heavy pseudo-component would require a viscosity on the order of 10^{28} cP at 60 °F. One of two possible approaches could have been followed in this section of the work: (a) use the Free Volume model to predict, based on certain group-specific physical characteristics, a typical aromatic pseudo-component, a typical resin pseudo-component and a typical asphaltene pseudo-component; or (b) lump resin and asphaltene together and use either the Free Volume model to predict the single heavy pseudo-component viscosity, or the colloidal system theory.

The present work followed the approach in (b), and both viscosity prediction methods were applied as a test. The saturates-aromatics 'pure' component characteristics (P_c, T_c, V_c) were based on boiling point fractions properties as described by Katz and Firoozabadi (1978). The viscosities of the initial 'pure' components were predicted by the extended Free Volume method (Chapter 5), and the grouped pseudo-component viscosities were calculated with the Arrhenius mixing rule as described in Chapters 2 and 3. The effects of the aromatics are assumed to be incorporated in the boiling point group properties and in the viscosity by the Free Volume parameters (l_m, E_0 and B) where literature values were based on the inclusion of more complex components such as highly branched alkanes, and aromatic components (Zéberg-Mikkelsen *et al.*, 2004; Boned *et al*., 2004).

The ranges of viscosities found for the oil mixture (distillable and undistillable) used by Lawal (2011), and those of aromatics by Chevalier *et al.* (1990), are comparable to the ranges of the twenty-four pure-components-mixture (SPE4-based study, Chapters 3 and 7 of this thesis) as calculated with the Free Volume Model, excluding the effects of complex molecules such as the asphaltenes. The molecular weights and other properties used in the Free Volume calculation were obtained from the generalised properties for SCN or carbon number fractions (Katz and Firoozabadi, 1978; Pedersen and Christensen, 2007), thus combining saturates and aromatics based on boiling points, and would therefore not require any further adjustment. The focus was thus on finding parameters suitable for using the

Free Volume model to correlate the heavy pseudo-component viscosity, assuming Newtonian behaviour.

Lawal's (Lawal and Adenuga, 2010; Lawal, 2011) investigation showed that a three pseudo-component scheme is satisfactory for prediction in a SAGD case of Nigerian Bitumen production. The components in their three-pseudo-components-scheme consisted of gas (0.25 wt.%, MW=16), maltenes (75.51 wt.%, MW=539), asphaltenes (24.24 wt.%, MW=1030), and provided the properties in terms of MW and density. They grouped the resins with the maltenes (75 wt%) and treated the asphaltenes as a separate component. In a four-pseudo-component scheme, the asphaltenes and resins were grouped together, with a 62.5% wt percentage and a MW of 813.

A similar scheme is proposed here, but the resins will be grouped with the asphaltenes as a heavy pseudo-component in a multi-component scheme, which will systematically be reduced to a three pseudo-component scheme of light (gas+distillable up to ~C12, depending on phase behaviour), medium (saturates and aromatics) and heavy components (resins and asphaltenes). The objective is to end up with the following three pseudo-components:

1. Gas and short-chain hydrocarbons up to C12
2. Saturates and aromatics
3. Asphaltenes and resins

In order to substantiate the assumptions of the proposed grouping, and ascertain appropriate assumptions to characterise the proposed pseudo-heavy-component in terms of the Free Volume viscosity model parameters, a review of the properties of resins and asphaltenes in recent research had been conducted, and is discussed in the next section. Firstly, the grouping and choice of ECN will be justified, then the molecular properties that will form the basis of the Free Volume parameter selections, will be investigated.

6.2 Resins and Asphaltenes Properties Review

6.2.1 Resin and asphaltene definitions

Resins and asphaltenes fall into the same geochemical group, the heteroatomic compounds (NSOs), but are usually separated into soluble resins and insoluble asphaltenes. Both are highly complex molecules containing additional elements, such as nitrogen (N), sulphur (S), and oxygen (O), combined with minor amounts of heavy metallic elements. Asphaltenes, in the absence of resins, tend to flocculate and eventually precipitate as solids. The SARA analysis division into resins and asphaltenes is 'man-made', according to Harriman (GHGeochem, 2004), as they form a continuum of increasingly higher molecular weight compounds, with resins at one end and asphaltenes at the other.

6.2.2 Resin-asphaltene grouping

Argillier and co-workers (Argillier *et al.,* 2002) stated that in order to 'understand the rheological behaviour of a heavy crude oil in relation with its internal structure, asphaltenes and resins have to be simultaneously considered'. They also found that the internal structure of these components, and thus the activation energy required in viscous flow, is based on thermal-dependent physical bonds, and influenced by resin and asphaltene 'critical' concentrations, after which rheology effects are more pronounced. Viscosity is therefore a strong function of all these factors. In the presence of resins, the contribution of asphaltenes towards increasing the crude viscosity by flocculation is lessened. Resins adsorb onto the surfaces of the asphaltenes, and could lower the relative viscosity by preventing the asphaltene particle associations (less overlapping). At higher temperatures desorption of these resins could again influence the bonds between the maltenes and asphaltenes, causing non-linearity in activation energy as a function of temperature.

Argillier visualized the SARA classifications as shown in Figure 6.1, indicating an overlap between resins and asphaltenes, depending on the *n*-alkane used to induce precipitation. In their study pentane (C5) *vs*. nonane (C9) were used and their results show that, due to the overlap, part of the resins is often grouped with the asphaltenes by definition.

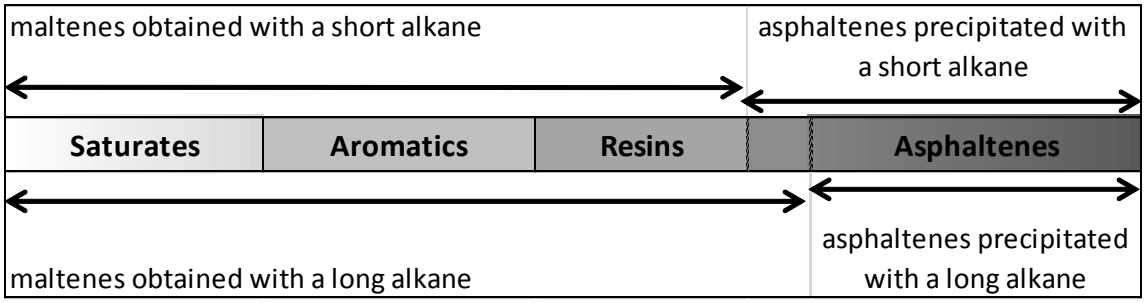


Figure 6.1. Separation of asphaltenes from heavy oil: influence of the precipitating alkane. (after Argillier *et al.*, 2002)

They found that, for a heavy oil from Venezuela, the percentage resins increase when using nonane instead of pentane for asphaltene precipitation. The percentage of asphaltenes decreased accordingly, implying there is an overlap between the molecules commonly defined as resins and those defined as asphaltenes (Figure 6.1).

In terms of the 'equivalent carbon numbers' Luo and Gu (2007) concluded that short-alkane (C5) -soluble asphaltenes carbon number are higher than C50. Their finding is based on the combination of the SARA and detailed compositional analysis of an oil sample from the Canadian Lloydminster field, with a density of 9.88 kg/m^3 (SG≅1), viscosity at standard conditions (23.9 °C; 1 bar) of 24,000 cP (or mPa s) and an asphaltene concentration of 14.5 wt.%.

In the present research, the continuum-assumption and resin-asphaltene interaction effects provided sufficient justification to grouping these two compounds into one pseudo-component.

6.2.3 Resin-asphaltene molecular weight

In terms of molecular weight, original compositional analysis in Lawal and Adenuga's work (2010) shows asphaltene molecular weights (MW_{asp}) of higher than 4000 g/mole. If combined with other components as pseudo-components for simulation purposes, they found, by using the asphaltene molecular weight as an adjustable parameter in mixing rules,

that MW_{asp} is in the order of 1000 g/mole (precipitable) and around 750 g/mole (non-precipitable), depending on the grouping and number of pseudo-components. This was consistent with previous findings: MW_{asp} = 750 g/mole (Badre *et al.*, 2006); Khan and co-workers show MW_{asp} of 3500 to 8140 g/mole from 4 bitumen samples (Peace River, Cold Lake, Wabasca and Athabasca) which clearly did not include any resins (Khan *et al.*, 1984). The specific gravity (SG) of the Lawal asphaltenes were 1.13, non-precipitable and 1.16 precipitable. Asphaltenes with resins had a SG of 1.13 and MW of 813.

6.2.4 Resin-asphaltenes physical properties: size and shape

Groenzin and Mullins (2000) calculated 'derived molecular major axis parameters' for both asphaltenes and resins. Their samples included heptanes (C7)-insoluble asphaltenes from crude oils from Kuwait (UG8 and BG5), California (Cal) and France (ST1) and resin samples obtained by precipitation by n-pentane (C5) followed by n-heptane (C7). Their finding are shown in Table 6.2, and based on a shape-assumption of an oblate spheroid with aspect ratio of 2 for the asphaltenes. Their results indicate resins and asphaltene molecular sizes to be very similar, and on the order of 11-28 Å.

Table 6.2. Molecular major axis diameters of asphaltenes and resins (from Groenzin and Mullins, 2000).

Molecular major axis diameters [Å]			
Asphaltenes			Resin
UG8 (Kuwait)	ST1 (France)	CAL (California)	
13.6	17.1	11.3	12.8
18	20	15.7	15.3
18.8	21.3	16.5	16.8
21.6	23.2	19.6	18.8
24.1	25.7	22.7	22.2
27.1	28.1	25.6	25.5

The shapes of the asphaltene particles had been heavily researched (Storm and Sheu, 1993; Luo and Gu, 2007) and it is acknowledged that they may differ between different reservoirs, oil samples, locations and vary with temperature, strongly affecting the intrinsic viscosities used in the colloidal-system based viscosity models. Many researchers found asphaltenes molecules to be spherical with a shape factor (used in calculating the intrinsic viscosity) of 2.5 (Storm and Sheu, 1993) but Luo and Gu (2007), based on the theoretical calculation, found this not to be the case in the Lloydminster sample, with shape factors up to 6 at lower temperatures. Furthermore, the interaction between individual particles, as well as with the resin in the maltenes, differ and change with temperature.

6.2.5 Resin-asphaltenes physical properties: energy of activation

It was also expected that the energy of activation in viscous flow of these molecules would be relatively high. This is confirmed from the papers from Argillier *et al.* (2002), and Luo and Gu (2007) who presented the activation energy, E_a, as a function of the asphaltene volume fraction in the maltenes (Table 6.3).

Table 6.3. Asphaltene volume fraction with associated activation energy (E_a).

Vol%	Energy of activation: slope of Eyring eq (E_a) (kJ/mole)
13.50	80.42
12.19	78.34
10.35	74.93
6.68	69.07
3.17	64.15
0	61.03

Luo and Gu (2007) performed experiments on a Lloydminster (Canada) crude oil sample to investigate the relationship between heavy oil (maltenes+asphaltenes) viscosity and the asphaltene weight percentage. They used the experimental data to calculate shape factors, salvation coefficients and maximum packing volume fractions for the dispersions,

maltenes+asphaltenes, based on colloid dispersion theories (Einstein, Pal-Phodes and Mooney). They used Eyring and collaborators's theory (Glasstone *et al.*, 1941) based on the Arrhenius-type equation, $\mu = A\exp(B/T)$, to relate the asphaltene percentage to the energy of activation (E_a) as a function of temperature.

6.2.6 Resin-asphaltenes physical properties: viscosity ranges

As previously mentioned, Luo and Gu (2007) reviewed heavy oil viscosities in terms of asphaltene content, and showed the high viscosity of heavy oil is predominantly determined by the asphaltene content. They mention Mack's research (Mack, 1932) where the asphaltenes were precipitated with petroleum ether, an earlier method, and did not include the resins. Increasing the weight percentage into their pertolenes (similar to maltenes), the viscosity at standard conditions (25 °C, 1 bar) of the mixture increased from 1.1×10^5 Poise to 4.03×10^7 Poise with a concentration (wt.%) increase from 0 to 20%, a relative increase of 367 times, concluding that this increase is probably due to strong aggregation of asphaltene particles. Dealy (1979) found that an Athabasca bitumen viscosity, with original asphaltene content of 16 wt.%,increased from 3×10^5 cP to 10^6 cP with the addition of 5 wt.% asphaltenes.

In terms of viscosity ranges for the combination of resins and asphaltenes, Lawal (2011) has shown that for the Nigerian bitumen, a pseudo-component that includes the resins in the maltenes, the maltenes viscosity at 20°C could be as high as around 32,000 cP, and asphaltene pseudo-component viscosity as high as 10^{16} cP (Figure 6.2). An asphaltene-resin pseudo-component was modelled with a viscosity of 10^{12} cP at 20°C (Figure 6.3). The original crude oil measured viscosities are shown in Figure 6.4.

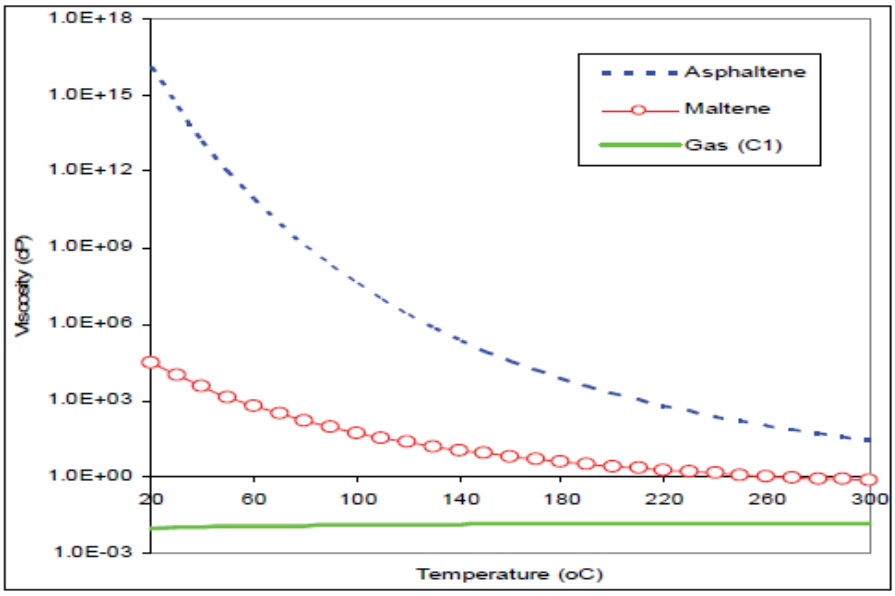


Figure 6.2. Lawal three-pseudo-component case with asphaltene pseudo-component viscosities (from Lawal, 2011).

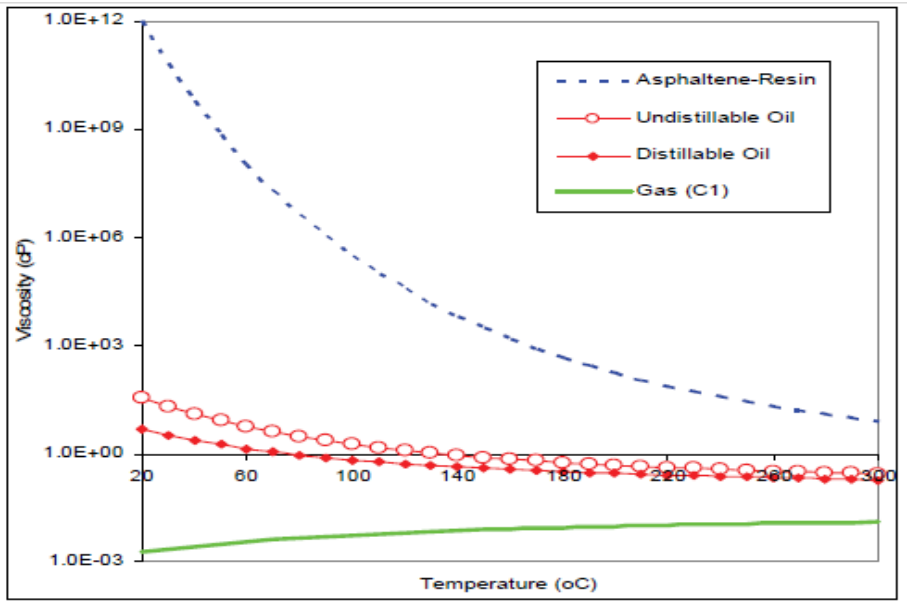


Figure 6.3. Lawal four-pseudo-component case with resin-asphaltene pseudo-component viscosity (from Lawal, 2011).

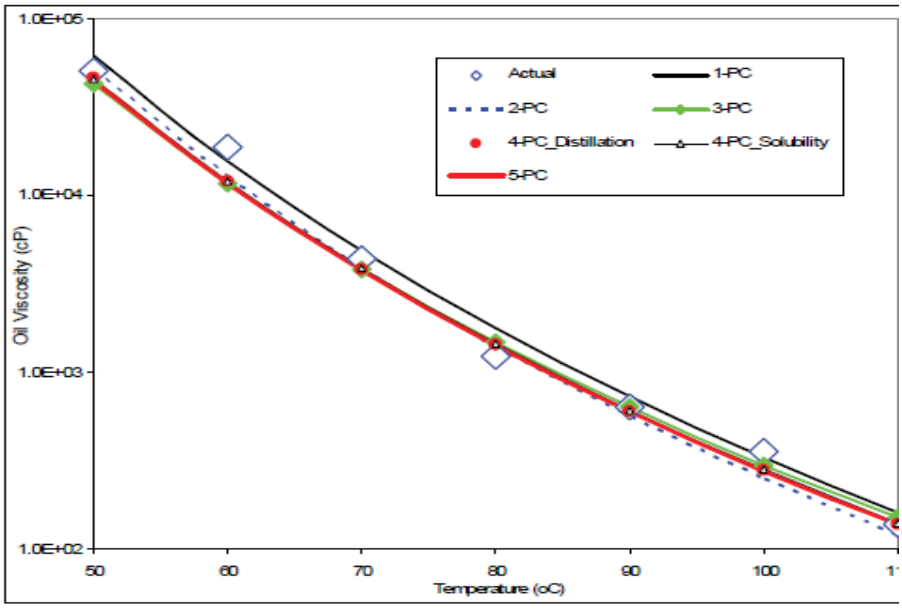


Figure 6.4. Nigerian bitumen measured viscosities (from Lawal, 2011).

6.3 Viscosity Modelling per Pseudo-Component

As stated in the beginning of the chapter, the objective was is to end up with the following three pseudo-components for thermal simulation purposes (a) gas and light hydrocarbons up to C12, (b) saturates and aromatics, and (c) asphaltenes and resins. The methods used to determine the liquid viscosities of each of the three pseudo-components will be discussed separately.

The gaseous/volatile pseudo-component, consisting of, roughly, C1 to C12, was based on an ECN (Chapter 3) and the Free Volume model was employed to calculate the viscosities of the pure components prior to grouping. The Free Volume parameters determined in Chapter 5, based on *n*-alkane data, were used. The individual pure component viscosities were grouped using the Arrhenius mixing method (Chapter 2).

In terms of defining the second pseudo-component, data from literature were used to provide an indication of expected ranges of viscosities and other properties for maltenes, ideally without resins. Most publications make the division of maltenes *vs*. asphaltenes by

including most of the resins in the maltenes group, but Lawal (2011) shows the pseudo-component viscosities and properties (MW and density) of two separate grouping schemes, namely the 3-PC and the 4-PC distillation-based) for the Nigerian heavy oil and bitumen. In the 3-PC scheme, he grouped the resins with the maltenes, which resulted in the following two oil components:

- Maltenes (with resins): MW =539 g/mole, SG=0.97;
- 'pure' asphaltene component with a MW of 1030 g/mole (SG=1.16).

In the 4-PC scheme, he included the resins in the heavy component (asphaltenes + resins), which resulted in a combined MW of 813 g/mole (SG=1.13). The maltenes/oil was divided into two pseudo-components, and if these two are combined again, the molefraction-weighted MW average is 398.98 g/mole and SG=0.868. The two resulting oil components, oil vs heavy fraction, would be

- Maltenes (without resins): MW=398.98, SG=0.868;
- Asphaltenes+resins: MW=813, SG=1.13.

A summary of the properties and the associated viscosity ranges between 20°C and 300 °C for the four different pseudo-components are provided in Table 6.4.

Table 6.4. Maltene and asphaltene properties, as estimated from Lawal and Adenuga (2010).

Component	MW g/mole	SG	Approx Visc (cP)	
			at 20 °C	at 300 °C
Maltenes (with resins):	539	0.97	35,000	1
'Pure' asphaltenes	1030	1.16	1E+16	100
Maltenes (without resins)	399	0.87	60	0.4
Asphaltenes+resins	813	1.13	1E+12	50

An interesting aspect to note is the large difference the presence of the resins makes to the maltenes pseudo-component viscosity. Without the resins, the viscosity at 20°C is three orders of magnitude lower. In the case of using the Free Volume model to predict viscosities, based on the extrapolated parameters from Chapter 5, the mixture viscosities

was of the same order as those of maltenes without resins in Table 6.4, providing some evidence that the combination of identifying an ECN based on the mixture molecular weight and Free Volume pure component viscosities, combined with the Arrhenius mixing method would be sufficient in modelling the combination of saturates and aromatics as the second,' live', pseudo-component.

In terms of the SPE4 test fluid and mixing methods described in Chapter 3, and based on the Lawal's grouping schemes, the expected ECN was around C29-C31, with a MW of 405 g/mole or higher, but depended on the actual composition and step-by-step grouping as proposed in Chapter 3. Viscosity was determined with the Free Volume model as before, combined with the Arrhenius mixing rule. As a reminder, in Chapter 3 this component's viscosity was based on a combination of Pedersen's Corresponding States method, used for prediction of the 'pure' components (single carbon number fractions), and the Arrhenius mixing rule. The viscosity-temperature relationship was a simple log-normal Andrade-type correlation. In the current section, the single component viscosities and relationships with temperature were computed with the Free Volume model, based on Free Volume parameters tuned to *n*-alkanes.

For the calculation of the viscosity of the last group, the heavy pseudo-component, both a colloid system approach, where the relative viscosity depended on the concentration of asphaltenes in the maltenes, as well as the use of the Free Volume Model, had been explored, as described in the next sections.

6.3.1 Heavy pseudo-component viscosity with Free Volume Model

The Free Volume model (Allal *et al*., 2000) as applied to *n*-alkanes in Chapter 5, is as formulated as follows (also eq. (5.24) in Chapter 5):

$$\mu = \frac{\rho \cdot l_m[(E_0 + (PM/\rho)]}{\sqrt{3RTM}} \exp\left[B\left(\frac{E_0 + (PM/\rho)}{2RT} \right)^{3/2} \right], \quad (6.1)$$

where μ is the viscosity (Pa s), ρ is the density (kg/m^3), P is the pressure (MPa), M is the molecular weight (kg/mole), R is the universal gas constant (8.31451 J/mole.K), T is the temperature (K), E_0 is the the energy associated with the molecular activation energy barrier (J/mole), l_m is associated with a molecular characteristic length, where $l_m=L^2/b_f$ (Å), and B is associated with the free volume overlap (dimensionless). The parameters l_m, E_0 and B are characteristic of a molecule and thus specific to the resin-asphaltene combination.

It was clear from the review on the characteristics of the resin-asphaltene compounds in the first section of this chapter, that it would be incorrect to assume the extrapolated parameters (Chapter 5), based on *n*-alkanes, would apply when applying the Free Volume model to the heavy pseudo-component viscosity. Instead, an attempt was made to choose parameters (l_m, E_0 and B) by using typical molecular size ranges to calculate l_m the characteristic length of the free volume, use ranges of measured energies of activation to select E_0, the energy associated with the energy required to break inter-molecular bonds, and, in the last instance, base B on molecular shape-factors.

The question which then remained was which approach should be followed to determine the resins+asphaltenes pseudo-component viscosities; would a colloidal system approach be more appropriate, or would the Free Volume approach provide more flexibility and accuracy? In order to answer this, the initial test fluid (SPE4), described in Chapter 3, had been used as a basis for the three pseudo-components, and each of the pseudo-component viscosities were calculated following the methods as discussed above. Since the SPE4 fluid was characterized by full composition only, it was necessary to find a real fluid from the literature where both the full composition, as well as the SARA analysis, were known, in order to understand the correlation between the two compositional break-downs. Jamaluddin *et al*. (1996) presented a rare combination of a SARA analysis, combined with a detailed oil composition (Table 6.5 and Table 6.6) for the Lindbergh field, Canada.

Table 6.5. Lindbergh oil properties and SARA analysis (Jamaluddin *et al*., 1996).

Oil Properties		**Lindbergh Oil**	**Sample A***
Density	g/mL	0.965	0.946
Viscosity	mPs.s at 20 °C	10,000	200 - 3,000
Molecular Weight		503	396
SARA Analysis (wt.%)			
Saturates		26	30
Aromatics		25	25
Resins		35	44
Asphaltene		14	<1

**Sample A: De-asphalted Oil (using n-pentane) + 12 wt% toluene*

This table shows that for the Lindbergh heavy oil with a viscosity of 10,000 cP at standard conditions, the resins account for 35 wt.%, and the asphaltenes 14%. Sample A shows the same oil, de-asphalted (DAO, using n-pentane, C_5H_{12}) and combined with 12% toluene (C_7H_8). Toluene is an aromatic with T_b=111°C, which, according to the SBN-method, would normally fall in the C8-group, but in this case, based on the relative increase observed in the C7-group (Table 6.6), was included in C7. Note the sharp decrease in asphaltene content from 14% to <1% (Table 6.5) and related decrease in C30+ from 21.48% to 5.27%, (Table 6.6), due to the de-asphalting process. Each of the components C12 to C29 showed the expected relative increase with the loss of part of the composition. It is also clear from Table 6.5 that the viscosities of the maltenes (resins included) are in the order of 200 to 3,000 cP at standard conditions. Table 6.6 shows that the de-asphalted oil (Sample A) still contained some (5%) C30+ molecules, which could possibly be classified as resins.

Table 6.6. Composition (mole%) of Lindbergh Oil and de-asphalted sample A (Jamaluddin *et al*., 1996).

Composition	Full Oil	Sample A
C1	0	0
C2	0.85	0
C3	0.74	0
i-C4	0	0
n-C4	0.55	0
i-C5	0	0
n-C5	0.38	0
C6	0.34	0.13
C7	0.28	0.83
C8	1.96	0.75
C9	2.91	1.46
C10	3.37	2.71
C11	5.17	5.52
C12	4.99	6.09
C13	5.04	6.3
C14	5.11	6.38
C15	5.05	8.43
C16	4.72	6.17
C17	3.45	4.51
C18	3.43	4.55
C19	3.65	4.93
C20	3.75	5.09
C21	3.38	4.71
C22	3.17	4.5
C23	2.69	3.87
C24	2.66	3.7
C25	2.53	3.56
C26	2.48	3.43
C27	2.25	2.96
C28	1.96	2.37
C29	1.66	1.78
C30+	21.48	5.27

These observations and characteristics had been used to ascertain that the test-case discussed in Chapter 3, based on the Fourth SPE Comparative study (SPE4) (Aziz *et al*., 1987), is realistic and that grouping/lumping all components from C30 and above together,

would be representative of a SARA group resins+asphaltenes. The new composition, introducing the new heavy pseudo-component with ECN=C40, is shown in Table 6.7.

Table 6.7. Pseudo-component grouping, with heavy resin-asphaltene pseudo-component.

Cn (ECN)	MW	Z_i	wt%	MW*Z_i
'C1'	16.043	0.1000	0.47	1.604
'C8'	107	0.0011	0.03	0.116
'C10'	134	0.0054	0.21	0.724
'C12'	161	0.0130	0.61	2.090
'C14'	190	0.0303	1.68	5.75
'C15'	206	0.0498	3.00	10.25
'C16'	222	0.0833	5.41	18.49
'C18'	251	0.1039	7.63	26.07
'C20'	275	0.1093	8.79	30.04
'C22'	305	0.0627	5.60	19.14
'C24'	331	0.0508	4.92	16.83
'C25'	345	0.0217	2.19	7.47
'C27'	374	0.0119	1.30	4.45
'C29'	402	0.0087	1.02	3.48
C40 (Asp+Res)	561	0.3483	57.14	195.3

This composition compares well with the real case composition in Table 6.6, where the intermediate hump is between C11 and C14, in this case at C18 to C20. The test fluid contains a higher fraction of methane, which is appropriate according to Lawal (2011). The 57 wt.% of the resin+asphaltenes pseudo-component compares well with the 50 wt.% of the combination in Table 6.5.

Using the Free Volume molecular characteristic parameters, l_m, E_0 and B, of the longest chain modelled in the previous section (Chapter 5), C64, resulted in viscosities that were too low (<1,000 cP at T_{std} = 15°C) to represent the proposed pseudo-component of asphaltene+resins. The expected viscosity for such a component is in the order of 10^{12} cP (Lawal, 2011), with the full oil mixture (heavy + light components) viscosity on the order of 10^5 cP at standard temperature. This applies to both the SPE4-based test case, as well as the Lawal example. With the objective to base the Free Volume parameters on physical properties, such as published properties for asphaltenes and resins (Groenzin and Mullins,

2000; Luo and Gu, 2007), the following Free Volume parameters were used as *a priori* information during a least-square fitting process:

- Molecular diameter in the order of 25 Å (assumes d=25 Å, therefore $L^2=3*d^2/20=95$ (Allal *et al*., 2000), assuming near-spherical molecules, and thus $l_m=L^2/b_f=25/b_f$, where b_f corresponds to the length of side of the cubic cage which surrounds the molecule (Å), including free volume;
- E_0 taken to be the activation energy E_a, in the order of 80-110 kJ/mole;
- B taken to be a shape-factor, where spherical-ellipsoidal shape-factors for asphaltenes only are around 2.5-3.

The Free Volume parameters required to fit the heavy pseudo-component viscosities to the estimated ones (back-calculated from the Arrhenius mixing rule and the SPE4 total oil viscosity, based on a C30+ heavy pseudo-component as in Table 6.7), are given in Table 8.

Table 6.8. Free Volume parameters for heavy pseudo-component (SPE4 case).

l_m (Å)	E_o (J/mole)	B
1.875×10^{-4}	106,000	0.276

In this case the value of b_f (where the characteristic length, $l_m=L^2/b_f$) that was required to fit the data was 500,000 Å (associated with the total molecular volume, hard-sphere+free). These parameters are not uniquely determined. In the case where the lower boundary of the E_0 was assumed (E_a = 90 kJ/mole), the best fit to data endpoints only, resulted in b_f=3000 Å (L = 25 Å and thus l_m=0.208 Å) and a 'shape factor' of B=0.28.

The Free Volume heavy pseudo-component viscosities for the SPE4 fluid, calculated using the parameters listed in Table 6.8, are shown in Table 6.9. The associated heavy component viscosity, required to result in the correct mixture viscosity, had very similar ranges as the Lawal asphaltene+resin viscosities in the temperature range of investigation. The densities shown were calculated in the same manner as described in Chapter 5, based on the extended Tait equation (Ciotta, 2010).

Table 6.9. Free Volume heavy pseudo-component viscosities for the SPE4 fluid, as a function of temperature.

T (°F)	Density(kg/m^3)	Viscosity (cP)
60	849	1.28E+09
100	834	4.65E+07
125	824	7.74E+06
150	815	1.54E+06
175	806	3.58E+05
200	797	9.53E+04
225	788	2.85E+04
250	779	9,465
275	770	3,441
300	762	1,356
400	727	62
500	691	6.2
600	648	1.02

As can be observed from Figure 6.5, the fit to the 'measured' (back-calculated from the Arrhenius mixing rule applied to the SPE4 fluid mixture, based on a C30+ heavy component) data is not perfect, with the average absolute deviation (AAD)[11] of 120%. The high deviations towards the endpoints could be an indication that the model may not be sufficiently flexible to represent such a complex mixture. The same phenomenon had also been observed in modelling real field data, where it is thought that the endpoint viscosities as measured in laboratories might deviate from theoretical models due to compositional changes when volatile components change phase at either low pressure or high

[11] $$AAD = \frac{\sum \frac{100 * |Exp - Calc|}{Exp}}{n}$$

temperatures. In both these instances priority should be given to the temperature ranges where accuracy is vital for the problem being modelled, as previously determined (Chapter 4).

In this case priority was given to minimise the average absolute deviation from $T=T_R$=125°F to $T=T_s$=400°F, based on the findings of the temperature range sensitivity research described in Chapter 4. Further oil recovery sensitivities to this heavy component viscosity had been simulated and are discussed in the next chapter.

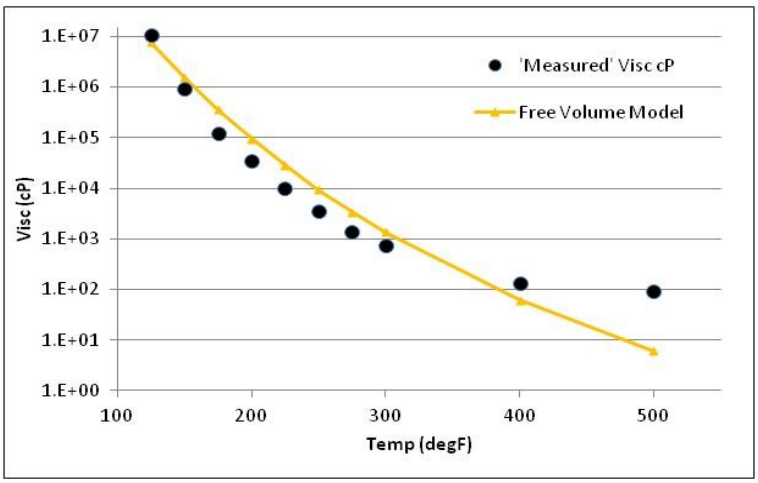


Figure 6.5. SPE4 Asphaltene+Resins pseudo-component viscosity (SPE4: black dots) modelled with the Free Volume Model (solid line).

6.3.2 Viscosities of colloid systems

Different researchers (Storm and Sheu, 1993; Argillier *et al.,* 2002; Luo and Gu, 2007) developed methods of using the asphaltene content of the oil to estimate heavy oil viscosities, based on colloidal dispersion theories such:

$$\mu_r = \frac{\mu_{disp}}{\mu_{maltene}} = 1 + [\mu]\phi + K_1\phi^2 + K_2\phi^3 + ... \tag{6.2}$$

where μ_r is the relative viscosity between those of the dispersion (maltenes+asphaltenes) and the maltenes. The parameter $[\mu]$ is the "intrinsic viscosity" of the asphaltene particles

and depends on the particle shapes (shape factor ν) and salvation constant (K); ϕ is the volume fraction of the asphaltenes in the mixture (more details are shown in Appendix C.). Eq. (6.3) below is a specific version of this method, based on field data.

The relationship shown in eq. (6.3) , based on work done by Luo and Gu (2007), had been tested in the present work.

$$\mu_r = \frac{\mu_{disp}}{\mu_{maltene}} = 1 + (53.483 - 0.1231T)\phi \tag{6.3}$$

It was found in the present work that colloidal dispersion relative viscosity method, as applied to the proposed grouping, resulted in oil mixture viscosities that were too low, compared to field measurements. This is due to the fact that the resins in the present study had been combined with the asphaltenes instead of the saturates and aromatics, and, as a consequence, the calculated 'maltenes'-pseudo-component viscosities were too low as a starting point. Further research is required in order to combine this method with the Free Volume viscosity model and different SARA pseudo-component lumping or groupings.

6.4 Conclusions

In this chapter a pseudo-heavy component has been characterized based on heavy crude resins and asphaltenes. Two methods to model the component viscosity as a function of temperature were tested: (1) the Free Volume method, based on physical properties such as the available free volume for molecules to move into, energy required to break inter-molecular bonds, and shape factors; (2) the colloidal system approach, in which the pseudo-heavy component viscosity is a function of the de-asphalted oil, in which case the asphaltenes were associated with particles mixed into a liquid, changing the viscosity.

It was found that the Free Volume method was again relatively easy to apply in modelling the newly defined pseudo-component viscosity and, in the test case used, gave good results, with an overall AAD of 120% when fitted to viscosity data between T_R and T_s. It was still

not possible to predict the heavy component viscosity in the absence of 'measured' data, using the extrapolations in Chapter 5 of this thesis, but a method has been proposed whereby the heavy component viscosity can be back-calculated from the measured oil mixture viscosity. The light to medium component viscosities can be calculated with the Free Volume method using the parameters in Chapter 5, after which the Arrhenius mixing rule can be used to 'extract' the heavy component viscosities. The Free Volume Model can consequently be used in a fitting procedure, with an appropriate objective function (incorporating physical characteristics of asphaltenes and resins), to find the Free Volume parameters. Once the Free Volume parameters had been established, the model can be used to predict the heavy component viscosities at all required pressures and temperatures.

The colloidal system approach was less successful, due to the grouping of the resins with the asphaltenes resulting in too low maltenes viscosities. More work is required to fully explore this method.

7 Thermal Simulation Sensitivities using Viscosities estimated by the Free Volume Model

7.1 Introduction

Following the investigations of pure component viscosity modelling (Chapter 5) and the characterisation and viscosity modelling of an extra-heavy pseudo-component (Chapter 6), the question remains as to whether it would still be possible to simulate heavy oil thermal recovery processes using only two pseudo-components, a gaseous live component and a heavy dead component, with the new methods implemented: component viscosities modelled using the Free Volume model, combined with lumping of heavy components into a single extra-heavy pseudo-component representing the resin-asphaltene fraction. The steam-line-drive case as described in Chapter 3, loosely based on the SPE Fourth Benchmark Study (Aziz *et al*., 1987), with an ambient oil viscosity in the order of 10,000 cP, was used to test the combination. In order to test the sensitivity to recovery method, further simulations followed, using a 100,000 cP oil in a SAGD case. It has already been illustrated in Chapter 3 that the initial reservoir pressure a determining factor is in cases where fluid-systems contain significant amounts of intermediate components (C2-C8), and that lumping beyond 10 pseudo-components resulted in high errors, if the initial reservoir pressure was below bubble point pressure. This case will not be repeated in this section.

7.2 Case Descriptions

Simulation of two separate recovery methods, steam-line-drive and SAGD, are tested for the sensitivity of oil recovery to Free Volume viscosity modelling, number of pseudo-components, and lumping strategy. The same fluid is used in both cases, only the dead-oil viscosities differ; with the steam-line-drive case the dead-oil viscosity of the order of 10,000 cP, was used while in the SAGD case the dead-oil viscosity of the order of 100,000 cP at 60 °F was chosen, incorporated in the very heavy pseudo-component viscosity.

7.2.1 Reservoir models and development strategies

7.2.1.1 Steam Line Drive (SLD)

In the case of steam-line-drive the model, as before, consisted of a 20×20×10 simulation grid with cell sizes of 5×5×5 ft. This translates into a reservoir of size 100×100×50 ft^3. The horizontal (*X* and *Y*) permeability in layers 1 to 2 was 2000 mD, in layers 3 to 5 was 500 mD, in layers 6 to 8 was 1000 mD, and in the last two layers, 9 to 10, was 2000 mD. The vertical to horizontal permeability ratio was set to unity, with porosity 30% in the full grid.Initial reservoir pressure and temperature were 400 psia and 125°F, respectively. The thermal conductivity of the rock was set to 24 btu/ft day °F (Somerton, 1992) and the rock heat capacity was 35 btu/ft^3 °F. The reservoir's outer boundaries were assumed to be non-conductive for the purposes of the sensitivity analysis.

In terms of saturation curves, the ECLIPSE default method of modelling three-phase saturation was used (where Figure 7.1 and Figure 7.2 show the two-phase relative permeability curves), with capillary pressures set to zero. The rock was set to be strongly water wet, with low water mobility, but high gas mobility. As the steam would be simulated as a gas component, the mobility of the steam was equal to that of the gas phase.[12]

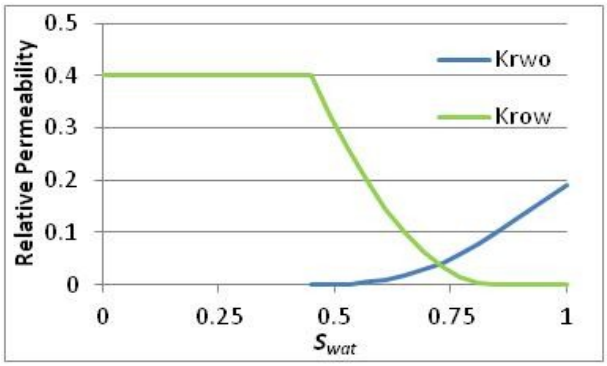


Figure 7.1. Oil-water relative permeabilities.

[12] Note: The gas-phase viscosity is determined by the following mixing rule during simulation, which differs from the oil-phase viscosity mixing equation: $\mu_g = \sum_{c=1}^{N_c+1} y^c \cdot \mu_g^c$.

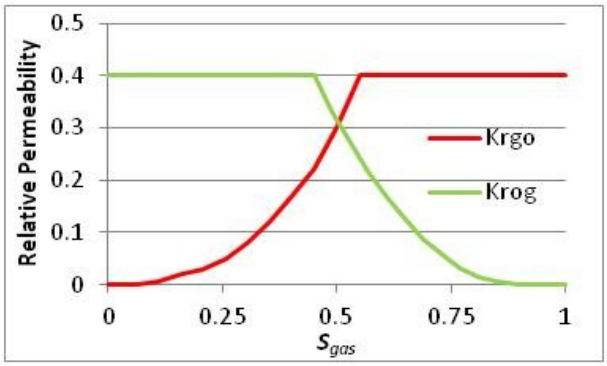


Figure 7.2. Oil-gas relative permeabilities.

The following production strategy was employed: steam was injected continuously into the upper left corner (Figure 7.3), while oil was produced from the bottom two corners. All three wells were perforated in all layers, and the steam was injected at a constant rate of 10 cold-water-equivalent (CWE) barrels per day, with a maximum bottomhole pressure of 1000 psi. Steam quality was set to 80%, and the injection temperature 450°F. Production in both producers started simultaneously, with the first steam injection on a very low bottomhole pressure control to limit interference with the rates. The well nearest to the injector, PNEAR, had a liquid target rate of 250 stb/d, whereas the well diagonally opposite from the injector, PFAR, had a target liquid rate of 125 stb/d. The maximum steam production rates for PNEAR and PFAR were 2.5 and 1.25 CWE bls/d, respectively. The model was run for five years, during which around 50% of oil initially in place was produced.

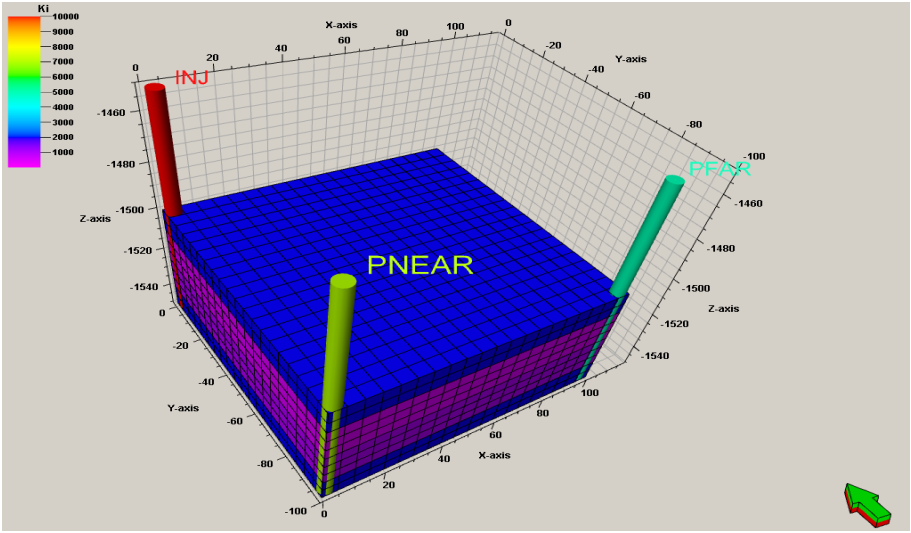


Figure 7.3. Steam-line-drive model: permeability distribution.

7.2.1.2 Steam Assisted Gravity Drainage (SAGD)

In the case of the SAGD model, a 8×20×40 simulation grid has been used, with cell-sizes 300×15×2.5 ft^3. (Note: Simulation gridcell sizes in the simulation of SAGD are limited to control numerical dispersion, more likely in these processes due to the high temperature differential between consequetive gridblocks, and the associated steep slope of the viscosity-temperature curve). Horizontal permeabilities in the top and bottom eight layers were 2000 mD, in layers 9 to 20 they were 500 mD, and in layers 21 to 32 they were 1000 mD, with vertical to horizontal permeability ratios equal to one. Porosity, thermal properties and saturation curves were as in SLD case.

The following production strategy was employed: steam was circulated for three months in two horizontal wells vertically separated by 15 feet. At the start of the third month, steam continued to be injected in the upper well at a target rate of 3800 CWE bls/d, limited by a bottomhole pressure of 1000 psi, while oil was produced from the lower well with a liquid target rate of 3800 stb/d and bottomhole pressure of 100 psi and a maximum liquid rate of 380 stb/d. Steam injection temperature was 480 °F and steam quality 65% (in realitity the quality could be closer to 95-100%). Both horizontal lengths were 1800 ft long, positioned in the bottom six layers of the model, as can be seen in Figure 7.4, at the centre of the model. The model was run for 25 years in order to see full effects.

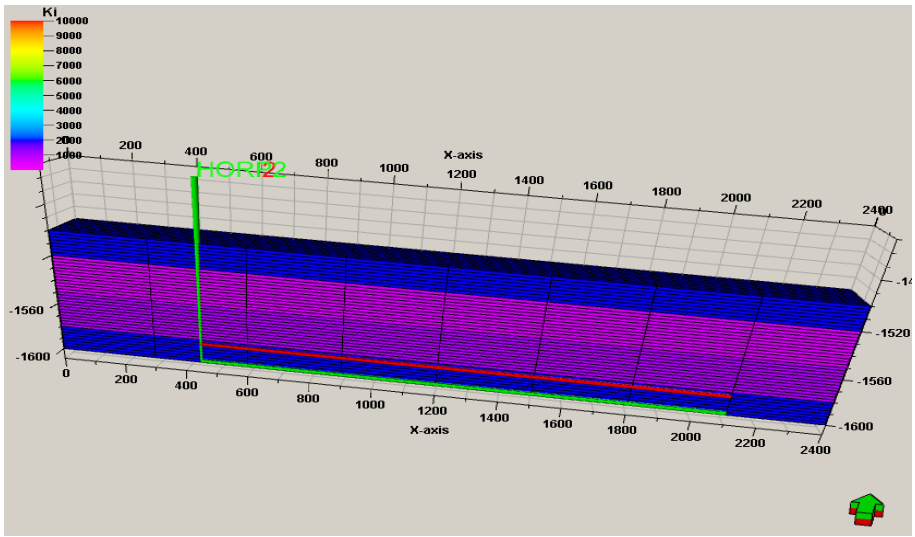


Figure 7.4. SAGD model: permeability distribution.

7.2.2 Component grouping/lumping

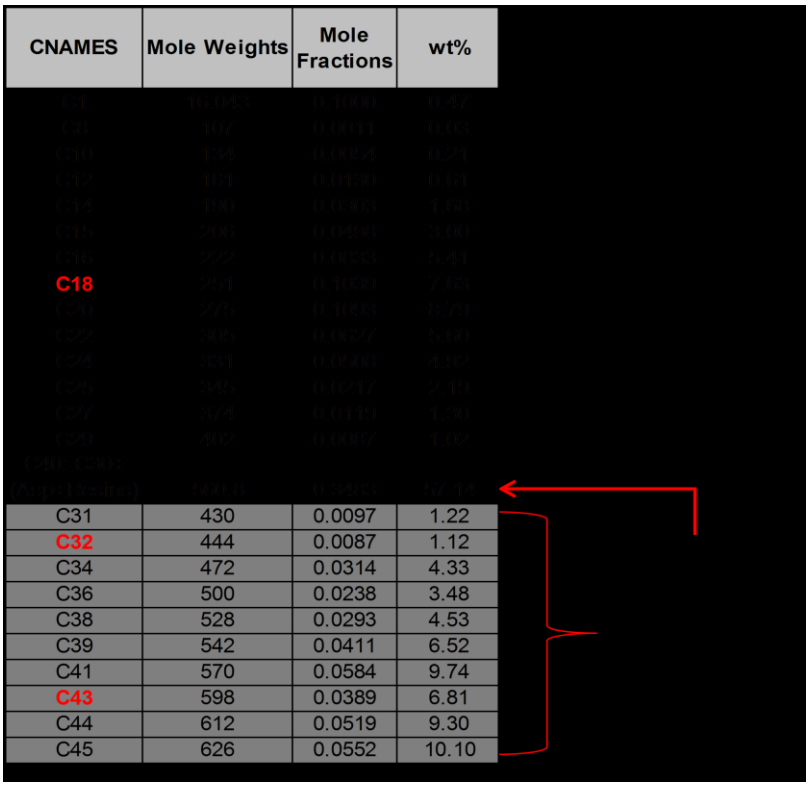
The original 24-component fluid, described in Chapter 3, was used, and the component grouping or lumping was performed in the same way in both cases. To represent the resin plus asphaltene component, all components from C30 and above were grouped together into one pseudo heavy component with a molecular weight of 560 g/mole, calculated as a mole-fraction weighted average. The equivalent carbon number (ECN) for this pseudo-component was C40 in this case, but it is acknowledged that in some heavy oil fluids this could be much higher. The resulting fluid consisted of 14 'pure' components and the heavy pseudo-component (Table 7.1). The rest of the components were lumped step by step into 8, 4, 3 and ultimately, 2 pseudo-components, with the molecular weight of each pseudo-component determined by eq. (7.1).

$$MW_{pc} = \frac{\sum_{i=ci}^{cj} MW_i Z_i}{\sum_{i=ci}^{cj} Z_i} \tag{7.1}$$

where *pc* represents the pseudo-component, lumping components *ci* to *cj*; MW_i the molecular weight of component *i* and z_i the mole-fraction of component *i*.

Each fluid was simulated with a cubic Peng-Robinson equation of state (Reid *et al*., 1987; PVTi 2010 reference manual), with regression after each lumping step, to the original P_{bub}=371 psi at 125 °F. This was done in order to preserve the original phase-behaviour. Each grouping step, and the resulting compositions, is shown in Table 7.1 to Table 7.6. The lines in the tables indicate the range of components lumped together in the following stage. In each of the tables, the newly determined molecular weight of the lumped components are shown, together with the ECN, new mole-fraction and weight percentage. The associated phase envelope as a function of pressure and temperature of each new composition is shown at each lumping stage as in Figure 7.5 to Figure 7.8. K-values, or equilibrium values, were supplied per ECN, or pseudo-component, in the form of look-up tables, as a function of pressure and temperature. These were generated with a Flash-calculation (PVTi SLB, 2010.1) for each combination.

Table 7.1. Detailed 24-component up-scaling to 15-components: 14 pure components plus 1 heavy pseudo-component. (Red components indicated the original SPE4 components).



CNAMES	Mole Weights	Mole Fractions	wt%
C18			
C31	430	0.0097	1.22
C32	444	0.0087	1.12
C34	472	0.0314	4.33
C36	500	0.0238	3.48
C38	528	0.0293	4.53
C39	542	0.0411	6.52
C41	570	0.0584	9.74
C43	598	0.0389	6.81
C44	612	0.0519	9.30
C45	626	0.0552	10.10

Table 7.2. 15-component composition.

Cn (ECN)	MW	z_i	Wt.%	MW*z_i
'C1'	16.043	0.1000	0.47	1.604
'C8'	107	0.0011	0.03	0.116
'C10'	134	0.0054	0.21	0.724
'C12'	161	0.0130	0.61	2.090
'C14'	190	0.0303	1.68	5.75
'C15'	206	0.0498	3.00	10.25
'C16'	222	0.0833	5.41	18.49
'C18'	251	0.1039	7.63	26.07
'C20'	275	0.1093	8.79	30.04
'C22'	305	0.0627	5.60	19.14
'C24'	331	0.0508	4.92	16.83
'C25'	345	0.0217	2.19	7.47
'C27'	374	0.0119	1.30	4.45
'C29'	402	0.0087	1.02	3.48
C40 (Asp+Res)	561	0.3483	57.14	195.3

Table 7.3. 8-PC composition.

Cn	MW	z_i	Wt.%	MW*z_i
C1	16.0	0.1000	0.47	1.60
C11	150.5	0.0195	0.86	2.93
C15	199.9	0.0800	4.68	16.00
C17	238.1	0.1871	13.03	44.56
C21	285.9	0.1720	14.39	49.18
C24	335.2	0.0725	7.11	24.30
C28	385.8	0.0206	2.32	7.93
C40	560.8	0.3483	57.15	195.35

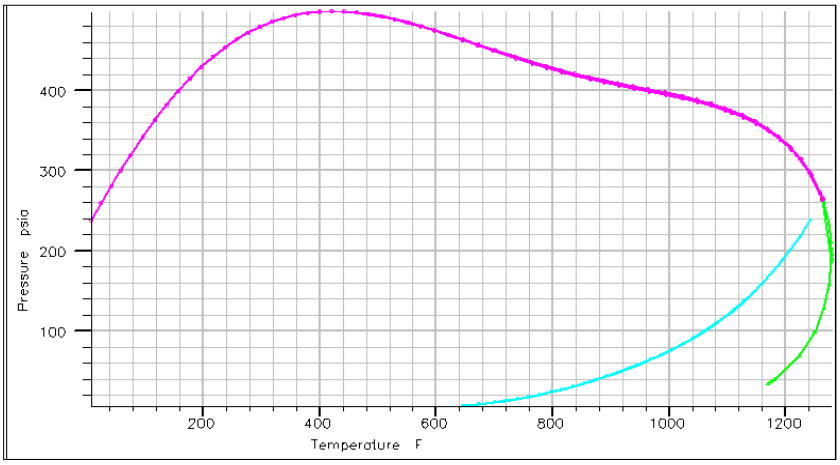


Figure 7.5. Phase envelope for 15 and 8-PC cases. Bubble-point line: pink, dew-point-line: green, 2-phase line: blue.

The phase diagrams of the 15 component case and the 8-pseudo-component (8-PC) case match perfectly.

Table 7.4. 4-PC composition.

Cn	MW	z_i	wt%	MW*z_i
C1	16.0	0.1000	0.47	1.60
C16	221.5	0.2866	18.57	63.49
C22	307.2	0.2650	23.81	81.40
C40	560.8	0.3483	57.15	195.35

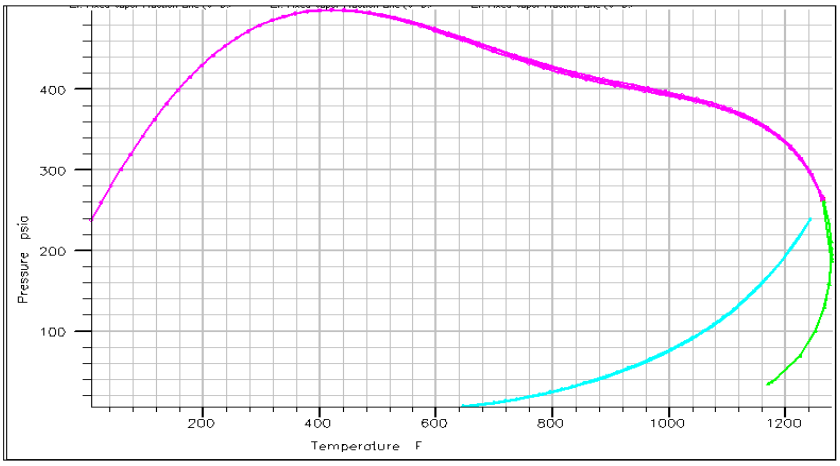


Figure 7.6. Phase envelope for 15 and 4 component cases.

The phase diagrams of the 4-PC case matches that of the 15-component case nearly perfectly.

Table 7.5. 3-PC composition.

Cn	MW	z_i	wt%	MW*z_i
C1	16.0	0.1	0.47	1.60
C19	262.6	0.552	42.39	145
C40	560.8	0.348	57.15	195

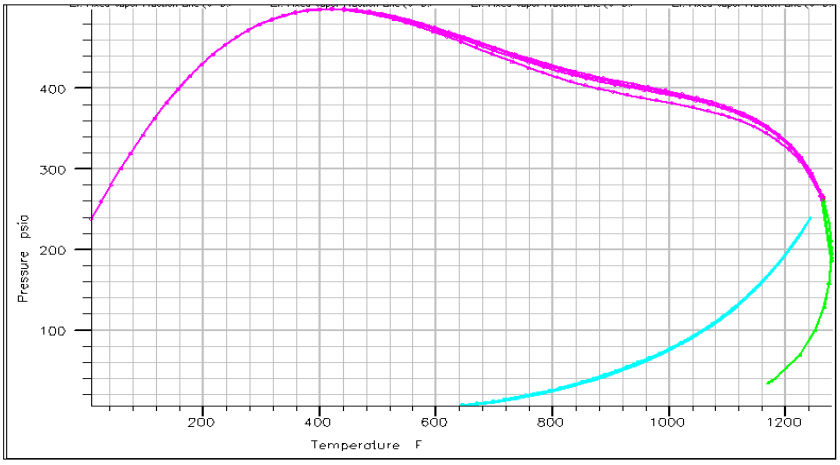


Figure 7.7. Phase envelopes for 15 and 4 component cases, together with 3-PC case.

A slight deviation in the 3-PC bubble-point line (pink) is visible on Figure 7.7, but the match is still reasonable.

The 2-PC bubble-point line (Figure 7.8) matches between the temperatures of interest: 125 and 600°F (*x*-axis), the range of temperatures expected to be encountered in the reservoir during thermal simulation. The composition is shown in Table 7.6.

Table 7.6. 2-PC composition.

Cn	MW	z_i	wt%	MW*z_i
C1	16.0	0.1	0.47	1.60
C27	378.0	0.9	99.53	340

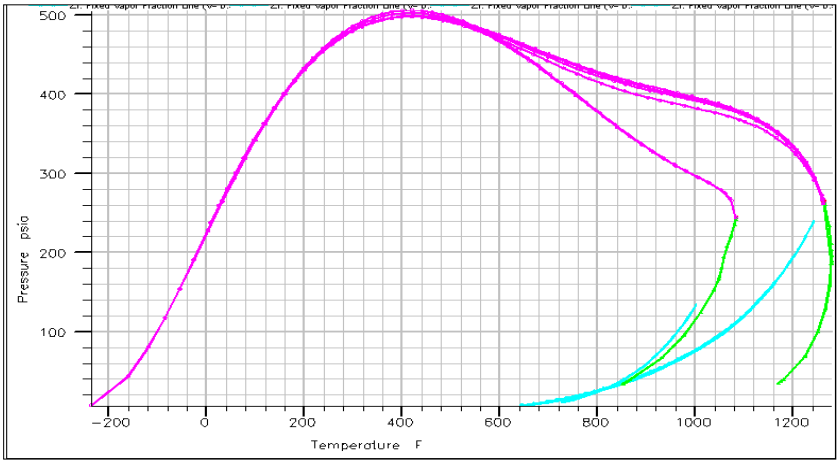


Figure 7.8. Phase envelope for 15, 4 and 3 component cases, compared with 2-PC case.

In conclusion, it can be observed that the phase behaviour was well preserved up until the three-pseudo-component (3-PC) fluid. In the 2-PC fluid priority was given to matching the phase behaviour for all reservoir pressure and temperature conditions expected during the simulated oil recovery process, but the effects on recovery results of the observed deviation in phase behaviour, will be quantified during simulations. An alternative grouping and simulation sensitivity results are shown later in this section.

7.2.3 Component viscosities

For all cases discussed in this section, the initial twenty-four pure component liquid viscosities had been modelled with the Free Volume model with parameters as discussed in Chapter 5, and the gas viscosities were modelled with an Andrade-type correlation. The

pure components from C30 and above were lumped into a single heavy pseudo-component and characterised as in Chapter 6, resulting in a fifteen-'pure'-component base case. During the upscaling or lumping process mentioned above, going from fifteen pseudo-pure species to eight, to four, three and eventually two pseudo-components, the Arrhenius rule, as described in Chapter 3, was used to predict the pseudo-component viscosities. The viscosity results of the component reductions are shown in Table 7.7 to Table 7.12. Table 7.7 and Table 7.8 show the Free Volume calculated viscosities for the 15 components used as a base case.

Table 7.7. 'Pure' component Free Volume viscosities: C1 to C16.

ECN	C1	C8	C10	C12	C14	C15	C16
MW	16.04	107	134	161	190	206	222
Mole %	10.0	0.108	0.54	1.30	3.03	4.98	8.33
T (°F)	1	2	3	4	5	6	7
60	0.006	0.551	1.000	1.643	2.567	4.811	4.000
100	0.005	0.430	0.740	1.146	1.737	3.046	2.557
125	0.004	0.375	0.627	0.941	1.402	2.371	2.001
150	0.003	0.330	0.539	0.785	1.153	1.888	1.601
175	0.002	0.294	0.469	0.665	0.964	1.533	1.306
200	0.001	0.264	0.412	0.571	0.817	1.267	1.083
225	0.0009	0.238	0.365	0.496	0.702	1.062	0.912
250	0.0008	0.217	0.327	0.435	0.610	0.902	0.777
275	0.0007	0.198	0.294	0.385	0.534	0.775	0.670
300	0.0006	0.182	0.267	0.343	0.473	0.673	0.583
400	0.0005	0.135	0.189	0.231	0.310	0.415	0.363
500	0.0004	0.105	0.142	0.167	0.220	0.282	0.248

Table 7.8.'Pure' component Free Volume viscosities: C18 to C29, plus heavy resin-asphaltene component.

ECN	C18	C20	C22	C24	C25	C27	C29	C30+ (Asph & Resins)
MW	251	275	305	331	345	374	402	560.8
Mole %	10.39	10.93	6.27	5.08	2.17	1.19	0.866	0.348
T (°F)	8	9	10	11	12	13	14	15
60	5.117	6.655	8.976	12.90	15.12	19.38	24.25	1.28E+09
100	3.189	4.046	5.306	7.37	8.51	10.66	13.08	4.65E+07
125	2.462	3.082	3.981	5.42	6.21	7.69	9.34	7.74E+06
150	1.946	2.407	3.067	4.11	4.67	5.72	6.88	1.54E+06
175	1.570	1.921	2.418	3.191	3.605	4.374	5.213	3.58E+05
200	1.289	1.562	1.944	2.531	2.843	3.418	4.043	9.53E+04
225	1.075	1.291	1.590	2.045	2.285	2.725	3.200	2.85E+04
250	0.908	1.083	1.321	1.680	1.867	2.211	2.580	9.47E+03
275	0.777	0.919	1.113	1.400	1.549	1.823	2.114	3.44E+03
300	0.672	0.790	0.948	1.182	1.303	1.523	1.757	1,356
400	0.409	0.470	0.551	0.665	0.723	0.829	0.939	62.0
500	0.275	0.311	0.357	0.422	0.454	0.512	0.573	6.20

Table 7.9. 8-PC case component viscosities, with heavy resin-asphaltene component.

ECN	C1	C11	C15	C17	C21	C24	C28	C40-PC
MW	16.043	151	200	238	286	335	386	561
Mole %	0.1	0.019	0.08	0.187	0.172	0.072	0.021	0.348
T (°F)	1	2	3	4	5	6	7	8
60	0.006	1.347	3.794	4.59	7.42	13.53	21.30	1.28E+09
100	0.005	0.962	2.463	2.891	4.47	7.69	11.62	4.65E+07
125	0.004	0.799	1.943	2.245	3.38	5.65	8.35	7.74E+06
150	0.003	0.674	1.567	1.784	2.630	4.27	6.19	1.54E+06
175	0.002	0.577	1.286	1.447	2.089	3.31	4.71	3.58E+05
200	0.001	0.500	1.073	1.193	1.692	2.62	3.67	9.53E+04
225	0.0009	0.437	0.908	0.999	1.393	2.11	2.92	2.85E+04
250	0.0008	0.386	0.778	0.847	1.164	1.734	2.36	9465
275	0.0007	0.344	0.674	0.727	0.986	1.443	1.940	3441
300	0.0006	0.309	0.589	0.631	0.844	1.217	1.617	1356
400	0.0005	0.212	0.372	0.388	0.498	0.682	0.874	62
500	0.0004	0.156	0.256	0.262	0.327	0.431	0.537	6.2

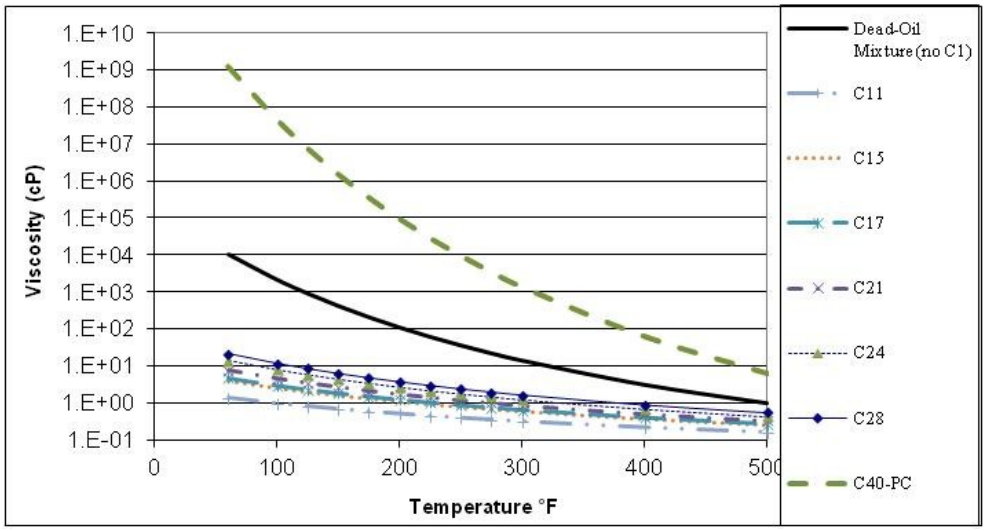


Figure 7.9. Dead-Oil mixture and component viscosities for 8-PC case.

Table 7.10. 4-PC case component viscosities, with heavy resin-asphaltene component.

ECN	C1	C16	C22	C40-PC
MW	16.043	221	307	562
Mole %	0.1	0.28663	0.26503	0.34834
T (°F)	1	2	3	4
60	6.0E-03	4.00	9.49	1.3E+09
100	5.0E-03	2.57	5.58	4.7E+07
125	4.0E-03	2.01	4.18	7.7E+06
150	3.0E-03	1.611	3.21	1.5E+06
175	2.0E-03	1.315	2.52	3.6E+05
200	1.0E-03	1.092	2.02	9.5E+04
225	9.0E-04	0.920	1.654	2.9E+04
250	8.0E-04	0.784	1.371	9465
275	7.0E-04	0.677	1.153	3441
300	6.0E-04	0.590	0.981	1356
400	5.0E-04	0.368	0.567	62
500	4.0E-04	0.252	0.366	6.2

Table 7.11. 3-PC case component viscosities, with heavy resin-asphaltene component.

ECN	C1	C19	C40-PC
MW	16.043	263	561
Mole %	0.1	0.552	0.348
T (°F)	1	2	3
60	6.0E-03	6.060	1.3E+09
100	5.0E-03	3.726	4.7E+07
125	4.0E-03	2.856	7.7E+06
150	3.0E-03	2.243	1.5E+06
175	2.0E-03	1.799	3.6E+05
200	1.0E-03	1.469	9.5E+04
225	9.0E-04	1.219	2.9E+04
250	8.0E-04	1.026	9465
275	7.0E-04	0.874	3441
300	6.0E-04	0.753	1356
400	5.0E-04	0.453	62
500	4.0E-04	0.301	6.2

Table 7.12. 2-PC case component viscosities.

ECN	C1	C27
MW	16.043	378
Mole %	0.1	0.9
T (°F)	1	2
60	6.0E-03	10105
100	5.0E-03	2079
125	4.0E-03	882
150	3.0E-03	407
175	2.0E-03	202
200	1.0E-03	107
225	9.0E-04	60
250	8.0E-04	35
275	7.0E-04	22
300	6.0E-04	13.7
400	5.0E-04	3.04
500	4.0E-04	0.972

7.3 Sensitivities

7.3.1 Steam-Line-Drive (SLD)

In this section, the original test case, consisting of a line-steam injection process, has been updated with the newly modelled oil viscosities. Sensitivities towards (a) Free Volume fit to a specific temperature range, (b) number of pseudo-components, and (c) specific combination of components in pseudo-component, has been tested.

The same SPE4-based case with the same fluid as before has been used, except that the oil viscosity as a function of temperature had been replaced in each case. The twenty-four-component fluid has been up-scaled to a fifteen-component fluid, in which all components above C30 were grouped together, as described in Chapter 3. The only difference was that the liquid viscosities of the pure components C1-C29 has been calculated with the Free Volume model, and the viscosity of the C30+ component, of which the characteristics (T_c,P_c,V_c) have been taken to be equivalent to C40, based on the molecular weight, have been calculated with the Free Volume method, as described in Chapter 6.

7.3.1.1 SLD Sensitivity 1: Oil Recovery to Heavy Component Viscosity Prediction

Three different predictions were made for the behaviour of the heavy pseudo-component viscosity, based on the priority that was given to specific data points. Each of these predictions were incorporated in the steam-line-drive model to establish exactly how sensitive the oil recovery predictions are to modelling decisions that may appear to be relatively unimportant.

Three cases were compiled: (a) the heavy pseudo-component viscosity was modelled such that the AAD was minimised at the endpoints of the 'experimental' data, and the case was named FV1, as seen in (Figure 7.10); (b) the heavy pseudo-component viscosity was modelled such that the AAD was minimised at 'experimental' viscosities $\mu(T_R)$ (T_R=125°F) and $\mu(T_s)$ (T_s=400°F). The AAD at these two point was 2.7%, with an AAD=207% for all points between T_R and T_s. This case was called FV2 and is shown with a blue dotted line in Figure 7.11. (c) The heavy pseudo-component viscosity was modelled

such that the total AAD was minimised at all 'experimental' viscosities from $\mu(T_R)$ up to $\mu(T_s)$. In this case the AAD at $\mu(T_R)$ and $\mu(T_s)$ combined was 40%, while the total AAD between these two temperatures was 120%. This case was called FV3 and is represented by the yellow line in Figure 7.11.

Four cases were simulated, three with the heavy pseudo-component viscosities modelled as described above, and one, the base case, with the 'experimental' heavy component viscosities. Comparative results are presented below.

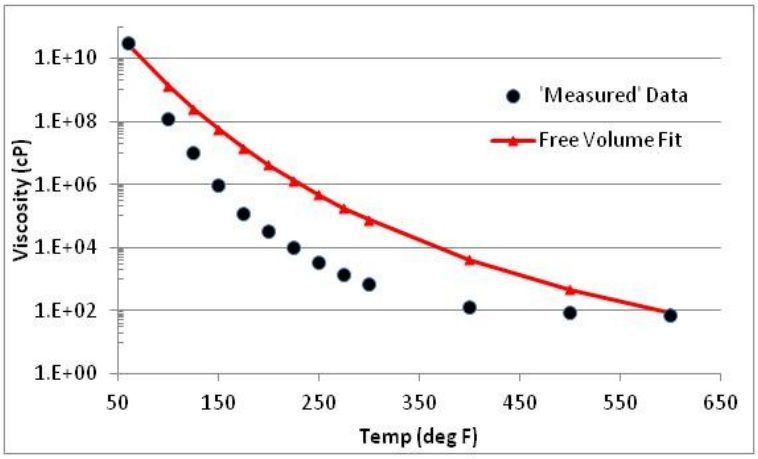


Figure 7.10. Heavy pseudo-component (asphaltene + resin) viscosity vs. temperature: priority on fitting measured endpoints.

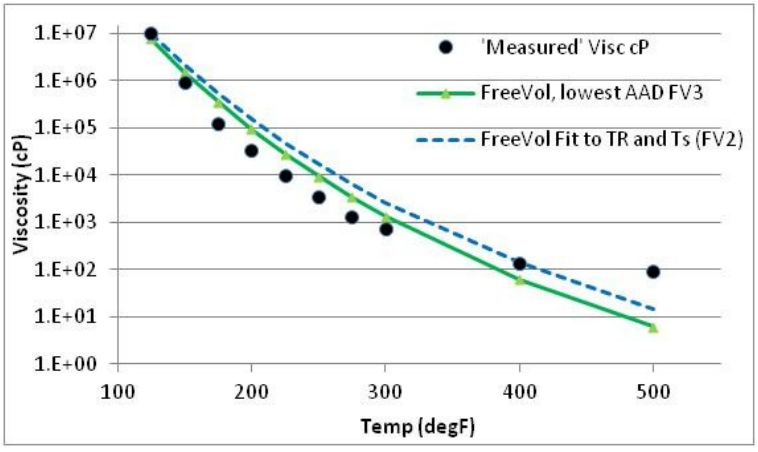


Figure 7.11. Heavy pseudo-component (asphaltene + resin) viscosity vs. temperature. FV2 (blue dotted line): priority on fitting T_R and T_s; FV3 (solid line): lowest AAD on all points between T_R and T_s.

Figure 7.12 shows the results in the cumulative oil production of the four simulated cases. The base case with 'experimental' viscosity data for the heavy component is shown in black (dots). Case FV2, in which the heavy component viscosity was modelled such to minimise the deviation at the two temperatures, T_R and T_s, is shown in blue, while FV3, with a total deviation minimisation of all data points from T_R up to T_s, is shown in green. Case FV1, fitted to end-points only, is shown in red. Results indicate that the oil recovery predictions would be most successfully simulated if one minimises the total deviation of modelled viscosities between the initial reservoir temperature (T_R) and the temperature at the steam-oil interface (T_s). It is very clear from this figure that the case where viscosity values only fitted the endpoints led to under-prediction of the recovery, by as much as 24% at the ultimate recovery. The error in case FV2 is 5%, and in case FV3 is 2.5%. Table 7.13 shows the actual cumulative oil produced in each case and Table 7.14 the relative deviations from the base case, where a negative number indicated over-prediction. In the case of steam-line drive, it is therefore important to fit all data values between the initial reservoir and the oil-steam interface temperatures.

The fact that the FV2 case prediction is slightly less representative than the FV3 case, shows that the majority of the produced oil is influenced by oil flowing at temperatures between these two boundaries at which the heavy component viscosities were slightly over-predicted. At early times (t < 800 days) the green line on Figure 7.12, representing case FV3, replicates the production of the base case exactly due to the good fit in 'cold' temperature viscosities. The deviations of the heavy component viscosity from the 'experimental' viscosity data at higher temperatures are visible in the cumulative production after 900 days, the time at which the steam front arrives at the far-end producer, increasing the temperature in the vicinity of the well above 200 °F. Both cases, FV2 and FV3, slightly over-predicts the oil viscosity at this temperature, with the FV2 viscosity slightly higher. However, the prediction deviations are well within normal reservoir simulation uncertainty ranges (around 10%).

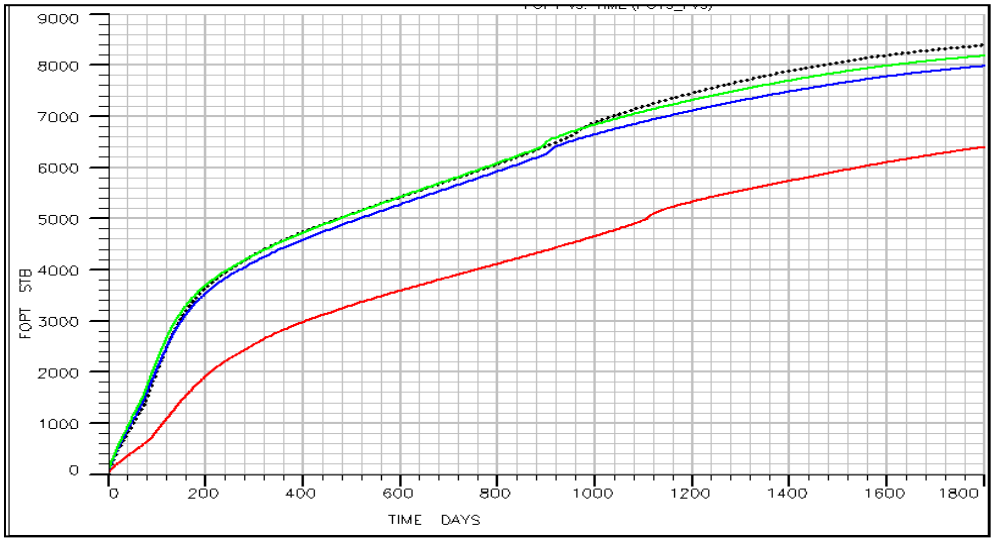


Figure 7.12. SLD Cumulative oil production (STB) for different heavy pseudo-component viscosity predictions. PC15 Experimental: black dots, PC15-FV1 case: red line, PC15-FV2 case: blue line, PC15-FV3 case: green line.

Table 7.13. SLD cumulative oil production (STB) for different heavy pseudo-component viscosity predictions.

Experimental	Endpoints	min AAD(T_R,T_s)	Total min AAD(T_R to T_s)
PC15-VEXP	PC15-FV1	PC15-FV2	PC-15_FV3
8393	6402	7980	8181

Table 7.14. SLD cumulative oil production deviations for different heavy pseudo-component viscosity predictions from base case with 'measured' values.

FV1 (min AAD(EndPoints))	FV2 (min AAD(T_R,T_s))	FV3 (Total min AAD(T_R to T_s))
23.7	4.9	2.5

7.3.1.2 SLD Sensitivity 2: Oil recovery to number of pseudo-components

In order to test the sensitivity of the ultimate recovery towards grouping, each of the three heavy components viscosity cases FV1, FV2 and FV3 had been 'upscaled', with the original fifteen components grouped sequentially into to eight, four, three and two pseudo-

components. Each of these cases was simulated, and the oil recovery (represented by the cumulative oil produced) was compared to both the 'experimental data'-based case, as well as the fifteen-component case of each of the models. The results are presented separately for each case.

7.3.1.2.1 FV1: $\mu_{hvpc}(AAD_{min}(T_{min},T_{max}))$

In the case where the heavy component viscosity end points of the 'experimental' viscosity data had been fitted (μ-AAD=1.7% at T_{min}=60 °F and T_{max}=600 °F), the majority of the heavy component viscosity *vs*. temperature points were well above the 'measured' values. This had a large effect on the recovery prediction as shown in section 1, with an error of 24%. The effects on oil recovery of the component grouping into pseudo-components can be seen in Figure 7.13. In this figure, the case containing the 'experimental' heavy pseudo-component viscosities is represented by a black dotted line. The FV1-base-case, the 15-PC case, is represented with a solid blue line and the 2-PC case in solid red.

Apart from the large error compared to the experimental values-case, the component-lumping itself resulted in no significant prediction deviations at late time (Table 7.15 and Table 7.16). At early times a significant error (of up to 16.2% at 520 days) is visible in the 2-PC case due to the lack of sufficient modelling of distillation effects as the very heavy pseudo-component is included in the single whole-oil pseudo-component. Once the steam reaches the PFAR well, at 1050 days, the error decreases to an insignificant value of 1.6% over-prediction at the end of the simulation period. The deviations in the 3-PC and 4-PC cases are less than 5%, and therefore within general simulation uncertainty margins.

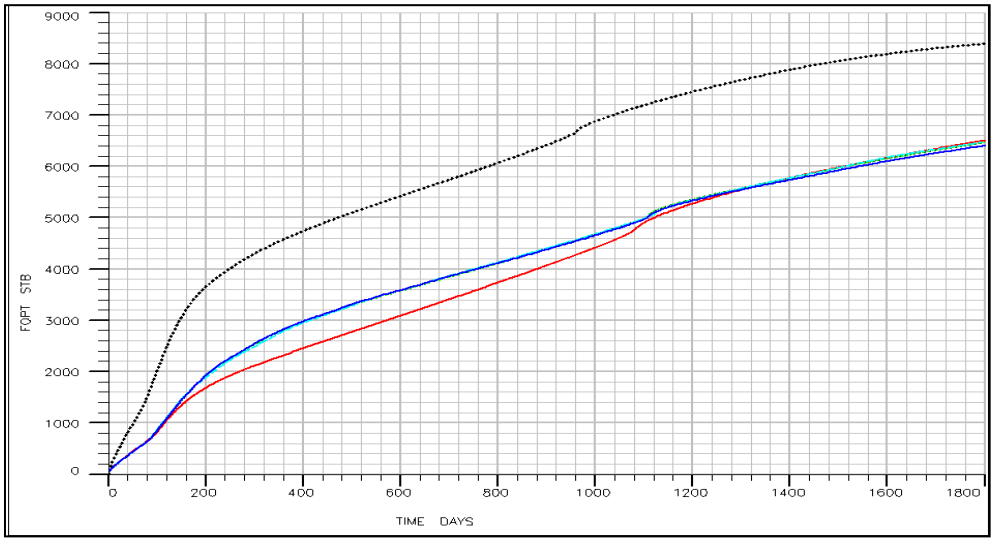


Figure 7.13. SLD-FV1 cumulative oil production (STB) as a function of number of pseudo-components. Case with 'measured' heavy oil viscosities shown in black dots, 15-PC base case in solid blue, 2-PC case in red. Other cases shown: 8-PC (dark green dotted), 4-PC (light green dotted), 3-PC (light blue dashed).

Table 7.15. SLD-FV1 cumulative oil production (STB) as a function of number of pseudo-components.

Experimental	Cum Oil STB ($\mu_{hvpc}(AAD_{min}(T_{min},T_{max}))$)			
PC15-VEXP	PC15-FV1	PC4-FV1	PC3-FV1	PC2-FV1
8393	6402	6461	6474	6502

Table 7.16. SLD-FV1 cumulative oil production deviation as a function of number of pseudo-components.

DEV % from 15-PC FV1			DEV % from 15-PC EXP		
PC4-FV1	PC3-FV1	PC2-FV1	PC4-FV1	PC3-FV1	PC2-FV1
-0.9	-1.1	-1.6	23.0	22.9	22.5

7.3.1.2.2 FV2: $\mu_{hvpc}(AAD_{min}(T_R,T_s))$

Each of the cases has been up-scaled step by step: fifteen to eight to four to three to two pseudo-components. In the case of FV2, with the heavy component viscosity deviation

minimised at two specific temperatures (in-between viscosity was higher than experimental values, whereas above T_s the predicted viscosity was lower than the experimental values), T_R and T_s, only a small deviation was observed when grouping. Even the two-pseudo-component case although presenting the largest overall deviation, gave ultimate recovery results similar to the FV2-15PC case (Figure 7.14). This is due to the fact that the heavy component was kept separate, and its viscosity was kept constant through the upscaling, except in the case of the two pseudo-components, when all 'pure' components from C2-C29 were grouped with the pseudo-heavy, containing the asphaltene. Only C1 remained as a single pure component. Figure 7.14 shows the base case (15-PC) with the 'experimental' heavy component viscosities in black dots, the 15-PC (FV2) in solid blue, 4-PC in dark-green dots, 3-PC in light-green dashed line. The 2-PC case is shown in red. Table 7.17 and Table 7.18 show the AAD per case, relative to the PC15-FV2 recovery results. It is clear that although the 2-PC case slightly over-predicts (2% more than the 15-PC case), the end result is actually closer to that of the experimental-data based 15-PC case. There is a clear change-over from under-predicting at early times to slightly over-predicting (compared to 15PC-FV2) after steam-break-through at the well furthest from the injector (at 900 days). The field production was mainly driven by this well, PFar (due to a production steam limit imposed which limited PNear where steam arrived very early), and the over-prediction of viscosity at temperatures between 125 and 400 °F shows at times less than 900 days. At the point the steam arrives, the oil temperature is greater than 400 °F, and the modelled heavy oil viscosity is now under-predicted, resulting in higher production. The reason for this effect being more pronounced in the 2-PC case, is that the distillation effects will be reduced, and any error in the heavy component is now contained in the oil as a whole.

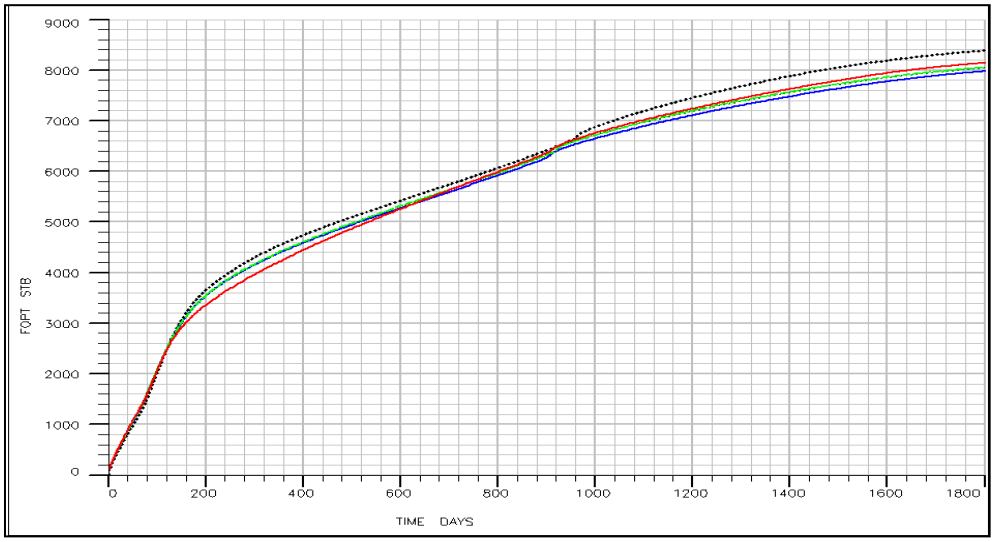


Figure 7.14. SLD-FV2 cumulative oil production (STB) as a function of number of pseudo-components. Case with 'measured' heavy oil viscosities shown in black dots, 15-PC base case in solid blue, 2-PC case in red. Other cases shown: 4-PC (dark green dotted), 3-PC (light green dashed).

Table 7.17. SLD-FV2 cumulative oil production (STB) as a function of number of pseudo-components.

Experimental	$T_R + T_s$ min AAD			
PC15-VEXP	PC15-FV2	PC4-FV2	PC3-FV2	PC2-FV2
8393	7980	8042	8057	8145

Table 7.18. SLD-FV2 cumulative oil production deviation as a function of number of pseudo-components.

DEV % from 15PC-FV2			DEV % from 15PC-EXP		
PC4-FV2	PC3-FV2	PC2-FV2	PC4-FV2	PC3-FV2	PC2-FV2
-0.8	-1.0	-2.1	4.2	4.0	2.9

7.3.1.2.3 FV3: $\mu_{hvpc}(AAD_{min}(T_R \text{ to } T_s))$

In case FV3, the heavy oil component viscosity deviation from 'experimental' values was minimised for all viscosity data points from T_R (125 °F) up to T_s (400 °F). Figure 7.15 shows the results of the 'upscaling' from fifteen components to two components. As before, the base case (15-PC) with the 'experimental' heavy component viscosities in black dots,

the 15-PC (FV3) in solid blue, 4-PC in dark-green dots, 3-PC in light-green dashed line. The 2-PC case is shown in red.

The deviation in recovery as a result of component-grouping or up-scaling, is again not significant and highest (2.2%) in the 2-PC case, compared to the FV3 15-PC base case (Table 7.19 and Table 7.20).

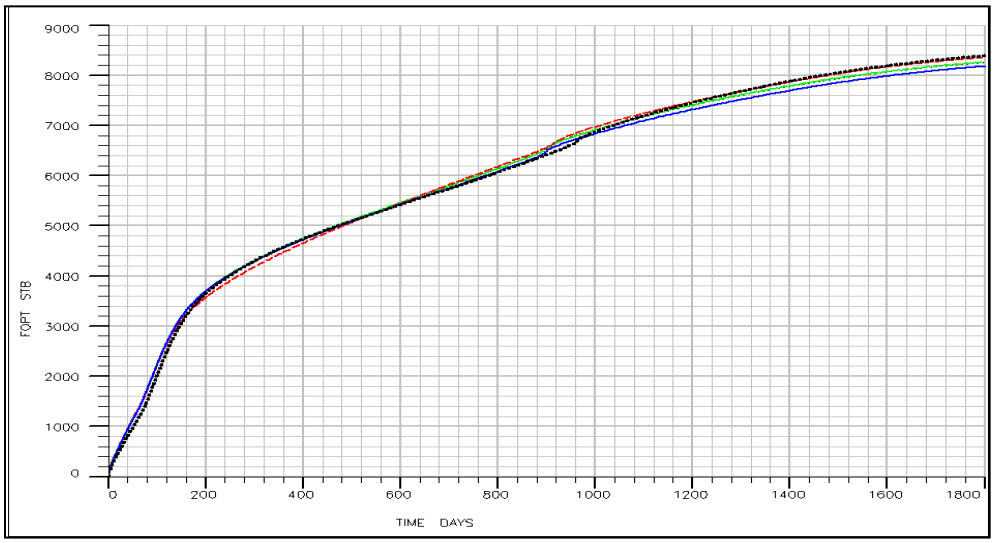


Figure 7.15. SLD-FV3 cumulative oil production (STB) as a function of number of pseudo-components. Case with 'measured' heavy oil viscosities shown in black dots, 15-PC base case in solid blue, 2-PC case in red, 4-PC (dark green dotted), 3-PC (light green dashed).

Table 7.19. SLD-FV3 cumulative oil production (STB) as a function of number of pseudo-components.

Experimental	Total min AAD (between T_R + T_s)			
PC15-VEXP	PC15-FV3	PC4-FV3	PC3-FV3	PC2-FV3
8393	8181	8251	8266	8358

Table 7.20. SLD-FV3 cumulative oil production deviation as a function of number of pseudo-components.

DEV % from 15PC-FV3			DEV % from 15PC-EXP		
PC4-FV3	PC3-FV3	PC2-FV3	PC4-FV3	PC3-FV3	PC2-FV3
-0.8	-1.0	-2.2	1.7	1.5	0.4

7.3.1.2.4 Discussion

Overall the cumulative production was well represented by 2-PC case. However, the larger deviation at early times observed in model FV1 shows that the success in representing heavy oil with only two pseudo-components very much depends on the successful modelling of the heavy pseudo-component viscosity, due to its a large influence on the average oil-mixture viscosity. In the FV1 model the mixture oil viscosity (all components C2+) was, on average, four times that of the oil in model FV3, with a viscosity of 3400 cP at 125 °F, as opposed to 900 cP in model FV3. This was solely due to a difference in the modelling of the heavy component viscosity. Clearly, the magnitude of the error at early times in the 2-PC cases is a function of the heavy pseudo-component viscosity. The more viscous this component is in comparison to the intermediate components mixture, the larger the error.

7.3.1.3 SLD Sensitivity 3: Oil Recovery to Lumping Strategy in 2-PC cases

In this sensitivity study the question was whether the case could possibly be simulated equally accurately with two pseudo-components in a different grouping scenario. In this case the heavy pseudo-component maintained its heavy character by only grouping it with all pure components from C20 and above. This was to allow for the observed phenomenon of the very heavy fraction remaining in the reservoir after the steam front had 'stripped' the oil of the lighter components. If the resin and asphaltenes are the compounds left in the reservoir, this grouping should be representative, consisting of one 'live' and one 'dead' component. All pure components from C1 to C18 had been grouped together into one light pseudo-component with ECN=C2. The composition and comparative phase diagrams are shown in Table 7.21 and Figure 7.16, with the associated component viscosities in Table 7.22.

Table 7.21. Alternative 2-PC component-lumping scenario.

C	MW	z_i	Wt.%	MW* z_i
C2	26.6	0.39	3.0	10.29
C39	540.6	0.61	97.0	331.56

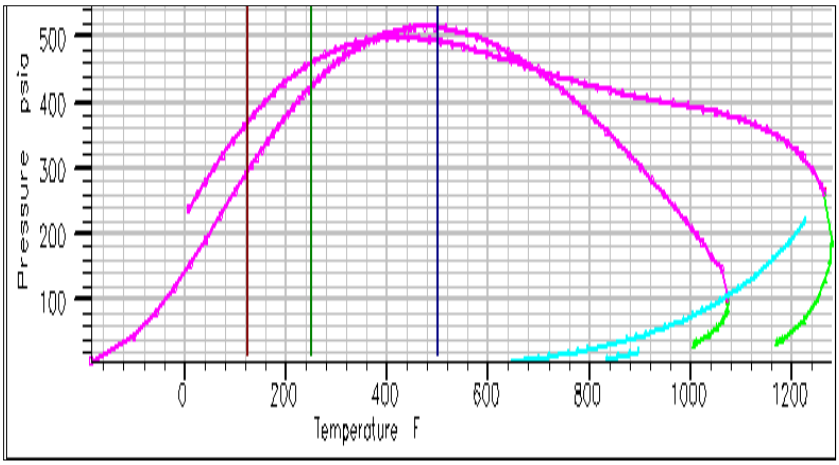


Figure 7.16. Phase envelope of alternative 2-PC grouping case, overlaying original fifteen-component case with dew-line >1200 °F.

It is clear that, even with regression, it was not possible to match the initial fifteen-component phase diagram between the temperatures of interest, which were 125 °F (T_{Res}) and 400 °F ($T_{steam\text{-}injection}$). However, a relatively close match was obtained for temperatures between 300 and 600 °F.

The effect on component viscosities was to significantly increase the viscosities of both components. The effect of increasing the lighter pseudo-component viscosity was to delay the progress of the steam front through the reservoir, as will be illustrated later.

Table 7.22. 2-PC case component viscosities, using alternative component lumping scheme.

ECN	C2	C39
MW	26	553
Mole %	0.35	0.65
T (°F)	1	2
60	5.4E-01	3.9E+05
100	3.6E-01	4.8E+04
125	3.0E-01	1.5E+04
150	2.5E-01	5404
175	2.1E-01	2127
200	1.7E-01	912
225	1.5E-01	421
250	1.4E-01	208
275	1.3E-01	108
300	1.2E-01	60
400	1.0E-01	8.2
500	8.9E-02	1.83

The results are presented per heavy-component viscosity modelled case:

1. FV1 (AAD at $\mu(T_{std})$ and $\mu(T_{max})$ minimised),
2. FV2(AAD of $\mu(T_R)$ and $\mu(T_s)$ at minimum) and
3. FV3 (total μ-AAD between T_R and T_s minimised)

Figure 7.17 to Figure 7.19 show that the second grouping, where the saturates and aromatics have been grouped with the gas component in order to create one distillable component, resulted in very large recovery deviations from the base case - present in all three viscosity models.

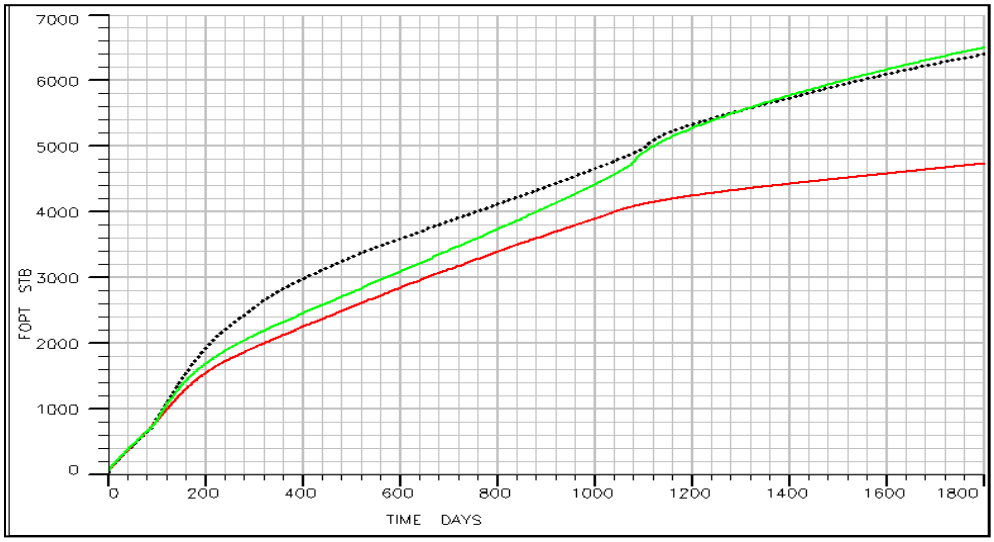


Figure 7.17. Cumulative oil production over time for the two 2-PC cases (FV1: heavy PC viscosity matched at endpoints), shown with the fifteen-component case (black dots). Original 2-PC case: green; new grouping: red.

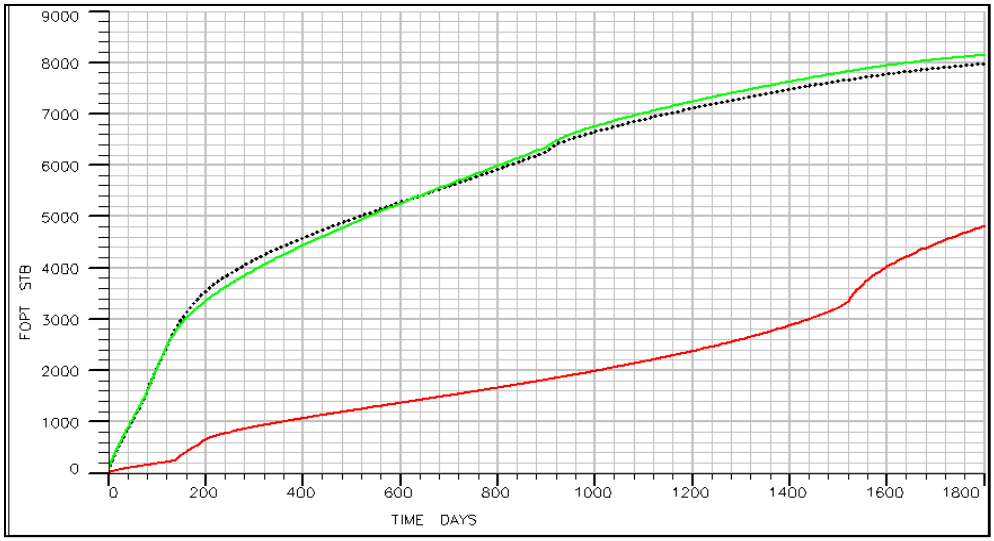


Figure 7.18. Cumulative oil production over time for the two 2-PC cases (FV2: heavy PC viscosity matched at T_R and T_s), shown with the fifteen-component case (black dots). Original 2-PC case: green; new grouping: red.

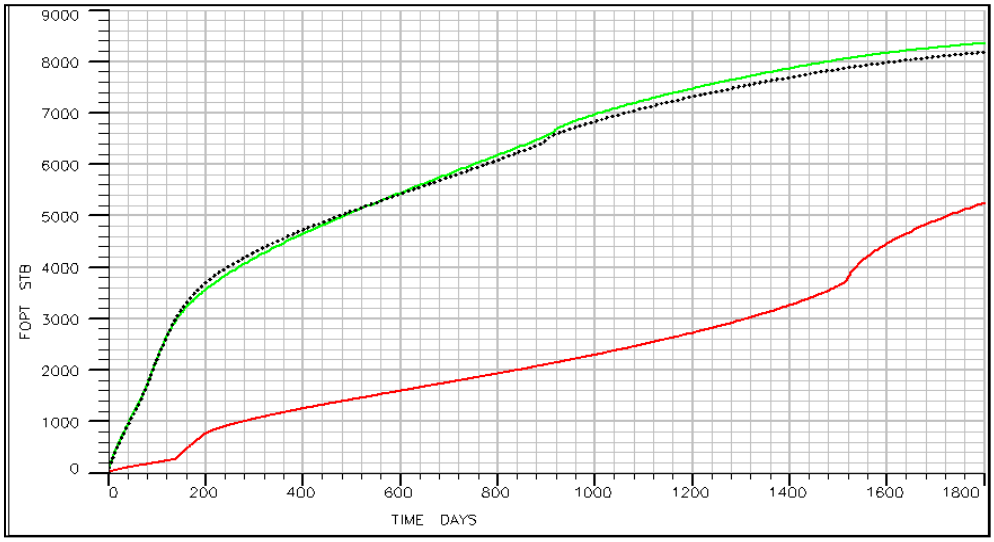


Figure 7.19. Cumulative oil production over time for the two 2-PC cases (FV3: heavy PC viscosity minimum AAD), shown with the 15-component case (black dots). (Original 2-PC case: green; new grouping: red).

It is clear from these results that it would be incorrect to lump the methane with the light oil components, ending up with a fluid of 39% C2 and 61% C39. The final recovery is much lower due to the fact that the gas-component was not correctly represented, consequently affecting the heavy component mobility adversely. Figure 7.20 shows the steam production rates at the well furthest away from the injector, PFAR, illustrating the late arrival of the steam front (red line), caused by the heavier gas-component in the alternative lumping scheme. Figure 7.21 shows the influence of the higher viscosity of the heavy oil component on the production rates at the well furthest away from the injector, prior to the steam-front arrival.

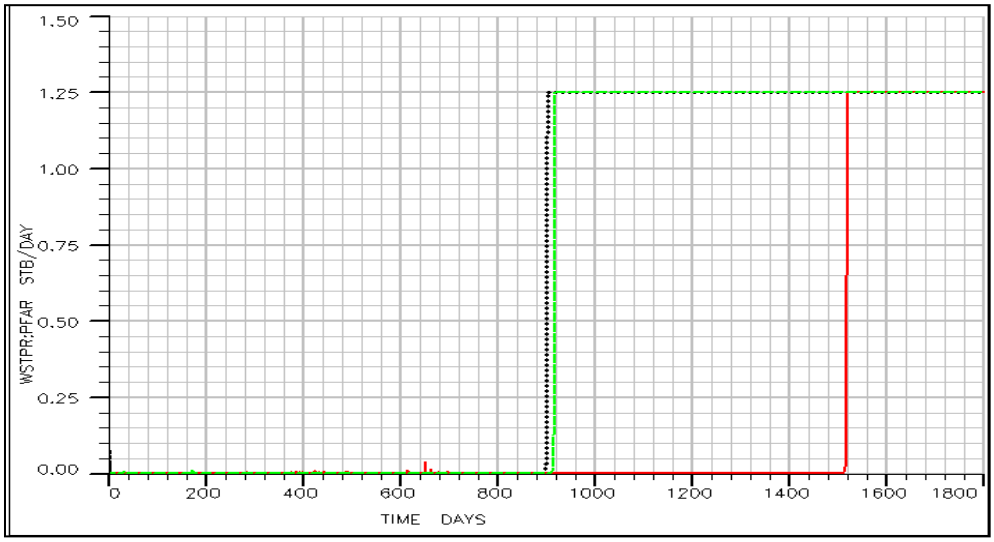


Figure 7.20. SLD-FV3: Steam production rates for 15-PC, 2-PC and alternative grouping 2-PC cases. Difference in steam-front arrival time at PFAR. (15-PC base case: black dotted line; 2-PC: green dashed line; 2-PC, alternative lumping: red line).

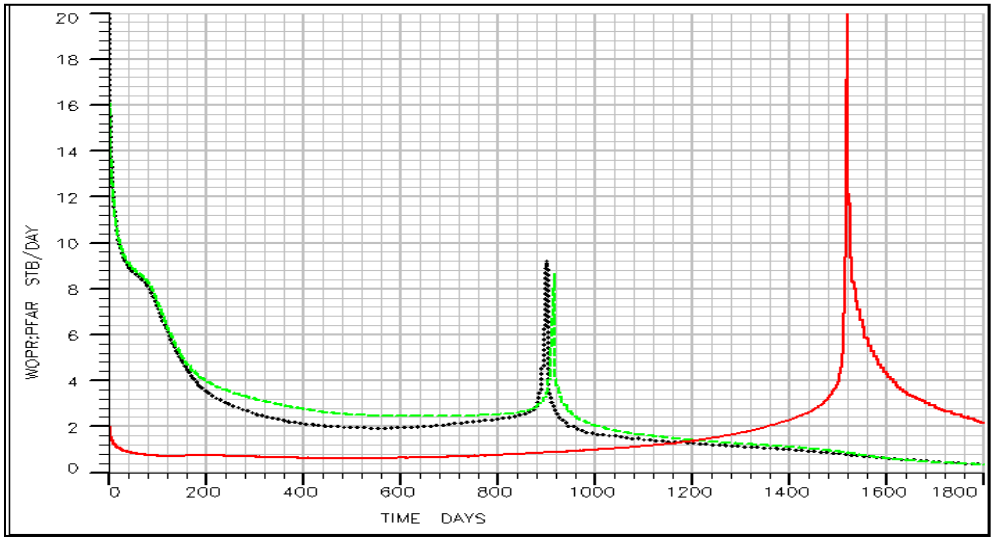


Figure 7.21. SLD-FV3: Oil production rates at PFAR. (15-PC base case: black dotted line; 2-PC: green dashed line; 2-PC, alternative lumping: red line).

Table 7.23 shows the predicted oil recoveries deviations in the 2-PC cases for each of the heavy component viscosity models, as compared to the original fifteen-component cases, as before.

Table 7.23. 2-PC alternative grouping recovery results and deviations from 15 component cases.

FOPT (STB)			Deviation% from 15-PC			Deviation% from 15-PC (experimental)		
FV1	FV2	FV3	FV1	FV2	FV3	FV1	FV2	FV3
4735	4811	5253	26	40	36	44	43	37

With this alternative lumping scenario the lowest deviation (26%) was in the case where the heavy pseudo-component viscosity end-points were matched, but is only due to the combination of the phase-behaviour and the heavy pseudo-component viscosity deviations and is not conclusive.

7.3.1.4 SLD Sensitivity 4: 10°API oil.

The oil recovery sensitivity to the molefraction distribution of an oil system, where the oil viscosities were determined with the Free Volume model, had been tested. The same fluid system (Pedersen, Christensen, 2007), as described in Chapter 3, Section 3.7., was used, and contained intermediate components (C2-C8). Liquid viscosities for components C1 to C26 were calculated with the extended Free Volume model, whilst the viscosity of the heavy end pseudo-component (C64) was derived with the Arrhenius equation, preserving the exact same deadoil viscosity as used in Chapter 3. The mixture viscosity is 1,500 cP at 100°F. The reservoir description, simulation grid, initial pressure (2000 psi) as well as the wells and well controls, remained the same.

For comparison purposes, the 30-component case from Chapter 3 will be assumed the base case. The five sensitivity cases consisted of 91) a 30-component case with the Free Volume oil component viscosities, (2) a 10-pseudo-component case, where the Free Volume oil viscosities were grouped with the Arrhenius method (component lumping remained the same as previously), (3) a 5-pseudo-component case, (4) a 3-pseudo-component case, and (5) a 2-pseudo-component case.

The field cumulative oil production for the cases is shown in Figure 7.22. The base case in this graph represents the original 30-component case, with oil viscosities determined with Pedersen's method. The rest of the lines represent the cases with the oil viscosities

calculated by the Free Volume method, but with the C30-plus-fraction viscosity chosen such that the deadoil viscosity remained the same. This was done in order to illustrate that the suggested method of modelling the C1 to C26 viscosities, using the Free Volume parameters optimised to alkane viscosities, will represent the saturates and aromatics viscosities in a similar fashion as the Pedersen method.

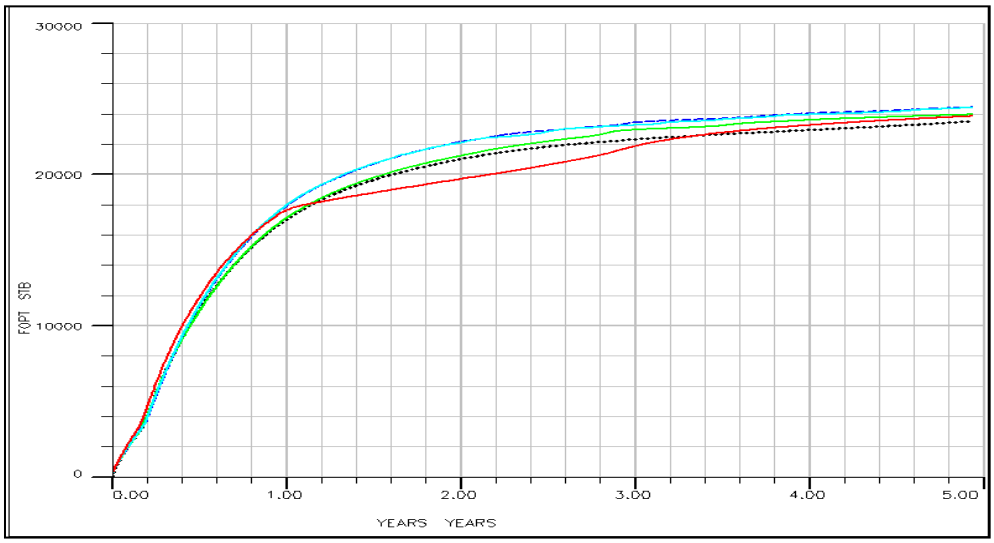


Figure 7.22. Field cumulative oil production for 10°API oil, with Free Volume viscosities. (Base case: black dotted; 10-PC: green; 5-PC: dark blue; 3-PC: light blue; 2-PC: red)

It can be observed that component lumpings, from 30 components to 10-, 5-, 3- and 2 pseudo-components, resulted in similar oil recoveries as in Chapter 3. The conclusion is that, using the Free Volume model method to determine component viscosities would not alter the modelled reservoir fluid behaviour. In general the Free Volume alkane liquid viscosities are lower than the SCNG Pedersen viscosities, which would explain the slight increase in the oil recovery. However, it is the viscosity of the heavy pseudo-component representing the plus-fraction, which has the determining effect, far overshowing the effect of the intermediate component viscosities.

Lumping of the components has an effect, but no more than previously found in Chapter 3. Table 7.24 shows the resulting oil recoveries over five years of simulation.

Table 7.24. Field cumulative oil production: 10°API oil with Free Volume viscosities.

30 Comp (Pedersen)	PC10(FV)	PC5(FV)	PC3(FV)	PC2(FV)
23,516	23,957	24,436	24,413	23,850

The cumulative oil production per well for each case is shown in Figure 7.23. It is clear that well interference may alter results when different lumping schemes are implemented and caution should be exercised when modelling wells where such interference may be a factor.

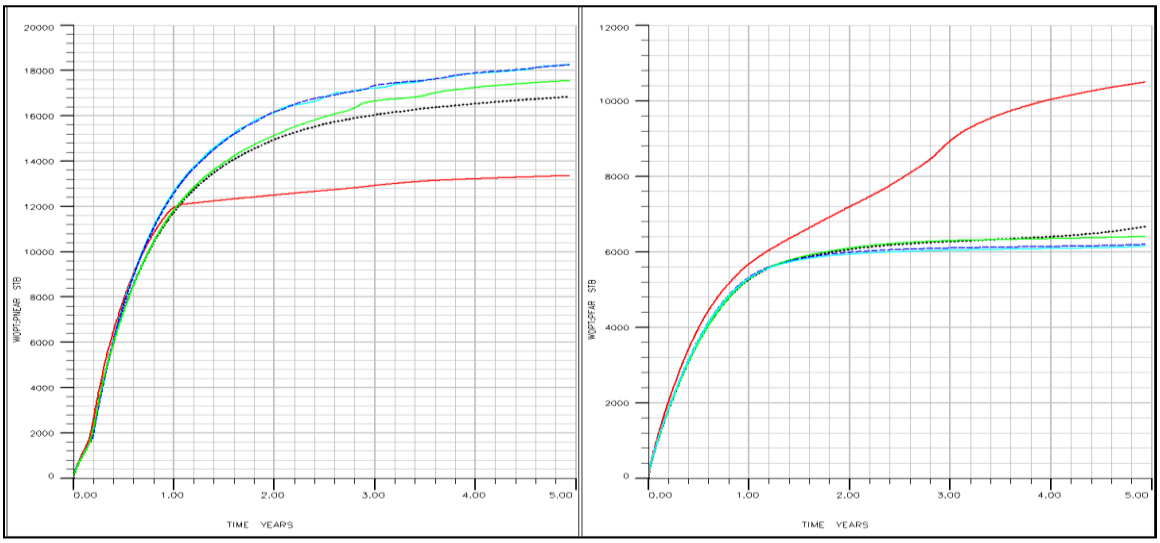


Figure 7.23. Well cumulative oil production in 10°API cases. Left: PNEAR, Right: PFAR. (Base case: black dotted; 10-PC: green; 5-PC: dark blue; 3-PC: light blue; 2-PC: red)

7.3.2 Steam-Assisted Gravity Drainage (SAGD)

In order to build a test case for SAGD sensitivities, the viscosities of the resin-asphaltene component were increased to produce a 100,000 cP (at T_{std}, P_{res}) and 7.8 cP (at T=500 °F and P_{res}) dead oil mixture. The mixture oil viscosities were generated with the Free Volume method, using l_m=0.1953125 Å, E_0=110 kJ/mole, and B=0.133, and are shown in Figure 7.24.

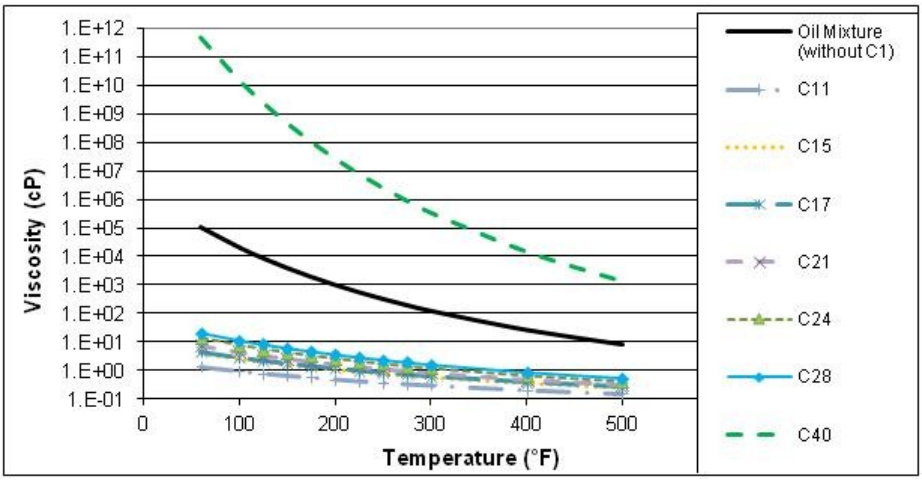


Figure 7.24. Very heavy oil component viscosities for SAGD 8-PC case. (Dead-oil mixture viscosities in solid black).

7.3.2.1 SAGD: Oil Recovery Sensitivity to Number of Pseudo-Components

The SAGD sensitivity showed similar results to that of the SLD, as seen in the cumulative oil production shown in Figure 7.25. The two pseudo-component case recovery results were slightly lower than that of the base case, with a deviation of 3.4% in the long term prediction (Table 7.25 and Table 7.26). In this case the lumping was done by keeping the methane separate, and the oil component was simulated with a C27 ECN. The slight under-prediction is due to the lower oil mobility (higher viscosity), however, Figure 7.26 shows the successfully simulated steam-oil-ratios and daily oil production rates, using only two pseudo-components.

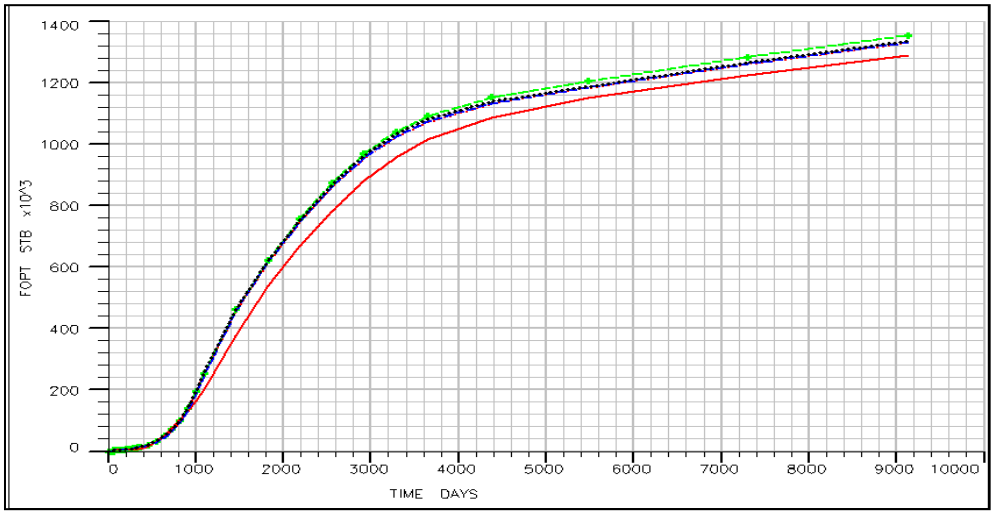


Figure 7.25. SAGD cumulative oil production sensitivity to number of pseudo-components. Base case (black dots), 8-PC case (red dotted line), 4-PC case (blue dashed line), 3-PC case (green dashed line), and 2-PC case (red).

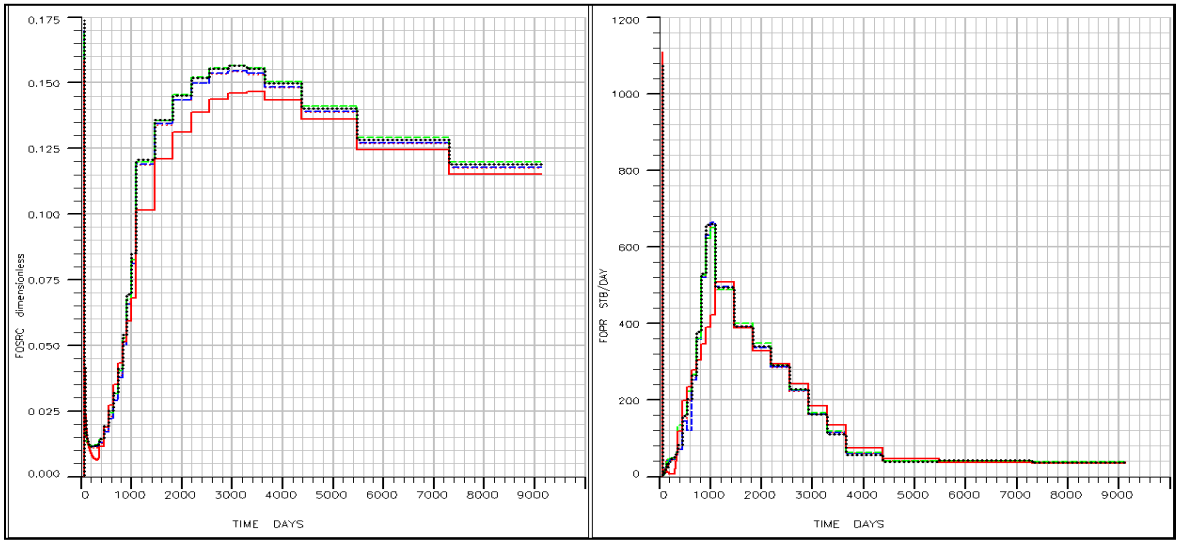


Figure 7.26. SAGD Steam-Oil ratio (left) and daily oil production rates (right) for base case (black dots), 2-PC case (red), 8-PC case (red dotted line), 4-PC case (blue dashed line), and 3-PC case (green dashed line).

Table 7.25. SAGD cumulative oil production for each case (PC15 is the base case).

PC15	PC8	PC4	PC3	PC2
1,334	1,327	1,330	1,353	1,288

Table 7.26. SAGD cumulative oil production deviations per sensitivity case.

DEV % from 15-PC-case			
PC8	**PC4**	**PC3**	**PC2**
0.5	0.3	-1.4	3.4

7.3.2.2 SAGD: Oil Recovery Sensitivity to 2-PC Lumping Strategy

The same alternative lumping strategy used for the two pseudo-component case in SLD, (section 7.3.1.3) has been used for the sensitivity testing with SAGD. The alternative lumping consisted of grouping C1 to C18 into an ECN of C2, with all heavier components from C20 and heavier, represented by an ECN of C39, as oppose to keeping Methane (C1) separate and lumping all components from C2 and above together.

The SAGD two-pseudo-component oil recovery shows a very high sensitivity towards the lumping strategy, as presented in Figure 7.27 and Table 7.27 to Table 7.28. The graph shows that the alternative lumping method under-predicts the recovery by 23%, over the simulated period.

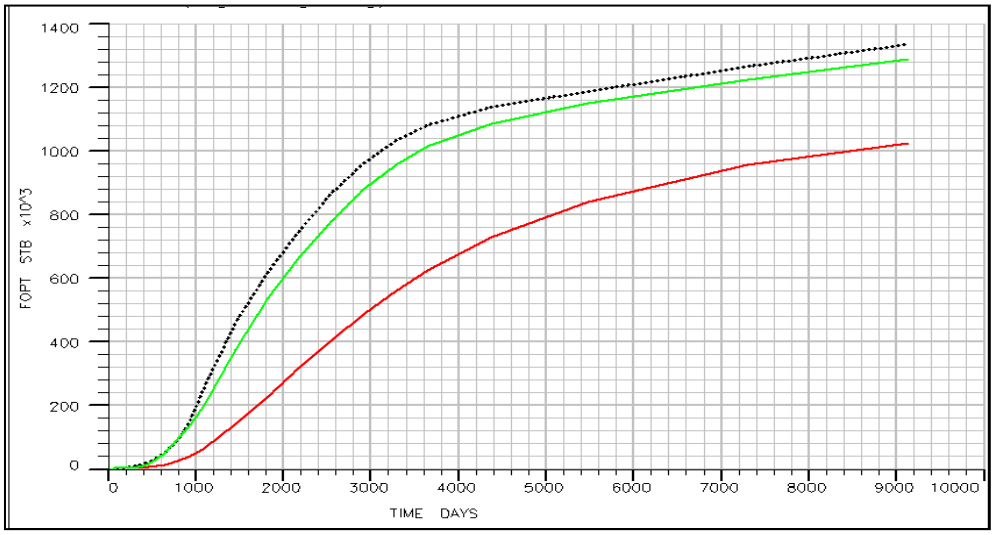


Figure 7.27. SAGD cumulative oil production sensitivity to lumping scenario. 15-component base case: black dotted line, 2-PC with original lumping: green, 2-PC with alternative lumping (grp2): red.

Table 7.27. SAGD cumulative oil (MSTB) produced per case: lumping strategy.

PC15	PC2_Grp1	PC2_Grp2
1,334	1,288	1,024

Table 7.28. SAGD Cumulative oil prediction deviations (%): lumping strategy.

DEV % from 15-PC-case	
PC2_Grp1	PC2_Grp2
3.4	23.3

7.4 Sensitivity Study Summary

A summary of all the results are presented as cumulative production (FOPT) and relative deviation from base case in Table 7.29 and Figure 7.28. Deviations are shown in terms of base case results, shown in bold for each section. In the case of the alternative groupings, the base cases are the 15-PC case of each heavy component viscosity case (FVi).

Table 7.29. Summary of Sensitivity Results.

Process	Sensitivity	Case #	Case name	Description	FOPT	Deviation* (%)
SLD	Heavy PC Viscosity	**1**	**PC15-Exp**	**'Experimental'**	**8393**	
		2	PC15-FV1	Match Experimental End-points	6402	23.7
		3	PC15-FV2	Match at T_R and T_S	7980	4.9
		4	PC15-FV3	Match all between T_R and T_S	8181	2.5
	Number of Pseudo-components	**6**	**PC15-FV1**	**Free-Volume1 (Match at Tmin and Tmax)', 14 'pure' components + 1 heavy pseudo-component**	**6402**	
		7	PC4-FV1	4 Pseudo-components, FV1	6461	-0.9
		8	PC3-FV1	3 Pseudo-components, FV1	6474	-1.1
		9	PC2-FV1	2 Pseudo-components, FV1	6502	-1.6
		10	**PC15-FV2**	**Free-Volume2 (match at T_R and T_s)', 14 'pure' components + 1 heavy**	**7980**	

Process	Sensitivity	Case #	Case name	Description	FOPT	Deviation* (%)
				pseudo-component		
		11	PC4-FV2	4 Pseudo-components, FV2	8042	-0.8
		12	PC3-FV2	3 Pseudo-components, FV2	8057	-1
		13	PC2-FV2	2 Pseudo-components, FV2	8145	-2.1
		14	**PC15-FV3**	**Free-Volume3 (match from TR to Ts)', 14 'pure' components + 1 heavy pseudo-component**	**8181**	
		15	PC4-FV3	4 Pseudo-components, FV3	8251	-0.8
		16	PC3-FV3	3 Pseudo-components, FV3	8266	-1
		17	PC2-FV3	2 Pseudo-components, FV3	8358	-2.2
	Lumping-strategy	18	PC2-FV1	2 Pseudo-components, FV1	6502	-1.6**
		19	PC2-FV2	2 Pseudo-components, FV2	8145	-2.1
		20	PC2-FV3	2 Pseudo-components, FV3	8358	-2.2
		21	PC2-GRP2-FV1	2-Pseudo-components, Alternative grouping, FV1	4735	26
		22	PC2-GRP2-FV2	2-Pseudo-components, Alternative grouping, FV2	4811	40
		23	PC2-GRP2-FV3	2-Pseudo-components, Alternative grouping, FV3	5253	36
SAGD	**Number of Pseudo-components**	**24**	**PC15**	**14 'pure' components + 1 heavy pseudo-component**	**1334**	
		25	PC8	8 Pseudo-components	1327	0.5
		26	PC4	4 Pseudo-components	1330	0.3
		27	PC3	3 Pseudo-components	1353	-1.4
		28	PC2	2 Pseudo-components	1288	3.4
	Lumping-strategy	**29**	**PC15**	**14 'pure' components + 1 heavy pseudo-component**	**1334**	
		30	PC2_Grp1	2 Pseudo-components	1288	3.4
		31	PC2_Grp2	2 Pseudo-components, alternative grouping	1024	23.3

**Deviations are in terms of the base case for each section, shown in bold. Negative signs are an indication of over-prediction.*

***PC2-case deviations are in terms of PC15-cases.*

It should be noted that since the deviations in Table 7.29 are in terms of each section's base case results, and not in terms of those of the 'experimental' base case, it may appear as if the prediction error, solely due to over-prediction in the heavy component viscosity, represented by the FV1 case, disappears when the alternative grouping is used (see cases PC2-GRP2-FV1, PC2- GRP2-FV2 and PC2- GRP2-FV3). However, this discrepancy is only due to it being a relative error. In absolute terms, the deviations for these three cases are 44%, 43% and 37%, respectively, indicating that the FV3 representation of the heavy component viscosity results in a lower deviation, consistent with other results.

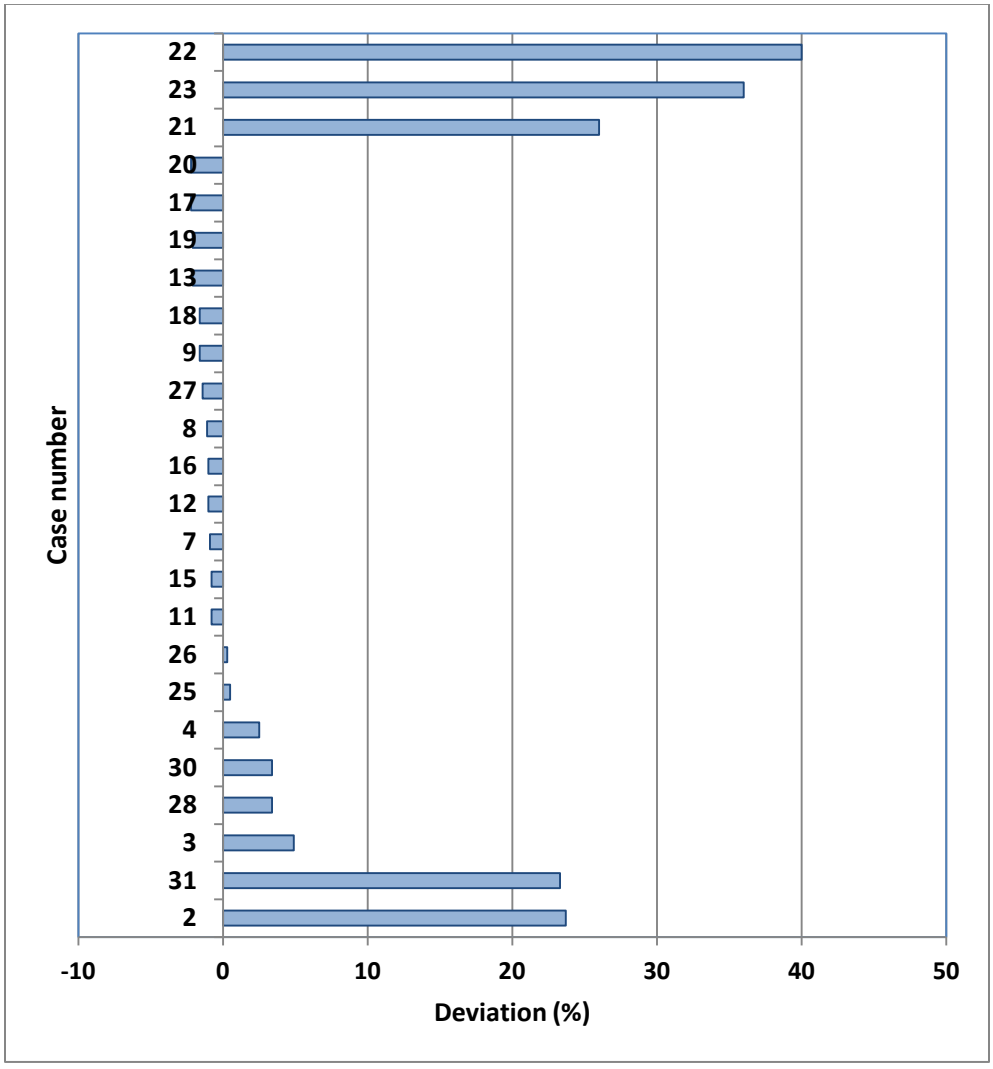


Figure 7.28. Oil recovery sensitivity to viscosity modelling and lumping results. (Deviations are relative to section-base case. Negative deviations indicate over-prediction).

It is clear that the heavy oil recovery predictions during numerical simulation of thermal recovery processes are most sensitive to lumping strategies (cases 21-23 and 31), irrespective of the process (SLD or SAGD). It is of critical importance to group components in a way to capture the phase behaviour in the reservoir during steam injection, and preserve relative mobilities of the fluids in the system. Secondly, the recovery is most sensitive to the heavy component viscosity (Cases 2 and 3). In this case it is important to model the viscosity between reservoir temperature and the steam-oil interface temperature correctly. In this study it was possible to match multi-component long-term recovery results using two pseudo-components within 5%, using the methodologies described.

7.5 Chapter Conclusions

Component lumping from fifteen components (one gas species, thirteen purecomponents, one asphaltene+resin) down to two had little effect on recovery prediction for both 10,000 cP oil in steam-line drive and a 100,000 cP oil in SAGD, with a deviation of only 2.2% on end recovery.

The accuracy of recovery prediction is very sensitive to the uncertainty in the heavy pseudo-component viscosity.

In the case of steam-line drive, it is important to minimise the deviation from the heavy component (resins with asphaltenes) viscosity data values for all values between the initial reservoir and the oil-steam interface temperatures.

Recovery prediction deviation in early time in 2-PC cases is a function of the heavy pseudo-component viscosity: the higher the component viscosity, the larger the early time prediction error.

Success of simulation with two pseudo-components is highly dependent on the lumping strategy, *i.e.,* the components grouped into each pseudo-component, as this affects phase-behaviour and thus the steam front movement. In this research it was found that the optimum lumping is specific to a fluid composition and the amount of gas in the system, and a few iterations may be required to find the correct lumping strategy during reservoir

modelling. Three pseudo-components are the safest option and delivered accurate results in all cases tested.

The specific thermal recovery process that was simulated (*i.e.,* steam-line-drive *vs.* SAGD) did not change the conclusions regarding number of pseudo-components and lumping strategies.

8 Conclusions and Recommendations

8.1 Overall Summary

This research had three main objectives. One was to investigate, in a heavy oil thermal simulation, whether one can obtain accurate oil recovery predictions while using a two-component characterisation, consisting of one light component (mostly methane), and one heavy pseudo-component. The second objective was to determine techniques to estimate the component viscosities, as a function of pressure and temperature, of (1) intermediate molecular weight hydrocarbon components (C10 to C64) representing saturates and aromatics, and of (2) heavy hydrocarbon plus-fraction components consisting mostly of resins and asphaltenes. The third objective was to determine the best technique of calculating an oil mixture viscosity, as a function of temperature, from the individual component viscosities.

The main contribution of this work is in the modelling of heavy oil viscosity, wherein the Free Volume viscosity model had been extended to model long-chain heavy oil pure components, as well a single complex heavy pseudo-component, representing resins and asphaltenes.

8.2 Specific Conclusions

8.2.1 Chapter 2: Evaluation of the Arrhenius Mixing Equation in Viscosity Modelling of Hydrocarbon Mixtures

1. The Arrhenius mixing equation has been found to accurately predict, with deviations < 10%, the viscosities of hydrocarbon mixture if specific guidelines are followed.

2. For binary mixtures containing a light component, such as methane, a maximum ΔC exists, beyond which the prediction deviations are higher, above 10%. Including intermediate components in the mixture improved the prediction accuracy.

3. The Arrhenius mixing equation has been found to be inadequate in the prediction of viscosities of mixtures of hydrocarbon with CO_2. A different method should be found in such cases.

8.2.2 Chapter 3: Thermal Recovery Sensitivity to Component Grouping and Viscosity Modelling.

1. It has been shown that it is possible to accurately simulate a steam line drive process using only two components, a gaseous component, consisting mostly of methane, and a heavy oil pseudo-component, even when the detailed composition has a bimodal mole-fraction distribution. Accuracy in this instance means recovery results are within 5% of those obtained using detailed, multi-component simulations. However, caution should be exercised with regard to well behaviours, where well interference may require at least three pseudo-components for accurate well predictions.

2. It has been shown that this accuracy is only obtainable if (a) the oil pseudo-component viscosities, as a function of temperature, is determined using the Arrhenius mixing equation, as is used in the simulator of choice; (b) no intermediate components (C2-C8) exist in the fluidsystem; (c) with intermediate components present, the initial reservoir pressure is above the bubble point pressure.

3. A technique of grouping, based on an equivalent carbon number method, has been demonstrated.

8.2.3 Chapter 4: Thermal Recovery Sensitivity to Uncertainty in Viscosity, as a Function of Temperature Range

1. It has been shown that the critical temperature range for viscosity modelling is dependent on the thermal recovery process.

2. Analytical models had been developed to calculate oil recovery sensitivity to viscosity uncertainty for steam-line-drive and SAGD.

3. In the case of steam line drive, it is critical to model the oil viscosity correctly at the initial reservoir temperature (low temperature range) to obtain accurate recovery results, while in the case of SAGD, it has been shown that the critical range is at the oil-steam interface temperature (higher temperature range).

8.2.4 Chapter 5: Viscosity Modelling of Individual Components

1. The preferred model to calculated viscosities of intermediate to long-chain components, C10 to C64, as a function of molecular weight, pressure and temperature, is the Free Volume model. These components will only be representative of the saturates and aromatics in heavy oil, and not the remaining, highly complex molecules, such as asphaltenes.

2. The critical parameters in the Free Volume model, characteristic of a component, have been provided as a function of molecular weight or chain-length. Recommended values for use in the industry are provided in Chapter 5.

8.2.5 Chapter 6: Characterisation of a Heavy Pseudo-Component

1. A very heavy pseudo-component, consisting of resins and asphaltenes, has been characterized. Viscosities have been determined by the Free Volume model as a function of molecular weight, pressure and temperature.

2. A technique of matching measured oil viscosity, and fine-tuning the Free Volume model parameters specific to this component, has been demonstrated.

8.2.6 Chapter 7: Thermal Simulation Sensitivities using Viscosities estimated by the Free Volume Model

1. The application of the Free Volume model in industry simulation workflows has been demonstrated. These apply to steam-enhanced heavy oil recovery processes, in reservoirs containing Newtonian fluids.

2. It was found that simulation results were most sensitive to the lumping strategy, after which accuracy of the viscosity of the heavy pseudo-component has the highest influence.

8.3 Recommendations

This research can be extended to investigate the effect of different compositions on (a) the two-pseudo-component case, and (b) the lumping strategy. The effect of higher concentrations of the intermediate components, such as C6 to C14, may have the effect that at least three pseudo-component will be required, as the weight percentage of the distillable components increase and have larger influence on the recovery results.

Further research should be conducted to investigate viscosity modelling and prediction of full maltenes mixtures: saturates, aromatics and resins, combined with the use of the colloidal system-approach to directly incorporate the effect of asphaltene concentration on the heavy oil mixture viscosity.

Thermal simulation sensitivities should be extended to incorporate economic effects of different factors, such as ultimate oil recovery, steam-oil ratio, and calendar daily oil rate. This can be done using the simple thermal efficiency parameter, STEP, introduced by Shin and Polikar (2005).

Also, more complex cases, which include hysteresis effects in the relative permeabilities with temperature increases (Polikar *et al*., 1990), should be investigated.

In the case of VAPEX processes, where steam is injected with carbon dioxide (CO_2), research into more accurate prediction methods for mixture viscosities is required, since this is the case where the Arrhenius mixing rule breaks down.

Research into *in situ* combustion problems, and the extent to which the two-pseudo-component problem helps simulation of this problem, is required. In these cases, the presence of additional non-hydrocarbon components, such as O_2, N, CO_2, and CO, exist in the combustion zone. This is also the zone where cracking of long-chain hydrocarbons, as well as complex molecules such as resins and asphaltenes occurs, which then burn. The rest of the production fluid is down-stream from the combustion zone, and is only affected by the temperature change. The fact that one would require only two pseudo-components in this region may simplify the problem greatly; however, recovery sensitivity towards detailed simulation of the processes in the combustion zone is unclear. Research in extending the current methodologies to these cases, and determining sensitivities, is recommended.

Appendix A: Viscosity Deviation Data for Arrhenius-Mixing Equation

1. Aucejo *et al.*, 1995

Temp 298.15 K
Pres 1 Bar

C5 - C6

x1	x2	Dens	Meas Visc		Calc Visc	Rel Dev	Abs Dev	MAD*	RMS*	BIAS*
		kg/m3	μPa.s		μPa.s	%	%			
0	1	655.1	298.7		296.3	0.81	0.81	**1.88**	**1.41**	**1.37**
0.10	0.90	652.1	289.8		286.9	0.99	0.99			
0.21	0.79	648.9	280.2		277.8	0.86	0.86			
0.31	0.69	645.8	272.4		269.3	1.14	1.14			
0.41	0.59	642.6	264.1		261.1	1.13	1.13			
0.51	0.49	639.4	257.4		253.3	1.61	1.61			
0.60	0.40	636.2	249.7		246.2	1.40	1.40			
0.70	0.30	632.7	243.2		238.6	1.87	1.87			
0.80	0.20	629.3	236.4		232.0	1.88	1.88			
0.90	0.10	625.3	228		224.7	1.44	1.44			
1	0	621.2	223		217.9	2.29	2.29			

**Defined in Chapter 2, equations (2.16 to 2.18)*

C5 - C7

x1	x2	Dens	Meas Visc		Calc Visc	Rel Dev	Abs Dev	MAD	RMS	BIAS
		kg/m3	μPa.s		μPa.s	%	%			
0	1	679.7	386.6		388.5	-0.49	0.49	**4.21**	**3.29**	**3.15**
0.10	0.90	675.0	369.1		365.7	0.93	0.93			
0.20	0.80	670.4	357.9		345.6	3.44	3.44			
0.31	0.69	665.0	332.5		325.0	2.26	2.26			
0.41	0.59	659.7	317.3		306.9	3.28	3.28			
0.50	0.50	654.7	300.4		291.3	3.03	3.03			
0.60	0.40	648.8	284.8		274.6	3.58	3.58			
0.66	0.34	645.0	276.2		264.9	4.10	4.10			
0.80	0.20	636.3	254		245.0	3.54	3.54			
0.89	0.11	629.6	242		231.8	4.21	4.21			
1	0	621.2	223		217.9	2.29	2.29			

C5 - C8

x1	x2	Dens	Meas Visc		Calc Visc	Rel Dev	Abs Dev	MAD	RMS	BIAS
		kg/m3	μPa.s		μPa.s	%	%			
0	1	698.4	509.4		509.7	-0.06	0.06	**6.14**	**4.45**	**4.21**
0.11	0.89	693.0	471.9		465.9	1.28	1.28			
0.20	0.80	687.8	443.9		431.0	2.90	2.90			
0.30	0.70	681.4	409.1		394.4	3.60	3.60			
0.40	0.60	674.6	380.6		361.6	4.99	4.99			
0.50	0.50	667.7	354.5		332.7	6.14	6.14			
0.60	0.40	659.8	322.8		304.9	5.54	5.54			
0.70	0.30	651.7	296.3		280.8	5.22	5.22			
0.80	0.20	642.4	270.2		257.7	4.63	4.63			
0.90	0.10	632.2	245.4		236.5	3.62	3.62			
1	0	621.2	223		217.9	2.29	2.29			

C5-C9

x1	x2	Dens	Meas Visc		Calc Visc	Rel Dev	Abs Dev	MAD	RMS	BIAS
		kg/m3	μPa.s		μPa.s	%	%			
0	1	713.8	660		654.0	0.91	0.91	**8.53**	**6.75**	**6.54**
0.09	0.91	708.6	611		590.8	3.31	3.31			
0.20	0.80	702.0	554.8		525.2	5.33	5.33			
0.31	0.69	694.5	501.6		466.2	7.06	7.06			
0.40	0.60	687.4	455.6		420.0	7.82	7.82			
0.49	0.51	680.6	417.9		383.3	8.28	8.28			
0.60	0.40	670.3	369.1		337.6	8.53	8.53			
0.70	0.30	660.2	326.8		302.3	7.48	7.48			
0.80	0.20	648.7	289.2		270.5	6.47	6.47			
0.90	0.10	635.6	253.8		242.1	4.59	4.59			
1	0	621.2	223		217.9	2.29	2.29			

C5 - C10

x1	x2	Dens	Meas Visc		Calc Visc	Rel Dev	Abs Dev	MAD	RMS	BIAS
		kg/m3	μPa.s		μPa.s	%	%			
0	1	726.3	846		848	-0.3	0.3	**12.77**	**9.62**	**9.35**
0.10	0.90	720.5	778		737	5.2	5.2			
0.21	0.79	713.5	697		639	8.3	8.3			
0.31	0.69	706.2	617		559	9.3	9.3			
0.41	0.59	697.8	545		487	10.6	10.6			
0.51	0.49	688.9	482		426	11.5	11.5			
0.60	0.40	679.2	429		374	12.8	12.8			
0.71	0.29	667.5	363		325	10.4	10.4			
0.80	0.20	654.6	314		284	9.5	9.5			
0.90	0.10	639.6	267		249	6.6	6.6			
1	0	621.2	223		218	2.3	2.3			

C5 - C11

x1	x2	Dens	Meas Visc		Calc Visc	Rel Dev	Abs Dev	MAD	RMS	BIAS
		kg/m3	μPa.s		μPa.s	%	%			
0	1	736.3	1084		1094	-0.9	0.9	**14.35**	**11.14**	**10.56**
0.10	0.90	730.9	965		937	2.9	2.9			
0.18	0.82	725.2	880		815	7.4	7.4			
0.27	0.73	718.4	784		703	10.3	10.3			
0.37	0.63	710.6	694		604	13.0	13.0			
0.48	0.52	700.0	583		502	13.9	13.9			
0.57	0.43	690.5	506		433	14.4	14.4			
0.66	0.34	680.4	433		377	12.9	12.9			
0.75	0.25	668.7	373		328	12.0	12.0			
0.90	0.10	643.4	281		257	8.2	8.2			
1	0	621.2	223		218	2.3	2.3			

C5 - C12

x1	x2	Dens	Meas Visc		Calc Visc	Rel Dev	Abs Dev	MAD	RMS	BIAS
		kg/m3	μPa.s		μPa.s	%	%			
0	1	745.0	1379		1359	1.5	1.5	**18.14**	**14.43**	**13.94**
0.11	0.89	738.8	1194		1112	6.9	6.9			
0.21	0.79	732.1	1037		930	10.4	10.4			
0.30	0.70	725.0	914		786	14.0	14.0			
0.41	0.59	715.4	771		644	16.5	16.5			
0.50	0.50	706.2	662		543	17.9	17.9			
0.60	0.40	694.5	550		451	18.1	18.1			
0.71	0.29	680.5	448		373	16.8	16.8			
0.81	0.19	664.3	363		311	14.4	14.4			
0.90	0.10	645.8	293		262	10.4	10.4			
1	0	621.2	223		218	2.3	2.3			

C5 -C16

x1	x2	Dens	Meas Visc		Calc Visc	Rel Dev	Abs Dev	MAD	RMS	BIAS
		kg/m3	μPa.s		μPa.s	%	%			
0	1	769.8	3093		3065	0.9	0.9	**33.52**	**26.63**	**25.63**
0.11	0.89	763.7	2574		2285	11.2	11.2			
0.21	0.79	757.3	2170		1751	19.3	19.3			
0.31	0.69	749.9	1816		1351	25.6	25.6			
0.42	0.58	740.2	1457		1019	30.0	30.0			
0.51	0.49	729.9	1172		791	32.5	32.5			
0.61	0.39	717.6	922		613	33.5	33.5			
0.70	0.30	702.8	700		477	31.8	31.8			
0.80	0.20	682.9	509		366	28.0	28.0			
0.90	0.10	656.6	346		282	18.7	18.7			
1	0	621.2	223		218	2.3	2.3			

Temp **298.15** **K**
Pressure **1** **Bar**

C6 - C7

x1	x2	Dens	Meas Visc		Calc Visc	Rel Dev	Abs Dev	MAD	RMS	BIAS
		kg/m3	μPa.s		μPa.s	%	%			
0	1	679.7	387		388	-0.49	0.49	**0.98**	**0.48**	**0.27**
0.11	0.89	677.3	379		377	0.45	0.45			
0.21	0.79	675.0	366		367	-0.42	0.42			
0.30	0.70	672.8	358		358	0.01	0.01			
0.41	0.59	670.3	349		348	0.14	0.14			
0.51	0.49	668.0	341		339	0.62	0.62			
0.61	0.39	665.5	331		330	0.26	0.26			
0.70	0.30	663.0	323		321	0.52	0.52			
0.80	0.20	660.5	312		313	-0.13	0.13			
0.90	0.10	657.9	308		304	0.98	0.98			
1	0	655.1	299		296	0.81	0.81			

C6 - C8

x1	x2	Dens	Meas Visc		Calc Visc	Rel Dev	Abs Dev	MAD	RMS	BIAS
		kg/m3	μPa.s		μPa.s	%	%			
0	1	698.4	509		510	-0.06	0.06	**2.05**	**1.20**	**1.00**
0.11	0.89	694.8	478		481	-0.57	0.57			
0.21	0.79	691.2	460		456	0.94	0.94			
0.30	0.70	687.6	441		432	2.05	2.05			
0.40	0.60	683.6	412		409	0.72	0.72			
0.51	0.49	679.1	392		386	1.41	1.41			
0.61	0.39	674.7	370		366	1.03	1.03			
0.71	0.29	670.4	351		348	0.97	0.97			
0.81	0.20	665.6	333		329	0.98	0.98			
0.90	0.10	660.6	317		312	1.48	1.48			
1	0	655.1	299		296	0.81	0.81			

C6-C9

x1	x2	Dens	Meas Visc		Calc Visc	Rel Dev	Abs Dev	MAD	RMS	BIAS
		kg/m3	μPa.s		μPa.s	%	%			
0	1	713.8	660		654	0.91	0.91	**5.21**	**3.19**	**3.04**
0.11	0.89	709.3	611		601	1.69	1.69			
0.21	0.79	704.7	569		554	2.72	2.72			
0.29	0.71	701.0	537		521	2.94	2.94			
0.40	0.60	695.1	502		476	5.21	5.21			
0.50	0.50	689.6	453		439	3.10	3.10			
0.61	0.39	683.5	420		404	3.74	3.74			
0.70	0.30	677.4	387		375	3.28	3.28			
0.80	0.20	670.4	355		346	2.45	2.45			
0.90	0.10	663.0	327		320	2.26	2.26			
1	0	655.1	299		296	0.81	0.81			

C6 - C10

x1	x2	Dens	Meas Visc		Calc Visc	Rel Dev	Abs Dev	MAD	RMS	BIAS
		kg/m3	μPa.s		μPa.s	%	%			
0	1	726.3	846		848	-0.26	0.26	**6.86**	**5.17**	**4.96**
0.11	0.89	721.3	781		758	2.99	2.99			
0.21	0.79	716.2	718		682	5.05	5.05			
0.30	0.70	711.0	652		617	5.33	5.33			
0.40	0.60	704.9	585		554	5.20	5.20			
0.50	0.50	698.5	532		499	6.09	6.09			
0.61	0.39	691.3	481		448	6.69	6.69			
0.71	0.29	683.5	434		404	6.86	6.86			
0.80	0.20	675.1	379		364	3.89	3.89			
0.90	0.10	665.5	337		328	2.56	2.56			
1	0	655.1	299		296	0.81	0.81			

C6 - C11

x1	x2	Dens	Meas Visc		Calc Visc	Rel Dev	Abs Dev	MAD	RMS	BIAS
		kg/m3	μPa.s		μPa.s	%	%			
0	1	736.3	1084		1094	-0.93	0.93	**8.04**	**5.79**	**5.39**
0.10	0.90	731.3	963		956	0.76	0.76			
0.20	0.80	726.2	876		844	3.66	3.66			
0.30	0.70	720.1	775		740	4.53	4.53			
0.41	0.59	713.2	693		645	7.03	7.03			
0.51	0.49	705.8	609		564	7.43	7.43			
0.61	0.39	698.0	539		496	8.04	8.04			
0.71	0.29	689.1	464		435	6.40	6.40			
0.80	0.20	679.2	404		382	5.45	5.45			
0.90	0.10	668.1	355		337	5.22	5.22			
1	0	655.1	299		296	0.81	0.81			

C6 - C12

x1	x2	Dens	Meas Visc		Calc Visc	Rel Dev	Abs Dev	MAD	RMS	BIAS
		kg/m3	μPa.s		μPa.s	%	%			
0	1	745.0	1379		1359	1.47	1.47	**11.59**	**8.63**	**8.29**
0.11	0.89	739.4	1196		1144	4.31	4.31			
0.21	0.79	733.7	1047		981	6.27	6.27			
0.30	0.70	728.1	933		857	8.09	8.09			
0.40	0.60	721.0	816		734	10.08	10.08			
0.51	0.49	713.1	708		628	11.24	11.24			
0.61	0.39	704.4	611		540	11.59	11.59			
0.72	0.28	692.7	501		452	9.70	9.70			
0.80	0.20	683.3	433		399	7.78	7.78			
0.90	0.10	670.1	363		343	5.51	5.51			
1	0	655.1	299		296	0.81	0.81			

C6 -C16

x1	x2	Dens	Meas Visc		Calc Visc	Rel Dev	Abs Dev	MAD	RMS	BIAS
		kg/m3	μPa.s		μPa.s	%	%			
0	1	769.8	3093		3065	0.89	0.89	**24.84**	**19.54**	**18.86**
0.10	0.90	764.8	2659		2401	9.70	9.70			
0.20	0.80	759.5	2251		1936	13.96	13.96			
0.30	0.70	752.7	1880		1521	19.12	19.12			
0.40	0.60	744.9	1547		1193	22.87	22.87			
0.51	0.49	735.2	1214		922	24.03	24.03			
0.61	0.39	725.6	987		742	24.84	24.84			
0.71	0.29	713.3	763		589	22.81	22.81			
0.80	0.20	698.1	580		468	19.39	19.39			
0.90	0.10	679.2	428		372	13.02	13.02			
1	0	655.1	299		296	0.81	0.81			

Temp 298.15 K
Pressure 1 Bar

C7 - C8

x1	x2	Dens	Meas Visc		Calc Visc	Rel Dev	Abs Dev	MAD	RMS	BIAS
		kg/m3	μPa.s		μPa.s	%	%			
0	1	698.4	509		510	-0.06	0.06	**1.48**	**0.73**	**-0.54**
0.11	0.89	696.6	494		495	-0.18	0.18			
0.21	0.79	694.8	477		481	-0.86	0.86			
0.31	0.69	693.0	461		468	-1.48	1.48			
0.41	0.59	691.3	454		457	-0.57	0.57			
0.51	0.49	689.4	443		444	-0.19	0.19			
0.61	0.39	687.4	429		432	-0.84	0.84			
0.71	0.29	685.5	420		421	-0.18	0.18			
0.81	0.19	683.5	410		409	0.22	0.22			
0.90	0.10	681.5	396		399	-0.82	0.82			
1	0	679.5	387		388	-0.51	0.51			

C7-C9

x1	x2	Dens	Meas Visc		Calc Visc	Rel Dev	Abs Dev	MAD	RMS	BIAS
		kg/m3	μPa.s		μPa.s	%	%			
0	1	713.8	660		654	0.91	0.91	**1.71**	**1.11**	**0.73**
0.11	0.89	710.7	613		618	-0.77	0.77			
0.20	0.80	708.0	592		588	0.71	0.71			
0.31	0.69	704.9	562		558	0.73	0.73			
0.41	0.59	701.7	537		529	1.51	1.51			
0.51	0.49	698.3	510		502	1.71	1.71			
0.61	0.39	694.8	484		477	1.48	1.48			
0.71	0.29	691.2	459		453	1.37	1.37			
0.80	0.20	687.5	431		431	0.15	0.15			
0.90	0.10	683.7	408		409	-0.30	0.30			
1	0	679.5	387		388	-0.51	0.51			

C7 - C10

x1	x2	Dens	Meas Visc		Calc Visc	Rel Dev	Abs Dev	MAD	RMS	BIAS
		kg/m3	μPa.s		μPa.s	%	%			
0	1	726.3	846		848	-0.26	0.26	**3.40**	**2.45**	**2.31**
0.10	0.90	722.8	805		785	2.45	2.45			
0.20	0.80	719.0	745		725	2.75	2.75			
0.31	0.69	715.0	681		668	1.82	1.82			
0.41	0.59	710.7	636		617	3.02	3.02			
0.51	0.49	706.3	589		571	3.14	3.14			
0.61	0.39	701.5	547		528	3.40	3.40			
0.71	0.29	696.4	498		488	2.10	2.10			
0.80	0.20	691.3	458		453	0.91	0.91			
0.90	0.10	685.5	424		419	1.21	1.21			
1	0	679.5	387		388	-0.51	0.51			

C7 - C11

x1	x2	Dens	Meas Visc		Calc Visc	Rel Dev	Abs Dev	MAD	RMS	BIAS
		kg/m3	μPa.s		μPa.s	%	%			
0	1	736.3	1084		1094	-0.93	0.93	**3.95**	**2.81**	**2.51**
0.11	0.89	732.1	982		978	0.38	0.38			
0.21	0.79	727.8	898		881	1.93	1.93			
0.30	0.70	723.6	817		800	2.06	2.06			
0.41	0.59	718.6	745		719	3.47	3.47			
0.51	0.49	713.2	672		647	3.65	3.65			
0.61	0.39	707.4	607		583	3.95	3.95			
0.70	0.30	701.4	548		528	3.67	3.67			
0.81	0.19	694.6	489		475	2.88	2.88			
0.90	0.10	687.6	434		431	0.59	0.59			
1	0	679.5	387		388	-0.51	0.51			

C7 - C12

x1	x2	Dens	Meas Visc		Calc Visc	Rel Dev	Abs Dev	MAD	RMS	BIAS
		kg/m3	μPa.s		μPa.s	%	%			
0	1	745.0	1379		1359	1.47	1.47	**6.04**	**4.32**	**3.98**
0.11	0.89	740.5	1219		1203	1.37	1.37			
0.21	0.79	735.9	1086		1057	2.66	2.66			
0.31	0.69	730.8	960		929	3.25	3.25			
0.41	0.59	725.7	866		822	5.06	5.06			
0.51	0.49	719.8	771		724	6.01	6.01			
0.61	0.39	713.1	677		636	6.04	6.04			
0.70	0.30	706.1	596		563	5.64	5.64			
0.80	0.20	698.1	516		496	3.87	3.87			
0.90	0.10	689.1	445		437	1.94	1.94			
1	0	679.5	387		387	0.00	0.00			

C7 -C16

x1	x2	Dens	Meas Visc		Calc Visc	Rel Dev	Abs Dev	MAD	RMS	BIAS
		kg/m3	μPa.s		μPa.s	%	%			
0	1	769.8	3093		3065	0.89	0.89	**19.00**	**14.49**	**13.85**
0.11	0.89	765.1	2618		2459	6.07	6.07			
0.20	0.80	760.4	2268		2036	10.22	10.22			
0.30	0.70	754.6	1922		1649	14.19	14.19			
0.41	0.59	747.8	1603		1327	17.27	17.27			
0.51	0.49	740.3	1308		1074	17.86	17.86			
0.61	0.39	731.8	1080		875	19.00	19.00			
0.71	0.29	721.7	855		709	17.09	17.09			
0.80	0.20	710.5	680		584	14.14	14.14			
0.90	0.10	696.4	522		476	8.81	8.81			
1	0	679.5	387		388	-0.51	0.51			

Temp 298.15 K
Pressure 1 Bar

C8 - C9

x1	x2	Dens	Meas Visc		Calc Visc	Rel Dev	Abs Dev	MAD	RMS	BIAS
		kg/m3	μPa.s		μPa.s	%	%			
0	1	713.8	660		654	0.91	0.91	**2.08**	**0.94**	**-0.27**
0.11	0.89	712.3	631		636	-0.87	0.87			
0.21	0.79	710.9	626		621	0.84	0.84			
0.30	0.70	709.5	607		606	0.10	0.10			
0.41	0.59	708.0	595		591	0.67	0.67			
0.51	0.49	706.4	577		577	0.03	0.03			
0.61	0.39	704.9	559		562	-0.63	0.63			
0.70	0.30	703.3	550		549	0.18	0.18			
0.80	0.20	701.7	532		535	-0.63	0.63			
0.90	0.10	700.1	512		522	-2.08	2.08			
1	0	698.4	509		510	-0.06	0.06			

C8 - C10

x1	x2	Dens	Meas Visc		Calc Visc	Rel Dev	Abs Dev	MAD	RMS	BIAS
		kg/m3	μPa.s		μPa.s	%	%			
0	1	726.3	846		848	-0.26	0.26	**2.06**	**1.44**	**1.33**
0.11	0.89	723.9	817		804	1.59	1.59			
0.21	0.79	721.2	775		760	1.83	1.83			
0.30	0.70	719.0	738		727	1.58	1.58			
0.41	0.59	716.3	694		690	0.53	0.53			
0.51	0.49	713.6	669		656	2.06	2.06			
0.61	0.39	710.8	631		623	1.20	1.20			
0.70	0.30	708.0	602		593	1.48	1.48			
0.80	0.20	705.0	572		564	1.38	1.38			
0.91	0.09	701.6	537		535	0.34	0.34			
1	0	698.4	509		510	-0.06	0.06			

C8 - C11

x1	x2	Dens	Meas Visc		Calc Visc	Rel Dev	Abs Dev	MAD	RMS	BIAS
		kg/m3	μPa.s		μPa.s	%	%			
0	1	736.3	1084		1094	-0.93	0.93	**2.09**	**1.11**	**0.86**
0.10	0.90	733.4	1012		1013	-0.05	0.05			
0.21	0.79	730.1	938		934	0.41	0.41			
0.31	0.69	726.7	862		863	-0.07	0.07			
0.41	0.59	723.5	811		802	1.08	1.08			
0.51	0.49	719.8	752		743	1.25	1.25			
0.61	0.39	715.9	702		687	2.09	2.09			
0.71	0.29	712.0	645		638	1.10	1.10			
0.80	0.20	707.8	601		592	1.61	1.61			
0.90	0.10	703.2	550		549	0.32	0.32			
1	0	698.4	509		510	-0.06	0.06			

C8 - C12

x1	x2	Dens	Meas Visc		Calc Visc	Rel Dev	Abs Dev	MAD	RMS	BIAS
		kg/m3	μPa.s		μPa.s	%	%			
0	1	745.0	1379		1359	1.47	1.47	**4.68**	**3.11**	**2.88**
0.11	0.89	741.3	1233		1218	1.18	1.18			
0.21	0.79	737.8	1138		1106	2.85	2.85			
0.30	0.70	734.3	1038		1010	2.70	2.70			
0.41	0.59	730.0	948		910	3.94	3.94			
0.51	0.49	725.7	867		827	4.68	4.68			
0.61	0.39	720.9	770		748	2.89	2.89			
0.70	0.30	716.1	710		682	3.99	3.99			

0.80	0.20	710.6	635		618	2.77	2.77			
0.90	0.10	704.6	565		560	0.90	0.90			
1	0	698.4	509		510	-0.06	0.06			

C8 -C16

x1	x2	Dens	Meas Visc		Calc Visc	Rel Dev	Abs Dev	MAD	RMS	BIAS
		kg/m3	μPa.s		μPa.s	%	%			
0	1	769.8	3093		3065	0.89	0.89	**14.44**	**10.98**	**10.44**
0.10	0.90	765.7	2656		2544	4.21	4.21			
0.21	0.79	760.9	2305		2095	9.13	9.13			
0.31	0.69	756.0	1973		1755	11.07	11.07			
0.41	0.59	750.4	1682		1465	12.90	12.90			
0.50	0.50	744.8	1452		1243	14.44	14.44			
0.61	0.39	737.7	1205		1032	14.35	14.35			
0.71	0.29	729.5	982		858	12.60	12.60			
0.81	0.19	720.7	796		721	9.39	9.39			
0.90	0.10	710.2	642		605	5.85	5.85			
1	0	698.4	509		510	-0.06	0.06			

Temp 298.15 K
Pressure 1 Bar

C9 - C10

x1	x2	Dens	Meas Visc		Calc Visc	Rel Dev	Abs Dev	MAD	RMS	BIAS
		kg/m3	μPa.s		μPa.s	%	%			
0	1	726.3	846		848	-0.26	0.26	**1.76**	**1.18**	**0.97**
0.11	0.89	725.0	839		825	1.60	1.60			
0.21	0.79	723.8	806		803	0.33	0.33			
0.30	0.70	722.7	784		784	-0.01	0.01			
0.40	0.60	721.5	776		763	1.63	1.63			
0.51	0.49	720.2	754		744	1.30	1.30			
0.61	0.39	718.9	734		724	1.41	1.41			
0.71	0.29	717.7	719		706	1.76	1.76			
0.81	0.19	716.3	691		688	0.50	0.50			
0.90	0.10	715.1	673		672	0.24	0.24			
1	0	713.8	660		654	0.91	0.91			

C9 - C11

x1	x2	Dens	Meas Visc		Calc Visc	Rel Dev	Abs Dev	MAD	RMS	BIAS
		kg/m3	μPa.s		μPa.s	%	%			
0	1	736.3	1084		1094	-0.93	0.93	**1.49**	**0.89**	**0.45**
0.10	0.90	734.3	1031		1038	-0.68	0.68			
0.30	0.70	730.3	931		937	-0.59	0.59			
0.41	0.59	728.1	893		887	0.63	0.63			
0.51	0.49	725.9	848		843	0.49	0.49			
0.60	0.40	723.7	814		802	1.49	1.49			
0.71	0.29	721.3	770		761	1.16	1.16			
0.80	0.20	718.9	733		725	1.13	1.13			
0.90	0.10	716.3	687		687	-0.03	0.03			
1	0	713.8	660		654	0.91	0.91			

C9 - C12

x1	x2	Dens	Meas Visc		Calc Visc	Rel Dev	Abs Dev	MAD	RMS	BIAS
		kg/m3	μPa.s		μPa.s	%	%			
0	1	745.0	1379		1359	1.47	0.48	**3.34**	**2.06**	**1.85**
0.10	0.90	742.7	1273		1267	0.48	1.04			
0.20	0.80	740.0	1187		1174	1.04	2.13			
0.30	0.70	737.1	1111		1087	2.13	1.20			
0.41	0.59	734.3	1022		1010	1.20	3.34			
0.51	0.49	731.2	969		937	3.34	2.88			
0.61	0.39	727.9	896		870	2.88	1.94			
0.70	0.30	724.8	828		812	1.94	2.30			
0.80	0.20	721.3	772		754	2.30	1.31			
0.90	0.10	717.6	712		702	1.31	0.91			
1	0	713.8	660		654	0.91	0.00			

C9 -C16

x1	x2	Dens	Meas Visc		Calc Visc	Rel Dev	Abs Dev	MAD	RMS	BIAS
		kg/m3	μPa.s		μPa.s	%	%			
0	1	769.8	3093		3065	0.89	4.21	**10.80**	**8.82**	**8.64**
0.11	0.89	766.0	2698		2584	4.21	6.86			
0.20	0.80	762.6	2416		2250	6.86	9.37			
0.32	0.68	757.7	2072		1878	9.37	10.57			
0.41	0.59	753.7	1832		1639	10.57	10.63			
0.51	0.49	748.7	1571		1404	10.63	10.79			
0.58	0.42	744.7	1404		1252	10.79	10.80			
0.71	0.29	736.9	1152		1027	10.80	8.08			
0.80	0.20	730.3	966		887	8.08	6.48			

0.90	0.10	722.8	818		765	6.48	0.91
1	0	713.8	660		654	0.91	0.00

C10 - C11

Temp 298.15 K
Pres 1 Bar

x1	*x2*	Dens kg/m3	Meas Visc	Calc Visc	Rel Dev	Abs Dev	MAD	RMS	BIAS
			µPa.s	µPa.s	%	%	8.45	3.83	2.55
0	1	736.3	1084	1094	-0.93	0.93	**1.10**	**0.62**	**-0.04**
0.11	0.89	735.3	1056	1065	-0.80	0.80			
0.21	0.79	734.3	1031	1037	-0.67	0.67			
0.31	0.69	733.4	1009	1012	-0.29	0.29			
0.41	0.59	732.4	985	986	-0.06	0.06			
0.51	0.49	731.4	956	961	-0.59	0.59			
0.61	0.39	730.4	939	937	0.22	0.22			
0.71	0.29	729.4	921	913	0.79	0.79			
0.80	0.20	728.4	901	891	1.10	1.10			
0.91	0.09	727.3	868	869	-0.09	0.09			
1	0	726.3	846	848	-0.26	0.26			

C10-C12

x1	*x2*	Dens	Meas Visc	Calc Visc	RelDev %				
0.00	1.00	745.0	1379	1359	1.47	1.47	**2.20**	**1.64**	**1.49**
0.11	0.89	743.3	1294	1292	0.18	0.18			
0.20	0.80	741.8	1243	1236	0.58	0.58			
0.30	0.70	740.0	1198	1179	1.57	1.57			
0.41	0.59	738.2	1146	1121	2.20	2.20			
0.51	0.49	736.3	1092	1070	2.07	2.07			
0.61	0.39	734.4	1036	1019	1.57	1.57			
0.81	0.19	730.5	949	930	2.01	2.01			
0.90	0.10	728.4	903	887	1.73	1.73			
1.00	0.00	726.3	846	848	-0.26	0.26			

C10-C16

x1	*x2*	Dens	Meas Visc	Calc Visc	RelDev %				
0	1	769.8	3093	3065	0.89	0.89	**8.45**	**6.42**	**6.09**
0.11	0.89	766.8	2749	2678	2.58	2.58			
0.21	0.79	763.5	2481	2348	5.36	5.36			
0.30	0.70	760.2	2200	2073	5.78	5.78			
0.40	0.60	756.5	1976	1823	7.75	7.75			
0.51	0.49	752.4	1733	1596	7.93	7.93			
0.61	0.39	747.9	1530	1401	8.45	8.45			

0.71	0.29	743.3	1336	1239	7.30	7.30
0.80	0.20	738.2	1170	1091	6.73	6.73
0.90	0.10	732.4	989	959	2.95	2.95
1	0	726.3	846	848	-0.26	0.26

C11 - C12

Temp 298.15 K
Pressure 1 Bar

x1	x2	Dens	Visc	EQ Visc	RelDev	Abs Dev	MAD	RMS	BIAS
			µPa.s	µPa.s	%	%	4.90	2.49	1.00
0	1	745.0	1379	1359	1.47	1.47	**1.82**	**1.09**	**-0.97**
0.11	0.89	744.2	1314	1328	-1.04	1.04			
0.21	0.79	743.4	1297	1300	-0.19	0.19			
0.31	0.69	742.5	1253	1271	-1.46	1.46			
0.41	0.59	741.6	1237	1242	-0.48	0.48			
0.56	0.44	740.4	1196	1205	-0.74	0.74			
0.61	0.39	739.9	1175	1191	-1.32	1.32			
0.72	0.28	738.9	1143	1163	-1.82	1.82			
0.81	0.19	738.0	1127	1139	-1.12	1.12			
0.91	0.09	737.1	1110	1116	-0.60	0.60			
1	0	736.3	1084	1094	-0.93	0.93			

C11-C16

x1	x2	Dens	Visc	EQ Visc	RelDev %				
0.00	1.00	769.8	3093	3065	0.89	0.89	**4.90**	**3.35**	**2.98**
0.11	0.89	767.1	2783	2738	1.60	1.60			
0.20	0.80	764.8	2549	2493	2.21	2.21			
0.31	0.69	761.7	2315	2224	3.96	3.96			
0.41	0.59	758.9	2108	2019	4.21	4.21			
0.51	0.49	755.7	1905	1818	4.54	4.54			
0.61	0.39	752.2	1723	1638	4.90	4.90			
0.71	0.29	748.7	1534	1483	3.35	3.35			
0.81	0.19	744.8	1363	1336	1.98	1.98			
0.90	0.10	740.7	1209	1209	0.02	0.02			
1.00	0.00	736.3	1084	1094	-0.93	0.93			

C12 - C16

Temp 298.15 K
Pressure 1 Bar

x1	x2	Dens	Meas Visc	Calc Visc	RelDev	Abs Dev	MAD	RMS	BIAS
			µPa.s	µPa.s	%	%	%		
0	1	769.8	3093	3065	0.89	0.89	**3.70**	**2.69**	**2.44**
0.11	0.89	767.7	2821	2808	0.45	0.45			
0.21	0.79	765.6	2643	2581	2.32	2.32			
0.31	0.69	763.6	2467	2390	3.12	3.12			
0.41	0.59	761.2	2281	2197	3.70	3.70			
0.51	0.49	758.9	2102	2029	3.48	3.48			
0.61	0.39	756.4	1936	1869	3.46	3.46			
0.71	0.29	753.8	1767	1727	2.27	2.27			
0.80	0.20	751.0	1636	1593	2.63	2.63			
0.91	0.10	748.0	1476	1468	0.51	0.51			
1	0	745.0	1379	1359	1.47	1.47			

2. Audonnet *et al*, 2004

C1 – C10

x C1	x C10	Temp (K)	Press (MPa)	Density (kg/m3)	Exp Mix Viscosity (mPa*s)	CalcVisc (uPa.s)	Rel Diff (%)	MAD	RMS	AVG Rel Dev	BIAS
0.227	0.773	303.15	10.12	702.2	0.605	345.00	42.98	42.98	37.29	37.12	37.12
0.227	0.773		15	706.2	0.633	372.37	41.17				
0.227	0.773		19.92	709.6	0.668	401.67	39.87				
0.227	0.773		30.19	717.3	0.734	461.83	37.08				
0.227	0.773		40.07	722.8	0.801	517.13	35.44				
0.227	0.773		49.93	728.5	0.868	571.31	34.18				
0.227	0.773		60.06	734.3	0.942	627.20	33.42				
0.227	0.773		75.72	742.4	1.065	715.76	32.79				
0.227	0.773	323.15	9.828	685.5	0.46	282.73	38.54	38.54	34.37	34.27	34.27
0.227	0.773		15.125	690.3	0.487	304.77	37.42				
0.227	0.773		20.143	694.4	0.512	327.06	36.12				
0.227	0.773		30.293	702.1	0.567	372.62	34.28				
0.227	0.773		40.113	709	0.62	415.54	32.98				
0.227	0.773		50.859	715.5	0.68	461.66	32.11				
0.227	0.773		60.325	721.3	0.736	502.22	31.76				
0.227	0.773		76.132	730.1	0.827	570.92	30.96				
0.227	0.773	353.15	10.13	661.1	0.36	222.92	38.08	38.08	34.29	34.19	34.19
0.227	0.773		15.1	666.5	0.381	237.66	37.62				
0.227	0.773		20.22	671.9	0.399	253.68	36.42				
0.227	0.773		30.06	680.7	0.43	285.35	33.64				

0.227	0.773		40.07	688.9	0.475	317.44	33.17				
0.227	0.773		50.02	696.1	0.513	348.94	31.98				
0.227	0.773		60.06	702.7	0.556	380.55	31.56				
0.227	0.773		75.4	711.8	0.622	429.09	31.02				
0.227	0.773	393.15	10.06	630.9	0.254	171.83	32.35	33.10	31.27	31.24	31.24
0.227	0.773		15.08	637.6	0.273	182.63	33.10				
0.227	0.773		20.27	644.2	0.288	194.20	32.57				
0.227	0.773		30.01	655.1	0.312	216.50	30.61				
0.227	0.773		39.89	664.1	0.349	239.28	31.44				
0.227	0.773		49.86	672.5	0.38	262.15	31.01				
0.227	0.773		59.97	681	0.407	285.22	29.92				
0.227	0.773		75.45	691.9	0.451	320.53	28.93				
0.41	0.59	303.15	20.02	674.3	0.457	195.10	57.31	57.31	53.01	52.95	52.95
0.41	0.59		25.09	678.8	0.48	213.10	55.60				
0.41	0.59		30.05	683	0.505	229.95	54.47				
0.41	0.59		40.12	689.9	0.541	261.98	51.57				
0.41	0.59		49.91	697.1	0.588	291.38	50.44				
0.41	0.59		60.07	703.6	0.648	321.08	50.45				
0.41	0.59		75.36	713.1	0.743	365.49	50.81				
0.41	0.59	323.15	20.05	656.9	0.356	165.05	53.64	53.64	50.01	49.95	49.95
0.41	0.59		24.92	662.1	0.374	178.41	52.30				
0.41	0.59		29.87	666.7	0.393	191.76	51.21				
0.41	0.59		40	675.8	0.435	217.85	49.92				
0.41	0.59		50.05	682.2	0.465	242.43	47.86				
0.41	0.59		60.29	690.1	0.506	266.74	47.29				
0.41	0.59		75.61	700.7	0.576	302.59	47.47				
0.41	0.59	353.15	20.09	634.2	0.279	135.29	51.51	51.51	49.24	49.21	49.21
0.41	0.59		25.01	640.2	0.295	145.00	50.85				
0.41	0.59		30.01	645.8	0.312	154.92	50.35				
0.41	0.59		39.94	654.5	0.336	174.26	48.14				
0.41	0.59		50.06	663.3	0.371	193.31	47.90				
0.41	0.59		60.26	671	0.408	211.98	48.05				
0.41	0.59		74.95	683.4	0.456	238.38	47.72				
0.41	0.59	393.15	20.05	602.3	0.204	110.41	45.88	46.66	45.88	45.87	45.87
0.41	0.59		25	610	0.22	117.35	46.66				
0.41	0.59		30.14	617.2	0.232	124.69	46.25				
0.41	0.59		40	627.9	0.255	138.79	45.57				
0.41	0.59		50.07	638.3	0.279	152.96	45.17				
0.41	0.59		60.03	647.6	0.306	166.72	45.52				
0.41	0.59		75.48	660.6	0.348	187.68	46.07				
0.601	0.399	303.15	24.84	615.1	0.274	101.35	63.01	63.01	59.78	59.75	59.75
0.601	0.399		30.14	621.2	0.289	111.42	61.45				
0.601	0.399		40.06	631.3	0.32	128.66	59.79				
0.601	0.399		49.95	640	0.352	144.39	58.98				
0.601	0.399		60.14	648.3	0.38	159.71	57.97				
0.601	0.399		75.15	659.2	0.425	181.47	57.30				
0.601	0.399	323.15	24.99	596.9	0.224	88.79	60.36	60.36	57.79	57.77	57.77
0.601	0.399		30.06	604	0.239	96.66	59.56				
0.601	0.399		40.04	615.9	0.264	111.22	57.87				
0.601	0.399		49.98	625.2	0.29	124.66	57.01				
0.601	0.399		59.97	634.4	0.313	137.45	56.09				

0.601	0.399		74.99	646	0.352	155.90	55.71				
0.601	0.399	353.15	24.99	569.2	0.18	76.03	57.76	57.76	56.63	56.62	56.62
0.601	0.399		30.07	578	0.193	82.01	57.51				
0.601	0.399		40.07	592.6	0.216	93.46	56.73				
0.601	0.399		50	603.7	0.237	104.26	56.01				
0.601	0.399		60.06	613.7	0.261	114.69	56.06				
0.601	0.399		74.91	626.5	0.292	129.49	55.66				
0.601	0.399	393.15	25.07	541.6	0.144	65.63	54.42	55.31	54.81	54.81	54.81
0.601	0.399		29.99	550.3	0.152	69.87	54.03				
0.601	0.399		40.16	567.5	0.176	78.66	55.31				
0.601	0.399		50.08	579.6	0.192	87.02	54.68				
0.601	0.399		59.95	590.5	0.212	95.08	55.15				
0.601	0.399		74.93	604.8	0.239	106.90	55.27				
0.799	0.201	303.15	40.11	527.7	0.147	61.65	58.06	58.89	57.86	57.86	57.86
0.799	0.201		45.04	535.4	0.16	65.78	58.89				
0.799	0.201		50.1	542.6	0.162	69.82	56.90				
0.799	0.201		60	553.4	0.182	77.29	57.53				
0.799	0.201		74.5	566.7	0.208	87.53	57.92				
0.799	0.201	323.15	40.16	508	0.129	55.47	57.00	57.42	56.79	56.78	56.78
0.799	0.201		45.02	516.7	0.137	59.07	56.88				
0.799	0.201		50.02	524.1	0.145	62.63	56.81				
0.799	0.201		60.05	537.6	0.157	69.38	55.81				
0.799	0.201		74.98	554.6	0.185	78.77	57.42				
0.799	0.201	353.15	40.07	480.2	0.106	48.92	53.85	54.67	54.12	54.12	54.12
0.799	0.201		45.09	490.6	0.113	52.05	53.94				
0.799	0.201		49.96	499.4	0.12	54.98	54.18				
0.799	0.201		60.09	515.4	0.132	60.80	53.94				
0.799	0.201		75.1	533.4	0.152	68.90	54.67				
0.799	0.201	393.15	40	447.6	0.086	43.50	49.41	54.17	51.48	51.46	51.46
0.799	0.201		45	460.8	0.094	46.00	51.06				
0.799	0.201		50.03	470.6	0.098	48.46	50.55				
0.799	0.201		60.02	486.7	0.111	53.19	52.08				
0.799	0.201		75.25	506.8	0.131	60.03	54.17				

3. Barrufet *et al*, 1996

CO2-C10

CO2	n-C10	Temp (K)	Press (MPa)	Density (g/cm3)	Exp Viscosity (mPa*s)	Calc Visc (uPa.s)	Rel Diff (%)	MAD	StdDev	BIAS
0.151	0.849	310.93	6.996	0.727	0.665	442.20	33.50	77.99	50.79	45.48
0.151	0.849	344.2	6.996	0.701	0.442	317.44	28.18			
0.151	0.849	373.15	6.996	0.677	0.332	252.51	23.94			
0.151	0.849	403.15	6.996	0.651	0.267	206.32	22.73			
0.301	0.699	310.93	6.996	0.733	0.546	254.62	53.37			
0.301	0.699	344.26	6.996	0.703	0.386	193.22	49.94			
0.301	0.699	373.15	6.996	0.675	0.28	161.31	42.39			
0.301	0.699	403.15	6.996	0.649	0.22	137.85	37.34			
0.505	0.495	310.93	6.996	0.749	0.546	120.19	77.99			
0.505	0.495	344.26	6.996	0.712	0.386	98.44	74.50			
0.505	0.495	373.15	10.443	0.684	0.202	94.26	53.34			
0.505	0.495	403.15	11.822	0.651	0.168	86.46	48.53			

CO2-C5-C10

CO2	n-C5	n-C10	Temp (K)	Press (MPa)	Density (g/cm3)	Exp Viscosity (mPa*s)	Calc Visc (uPa.s)	Rel Diff (%)	MAD	StdDev	BIAS
0	0.288	0.712	354.26	0.239	0.649	0.334	312.93	6.31	41.40	30.84	28.22
0	0.288	0.712	365.93	0.308	0.639	0.297	281.36	5.27			
0	0.288	0.712	377.59	0.377	0.629	0.259	253.92	1.96			
0	0.288	0.712	389.82	0.446	0.618	0.237	228.58	3.55			
0	0.288	0.712	401.48	0.515	0.607	0.21	206.98	1.44			
0.087	0.258	0.655	354.26	2.514	0.628	0.321	252.76	21.26			
0.087	0.258	0.655	365.93	2.514	0.617	0.291	230.12	20.92			
0.087	0.258	0.655	377.59	2.514	0.605	0.266	210.30	20.94			
0.087	0.258	0.655	389.82	2.514	0.592	0.243	191.90	21.03			
0.087	0.258	0.655	401.48	2.514	0.579	0.223	176.16	21.00			
0.223	0.224	0.553	354.26	4.928	0.634	0.299	175.20	41.40			
0.223	0.224	0.553	365.93	4.928	0.621	0.262	162.54	37.96			
0.223	0.224	0.553	377.59	4.928	0.611	0.233	151.33	35.05			
0.223	0.224	0.553	389.82	4.928	0.597	0.208	140.81	32.31			
0.223	0.224	0.553	401.48	4.928	0.585	0.189	131.73	30.30			

CO2-C4-C6-C10

CO2	n-C4	n-C6	n-C10	Temp (K)	Press (MPa)	Density (g/cm3)	Exp Viscosity (mPa*s)	Calc Visc (uPa.s)	Rel Diff (%)	MAD	StdDev	BIAS
0	0.193	0.193	0.614	324.26	0.308	0.661	0.381	368.90	3.18	38.78	32.46	29.88
0	0.193	0.193	0.614	342.04	0.377	0.647	0.336	306.40	8.81			
0	0.193	0.193	0.614	359.82	0.446	0.632	0.287	257.54	10.26			

0	0.193	0.193	0.614	377.59	0.515	0.616	0.246	217.51	11.58	
0	0.193	0.193	0.614	395.37	0.653	0.601	0.217	173.58	20.01	
0.086	0.177	0.177	0.56	324.26	2.514	0.668	0.35	289.94	17.16	
0.086	0.177	0.177	0.56	342.04	2.514	0.653	0.307	246.03	19.86	
0.086	0.177	0.177	0.56	359.82	2.514	0.638	0.275	211.26	23.18	
0.086	0.177	0.177	0.56	377.59	2.514	0.622	0.25	182.72	26.91	
0.086	0.177	0.177	0.56	395.37	2.514	0.605	0.232	158.05	31.88	
0.224	0.15	0.15	0.476	324.26	4.928	0.678	0.304	195.10	35.82	
0.224	0.15	0.15	0.476	342.04	4.928	0.663	0.279	170.80	38.78	
0.224	0.15	0.15	0.476	359.82	4.928	0.647	0.244	151.25	38.01	
0.224	0.15	0.15	0.476	377.59	4.928	0.629	0.216	134.99	37.51	
0.224	0.15	0.15	0.476	395.37	4.928	0.612	0.172	120.99	29.66	

CO2-C5-C6-C7-C10

CO2	n-C5	n-C6	n-C7	n-C10	Temp (K)	Press (MPa)	Density (g/cm3)	Exp Viscosity (mPa*s)	Calc Visc (uPa.s)	Rel Diff (%)	MAD	StdDev	BIAS
0	0.097	0.289	0.103	0.511	359.82	0.273	0.655	0.266	266.98	-0.37	36.18	29.68	27.06
0	0.097	0.289	0.103	0.511	377.59	0.308	0.639	0.241	228.89	5.02			
0	0.097	0.289	0.103	0.511	383.15	0.343	0.634	0.228	218.56	4.14			
0	0.097	0.289	0.103	0.511	395.37	0.412	0.622	0.217	197.80	8.85			
0.087	0.088	0.264	0.094	0.467	359.82	2.514	0.645	0.278	218.01	21.58			
0.087	0.088	0.264	0.094	0.467	377.59	2.514	0.629	0.252	190.54	24.39			
0.087	0.088	0.264	0.094	0.467	383.15	2.514	0.624	0.231	182.97	20.79			
0.087	0.088	0.264	0.094	0.467	395.37	2.514	0.612	0.209	167.71	19.76			
0.223	0.075	0.225	0.08	0.397	359.82	4.928	0.625	0.243	155.62	35.96			
0.223	0.075	0.225	0.08	0.397	377.59	4.928	0.608	0.219	139.77	36.18			
0.223	0.075	0.225	0.08	0.397	383.15	4.928	0.604	0.197	135.36	31.29			
0.223	0.075	0.225	0.08	0.397	395.37	4.928	0.592	0.172	126.39	26.52			

4. Caudwell *et al*., 2004.

C8-C10

C8	C10	Temp (K)	Press (MPa)	Density (kg/m3)	Exp Viscosity (mPa*s)	Calc Visc (uPa.s)	Rel Diff (%)	MAD	RMS	BIAS
0.743	0.257	323.15	0.1	694.7	0.502	482.71	3.84	3.84	3.46	3.45
0.743	0.257		0.1	694.6	0.501	482.71	3.65			
0.743	0.257		0.1	694.6	0.502	482.71	3.84			
0.743	0.257		0.1	694.6	0.502	482.71	3.84			
0.743	0.257		39.6	726.1	0.742	715.62	3.56			
0.743	0.257		79.9	749	1.02	988.36	3.10			
0.743	0.257		81.6	749.7	1.03	1000.79	2.84			
0.743	0.257		120	767.2	1.35	1304.31	3.38			
0.743	0.257		161.5	783.1	1.74	1689.10	2.93			
0.743	0.257		161.5	783.1	1.75	1689.10	3.48			
0.743	0.257		161.5	783	1.75	1689.10	3.48			
0.743	0.257		161.5	782.9	1.75	1689.10	3.48			
0.743	0.257		201	796.1	2.2	2123.82	3.46			
0.743	0.257		201.1	796.1	2.2	2125.02	3.41			
0.743	0.257		201.1	796.2	2.2	2125.02	3.41			
0.743	0.257	373.15	0.1	653.6	0.306	297.25	2.86	3.71	3.06	3.02
0.743	0.257		0.1	653.7	0.306	297.25	2.86			
0.743	0.257		39.9	695.2	0.465	448.94	3.45			
0.743	0.257		80.5	723.1	0.632	614.48	2.77			
0.743	0.257		80.5	723.1	0.633	614.48	2.93			
0.743	0.257		80.7	723.2	0.634	615.34	2.94			
0.743	0.257		120.3	744.1	0.814	793.02	2.58			
0.743	0.257		161.5	762	1.02	998.01	2.16			
0.743	0.257		162	762.3	1.03	1000.63	2.85			
0.743	0.257		162	762.3	1.03	1000.63	2.85			
0.743	0.257		200.4	776.6	1.26	1213.24	3.71			
0.743	0.257		200.5	776.6	1.26	1213.83	3.66			
0.743	0.257		200.5	776.5	1.26	1213.83	3.66			
0.743	0.257	423.15	21.4	644.9	0.274	263.27	3.92	3.92	3.14	3.10
0.743	0.257		21.5	644.6	0.273	263.56	3.46			
0.743	0.257		21.5	644.7	0.273	263.56	3.46			
0.743	0.257		40.8	666.3	0.331	319.18	3.57			
0.743	0.257		80.4	698.2	0.45	435.12	3.31			
0.743	0.257		80.8	698.5	0.452	436.32	3.47			
0.743	0.257		80.9	698.4	0.451	436.62	3.19			
0.743	0.257		120.4	722.1	0.575	558.74	2.83			
0.743	0.257		160.1	741.3	0.708	689.97	2.55			
0.743	0.257		160.2	741.3	0.708	690.31	2.50			
0.743	0.257		201.8	758.4	0.86	838.41	2.51			
0.743	0.257		201.9	758.4	0.86	838.78	2.47			
0.434	0.566	323.15	0.1	710	0.657	630.07	4.10	4.92	4.49	4.48
0.434	0.566		0.1	710	0.658	630.07	4.24			
0.434	0.566		0.1	709.9	0.657	630.07	4.10			
0.434	0.566		39.9	739.7	0.995	949.95	4.53			
0.434	0.566		79.4	761.3	1.38	1318.21	4.48			

0.434	0.566		79.5	761.4	1.38	1319.22	4.40			
0.434	0.566		81.4	762.3	1.4	1338.53	4.39			
0.434	0.566		119.6	779.2	1.85	1763.64	4.67			
0.434	0.566		160.3	794.3	2.43	2310.45	4.92			
0.434	0.566		160.6	794.5	2.43	2314.91	4.74			
0.434	0.566		160.6	794.5	2.43	2314.91	4.74			
0.434	0.566		201.6	807.6	3.14	2998.83	4.50			
0.434	0.566		201.6	807.7	3.14	2998.83	4.50			
0.434	0.566	373.15	0.1	670.6	0.385	371.55	3.49	5.59	4.32	4.23
0.434	0.566		0.1	670.6	0.386	371.55	3.74			
0.434	0.566		0.1	670.7	0.385	371.55	3.49			
0.434	0.566		39.8	709.2	0.585	565.70	3.30			
0.434	0.566		80	735.5	0.803	775.32	3.45			
0.434	0.566		80	735.5	0.802	775.32	3.33			
0.434	0.566		80.3	735.7	0.805	776.96	3.48			
0.434	0.566		119.7	755.5	1.05	1003.82	4.40			
0.434	0.566		160.3	772.5	1.34	1265.15	5.59			
0.434	0.566		160.3	772.4	1.34	1265.15	5.59			
0.434	0.566		160.3	772.5	1.33	1265.15	4.88			
0.434	0.566		160.4	772.7	1.33	1265.83	4.82			
0.434	0.566		199.8	786.9	1.64	1551.65	5.39			
0.434	0.566	423.15	20.2	659.7	0.331	318.80	3.68	5.93	4.13	4.05
0.434	0.566		20.2	659.8	0.331	318.80	3.68			
0.434	0.566		40.6	681.3	0.406	391.24	3.63			
0.434	0.566		79.6	711	0.549	531.07	3.27			
0.434	0.566		79.9	711.3	0.551	532.17	3.42			
0.434	0.566		120.2	734.5	0.71	684.24	3.63			
0.434	0.566		159.5	752.7	0.885	842.96	4.75			
0.434	0.566		160.5	753.3	0.887	847.15	4.49			
0.434	0.566		201.3	769.1	1.09	1025.40	5.93			

C3-C8-C10

C8	C10	C3	Temp (K)	Press (MPa)	Density (kg/m3)	Exp Viscosity (mPa*s)	Calc Visc (uPa.s)	Rel Diff (%)	MAD	RMS	BIAS
0.611	0.211	0.178	323.15	21.5	700.8	0.514	445.71	13.29	14.20	12.87	12.85
0.611	0.211	0.178		21.6	700.4	0.52	446.17	14.20			
0.611	0.211	0.178		21.7	700.9	0.515	446.63	13.28			
0.611	0.211	0.178		40.2	714.8	0.614	532.18	13.33			
0.611	0.211	0.178		60.5	728.4	0.717	629.61	12.19			
0.611	0.211	0.178		61	728.5	0.723	632.08	12.58			
0.611	0.211	0.178		61	728.4	0.724	632.08	12.70			
0.611	0.211	0.178		79.9	739.3	0.829	727.84	12.20			
0.611	0.211	0.178		103.2	751.1	0.969	853.79	11.89			
0.611	0.211	0.178	373.15	20.1	662.2	0.323	279.93	13.33	13.98	13.33	13.33
0.611	0.211	0.178		20.4	662.5	0.323	280.92	13.03			
0.611	0.211	0.178		40.6	682.5	0.401	344.93	13.98			
0.611	0.211	0.178		61	698.6	0.471	408.63	13.24			
0.611	0.211	0.178		61	698.7	0.47	408.63	13.06			
0.312	0.405	0.283	323.15	21.3	702.3	0.563	452.03	19.71	19.71	18.43	18.41

0.312	0.405	0.283		21.3	702.3	0.562	452.03	19.57			
0.312	0.405	0.283		21.6	702.9	0.56	453.50	19.02			
0.312	0.405	0.283		40.9	717.5	0.673	548.06	18.56			
0.312	0.405	0.283		59.5	729.8	0.781	641.39	17.88			
0.312	0.405	0.283		60.4	730.3	0.789	646.01	18.12			
0.312	0.405	0.283		60.4	730.3	0.788	646.01	18.02			
0.312	0.405	0.283		80.6	741.8	0.916	752.57	17.84			
0.312	0.405	0.283		99.8	751.6	1.05	860.09	18.09			
0.312	0.405	0.283		99.8	751.7	1.04	860.09	17.30			
0.312	0.405	0.283	373.15	20.5	664.6	0.346	279.88	19.11	19.36	18.56	18.55
0.312	0.405	0.283		20.5	664.6	0.347	279.88	19.34			
0.312	0.405	0.283		20.6	664.7	0.346	280.24	19.01			
0.312	0.405	0.283		40.4	684.2	0.43	346.73	19.36			
0.312	0.405	0.283		62.7	701.7	0.514	418.23	18.63			
0.312	0.405	0.283		62.6	701.7	0.513	418.55	18.41			
0.312	0.405	0.283		80.6	713.8	0.582	476.70	18.09			
0.312	0.405	0.283		100	725.4	0.659	541.24	17.87			
0.312	0.405	0.283		100.2	725.6	0.66	541.91	17.89			
0.312	0.405	0.283		100.4	725.7	0.66	542.59	17.79			
0.344	0.231	0.425	323.15	20.7	676.8	0.394	311.26	21.00	21.00	19.01	18.98
0.344	0.231	0.425		20.9	677.5	0.391	311.96	20.21			
0.344	0.231	0.425		41	694.8	0.474	380.71	19.68			
0.344	0.231	0.425		60.1	709.1	0.545	445.83	18.20			
0.344	0.231	0.425		60.7	709.3	0.552	447.90	18.86			
0.344	0.231	0.425		60.7	709.3	0.551	447.90	18.71			
0.344	0.231	0.425		60.8	709.3	0.552	448.24	18.80			
0.344	0.231	0.425		81.7	722.3	0.639	521.72	18.35			
0.344	0.231	0.425		100.3	732.6	0.719	589.96	17.95			
0.344	0.231	0.425		100.3	732.6	0.72	589.96	18.06			
0.344	0.231	0.425	373.15	20.9	636.7	0.253	202.36	20.02	20.02	19.31	19.30
0.344	0.231	0.425		20.9	636.8	0.253	202.36	20.02			
0.344	0.231	0.425		21	636.7	0.253	202.64	19.91			
0.344	0.231	0.425		40.3	659.5	0.31	251.97	18.72			
0.344	0.231	0.425		59.9	677.5	0.366	298.49	18.45			
0.344	0.231	0.425		60.9	677.8	0.374	300.84	19.56			
0.344	0.231	0.425		60.9	677.9	0.374	300.84	19.56			
0.344	0.231	0.425		80.5	692.5	0.428	346.83	18.97			
0.344	0.231	0.425		101.2	706	0.486	395.99	18.52			

5. Dymond *et al*, 1981

C8-C12

C8	C12	Temp (K)	Press (MPa)	Density (kg/m3)	Exp Viscosity (mPa*s)	Calc Visc (uPa.s)	Rel Diff (%)	MAD	RMS	BIAS
0.5	0.5	298.2	0.1	725.9	0.869	832	4.30	5.34	4.57	4.48
0.5	0.5		25.7	744.1	1.151	1098	4.57			
0.5	0.5		74.8	770.9	1.81	1717	5.15			
0.5	0.5		103.4	783.3	2.286	2164	5.34			
0.5	0.5		150.1	800.5	3.255	3095	4.92			
0.5	0.5		197.9	815.6	4.569	4451	2.58			
0.5*	0.5		238.6	827.3	5.992	6196	-3.40			
0.5	0.5	323.22	0.1	706.9	0.623	595	4.54	6.82	5.71	5.63
0.5	0.5		25.4	728.2	0.818	780	4.60			
0.5	0.5		96.1	768.2	1.482	1400	5.50			
0.5	0.5		153.5	790.2	2.215	2064	6.82			
0.5	0.5		197.6	804.2	2.912	2717	6.68			
0.5	0.5		252.4	819.4	4.017	3792	5.61			
0.5	0.5		302.9	832.4	5.31	5200	2.07			
0.5	0.5		353	844.8	6.908	7350	-6.40			
0.5	0.5		395.6	855.3	8.589	10510	-22.37			
0.5	0.5	348.17	0.1	687.7	0.472	451	4.55	6.98	5.46	5.38
0.5	0.5		51	730.4	0.781	746	4.51			
0.5	0.5		94.1	754.5	1.083	1030	4.87			
0.5	0.5		149.6	777.5	1.555	1462	5.96			
0.5	0.5		197.3	793.3	2.054	1911	6.98			
0.5	0.5		248.9	808.1	2.708	2502	7.62			
0.5	0.5		301.1	821.6	3.516	3254	7.46			
0.5	0.5		351	833.7	4.453	4182	6.09			
0.5	0.5		404.4	846.4	5.664	5529	2.39			
0.5	0.5		455.1	858.5	7.069	7395	-4.61			
0.5	0.5		502	869.9	8.602	10156	-18.07			
0.5	0.5	373.17	0.1	668	0.37	354	4.27	6.29	5.05	4.98
0.5	0.5		49.7	712	0.612	586	4.31			
0.5	0.5		99.6	741	0.886	841	5.06			
0.5	0.5		152.6	763.7	1.229	1152	6.29			
0.5	0.5		202.6	780.9	1.608	1491	7.25			
0.5	0.5		251.2	795.3	2.045	1876	8.27			
0.5	0.5		300	808.5	2.554	2329	8.79			
0.5	0.5		349.5	820.9	3.171	2878	9.24			
0.5	0.5		401.2	833.5	3.919	3577	8.71			
0.5	0.5		452.5	845.9	4.798	4448	7.29			
0.5	0.5		505.5	858.9	5.858	5622	4.03			

**Shaded data at P>200 MPa not included in RMS, MAD and BIAS*

C6-C16

C6	C16	Temp (K)	Press (MPa)	Density (kg/m3)	Exp Viscosity (mPa*s)	Calc Visc (uPa.s)	Rel Diff (%)	MAD	RMS	BIAS
0.8	0.2	298.22	0.1	698.9	0.584	465.17	20.35	27.55	23.29	23.17
0.8	0.2		1.4	700.1	0.599	471.35	21.31			
0.8	0.2		9	707	0.646	507.90	21.38			
0.8	0.2		18.5	714.7	0.709	554.47	21.80			
0.8	0.2		41.4	730.2	0.877	670.70	23.52			
0.8	0.2		61.2	741.2	1.023	775.68	24.18			
0.8	0.2		80.9	750.8	1.184	884.27	25.31			
0.8	0.2		103.9	760.9	1.403	1016.44	27.55			
0.8	0.2	323.19	0.1	678.1	0.4426	354.74	19.85	24.31	22.17	22.10
0.8	0.2		1.6	679.9	0.4508	360.24	20.09			
0.8	0.2		8.4	687.3	0.4868	385.44	20.82			
0.8	0.2		48.5	720.2	0.701	543.89	22.41			
0.8	0.2		98.7	747	1.002	768.95	23.26			
0.8	0.2		127.9	759	1.206	916.80	23.98			
0.8	0.2		152.5	768	1.392	1053.56	24.31			
0.8	0.2		204.5	785	1.857	1391.35	25.08			
0.8	0.2		230.4	792.9	2.145	1592.72	25.75			
0.8	0.2	348.07	0.1	656.4	0.3501	281.30	19.65	24.79	22.12	22.03
0.8	0.2		3.1	659.9	0.3632	289.91	20.18			
0.8	0.2		9.4	667	0.3902	308.20	21.01			
0.8	0.2		48.3	701.5	0.552	427.93	22.48			
0.8	0.2		101.1	733.6	0.804	610.28	24.09			
0.8	0.2		152.7	756.4	1.082	813.82	24.79			
0.8	0.2		202.5	774	1.401	1039.61	25.80			
0.8	0.2		248.7	788	1.736	1282.02	26.15			
0.8	0.2		296	800.9	2.138	1572.94	26.43			
0.8	0.2		351.1	814.8	2.68	1984.96	25.93			
0.8	0.2		401.8	827.1	3.31	2459.53	25.69			
0.8	0.2		450.4	838.6	3.982	3034.42	23.80			
0.8	0.2		482.2	846.2	4.399	3495.99	20.53			
0.8	0.2	373.12	0.1	634.5	0.2803	228.90	18.34	24.84	22.07	21.94
0.8	0.2		48.6	685.6	0.4572	358.99	21.48			
0.8	0.2		101.8	720.3	0.66	507.56	23.10			
0.8	0.2		151.6	743.2	0.874	656.87	24.84			
0.8	0.2		201.4	761.4	1.109	821.65	25.91			
0.8	0.2		249.5	776.3	1.368	1002.18	26.74			
0.8	0.2		302.2	790.8	1.709	1234.38	27.77			
0.8	0.2		351.5	803.3	2.061	1497.57	27.34			

0.8	0.2		398.3	814.8	2.446	1805.34	26.19			
0.8	0.2		447.7	826.6	2.896	2216.82	23.45			
0.8	0.2		501.9	839.6	3.498	2817.81	19.45			
0.6	0.4	298.12	0.1	726.4	0.991	747.48	24.57	31.58	26.99	26.87
0.6	0.4		4.6	730	1.027	785.97	23.47			
0.6	0.4		10.6	734.5	1.108	837.71	24.39			
0.6	0.4		19.6	740.9	1.227	916.08	25.34			
0.6	0.4		32	749	1.396	1025.39	26.55			
0.6	0.4		40.7	754.2	1.5	1102.89	26.47			
0.6	0.4		50.7	759.8	1.646	1192.72	27.54			
0.6	0.4		61.9	765.6	1.806	1294.20	28.34			
0.6	0.4		70.8	769.8	1.978	1375.46	30.46			
0.6	0.4		82	774.8	2.161	1478.50	31.58			
0.6	0.4	323.33	0.1	707	0.703	537.87	23.49	30.47	26.91	26.79
0.6	0.4		5.3	711.9	0.75	568.77	24.16			
0.6	0.4		10.5	716.4	0.785	600.18	23.54			
0.6	0.4		26.2	728.7	0.928	698.20	24.76			
0.6	0.4		50.7	744.6	1.151	861.32	25.17			
0.6	0.4		75	757.5	1.414	1036.93	26.67			
0.6	0.4		101.5	769.6	1.73	1247.23	27.91			
0.6	0.4		121.5	777.8	2.005	1421.70	29.09			
0.6	0.4		153.8	789.9	2.479	1739.84	29.82			
0.6	0.4		172.1	796.2	2.762	1945.10	29.58			
0.6	0.4		199.2	805.4	3.297	2292.37	30.47			
0.6	0.4	348.29	0.1	687.1	0.522	409.38	21.57	28.81	25.36	25.20
0.6	0.4		9.2	696.4	0.581	449.14	22.70			
0.6	0.4		51.1	729.5	0.865	648.56	25.02			
0.6	0.4		101.4	757	1.284	925.61	27.91			
0.6	0.4		153	778.1	1.769	1259.42	28.81			
0.6	0.4		202.7	794.8	2.388	1640.77	31.29			
0.6	0.4		249.7	808.7	3.033	2072.41	31.67			
0.6	0.4		298.4	822	3.834	2617.77	31.72			
0.6	0.4		341.7	833.3	4.717	3216.40	31.81			
0.6	0.4	373.24	0.1	667	0.4147	324.01	21.87	28.30	24.93	24.82
0.6	0.4		5.2	673.2	0.4445	342.84	22.87			
0.6	0.4		10.5	679.3	0.4753	362.57	23.72			
0.6	0.4		49.8	714.6	0.686	514.29	25.03			
0.6	0.4		103.3	746.7	1.015	739.54	27.14			
0.6	0.4		152.3	767.8	1.353	970.15	28.30			
0.6	0.4		203.7	785.5	1.797	1245.41	30.69			
0.6	0.4		251.9	799.6	2.254	1545.40	31.44			
0.6	0.4		303.3	813.2	2.852	1926.44	32.45			

0.6	0.4		351.3	825	3.502	2360.50	32.60			
0.6	0.4		402.3	837.1	4.323	2937.41	32.05			
0.6	0.4		451.7	848.7	5.225	3657.01	30.01			
0.6	0.4		478.3	855	5.888	4133.48	29.80			
0.6	0.4		502.8	860.8	6.334	4643.32	26.69			
0.4	0.6	298.15	0.1	745.4	1.518	1199.06	21.01	27.56	24.44	24.36
0.4	0.6		4.3	748.9	1.648	1262.63	23.38			
0.4	0.6		9	752.6	1.737	1334.10	23.20			
0.4	0.6		15.7	757.5	1.881	1436.43	23.63			
0.4	0.6		21.6	761.4	2.011	1526.85	24.08			
0.4	0.6		31.6	767.5	2.248	1680.44	25.25			
0.4	0.6		36.9	770.5	2.277	1761.89	22.62			
0.4	0.6		41.8	773.1	2.493	1837.18	26.31			
0.4	0.6		46.2	775.3	2.595	1904.73	26.60			
0.4	0.6		57.2	780.4	2.862	2073.28	27.56			
0.4	0.6	323.13	0.1	726.8	1.028	818.99	20.33	27.64	24.55	24.41
0.4	0.6		25.8	747.1	1.379	1075.09	22.04			
0.4	0.6		52.1	762.8	1.749	1363.45	22.04			
0.4	0.6		77.6	775.3	2.19	1673.22	23.60			
0.4	0.6		111	789.2	2.891	2136.75	26.09			
0.4	0.6		126.9	795.3	3.247	2386.81	26.49			
0.4	0.6		153.2	804.9	3.915	2854.77	27.08			
0.4	0.6		178.4	813.8	4.678	3385.09	27.64			
0.4	0.6	348.31	0.1	708	0.754	596.80	20.85	26.20	23.59	23.50
0.4	0.6		4.9	712.5	0.798	628.19	21.28			
0.4	0.6		8.7	716	0.833	653.50	21.55			
0.4	0.6		49.8	746.4	1.265	953.75	24.60			
0.4	0.6		102	773.8	1.881	1409.41	25.07			
0.4	0.6		137.1	788.2	2.358	1769.65	24.95			
0.4	0.6		167.3	799	2.874	2121.14	26.20			
0.4	0.6		202.6	810.4	3.563	2590.80	27.29			
0.4	0.6		249.9	824.1	4.666	3346.12	28.29			
0.4	0.6		297.1	836.7	6.219	4293.13	30.97			
0.4	0.6	373.18	0.1	689	0.568	459.31	19.14	26.45	22.51	19.14
0.4	0.6		4.3	693.4	0.595	480.83	19.19			
0.4	0.6		9.6	698.6	0.64	508.35	20.57			
0.4	0.6		49.9	731.2	0.96	731.61	23.79			
0.4	0.6		91.4	755.5	1.317	989.93	24.83			
0.4	0.6		140.9	777.7	1.824	1341.52	26.45			
0.4	0.6		202.2	799.2	2.597	1858.34	28.44			
0.4	0.6		298.9	826.1	4.282	2939.59	31.35			
0.4	0.6		400	850.1	6.791	4662.77	31.34			

0.4	0.6		418.4	854.2	7.398	5078.69	31.35			
0.2	0.8	298.09	0.1	759.6	2.236	1926.55	13.84	16.70	14.84	14.76
0.2	0.8		4.3	762.8	2.327	2038.33	12.41			
0.2	0.8		10.2	767.1	2.531	2195.96	13.24			
0.2	0.8		19.8	773.3	2.868	2453.01	14.47			
0.2	0.8		30.1	779.2	3.275	2728.17	16.70			
0.2	0.8		34.3	781.4	3.4	2839.88	16.47			
0.2	0.8		39.5	784	3.552	2977.60	16.17			
0.2	0.8	323.21	0.1	741.7	1.409	1242.47	11.82	20.83	16.15	15.75
0.2	0.8		5	745.7	1.488	1317.82	11.44			
0.2	0.8		9.8	749.4	1.586	1393.14	12.16			
0.2	0.8		39	768.5	2.167	1884.81	13.02			
0.2	0.8		61.4	780.2	2.69	2305.94	14.28			
0.2	0.8		79	788.4	3.156	2669.35	15.42			
0.2	0.8		101.3	797.7	3.882	3180.52	18.07			
0.2	0.8		123.4	806.2	4.714	3757.36	20.29			
0.2	0.8		142.9	813.4	5.483	4340.64	20.83			
0.2	0.8		156.6	818.3	6.014	4802.40	20.15			
0.2	0.8	348.09	0.1	723.9	0.988	872.64	11.68	19.78	14.64	14.29
0.2	0.8		4.5	727.8	1.034	916.11	11.40			
0.2	0.8		9.7	732.2	1.102	968.74	12.09			
0.2	0.8		48.9	759.4	1.628	1410.51	13.36			
0.2	0.8		99.4	784.7	2.549	2105.29	17.41			
0.2	0.8		148.2	803.7	3.661	2936.99	19.78			
0.2	0.8		201.8	821.1	5.184	4090.26	21.10			
0.2	0.8		246.8	834.2	6.733	5325.76	20.90			
0.2	0.8		300.4	849	9.344	7259.02	22.31			
0.2	0.8	373.17	0.1	705.6	0.729	650.85	10.72	19.47	16.03	15.70
0.2	0.8		48.2	744.7	1.208	1025.06	15.14			
0.2	0.8		100.1	773.5	1.834	1513.87	17.46			
0.2	0.8		158.5	797.2	2.714	2185.66	19.47			
0.2	0.8		202.2	811.6	3.515	2791.01	20.60			
0.2	0.8		251	825.7	4.627	3599.17	22.21			
0.2	0.8		302.1	839	6.163	4639.91	24.71			
0.2	0.8		351.4	850.8	7.85	5897.55	24.87			
0.2	0.8		401	862.3	9.859	7508.12	23.85			
0.2	0.8		446.1	872.5	12.139	9387.72	22.66			

C6-C12

C6	C12	Temp (K)	Press (MPa)	Density (kg/m3)	Exp Viscosity (mPa.s)	Calc Visc (uPa.s)	Rel Diff (%)	MAD	RMS	BIAS
0.501	0.499	298.1	0.1	713.8	0.719	627.31	12.75	15.61	14.57	14.54
0.501	0.499		49.7	746.4	1.181	1004.90	14.91			
0.501	0.499		102.2	771.3	1.802	1520.73	15.61			
0.501	0.499		152.2	790	2.57	2184.67	14.99			
0.501	0.499		177.7	798.3	3.065	2622.41	14.44			
0.501	0.499		203.6	806.2	3.605	3169.77	12.07			
0.501	0.499	348.12	0.1	673.7	0.403	357.81	11.21	15.88	13.78	13.68
0.501	0.499		52.1	717	0.667	579.11	13.18			
0.501	0.499		96.3	741.8	0.923	789.74	14.44			
0.501	0.499		150.4	764.7	1.293	1087.65	15.88			
0.501	0.499		210	781.9	1.711	1485.13	13.20			
0.501	0.499		248.5	795.9	2.178	1794.33	17.62			
0.501	0.499		302.5	810.3	2.811	2325.58	17.27			
0.501	0.499		355.7	823.7	3.569	3011.43	15.62			
0.501	0.499		403.4	835.3	4.378	3843.72	12.20			
0.501	0.499		455.1	847.9	5.411	5151.85	4.79			
0.501	0.499	373.16	0.1	652.8	0.3214	286.17	10.96	15.13	12.63	12.52
0.501	0.499		51.8	701.9	0.533	473.56	11.15			
0.501	0.499		98	729.2	0.743	647.72	12.82			
0.501	0.499		150.8	752	1.019	864.86	15.13			
0.501	0.499		203.3	770.1	1.339	1109.83	17.11			
0.501	0.499		250.8	784.4	1.675	1366.91	18.39			
0.501	0.499		303.4	799.2	2.112	1706.63	19.19			
0.501	0.499		351.8	812.3	2.579	2090.74	18.93			

6. Wakefield *et al.*, 1988

C8-C14 (T=303.16 K, P=1 Bar)

C8	C14	Density (kg/m3)	Exp Viscosity (uPa.s)	Calc Visc (uPa.s)	Rel Diff (%)	MAD	RMS	BIAS
1	0	694.59	484.33	480	0.81	9.37	7.66	7.39
0.84958	0.15042	708.44	630.29	591	6.21			
0.64959	0.35041	723.53	858.89	779	9.33			
0.50006	0.49994	732.93	1056	957	9.37			
0.35146	0.64854	740.99	1275.9	1175	7.93			
0.1525	0.8475	749.65	1612.1	1545	4.13			
0	1	756.08	1901	1907	-0.32			
1	0	690.59	456.77	454	0.65	9.52	7.70	7.43
0.84958	0.15042	704.58	592.54	555	6.29			
0.64959	0.35041	719.75	802.57	726	9.52			
0.50006	0.49994	729.12	978.86	887	9.34			
0.35146	0.64854	737.17	1175.7	1083	7.86			
0.1525	0.8475	746.24	1475.6	1415	4.13			
0	1	752.5	1728.6	1736	-0.42			

C8-C16 (T=318.16 K, P=1 Bar)

C8	C16	Density (kg/m3)	Exp Viscosity (uPa.s)	Calc Visc (uPa.s)	Rel Diff (%)	MAD	RMS	BIAS
1	0	682.77	413.8	407.21	1.59	14.58	12.21	11.96
0.84996	0.15004	700.95	575.8	519.40	9.79			
0.65006	0.34994	719.7	837.8	718.30	14.26			
0.49989	0.50011	730.83	1072.8	916.38	14.58			
0.36018	0.63982	740.35	1317.3	1149.43	12.74			
0.20044	0.79956	749.4	1626.6	1489.35	8.44			
0	1	756.29	2039.2	2061.47	-1.09			
1	0	674.48	370.6	367.86	0.74	14.47	12.17	11.91
0.84996	0.15004	692.96	512.8	463.84	9.55			
0.65006	0.34994	712.14	738.6	631.71	14.47			
0.49989	0.50011	723.52	931.4	796.70	14.46			
0.36018	0.63982	732.93	1132.5	988.66	12.70			
0.20044	0.79956	742.26	1380.8	1265.45	8.35			
0	1	749.25	1703.2	1724.86	-1.27			
1	0	666.07	341.5	334.20	2.14	14.40	12.08	11.80
0.84996	0.15004	685.01	460.1	417.21	9.32			
0.65006	0.34994	704.5	655	560.67	14.40			
0.49989	0.50011	716.09	817.8	700.06	14.40			
0.36018	0.63982	725.72	985.8	860.68	12.69			
0.20044	0.79956	734.95	1187.2	1089.97	8.19			
0	1	742.26	1450	1465.95	-1.10			

C6-C10-C12-C16 (*T*=303.16 K, *P*=1 Bar)

C6	C10	C12	C16	Density (kg/m3)	Exp Viscosity (uPa*s)	Calc Visc (uPa.s)	Rel Diff (%)	MAD	RMS	BIAS
1	0	0	0	646.13	284.5	281.4	1.08	14.37	12.32	12.14
0	1	0	0	722.29	796.03	789.7	0.80			
0	0	1	0	741.79	1257.2	1246.0	0.89			
0	0	0	1	766.72	2753.4	2772.3	-0.69			
0.08312	0.07472	0.42175	0.42041	749.51	1626.6	1489.5	8.43			
0.17435	0.17551	0.32506	0.32508	740.99	1312.5	1150.8	12.32			
0.24928	0.24931	0.2509	0.25051	733.11	1090.2	937.7	13.99			
0.3288	0.32389	0.17333	0.17398	723.71	884.58	757.4	14.37			
0.42524	0.42483	0.07514	0.07479	708.69	654.66	578.9	11.58			
1	0	0	0	646.13	272.4	267.7	1.73	14.18	12.30	12.10
0	1	0	0	718.64	743.09	737.5	0.75			
0	0	1	0	738.09	1157.7	1147.5	0.88			
0	0	0	1	763.45	2477.8	2509.9	-1.29			
0.08312	0.07472	0.42175	0.42041	745.93	1487.8	1367.0	8.12			
0.17435	0.17551	0.32506	0.32508	737.32	1212	1062.5	12.33			
0.24928	0.24931	0.2509	0.25051	729.45	1012.8	869.9	14.11			
0.3288	0.32389	0.17333	0.17398	719.46	822.73	706.1	14.18			
0.42524	0.42483	0.07514	0.07479	704.69	615.31	543.0	11.75			

C7-C9-C12-C16 (*T*=303.16 K, *P*=1 Bar)

C7	C9	C12	C16	Density (kg/m3)	Exp Viscosity (uPa.s)	Calc Visc (uPa.s)	Rel Diff (%)	BIAS
1	0	0	0	676.52	366.46	367.5	-0.28	10.25
0	1	0	0	709.98	626.34	614.2	1.93	
0	0	1	0	741.79	1257.2	1246.0	0.89	
0	0	0	1	766.72	2753.4	2772.4	-0.69	
0.07483	0.07466	0.42552	0.42499	749.86	1636.4	1515.4	7.4	
0.17416	0.17445	0.32635	0.32504	741.1	1299.3	1154.7	11.13	
0.25004	0.24921	0.25028	0.25047	733.27	1071.1	940.5	12.19	
0.32462	0.32501	0.17506	0.17531	723.8	870.37	766.4	11.95	
0.42475	0.42538	0.07493	0.07494	708.9	637.66	583.0	8.58	
1	0	0	0	672.55	345.56	348.2	-0.76	10.05
0	1	0	0	706.1	589.08	578.5	1.8	
0	0	1	0	738.09	1157.7	1147.5	0.88	
0	0	0	1	763.45	2477.8	2509.9	-1.29	
0.07483	0.07466	0.42552	0.42499	746.28	1496.06	1390.7	7.04	
0.17416	0.17445	0.32635	0.32504	737.42	1197.96	1066.9	10.94	
0.25004	0.24921	0.25028	0.25047	729.42	992.93	873.5	12.03	
0.32462	0.32501	0.17506	0.17531	720.11	810.81	715.4	11.77	
0.42475	0.42538	0.07493	0.07494	704.85	598.6	547.9	8.47	

7. Wu *et al*., 1998

4-Component mixtures at *P*=1 Bar

#T = 293.15 K										
C7	C8	C11	C13	Density (kg/m3)	Exp Viscosity (uPa.s)	Calc Visc (uPa.s)	Rel Diff (%)	MAD	RMS	BIAS
0.2194	0.1073	0.5242	0.1491	730.7	964.7	927.4	3.86	6.68	5.24	5.15
0.0905	0.5375	0.2202	0.1518	721.6	795	758.8	4.55			
0.1213	0.1148	0.2462	0.5177	741.7	1271.3	1208.2	4.96			
0.335	0.316	0.1765	0.1725	718.1	745.7	703.1	5.71			
0.5416	0.1151	0.1764	0.1669	714.8	706.8	659.6	6.68			
# T = 298.15 K										
C7	C8	C11	C13	Density (kg/m3)	Exp Viscosity (uPa.s)	Calc Visc (uPa.s)	Rel Diff (%)	MAD	RMS	BIAS
0.067	0.0665	0.7109	0.1556	734.6	1053.5	1040.0	1.28	8.00	5.57	5.21
0.0554	0.0316	0.1948	0.7182	745.8	1409.8	1383.0	1.90			
0.1767	0.1413	0.5794	0.1026	726.6	885.5	856.4	3.28			
0.1107	0.656	0.0913	0.142	711.6	657	629.2	4.22			
0.1528	0.3674	0.3159	0.1639	721.5	800.2	758.5	5.21			
0.1831	0.1419	0.3025	0.3725	732.1	1013.5	957.0	5.57			
0.1641	0.1442	0.0999	0.5918	737	1138.8	1072.5	5.82			
0.3628	0.3421	0.1008	0.1943	712.2	669.9	630.3	5.91			
0.1679	0.5003	0.1067	0.2251	717.1	736.4	692.8	5.92			
0.4293	0.1376	0.2687	0.1644	716	724.1	679.1	6.22			
0.1676	0.3678	0.1004	0.3642	725.6	872.4	815.2	6.56			
0.4303	0.1366	0.0948	0.3383	720.5	795.2	732.6	7.87			
0.3264	0.1127	0.0787	0.4822	729.3	962	885.0	8.00			
# T = 308.15 K										
C7	C8	C11	C13	Density (kg/m3)	Exp Viscosity (uPa.s)	Calc Visc (uPa.s)	Rel Diff (%)	MAD	RMS	BIAS
0.107	0.645	0.0888	0.1592	705.2	592.6	564.4	4.76	7.04	6.19	6.12
0.6585	0.1065	0.1679	0.0671	693.4	491	465.0	5.30			
0.1574	0.2461	0.0923	0.5042	725.4	886.2	827.9	6.58			
0.2114	0.1204	0.5858	0.0824	718	775.2	721.6	6.92			
0.322	0.3136	0.1504	0.214	708.5	638.5	593.5	7.04			
C8	C10	C11	C15	Density (kg/m3)	Exp Viscosity (uPa.s)	Calc Visc (uPa.s)	Rel Diff (%)	MAD	RMS	BIAS
0.1137	0.1002	0.3688	0.4173	739.7	1235.3	1180.7	4.42	6.39	5.23	5.16
0.2064	0.2954	0.2017	0.2965	731.5	1014.8	963.1	5.10			
0.3047	0.1986	0.2025	0.2942	729.5	975.3	913.0	6.39			
0.396	0.202	0.203	0.199	722.9	840.4	791.4	5.83			
0.506	0.2965	0.1037	0.0938	713.2	686.8	658.9	4.06			
C8	C11	C13	C15	Density (kg/m3)	Exp Viscosity (uPa.s)	Calc Visc (uPa.s)	Rel Diff (%)	MAD	RMS	BIAS
0.1092	0.1028	0.3805	0.4075	745.9	1468.4	1405.3	4.30	7.03	5.87	5.79

0.2042	0.3021	0.1996	0.2941	737.5	1171.8	1111.4	5.15			
0.3039	0.2044	0.1984	0.2933	734.9	1106	1032.6	6.64			
0.4012	0.2007	0.1995	0.1986	728.8	960	892.5	7.03			
0.5017	0.299	0.1017	0.0976	719.5	780.4	735.0	5.82			
C7	C10	C13	C16	Density (kg/m3)	Exp Viscosity (uPa.s)	Calc Visc (uPa.s)	Rel Diff (%)	MAD	RMS	BIAS
0.095	0.1016	0.399	0.4044	747.8	1553.6	1471.3	5.29	11.54	9.40	9.14
0.1956	0.3018	0.2002	0.3024	736.4	1167	1064.1	8.82			
0.2919	0.2021	0.2023	0.3037	734	1112.4	989.3	11.06			
0.3903	0.2031	0.2016	0.205	725.6	919.9	813.7	11.54			
0.4975	0.3061	0.0985	0.0979	711.1	678.4	617.5	8.97			
C7	C8	C12	C16	Density (kg/m3)	Exp Viscosity (uPa.s)	Calc Visc (uPa.s)	Rel Diff (%)	MAD	RMS	BIAS
0.0907	0.1085	0.3981	0.4027	743.4	1387.1	1096.6	20.94	20.94	18.77	18.58
0.1947	0.3072	0.1971	0.301	728.9	992.7	803.5	19.06			
0.2907	0.2057	0.2015	0.3021	728.3	982.8	786.7	19.96			
0.3943	0.2022	0.1992	0.2043	718.8	803.1	646.5	19.50			
0.499	0.2977	0.1019	0.1014	701.8	577.8	500.0	13.46			
# T = 313.15 K										
C7	C8	C11	C13	Density (kg/m3)	Exp Viscosity (uPa.s)	Calc Visc (uPa.s)	Rel Diff (%)	MAD	RMS	BIAS
0.0738	0.1142	0.0907	0.7213	732.6	1038.8	1003.7	3.38	7.13	5.01	4.60
0.0862	0.0887	0.7	0.1251	721.7	807.9	793.5	1.79			
0.1377	0.5714	0.1702	0.1207	701.6	558.8	534.8	4.29			
0.2855	0.2511	0.2509	0.2125	708.9	645	603.5	6.43			
0.4957	0.0984	0.2237	0.1822	703.1	583.2	541.6	7.13			
C8	C10	C11	C15	Density (kg/m3)	Exp Viscosity (uPa.s)	Calc Visc (uPa.s)	Rel Diff (%)	MAD	RMS	BIAS
0.1034	0.0983	0.3947	0.4036	736	1134	1095.8	3.37	5.10	3.86	3.73
0.2015	0.3007	0.2011	0.2967	728	944.4	914.8	3.14			
0.2998	0.1991	0.2004	0.3007	726.3	914.5	867.8	5.10			
0.4008	0.2026	0.1951	0.2015	719.2	783.7	747.5	4.62			
0.5093	0.2896	0.1019	0.0992	709.7	647.3	631.6	2.43			
C8	C11	C13	C15	Density (kg/m3)	Exp Viscosity (uPa.s)	Calc Visc (uPa.s)	Rel Diff (%)	MAD	RMS	BIAS
0.11	0.1024	0.3895	0.3981	742.3	1328.1	1288.6	2.97	6.89	5.60	5.42
0.2063	0.3023	0.1992	0.2922	733.9	1079.9	1026.3	4.96			
0.3042	0.2005	0.2005	0.2948	731.5	1027.3	959.8	6.57			
0.3949	0.2002	0.1975	0.2074	725.7	902	839.9	6.89			
0.5035	0.2957	0.1019	0.0989	715.8	729.4	687.6	5.73			
C7	C10	C13	C16	Density (kg/m3)	Exp Viscosity (uPa.s)	Calc Visc (uPa.s)	Rel Diff (%)	MAD	RMS	BIAS
0.1039	0.1006	0.3867	0.4088	744.1	1416	1343.8	5.10	10.57	8.38	8.14
0.1987	0.2999	0.202	0.2994	732.7	1074.3	997.1	7.19			
0.2882	0.2023	0.2036	0.3059	730.7	1036.5	932.7	10.01			

0.3928	0.2035	0.1999	0.2038	721.8	853.5	763.3	10.57			
0.4969	0.2995	0.1019	0.1017	707.7	644.1	593.7	7.83			
C7	C8	C12	C16	Density (kg/m3)	Exp Viscosity (uPa.s)	Calc Visc (uPa.s)	Rel Diff (%)	MAD	RMS	BIAS
0.0975	0.1116	0.3937	0.3972	739.5	1262.1	1024.0	18.87	19.13	17.62	17.46
0.1921	0.3048	0.1995	0.3036	725.6	929.7	761.7	18.07			
0.2866	0.2086	0.2011	0.3037	724.8	919.9	743.9	19.13			
0.3886	0.2073	0.2001	0.204	715.2	752.3	613.3	18.47			
0.4966	0.3023	0.0985	0.1026	697.9	543.4	474.2	12.74			

5-Component mixtures at T=298.15 K, P=1 Bar.

C7	C8	C11	C13	C15	Density (kg/m3)	Exp Viscosity (uPa.s)	Calc Visc (uPa.s)	Rel Diff (%)	MAD	RMS	BIAS
0.0893	0.0946	0.0439	0.0942	0.678	754.1	1849.9	1711.0	7.51	8.86	7.55	7.51
0.129	0.1174	0.1174	0.4869	0.1493	742.4	1311.6	1229.2	6.28			
0.1657	0.3208	0.262	0.1352	0.1163	727	910.4	844.5	7.24			
0.2051	0.2424	0.3417	0.0935	0.1173	727	908.9	846.0	6.92			
0.2742	0.2241	0.198	0.1587	0.145	727.2	922.8	841.0	8.86			
0.4291	0.3308	0.1134	0.0298	0.0969	709.6	649	599.1	7.68			
0.589	0.1747	0.0759	0.0874	0.073	707.5	625.5	575.0	8.08			

Appendix B: Viscosity Modelling of Individual Components

B.1. Available Measured Data.

Cn	Reference	# Data points	*P* Range (Mpa)	*T* range (K)	Dens	Visc	Inc in Anal	Reason for exclusion
5	Giller *et al.,* 1949	18	0.1	137.15 - 283.15	Yes	Yes	No	mostly T<0 degC
	Doolittle *et al.,* 1951	2	0.1	263.15 -283.15	Yes	Yes	No	only 2 points: at -10 and 20 deg C
6	Aasen *et al.,* 1990	4	0.1	288.15 - 326.15	No	Yes	No	Knapstad et al 1989
	Giller *et al.,* 1949	14	0.1	175.15 - 283.15	Yes	Yes	No	mostly T<0 degC
	Wakefield *et al.,* 1988a	3	0.1	318 - 338	Yes	Yes	No	Dymond more comprehensive
	Dymond *et al.,* 1980 (I)	14	Psat	283 - 395	Yes	Yes	No	Dymond (II) more comprehensive
	Dymond *et al.,* 1980 (II)	**37**	**0.1 - 419**	**298 - 373**	**Yes**	**Yes**	**Yes, up to 100 Mpa**	
	Assael *et al.,* 1992	2	0.1	303 - 323	No	Yes	No	Mixtures only
7	Giller *et al.,* 1949	15	0.1	180.15 -283.15	Yes	Yes	No	mostly T<0 degC
	Quiemada *et al.,* 2003	4	0.1	293.15 - 323.15	Yes	Yes	No	Doolittle wider range of T, values ~same
	Assael *et al.,* 1992	2	0.1	303-323	No	Yes	No	Mixtures only
	Doolittle *et al.,* 1951	**4**	**0.1**	**263.15 - 373.15**	**Yes**	**Yes**	**Yes**	
8	Aasen *et al.,* 1990	5	0.1	293.15 - 370.15	No	Yes	No	Knapstad et al 1989, no densities
	Giller *et al.,* 1949	15	0.1	211.15 - 293.15	Yes	Yes	No	mostly T<0 degC

Cn	Reference	# Data points	*P* Range (Mpa)	*T* range (K)	Dens	Visc	Inc in Anal	Reason for exclusion
	Wakefield *et al.,* 1988a	3	0.1	318 - 338	Yes	Yes	No	Dymond (II) more comprehensive
	Dymond *et al.,* 1981 (III)	**41**	**0.1 - 505**	**298.15 -373.15**	**Yes**	**Yes**	**Yes**	
	Dymond *et al.,* 1980 (I)	8	Psat	283 - 393	Yes	Yes	No	Dymond (II) more comprehensive
	Doolittle *et al.,* 1951	**4**	**0.1**	**263.15 -373.15**	**Yes**	**Yes**	**Yes**	
9	Assael *et al.,* 1992	2	0.1	303-323	No	Yes	No	Mixtures only
	Doolittle *et al.,* 1951	**5**	**0.1**	**263.15 -423.15**	**Yes**	**Yes**	**Yes**	
10	Aasen *et al.,* 1990	7	0.1	292.15 - 423.15	No	Yes	No	Knapstad et al 1989
	Giller *et al.,* 1949	14	0.1	240.15 - 293.15	Yes	Yes	No	mostly T<0 degC
	Wakefield *et al.,* 1988a	3	0.1	318 - 338	Yes	Yes	No	Queimada more comprehensive
	Quiemada *et al.,* 2005	**6**	**0.1**	**293 - 343**	**Yes**	**Yes**	**Yes**	
11	Assael *et al.,* 1992	2	0.1	303-323	No	Yes	No	Mixtures only
	Doolittle *et al.,* 1951	**6**	**0.1**	**263.15 - 473.15**	**Yes**	**Yes**	**Yes**	
12	**Giller *et al.,* 1949**	**11**	**0.1**	**262.15 - 293.15**	**Yes**	**Yes**	**Yes**	mostly T<0 degC
	Dymond *et al.,* 1981 (III)	**32**	**0.1 - 501.6**	**298-373**	**Yes**	**Yes**	**Yes, up to 100 Mpa**	
	Dymond *et al.,* 1980 (I)	8	Psat	283 - 393	Yes	Yes	No	Dymond (II) more comprehensive
	Doolittle *et al.,* 1951	6	0.1	263.15 - 473.15	Yes	Yes	No	Dymond (II) more comprehensive

Cn	Reference	# Data points	*P* Range (Mpa)	*T* range (K)	Dens	Visc	Inc in Anal	Reason for exclusion
14	Aasen *et al.,* 1990	7	0.1	292.15 -423.15	No	Yes	No	Knapstad et al 1989, densities missing
	Giller *et al.,* 1949	**10**	**1**	**277.65 - 293.15**	**Yes**	**Yes**	**Yes**	
16	Quiemada *et al.,* 2003	6	0.1	293 - 343	No	Yes		Ciotta mode comprehensive
	Ciotta, 2010	**54**	**1 - 101**	**298 - 473**	**Yes**	**Yes**	**Yes**	
	Dymond *et al.,* 1980 (I)	10	Psat	289 - 393	Yes	Yes	No	Ciotta mode comprehensive
	Dymond *et al.,* 1980 (II)	28	0.1 - 425	298 - 373	Yes	Yes	No	Ciotta mode comprehensive
17	Aasen *et al.,* 1990	6	0.1	300.15 - 523.15	No	Yes	No	Same as Doolittle
	Doolittle *et al.,* 1951	**7**	**0.1**	**293.15 - 573.15**	**Yes**	**Yes**	**Yes**	
20	Aasen *et al.,* 1990	4	0.1	323.15 -423.15	Yes	No	No	Flory et al (1964), no visc data
	Quiemada *et al.,* 2005	**4**	**0.1**	**313 - 343**	**Yes**	**Yes**	**Yes**	
	Quiemada *et al.,* 2003	4	0.1	313 - 343	Yes	Yes	No	same as Queimada 2005
22	**Quiemada *et al.,* 2005**	**3**	**0.1**	**323 - 343**	**Yes**	**Yes**	**Yes**	
	Quiemada *et al.,* 2003	3	0.1	323 - 343	Yes	Yes	No	same as Queimada 2005
24	**Wakefield *et al.,* 1988a**	**3**	**0.1**	**318 - 338**	**Yes**	**Yes**	**Yes**	**Estimated values**
	Quiemada *et al.,* 2005	**2**	**0.1**	**333 - 343**	**Yes**	**Yes**	**Yes**	
	Quiemada *et al.,* 2003	2	0.1	333 - 343	Yes	Yes	No	same as Queimada 2005

Cn	Reference	# Data points	*P* Range (Mpa)	*T* range (K)	Dens	Visc	Inc in Anal	Reason for exclusion
28	Aasen *et al.,* 1990	2	0.1	373.15 - 423.15	Yes	No	No	Flory et al (1964), no visc data
	Aasen *et al.,* 1990	5	0.1	373.15 - 573.15	No	Yes	No	Same as Doolittle
	Doolittle *et al.,* 1951	**7**	**0.1**	**293.15 - 573.15**	**Yes**	**Yes**	**Yes**	
30	Aasen *et al.,* 1990	2	0.1	373.15 - 423.15	Yes	No	No	Flory et al (1964), no visc data
32	**Aasen *et al.,* 1990**	**8**	**0.3**	**353.15 - 473.15**	**Yes**	**Yes**	**Yes**	
36	Aasen *et al.,* 1990	2	0.1	373.15 - 423.15	Yes	No	No	Flory et al (1964), no visc data
	Aasen *et al.,* 1990	5	0.1	373.15 - 573.15	No	Yes	No	Same as Doolittle
	Doolittle *et al.,* 1951	**5**	**0.1**	**323.15 -573.15**	**Yes**	**Yes**	**Yes**	
40	Aasen *et al.,* 1990	1	0.1	423.15	Yes	No	No	Flory et al (1964), no visc data
44	**Aasen *et al.,* 1990**	**5**	**0.3**	**369.15 - 473.15**	**Yes**	**Yes**	**Yes**	
60	**Aasen *et al.,* 1990**	**5**	**0.3**	**407.15 -466.15**	**Yes**	**Yes**	**Yes**	
64	Aasen *et al.,* 1990	1	0.1	423.15	Yes	No	No	Flory et al (1964), no visc data
	Doolittle *et al.,* 1951	**5**	**0.1**	**323.15 - 573.15**	**Yes**	**Yes**	**Yes**	

B.2. Viscosity Comparison Results: Hard Sphere *vs.* Free Volume

Component: C6

Mw: 86 x 10^{-3} kg/mol

Dymond *et al.,* 1980 (II)

		Measured data		Calculated data			Deviations %		
Ref P (atm)	Temp (K)	Dens (kg/m3)	Visc (mPa.s)	Densities (kg/m3) (Tait+ Ciotta + a0 extrapolation)	Free Volume Visc (cP)	ST-HS Visc(cP)	Dens	FV Visc	ST-HS Visc
1	298.3	655	0.30	659	0.29	0.32	0.6	-2.4	6.7
1	323.2	632	0.24	641	0.24	0.26	1.5	0.4	12.2
1	348.4	607	0.19	623	0.20	0.23	2.7	3.3	18.0
1	373.4	581	0.16	605	0.17	0.20	4.3	5.3	22.8
208	298.3	674	0.36	670	0.35	0.35	-0.6	-2.5	-3.1
416	298.3	690	0.43	679	0.43	0.39	-1.5	0.4	-9.7
478	323.2	677	0.37	666	0.36	0.33	-1.6	-1.1	-10.4
491	348.4	659	0.31	652	0.30	0.28	-0.9	-2.0	-8.3
518	373.4	645	0.27	639	0.26	0.25	-0.9	-2.3	-5.9
590	298.3	701	0.49	686	0.50	0.41	-2.1	3.1	-14.7
815	298.3	714	0.56	694	0.61	0.45	-2.8	8.6	-19.5
996	348.4	693	0.42	673	0.45	0.34	-2.8	5.7	-20.4
1002	323.2	710	0.51	687	0.56	0.40	-3.2	9.1	-22.2
1009	298.3	724	0.63	701	0.72	0.48	-3.2	13.3	-23.7
1009	373.4	680	0.37	661	0.38	0.30	-2.8	2.7	-18.9

Component: C7

Mw: 100 x 10^{-3} kg/mol

Doolittle *et al.,* 1951

		Measured data		Calculated data			Deviations %		
Ref *P* (atm)	Temp (K)	Dens (kg/m3)	Visc (mPa.s)	Densities (kg/m3) (Tait+ Ciotta + a0 extrapolation)	Free Volume Visc (cP)	ST-HS Visc(cP)	Dens	FV Visc	ST-HS Visc
1	263.15	709	0.60	708	0.57	0.62	-0.2	-5.3	2.8
1	293.15	684	0.42	686	0.41	0.44	0.3	-1.9	4.6
1	323.15	658	0.31	665	0.31	0.33	1.0	1.0	7.9
1	373.15	612	0.21	629	0.22	0.24	2.9	4.0	13.8

Component: C8

Mw: 114 x 10^{-3} kg/mol

Doolittle *et al.,* 1951

		Measured data		Calculated data			Deviations %		
Ref *P* (atm)	Temp (K)	Dens (kg/m3)	Visc (mPa.s)	Densities (kg/m3) (Tait+ Ciotta + a0 extrapolation)	Free Volume Visc (cP)	ST-HS Visc(cP)	Dens	FV Visc	ST-HS Visc
1	263.2	727	0.83	727	0.79	0.86	0.0	-4.6	3.7
1	293.2	703	0.55	705	0.54	0.57	0.4	-1.6	4.3
1	323.2	678	0.39	684	0.39	0.42	0.8	0.2	6.6
1	373.2	635	0.26	648	0.26	0.29	2.1	1.5	11.4

Component: C8

Dymond *et al.,* 1981

Mw: 114 x 10^{-3} kg/mol

		Measured data		Calculated data			Deviations %		
Ref *P* (atm)	Temp (K)	Dens (kg/m3)	Visc (mPa.s)	Densities (kg/m3) (Tait+ Ciotta + a0 extrapolation)	Free Volume Visc (cP)	ST-HS Visc(cP)	Dens	FV Visc	ST-HS Visc
1	298.2	699	0.51	702	0.48	0.54	0.5	-5.8	5.9
1	323.3	678	0.39	684	0.37	0.42	0.8	-4.3	8.1
1	348.3	657	0.30	666	0.30	0.34	1.4	-2.3	11.9
1	373.1	636	0.25	648	0.24	0.29	2.0	-0.5	16.2
469	348.3	702	0.48	696	0.46	0.45	-0.8	-3.5	-5.5
482	373.1	687	0.40	683	0.38	0.38	-0.6	-4.8	-3.9
517	323.3	720	0.62	713	0.61	0.57	-1.1	-2.2	-8.6
529	298.2	737	0.85	728	0.82	0.75	-1.2	-3.6	-12
986	323.3	746	0.88	732	0.93	0.72	-1.8	6.2	-18
1012	298.2	761	1.20	746	1.31	0.96	-1.9	8.7	-20
1018	348.3	734	0.70	720	0.73	0.58	-1.9	4.7	-17
1022	373.1	722	0.57	709	0.59	0.49	-1.8	2.4	-15
1474	298.2	779	1.67	761	2.02	1.20	-2.3	21	-28
1486	323.3	766	1.21	749	1.44	0.89	-2.3	20	-26
1519	348.3	755	0.95	738	1.11	0.71	-2.3	17	-24
1600	373.1	747	0.80	730	0.92	0.61	-2.3	15	-24
1951	373.1	759	0.95	740	1.19	0.69	-2.5	25	-28
1976	323.3	782	1.59	762	2.19	1.09	-2.6	38	-32

		Measured data		Calculated data			Deviations %		
Ref *P* (atm)	Temp (K)	Dens (kg/m3)	Visc (mPa.s)	Densities (kg/m3) (Tait+ Ciotta + a0 extrapolation)	Free Volume Visc (cP)	ST-HS Visc(cP)	Dens	FV Visc	ST-HS Visc
1994	298.2	795	2.27	774	3.26	1.50	-2.6	44	-34
2007	348.3	772	1.22	752	1.63	0.85	-2.6	34	-30
2476	373.1	776	1.21	754	1.75	0.81	-2.8	45	-33
2488	298.2	809	3.04	786	5.13	1.83	-2.8	69	-40
2502	323.3	797	2.10	775	3.42	1.32	-2.8	63	-37
2504	348.3	787	1.56	764	2.40	1.01	-2.8	55	-35
2981	323.3	810	2.65	785	5.10	1.55	-3.1	92	-41
2983	373.1	790	1.49	766	2.52	0.94	-3.0	70	-37
2991	348.3	800	1.94	775	3.51	1.18	-3.1	81	-39
3011	298.2	822	4.06	796	8.26	2.22	-3.1	104	-45
3475	348.3	812	2.38	785	5.08	1.36	-3.4	114	-43
3490	298.2	833	5.23	805	12.77	2.64	-3.3	144	-50
3497	323.3	823	3.39	795	7.83	1.84	-3.4	131	-46
3498	373.1	803	1.83	776	3.64	1.09	-3.4	100	-40
3962	298.2	844	6.68	813	19.63	3.10	-3.6	194	-54
3993	373.1	816	2.21	785	5.18	1.24	-3.7	135	-44
4000	348.3	825	2.95	794	7.60	1.58	-3.8	158	-46
4035	323.3	836	4.31	804	12.25	2.17	-3.7	184	-50
4467	348.3	837	3.54	802	10.87	1.80	-4.2	207	-49
4471	298.2	855	8.67	821	31.21	3.66	-3.9	260	-58
4491	323.3	846	5.26	812	17.90	2.49	-4.1	240	-53
4964	348.3	851	4.27	810	15.90	2.06	-4.8	272	-52
4989	323.3	859	6.50	819	27.12	2.87	-4.6	317	-56

Component: C9

Doolittle *et al.,* 1951

Mw: 128×10^{-3} kg/mol

		Measured data		Calculated data			Deviations %		
Ref *P* (atm)	Temp (K)	Dens (kg/m3)	Visc (mPa.s)	Densities (kg/m3) (Tait+ Ciotta + a0 extrapolation)	Free Volume Visc (cP)	ST-HS Visc(cP)	Dens	FV Visc	ST-HS Visc
1	263.2	741	1.15	742	1.09	1.19	0.1	-5.4	2.9
1	293.2	718	0.72	720	0.71	0.74	0.4	-1.3	3.0
1	323.2	694	0.50	699	0.50	0.52	0.7	0.4	4.0
1	373.2	653	0.31	664	0.32	0.34	1.6	2.0	8.6
1	423.2	609	0.21	628	0.22	0.25	3.2	3.5	15.0

Component: C10

Queimada *et al.,* 2005

Mw: 142×10^{-3} kg/mol

		Measured data		Calculated data			Deviations %		
Ref *P* (atm)	Temp (K)	Dens (kg/m3)	Visc (mPa.s)	Densities (kg/m3) (Tait+ Ciotta + a0 extrapolation)	Free Volume Visc (cP)	ST-HS Visc(cP)	Dens	FV Visc	ST-HS Visc
1	293.2	729	0.90	733	0.91	0.95	0.5	1.4	5.3
1	303.2	722	0.77	725	0.80	0.82	0.4	3.9	6.7
1	313.2	715	0.67	718	0.70	0.71	0.5	5.2	7.3
1	323.2	707	0.59	711	0.62	0.63	0.6	6.0	7.8
1	333.2	699	0.52	704	0.56	0.57	0.7	6.7	8.4
1	343.2	692	0.47	697	0.50	0.51	0.8	6.2	8.2

Component: C11

Doolittle *et al.,* 1951

Mw: 156×10^{-3} kg/mol

		Measured data		Calculated data			Deviations %		
Ref *P* (atm)	Temp (K)	Dens (kg/m3)	Visc (mPa.s)	Densities (kg/m3) (Tait+ Ciotta + a0 extrapolation)	Free Volume Visc (cP)	ST-HS Visc(cP)	Dens	FV Visc	ST-HS Visc
1	263.2	762	2.17	764	2.27	2.18	0.2	4.4	0.3
1	293.2	740	1.19	742	1.31	1.20	0.3	10.8	1.0
1	323.2	718	0.76	721	0.85	0.77	0.4	11.6	0.7
1	373.2	680	0.44	686	0.48	0.45	0.8	9.8	2.8
1	423.2	639	0.29	650	0.31	0.31	1.7	8.3	8.1
1	473.2	595	0.20	614	0.22	0.24	3.3	9.0	15.9

Component: C12

Giller *et al.,* 1949

Mw: 170×10^{-3} kg/mol

		Measured data		Calculated data			Deviations %		
Ref *P* (atm)	Temp (K)	Dens (kg/m3)	Visc (mPa.s)	Densities (kg/m3) (Tait+ Ciotta + a0 extrapolation)	Free Volume Visc (cP)	ST-HS Visc(cP)	Dens	FV Visc	ST-HS Visc
1	282.2	757	1.81	758	1.79	1.87	0.1	-0.9	3.1
1	272.2	766	2.26	765	2.17	2.32	-0.1	-3.8	2.8
1	267.2	768	2.55	769	2.41	2.62	0.1	-5.6	2.6
1	265.2	770	2.68	770	2.51	2.75	0.0	-6.4	2.5
1	264.2	770	2.75	771	2.56	2.82	0.1	-6.8	2.4
1	263.2	770	2.82	772	2.62	2.89	0.2	-7.2	2.4
1	262.7	771	2.86	772	2.65	2.92	0.2	-7.5	2.2
1	262.2	773	2.90	773	2.68	2.96	-0.1	-7.7	2.1
1	261.7	774	2.94	773	2.70	3.00	-0.1	-8.0	2.0
1	261.2	771	2.97	773	2.73	3.04	0.2	-7.9	2.3

Component: C12

Dymond *et al.,* 1981

Mw: 170×10^{-3} kg/mol

		Measured data		Calculated data			Deviations %		
Ref *P* (atm)	Temp (K)	Dens (kg/m3)	Visc (mPa.s)	Densities (kg/m3) (Tait+ Ciotta + a0 extrapolation)	Free Volume Visc (cP)	ST-HS Visc(cP)	Dens	FV Visc	ST-HS Visc
1	298.3	745	1.36	747	1.36	1.37	0.2	0.2	0.8
1	323.4	727	0.92	729	0.93	0.92	0.3	2.1	0.1
1	348.1	709	0.67	711	0.68	0.67	0.4	2.4	0.3
1	373.2	690	0.51	694	0.52	0.52	0.5	2.2	1.6
90	348.1	717	0.74	719	0.75	0.73	0.2	0.3	-1.8
127	323.4	737	1.07	738	1.06	1.04	0.0	-0.2	-2.6
238	373.2	714	0.67	714	0.65	0.64	0.0	-3.4	-4.1
517	323.4	763	1.59	760	1.56	1.46	-0.4	-1.8	-7.8
522	298.3	778	2.43	775	2.35	2.24	-0.4	-3.2	-7.7
685	348.1	758	1.32	755	1.29	1.19	-0.4	-2.4	-9.9
946	373.2	760	1.23	755	1.18	1.08	-0.7	-3.8	-12.3
997	323.4	786	2.40	781	2.43	2.10	-0.7	1.5	-12.3
1026	348.1	774	1.73	770	1.73	1.51	-0.6	0.3	-12.6
1031	298.3	800	3.92	795	3.92	3.38	-0.7	0.0	-13.7
1176	298.3	806	4.45	800	4.52	3.77	-0.7	1.6	-15.4

Component: C13

Doolittle *et al.,* 1951

Mw: 184×10^{-3} kg/mol

		Measured data		Calculated data			Deviations %		
Ref *P* (atm)	Temp (K)	Dens (kg/m3)	Visc (mPa.s)	Densities (kg/m3) (Tait+ Ciotta + a0 extrapolation)	Free Volume Visc (cP)	ST-HS Visc(cP)	Dens	FV Visc	ST-HS Visc
1	263.2	778	3.45	779	4.46	3.78	0.1	29.5	9.8
1	293.2	756	1.88	757	2.36	1.86	0.1	25.2	-1.2
1	323.2	735	1.12	736	1.42	1.09	0.1	27.1	-2.2
1	373.2	699	0.60	700	0.74	0.59	0.3	23.1	-2.5
1	423.2	660	0.38	665	0.45	0.38	0.7	20.2	2.1
1	473.2	620	0.26	629	0.31	0.28	1.5	17.9	8.3

Component: C14

Giller *et al.,* 1949

Mw: 198×10^{-3} kg/mol

		Measured data		Calculated data			Deviations %		
Ref *P* (atm)	Temp (K)	Dens (kg/m3)	Visc (mPa.s)	Densities (kg/m3) (Tait+ Ciotta + a0 extrapolation)	Free Volume Visc (cP)	ST-HS Visc(cP)	Dens	FV Visc	ST-HS Visc
1	292.2	763	2.29	764	2.34	2.35	0.1	2.0	2.5
1	287.2	768	2.58	767	2.57	2.63	-0.1	-0.5	1.9
1	282.2	770	2.92	771	2.83	2.96	0.1	-3.0	1.4
1	280.2	777	3.06	772	2.95	3.11	-0.6	-3.6	1.7
1	279.2	775	3.13	773	3.01	3.19	-0.2	-3.8	1.9
1	278.2	773	3.21	774	3.07	3.27	0.0	-4.3	1.9
1	277.7	774	3.25	774	3.10	3.31	0.0	-4.5	1.9
1	277.2	774	3.29	774	3.14	3.35	0.0	-4.7	2.0
1	277	775	3.31	775	3.15	3.37	-0.1	-4.8	1.9
1	276.7	775	3.34	775	3.17	3.40	0.0	-5.1	1.7

Component: C16

Ciotta, 2010

Mw: 226×10^{-3} kg/mol

		Measured data		Calculated data			Deviations %		
Ref *P* (atm)	Temp (K)	Dens (kg/m3)	Visc (mPa.s)	Densities (kg/m3) (Tait+ Ciotta + a0 extrapolation)	Free Volume Visc (cP)	ST-HS Visc(cP)	Dens	FV Visc	ST-HS Visc
10	298.4	769	3.11	770	3.20	3.18	0.1	2.9	2.5
11	298.4	769	3.11	770	3.20	3.18	0.1	2.9	2.4
11	323.2	752	1.87	752	2.02	1.87	0.1	7.7	-0.2
12	323.2	752	1.87	752	2.02	1.87	0.1	8.0	0.1
10	348.2	734	1.26	734	1.36	1.22	0.0	8.7	-2.9
12	373.1	717	0.91	717	0.98	0.87	0.0	7.6	-4.7
12	398.2	700	0.69	699	0.73	0.66	-0.1	5.7	-5.3
13	423.3	682	0.54	682	0.57	0.52	0.0	4.8	-3.8
11	448.2	664	0.44	664	0.45	0.43	0.0	3.4	-2.1
12	473.5	645	0.36	647	0.37	0.36	0.2	2.7	0.7
99	298.4	775	3.50	775	3.55	3.59	0.0	1.6	2.6
208	298.4	781	4.03	782	4.04	4.13	0.1	0.3	2.5

		Measured data		Calculated data			Deviations %		
Ref *P* (atm)	Temp (K)	Dens (kg/m3)	Visc (mPa.s)	Densities (kg/m3) (Tait+ Ciotta + a0 extrapolation)	Free Volume Visc (cP)	ST-HS Visc(cP)	Dens	FV Visc	ST-HS Visc
208	323.2	765	2.39	766	2.52	2.40	0.1	5.4	0.7
198	348.2	749	1.57	749	1.67	1.54	0.0	6.1	-2.1
198	373.1	734	1.14	734	1.19	1.09	0.0	4.3	-4.2
202	398.2	719	0.87	719	0.88	0.82	0.0	1.4	-5.4
205	423.3	704	0.69	705	0.69	0.66	0.0	-0.9	-4.8
200	448.2	689	0.56	690	0.54	0.54	0.1	-2.9	-3.4
205	473.5	674	0.47	676	0.44	0.46	0.2	-5.3	-1.9
301	298.4	786	4.53	787	4.51	4.63	0.0	-0.6	2.2
405	323.2	777	2.96	777	3.11	3.02	0.0	5.1	2.0
400	348.2	763	1.94	762	2.05	1.93	0.0	5.5	-0.7
402	373.1	749	1.40	749	1.44	1.35	0.0	3.3	-3.1
402	398.2	735	1.07	735	1.07	1.02	0.0	-0.1	-4.6
404	423.3	722	0.85	722	0.82	0.81	0.1	-3.1	-4.6
400	448.2	708	0.69	709	0.65	0.66	0.2	-6.1	-4.0
404	473.5	695	0.58	697	0.53	0.56	0.2	-9.0	-3.4
597	323.2	787	3.60	787	3.81	3.71	0.0	5.8	3.2
599	348.2	774	2.36	774	2.49	2.36	0.0	5.7	0.2
600	373.1	761	1.68	761	1.74	1.64	0.0	3.4	-2.0
598	398.2	748	1.27	749	1.27	1.22	0.0	0.1	-3.4
593	423.3	735	1.00	736	0.96	0.96	0.2	-3.7	-4.1
597	448.2	724	0.82	725	0.76	0.79	0.2	-7.3	-4.2
600	473.5	712	0.69	713	0.62	0.66	0.2	-10.6	-4.2
793	323.2	796	4.38	796	4.66	4.52	0.0	6.4	3.2
794	348.2	784	2.81	783	3.00	2.85	0.0	7.1	1.4
797	373.1	771	1.99	772	2.08	1.97	0.0	4.4	-1.1
793	398.2	759	1.49	760	1.50	1.45	0.1	0.7	-2.7
794	423.3	748	1.17	749	1.13	1.13	0.2	-3.2	-3.4
794	448.2	737	0.96	738	0.89	0.92	0.3	-7.4	-4.1
794	473.5	726	0.80	727	0.71	0.76	0.2	-11.2	-5.0
1015	323.2	803	5.08	805	5.84	5.58	0.3	15.0	9.9
996	348.2	792	3.28	793	3.64	3.41	0.1	11.0	4.2
989	373.1	781	2.30	781	2.46	2.32	0.0	6.8	0.6
991	398.2	769	1.71	770	1.77	1.70	0.1	3.4	-0.6
987	423.3	758	1.35	760	1.32	1.31	0.2	-2.0	-2.7
990	448.2	748	1.10	750	1.03	1.06	0.3	-6.2	-3.5
998	473.5	738	0.92	740	0.83	0.88	0.2	-10.6	-5.1

Component: C17

Doolittle *et al.,* 1951

Mw: 240×10^{-3} kg/mol

		Measured data		Calculated data			Deviations %		
Ref *P* (atm)	Temp (K)	Dens (kg/m3)	Visc (mPa.s)	Densities (kg/m3) (Tait+ Ciotta + a0 extrapolation)	Free Volume Visc (cP)	ST-HS Visc(cP)	Dens	FV Visc	ST-HS Visc
1	293.2	778	4.00	777	4.28	4.22	-0.1	6.9	5.6
1	323.2	758	2.17	756	2.36	2.12	-0.2	8.8	-2.3
1	373.2	723	1.02	720	1.11	0.95	-0.4	8.3	-7.5
1	423.2	688	0.60	685	0.63	0.55	-0.5	4.6	-7.4
1	473.2	651	0.39	649	0.40	0.38	-0.3	2.6	-2.7
1	523.2	612	0.28	613	0.28	0.28	0.3	-1.3	0.7
1	573.2	569	0.20	578	0.20	0.22	1.6	0.7	9.8

Component: C20

Queimada *et al.,* 2005

Mw: 283×10^{-3} kg/mol

		Measured data		Calculated data			Deviations %		
Ref *P* (atm)	Temp (K)	Dens (kg/m3)	Visc (mPa.s)	Densities (kg/m3) (Tait+ Ciotta + a0 extrapolation)	Free Volume Visc (cP)	ST-HS Visc(cP)	Dens	FV Visc	ST-HS Visc
1	313.2	775	4.01	774	3.75	4.46	-0.1	-6.5	11.2
1	323.2	768	3.20	767	3.09	3.49	-0.2	-3.4	9.2
1	333.2	762	2.61	760	2.57	2.79	-0.2	-1.5	6.8
1	343.2	755	2.17	753	2.17	2.27	-0.3	0.0	4.6

Component: C22

Queimada *et al.,* 2005

Mw: 311×10^{-3} kg/mol

		Measured data		Calculated data			Deviations %		
Ref *P* (atm)	Temp (K)	Dens (kg/m3)	Visc (mPa.s)	Densities (kg/m3) (Tait+ Ciotta + a0 extrapolation)	Free Volume Visc (cP)	ST-HS Visc(cP)	Dens	FV Visc	ST-HS Visc
1	323.2	774	4.13	774	3.99	4.91	0.0	-3.3	18.8
1	333.2	768	3.34	767	3.30	3.83	-0.1	-1.4	14.7
1	343.2	761	2.75	760	2.75	3.06	-0.2	0.0	11.0

Component: C24

Queimada *et al.,* 2005

Mw: 339×10^{-3} kg/mol

		Measured data		Calculated data			Deviations %		
Ref *P* (atm)	Temp (K)	Dens (kg/m3)	Visc (mPa.s)	Densities (kg/m3) (Tait+ Ciotta + a0 extrapolation)	Free Volume Visc (cP)	ST-HS Visc(cP)	Dens	FV Visc	ST-HS Visc
1	333.2	773	4.48	773	4.44	0.28	0.1	-0.8	-93.7
1	343.2	766	3.67	766	3.67	4.13	0.0	0.1	12.6

Component: C24

Wakefield *et al.,* 1988 (estimated values)

Mw: 339×10^{-3} kg/mol

		Measured data		Calculated data			Deviations %		
Ref *P* (atm)	Temp (K)	Dens (kg/m3)	Visc (mPa.s)	Densities (kg/m3) (Tait+ Ciotta + a0 extrapolation)	Free Volume Visc (cP)	ST-HS Visc(cP)	Dens	FV Visc	ST-HS Visc
1	318.2	782	5.73	784	6.07	7.97	0.3	6.0	39.1
1	328.2	776	4.79	777	4.92	6.03	0.1	2.7	25.9
1	338.2	770	3.85	770	4.04	4.66	0.0	4.8	21.1

Component: C28

Doolittle *et al.,* 1951

Mw: 395×10^{-3} kg/mol

		Measured data		Calculated data			Deviations %		
Ref *P* (atm)	Temp (K)	Dens (kg/m3)	Visc (mPa.s)	Densities (kg/m3) (Tait+ Ciotta + a0 extrapolation)	Free Volume Visc (cP)	ST-HS Visc(cP)	Dens	FV Visc	ST-HS Visc
1	323.2	788	5.97	791	7.79	13.41	0.5	30.6	124.8
1	373.2	756	2.90	756	3.00	3.58	0.0	3.4	23.6
1	423.2	724	1.46	720	1.48	1.48	-0.5	0.9	1.5
1	473.2	691	0.87	685	0.85	0.82	-0.9	-2.7	-6.4
1	523.2	658	0.60	649	0.55	0.54	-1.3	-9.0	-10.4
1	573.2	623	0.42	614	0.38	0.39	-1.5	-9.4	-6.3

Component: C32

Assen *et al.,* 1990

Mw: 451×10^{-3} kg/mol

		Measured data		Calculated data			Deviations %		
Ref *P* (atm)	Temp (K)	Dens (kg/m3)	Visc (mPa.s)	Densities (kg/m3) (Tait+ Ciotta + a0 extrapolation)	Free Volume Visc (cP)	ST-HS Visc(cP)	Dens	FV Visc	ST-HS Visc
3	353.1	774	5.37	778	5.40	9.53	0.5	0.7	77.5
3	372.1	762	3.81	764	3.84	5.78	0.3	1.0	51.8
3	372.2	762	3.79	764	3.84	5.77	0.3	1.4	52.4
3	396.7	747	2.57	747	2.61	3.34	0.0	1.2	29.9
3	424.3	729	1.81	727	1.79	2.03	-0.3	-1.2	12.4
3	449.7	713	1.37	709	1.32	1.40	-0.6	-3.5	2.6
3	457.2	709	1.25	704	1.21	1.27	-0.7	-3.2	1.6
3	465.3	704	1.17	698	1.11	1.15	-0.8	-4.8	-1.3

Component: C36

Doolittle *et al.,* 1951

Mw: 507×10^{-3} kg/mol

		Measured data		Calculated data			Deviations %		
Ref *P* (atm)	Temp (K)	Dens (kg/m3)	Visc (mPa.s)	Densities (kg/m3) (Tait+ Ciotta + a0 extrapolation)	Free Volume Visc (cP)	ST-HS Visc(cP)	Dens	FV Visc	ST-HS Visc
1	373.2	767	4.89	769	5.00	8.47	0.3	2.2	73.1
1	423.2	736	2.32	733	2.31	2.79	-0.3	0.0	20.5
1	473.2	705	1.33	698	1.27	1.32	-1.0	-4.2	-1.0
1	523.2	673	0.89	662	0.79	0.78	-1.6	-11.2	-11.8
1	573.2	640	0.61	627	0.53	0.54	-2.1	-12.5	-11.6

Component: C44

Assen *et al.,* 1990

Mw: 619×10^{-3} kg/mol

		Measured data		Calculated data			Deviations %		
Ref *P* (atm)	Temp (K)	Dens (kg/m3)	Visc (mPa.s)	Densities (kg/m3) (Tait+ Ciotta + a0 extrapolation)	Free Volume Visc (cP)	ST-HS Visc(cP)	Dens	FV Visc	ST-HS Visc
3.0	368.4	776.5	8.338	784.1	8.740	23.691	1.0	4.8	184.1
3.0	398.9	757.8	4.696	762.5	5.082	9.663	0.6	8.2	105.8
3.0	425	741.9	3.232	744.0	3.422	5.166	0.3	5.9	59.8
3.0	447.5	728.1	2.452	728.0	2.532	3.294	0.0	3.3	34.3
3.0	473.1	712.4	1.865	709.9	1.866	2.153	-0.4	0.0	15.4

Component: C60

Aasen *et al.,* 1990

Mw: 844×10^{-3} kg/mol

		Measured data		Calculated data			Deviations %		
Ref *P* (atm)	Temp (K)	Dens (kg/m3)	Visc (mPa.s)	Densities (kg/m3) (Tait+ Ciotta + a0 extrapolation)	Free Volume Visc (cP)	ST-HS Visc(cP)	Dens	FV Visc	ST-HS Visc
3.0	407.9	762	7.305	767.2	6.458	24.900	0.7	-12	241
3.0	423.5	752.6	5.762	756.1	5.108	15.690	0.5	-11	172
3.0	441.5	741.7	4.513	743.4	3.991	9.769	0.2	-12	116
3.0	462	771.6	9.65	728.8	3.085	6.084	-5.5	-68	-37
3.0	465.5	727.3	3.379	726.3	2.959	5.646	-0.1	-12	67

Component: C64

Doolittle *et al.,* 1951

Mw: 899.7×10^{-3} kg/mol

		Measured data		Calculated data			Deviations %		
Ref *P* (atm)	Temp (K)	Dens (kg/m3)	Visc (mPa.s)	Densities (kg/m3) (Tait+ Ciotta + a0 extrapolation)	Free Volume Visc (cP)	ST-HS Visc(cP)	Dens	FV Visc	ST-HS Visc
1.0	383.2	781.8	14.346	786.6	10.266	76.183	0.6	-28	431
1.0	423.2	757.9	7.140	758.2	5.420	20.260	0.0	-24	184
1.0	474.4	728.3	3.705	721.7	2.833	5.663	-0.9	-24	53
1.0	521.4	698.1	2.326	688.3	1.757	2.503	-1.4	-24	8
1.0	573.8	668	1.519	651.1	1.132	1.326	-2.5	-26	-13

B.3. Matlab Codes

B.3.1. Density

```
%This program estimates the a0 values of n-alkanes in the Ciotta-version
of the modified Tait eq.
%It calculates the densities of 'pure' Hydrocarbons between 1 and 64 at
the user-required pressures and temperatures, using the Tait Equation as
in ref Assael-Dymond, 1994, International Journal of Thermophysics, Vol
15, No 1. 'An Improved Representations for n-Alkane Liquid densities' and
using Ciotta's (2010) formulae for calculating Rho_0 and B.
% It then compares the calculated densities with the measured and adjusts
a0. A0 is required to monotonically increase in values and should be
around 4.1*Rho_c

M_db=[0.016043,0.03007,0.044097,0.058124,0.07215,0.086177,0.100205,0.1142
3,0.1283,0.142284,0.156313,0.170337,0.184367,0.198391,0.212421,0.226,0.24
05,0.2545,0.2685,0.28256,0.29657,0.3106,0.3246,0.33865,0.35268,0.366707,0
.3807335,0.3947601,0.4087867,0.4228133,0.4368399,0.4508664,0.464893,0.478
9196,0.4929462,0.5069728,0.5209993,0.5350259,0.549,0.5630791,0.577,0.5911
322,0.6051588,0.6191854,0.633212];
rhoc_db=[162.0;210.0;221.0;227.0;232.0;234.0;236.0;237.0;238.0;239.0;240.
0;240.0;240.0;241.0;241.0;241.0;240.5;241.5;241.7;242.0;242.2;242.4;242.5
;242.7;242.9;243.1;243.2;243.4;243.5;243.7;243.8;244.0;244.1;244.2;244.3;
244.5;244.6;244.7;244.8;244.9;245.0;245.1;245.2;245.3;245.4];
%Carbon numbers in measured DB
nC_db=[5,6,7,8,10,12,14,16,17,20,22,24,28,30,32,36,40,44,60,64];
%Number of data points:
np_db=length(nC_db);

%First guess for a0 in the Ciotta& Mofidied Tait Equation: extrapolation
to C64
a0_init=[840,870,898,915,938.5,957.5,971.5,981,986,998,1004,1008.5,1017.1
25,1021.34,1025,1033,1040,1045,1057,1059];
%Rest of Ciotta coeff:
a1=-0.711;
a2=0;
b0=410;
b1=-1.42;
b2=0.0013;
C=0.198;
a0=a0_init;
R=8.3144621 ;
%Pressure in Mpa. (=>10^-6Pa) P0 at atmospheric.
P0=.1;

fid1= fopen('densities1.txt','w');
fid2= fopen('measured_dens1.txt');

%10 different components have measurements:
for n=1:10;
    data_comp=fscanf(fid2,'%u %u\n',[2,1]);
    compx=data_comp(1);
    nt=data_comp(2);

    rho0 = zeros(1,nt);
```

```
    rho = zeros(1,nt);
    rho_meas = zeros(1,nt);
    Pp = zeros(1,nt);
    T = zeros(1,nt);
    err = zeros(1,nt);
    B= zeros(1,nt);

    data_in=fscanf(fid2,'%f %f %f\n',[3,nt]);
    data_in=data_in';

    %Pressure in Mpa (Pref in atm)
    Pp=data_in(1:nt,1).*0.10132501;
    T = data_in(1:nt,2);
    rho_meas = data_in(1:nt,3);

    %ans=input('Press return to continue');

    !Find the component in DB:
    Found=0;
    ip=1;
    idb=ip;
    while (Found==0) && (ip<=np_db);
        if compx==nC_db(ip);
           idb=ip;
           Found=1;
        else
           ip=ip+1;
        end
    end
    if Found==0;
        disp('Error: component not in DB. Comp: %u', compx)
        break;
    end;



%=========================================================================
=========================================================================
===
    repeat=1;
    iter1=0;
    rms=1000;
    rms_min=rms
    while repeat==1;
        iter1=iter1+1;

        rel_err=0;
        for it=1:nt;
            %Calc B as in modified Tait eq (Ciotta 2010):
            B(it)=b0 + (b1*T(it)) + (b2*T(it)^2);

            %Determine atmospheric densities rho0 (Ciotta, 2010) in
kg/m3:
            rho0(it)=a0(idb) + (a1*T(it)) + (a2*(T(it)^2));
```

```
            %Tait eq => Assael 2009, eq 1, giving densities (kg/m3) at
all T and Pp(Mpa). P0 (Mpa) taken as atmospheric
            rho(it) =rho0(it)/(1-(C*log10((B(it)+Pp(it))/(B(it)+P0))));

            err(it)=(rho(it)-rho_meas(it));
            rel_err(it)=err(it)/rho_meas(it);
        end;

        err_sqr(it) = err(it)^2;

        rms=sqrt((sum(err_sqr))/nt);
        a0_save=a0(idb);

        %If rms is decreasing and a0 still withing limits, adjust a0 and
repeat the full procedure
        if  (abs(rms)<abs(rms_min)| iter1==1) ;
            %& ((a0(idb)-.1)>a0(idb-1)) & (a0(idb)+0.1<a0(idb+1)));
            repeat=1;
            rms_min=rms;
            %Adjust a0 to see if rms can still be reduced:
            if sum(err)/nt>0 ;
                a0(idb)=a0(idb)-.1;
            elseif sum(err(it))/nt<0;
                a0(idb)=a0(idb)+.1;
            end
        %If rms is now increasing, or a0 out of limits take one step back
and end iterations:
        elseif (abs(rms)>abs(rms_min)& iter1~=1) ;
            %| (((a0(idb)-.1)<a0(idb-1)) & (a0(idb)+0.1>a0(idb+1)))
            %Calculate final numbers with minimum rms a0:
            repeat=0;
            a0(idb)=a0_save;
            for it=1:nt;
                %Calc B as in modified Tait eq (Ciotta 2010):
                B(it)=b0 + (b1*T(it)) + (b2*T(it)^2);

                %Determine atmospheric densities rho0 (Ciotta, 2010) in
kg/m3:
                rho0(it)=a0(idb) + (a1*T(it)) + (a2*(T(it)^2));

                %Tait eq => Assael 2009, eq 1, giving densities (kg/m3)
at all T and Pp(Mpa). P0 (Mpa) taken as atmospheric
                rho(it) =rho0(it)/(1-
(C*log10((B(it)+Pp(it))/(B(it)+P0))));

                err(it)=(rho(it)-rho_meas(it));
                rel_err(it)=err(it)/rho_meas(it);
            end;
            err_sqr(it) = err(it)^2;
            rms_min=sqrt((sum(err_sqr))/nt)
        %else, if rms=min and a0 within limits, then accept results
        else (abs(rms)==abs(rms_min)& iter1~=1) ;
            rsm_min = rms;
            repeat = 0;
        end;
    end
    fprintf(fid1,' Component: %d\r\n',compx);
```

```
    fprintf(fid1,' Mw: %12.3f \r\n', M_db(idb));
    fprintf(fid1,' a0_init=%f , new a0=%f , rms=%f \r\n', a0_init(idb),
a0(idb), rms_min);
    fprintf(fid1,' Ref P(atm) %12.3f \r\n', Pp./.10132501);
    fprintf(fid1,' Temp(K): %6.1f\r\n', T);
    fprintf(fid1,'Calculated densities (kg/m3):\r\n');
    fprintf(fid1,'%12.3f  \r\n', rho);
    fprintf(fid1,'vs Measured Densities (kg/m3):\r\n');
    fprintf(fid1,'%12.3f  \r\n', rho_meas);
end;


subplot(1,2,1)
%plot(nC_db,a0);
coeff=polyfit(nC_db,a0,7);
a0_fit1=polyval(coeff,nC_db);
plot(nC_db,a0,'o',nC_db,a0_fit1);
nC_fine=1:1:64;
a0_fit64=polyval(coeff,nC_fine);
subplot(1,2,2)
plot(nC_db,a0,'o',nC_fine,a0_fit64);

fprintf(fid1,'Extrapolated a0 (Cn 1 to 64):\n')
fprintf(fid1,'%f \n',a0_fit64);
fprintf(fid1,'polynomal coeff: %20.15e \n',coeff);

fclose(fid1);
fclose(fid2);
type densities1.txt;
```

B.3.2. Pedersen Corresponding States Viscosities

```
%Pedersen Viscosity calculation for a single component at multiple
%temperatures (K), say 60, 80, 100, 150, 200, 250, 300 deg C
% Chapter 10, Pedersen,Christensen book 'Phase Behaviour of Petroleum
% Fluid', 2007.
% Units: Visc in cP, P in atm, dens in mol/l, T in Kelvin, R in atm/mol.K

%Molecular weights in Kg-mole
M_db=[0.016043,0.03007,0.044097,0.058124,0.07215,0.086177,0.100205,0.1142
3,0.1283,0.142284,0.170337,0.198391,0.226,0.058124,0.07215,0.226,0.269,0.
078113,0.09214,0.106167,0.106167,0.106167,0.134221,0.204335,0.246,0.13825
2,0.138252,0.142201,0.084161,0.0981888,0.0601,0.11616,0.032042,0.046069,0
.0601,0.074122,0.13737,0.12091,0.06605,0.153823,0.04402];
%Carbon numbers
nC_db=[1,2,3,4,5,6,7,8,9,10,12,14,16];
Tc_db=[190.6,305.43,369.8,425.2,465.9,507.5,548,575,603,626,668,706,740];
Pc_db=[45.44,48.2,41.9,37.47,33.15,29.71,29.,28.42,25.96,23.88,20.53,18.3
6,16.38];
%Number of data points:
np_db=length(M_db);
%Mw in g/cc
M_dbg=M_db.*1000;
```

```
T=input('Please enter temperature range in K: ');
Pref=input('Please enter pressure in atm: ');
%temp_c=(50:50:300);
%Temp in Kelvin:
%T=(temp_c + 273.15);
nt=length(T);
%pre-allocate memory
mu_ox = zeros(1,nt);
mu_ox1 = zeros(1,nt);
mu_x = zeros(1,nt);
mu_x1 = zeros(1,nt);
To_refx = zeros(1,nt);
%res pressure at 1500psi in atmospheres:
%Pref=105.5 ;

%Critical properties Methane
%Mw in g/mole
Mw_o=16.043 ;
%Critical temp in K
Tc_o=190.4 ;
%Critical press in atm
Pc_o=46.042/1.01325 ;
%Methane freezing point - temp in K:
TF=91.0 ;
%methane density in g/cm3 rhoc_o=0.16284
% g/cm3: rho_o=[0.071416 0.0581 0.04955 0.04346 0.388455 0.035194];
%Critical density in mol/l
rhoc_o=10.139;
%Methane dens at Pref and T: rho_o=[4.4600 3.6276 3.0943 2.7143 2.4259
2.1977 ]
%any comp
answ='Y';

while answ=='Y'
   answ=input('Do you want another component? (Y/n): ');
   if answ=='N'
       break
   end
   Compx=input('Please enter component number: ');


    !Find the component in DB:
    Found=0;
    ip=1;
    idb=ip;
    while (Found==0) && (ip<=np_db);
        if Compx==nC_db(ip);
           idb=ip;
           Found=1;
        else
           ip=ip+1;
        end
    end
   %Mw_x=input('Please enter Mw of component (g/mole): ');
   Mw_x=M_dbg(idb);
```

```
   %Tc_x=input('Please enter Tc of component (K): ');
   Tc_x=Tc_db(idb);
   %Pc_x=input('Please enter Pc of component (atm): ');
   Pc_x=Pc_db(idb)


%constants
GV=[-2.090975*10^5 2.647269*10^5 -1.472818*10^5 4.71674*10^4 -
9.491872*10^3 1.219979*10^3 -9.627993*10 4.274152 -8.141531*10^-2] ;
A=1.696985927 ;
B=-0.133372346 ;
C=1.4 ;
F=168.0 ;
j=[-10.3506 17.5716 -3019.39 188.73 0.0429036 145.29 6127.68] ;
k=[-9.74602 18.0834 -4126.66 44.6055 0.976544 81.8134 15649.9] ;
%R gas const atm/mole-K
R=8.205746*10^-2 ;
N=[-1.8439486666*10^-2 1.0510162064 -1.6057820303*10 8.4844027562*10^2 -
4.2738409106*10^4 7.6565285254*10^-4 -4.8360724197*10^-1 8.5195473835*10
-1.6607434721*10^4 -3.7521074532*10^-5 2.8616309259*10^-2 -2.8685295973
1.1906973942*10^-4 -8.5315715699*10^-3 3.8365063841 2.4986828379*10^-5
5.7974531455*10^-6 -7.1648329297*10^-3 1.2577853784*10^-4
2.2240102466*10^4 -1.4800512328*10^6 5.0498054887*10 1.6428375992*10^6
2.1325387196*10^-1 3.7791273422*10 -1.1857016815*10^-5 -3.1630780767*10 -
4.1006782941*10^-6 1.4870043284*10^-3 3.1512261532*10^-9 -
2.1670774745*10^-6 2.4000551079*10^-5] ;
gamma=0.0096;


%Calc Component viscosities at different temps:Eq 10.5
%('Phase Behaviour of Petroleum Fluids', Pedersen&Christensen,2007)
for i=1:nt
    %Methane reference pressure and temp:density (eq 10.5)
    Po_refx=Pref*Pc_o/Pc_x;
    To_refx(i)=T(i)*Tc_o/Tc_x;
end
Po_refx
To_refx

%Instead of using eq(10.11) to calculate, enter methane density at
calculated (P,T):
rho_ox=input('Please enter methane rho (g-mol/l for this (P,T): ')
mu_ox1=input('Please enter methane visc (cP) for this (P,T): ')

%Methane reduced density (eq 10.27):
rhor_o=rho_ox./rhoc_o

%Use eq(10.11) to test whether the methane densities input are correct:
for i=1:nt
    %a constants as in Table 10.2, used in eq(10.11):
    a=[R*To_refx(i)
N(1)*To_refx(i)+N(2)*To_refx(i)^.5+N(3)+N(4)/To_refx(i)+N(5)/To_refx(i)^2
N(6)*To_refx(i)+N(7)+N(8)/To_refx(i)+N(9)/To_refx(i)^2
N(10)*To_refx(i)+N(11)+N(12)/To_refx(i) N(13)
N(14)/To_refx(i)+N(15)/To_refx(i)^2 N(16)/To_refx(i)
N(17)/To_refx(i)+N(18)/To_refx(i)^2 N(19)/To_refx(i)^2
N(20)/To_refx(i)^2+N(21)/To_refx(i)^3
```

```
N(22)/To_refx(i)^2+N(23)/To_refx(i)^4
N(24)/To_refx(i)^2+N(25)/To_refx(i)^3
N(26)/To_refx(i)^2+N(27)/To_refx(i)^4
N(28)/To_refx(i)^2+N(29)/To_refx(i)^3
N(30)/To_refx(i)^2+N(31)/To_refx(i)^3+N(32)/To_refx(i)^4 ];
    %Test: Back calc P from eq 10.11
    suma1=0;
    suma2=0;
    for ii=1:9
        suma1=a(ii)*To_refx(i)*rho_ox(i)^ii;
    end
    for n=10:15
        suma2=a(n)*To_refx(i)*rho_ox(i)^(2*n-17)*exp(-
gamma*(rho_ox(i)^2));
    end
    P=suma1+suma2;
end

%Use eq(10.5) to calculate viscosity for comp x at each temperature:
for i=1:nt
    %1. Calc methane mu at reference P,T  (second term of eq(10.5)),
    %using eq(10.29) as for Heavy Oil:
    %Eq 10.32:
    dT =To_refx(i)- TF;
    %Eq 10.31:
    HTAN = (exp(dT) - exp(-dT))/(exp(dT+exp(-dT)));
    %Eq 10.30:
    F1=(HTAN+1)/2;
    F2=(1-HTAN)/2;
    %Eq 10.10:
    theta=(rho_ox(i)-rhoc_o)/rhoc_o ;
    %Eq 10.7:

mu_0=(GV(1)/To_refx(i))+(GV(2)/To_refx(i)^(2/3))+(GV(3)/To_refx(i)^(1/3))
+GV(4)+(GV(5)*To_refx(i)^(1/3)) + (GV(6)*To_refx(i)^(2/3)) +
(GV(7)*To_refx(i)) + (GV(8)*To_refx(i)^(4/3)) + (GV(9)*To_refx(i)^(5/3));
    %Eq 10.8:
    mu_1=A+B*((C-log(To_refx(i)/F))^2);
    %Eq 10.9:
    dmu_ax= exp(j(1))+(j(4)/To_refx(i)) * (exp
(rho_ox(i)^0.1*(j(2)+(j(3)/To_refx(i)^(3/2)))  +  theta*rho_ox(i)^0.5  *
(j(5)+(j(6)/To_refx(i)+j(7)/To_refx(i)^2) )   )-1.0);
    %Eq 10.28:
    dmu_aax= exp(k(1)+(k(4)/To_refx(i))) * (exp   (  rho_ox(i)^0.1  *
(k(2)+(k(3)/(To_refx(i)^(3/2)) ))   +   theta*rho_ox(i)^0.5  *
(k(5)+(k(6)/To_refx(i))+(k(7)/To_refx(i)^2))   )  - 1.0 );
    %Eq 10.29:
    mu_ox(i)=mu_0 + mu_1 + F1*dmu_ax+ F2*dmu_aax;

    %2. Calc new comp visc in 10^-4 cP  (eq 10.5)
    %(where mu_ox is methane visc calculated and mu_ox1 is methane visco
from input)

mu_x(i)=((((Pc_x/Pc_o)^(2/3))*((Mw_x/Mw_o)^(.5)))/((Tc_x/Tc_o)^(1/6)))*
mu_ox(i);

mu_x1(i)=((((Pc_x/Pc_o)^(2/3))*((Mw_x/Mw_o)^(.5)))/((Tc_x/Tc_o)^(1/6)))*
mu_ox1(i);
```

```
end

disp('temp(C) mu_C1   Mu_C10  mu_x visc in cP')
temp_c
%mu_ox*10^4
mu_ox1
%mu_x*10^4
mu_x1

fid= fopen('corrstates-output.txt','w');
fprintf(fid,' Component: %s\r\n',Compx);
fprintf(fid,' Mw: %12.3f   Pc: %12.3f  Tc: %12.3f\r\n', Mw_x, Pc_x,
Tc_x);
fprintf(fid,' Ref P(atm) %12.3f   Temp(C): \r\n', Pref);
fprintf(fid,' %12.3f\r\n', temp_c);
fprintf(fid,' Visc:')
fprintf(fid,' %12.3f\r\n', mu_x1);
fclose(fid);
type corrstates-output.txt

plot(temp_c,mu_x1)
end
```

B.3.3. Assael-Dymond Hard Sphere Model as implemented by Sun&Teja and Free Volume model

```
%This program calculates the viscosities of 'pure' Hydrocarbons between 1
%and 64 at the user-required pressures and temperatures, using 2
different
%methods:  Allal&Boned's Free Volume Model and the Dymond-Assael
HardSphere model.

%CALCULATE densities, using (Tait+Ciotta-mod+refined a0).

%Read temp (K) and pressure (bar) data from file.

%Freevolume Coefficients had been extrapolated from C16 to C64, using
C22,
%C32 and C44 data to control the extrapolation. This version contains
%the 'fine-tuned' extrapolated coefficients from Polyfit4+ manual
optimizations of various components.
%C8 and  C16 published parameters are overwritten by optimized values.
%See OptResults1.xls (sheet: Final Coeff(2))and
%FinetuneCoeff-on-Heavies2-1Dec11.xls

%Step 1: Set up Pures DB of molecular weights, Tc's and Pc's.
%Molecular weights in Kg/mol (Pures, with number of Carbons as in nC_db),
%from Reid's book and NIST.
M_db=[0.016043,0.03007,0.044097,0.058124,0.07215,0.086177,0.100205,0.1142
3,0.1283,0.142284,0.156313,0.170337,0.184367,0.198391,0.212421,0.226,0.24
05,0.2545,0.2685,0.28256,0.29657,0.3106,0.3246,0.33865,0.35268,0.366707,0
.3807335,0.3947601,0.4087867,0.4228133,0.4368399,0.4508664,0.464893,0.478
```

```
9196,0.4929462,0.5069728,0.5209993,0.5350259,0.549,0.5630791,0.577,0.5911
322,0.6051588,0.6191854,0.633212,.8436107,0.89968];
%Mw in g/mole
M_dbg=M_db.*1000;
%Carbon numbers
nC_db=[1,2,3,4,5,6,7,8,9,10,11,12,13,14,15,16,17,18,19,20,21,22,23,24,25,
26,27,28,29,30,31,32,33,34,35,36,37,38,39,40,41,42,43,44,45,60,64];
%Critical temperatures in K (from Assael 1994 paper)
Tc_db=[190.4,305.4,369.8,425.2,469.7,507.5,540.3,568.8,594.6,617.7,638.8,
658.2,676,693,707,722,733,748,756,767,777.6,785.5,789.7,799.6,820,816,813
,824,833,843,896,854,849,853,860,872,880,888,910,867,903,993,929,947,1017
];
%Critical Pressures in atm (Reid's book)
Pc_db=[45.40,48.16,41.94,37.50,33.26,29.71,27.04,24.57,22.60,20.92,19.44,
17.96,16.98,14.21,15.00,13.92,12.83,11.84,10.95,10.95,10.17,9.77,8.98,8.5
9,7.99,7.80,7.50,7.40,6.81,6.42,6.51,6.22,6.02,5.82,5.03,4.66,4.74,4.64,4
.64,3.75,4.24,4.05,4.05,3.95,3.65];
%Critical Densities for n-Alkanes 1-16(kg/m3), Tab1 (Assael 1994):
rhoc_db=[162,210,221,227,232,234,236,237,238,239,240,240,240,241,241,241,
241,242,242,242,242,242,243,243,243,243,243,243,244,244,244,244,244,244,2
44,244,245,245,245,245,245,245,245,245,245];
%Number of data points:
np_db=length(nC_db);
%R gas const J/mole-K
R=8.3144621 ;
%Pressure in MPa. (=>10^-6Pa) P0 at atmospheric.
P0=.101;


%Ciotta density coefficients:
a1=-0.711;
a2=0;
b0=410;
b1=-1.42;
b2=0.0013;
C=0.198;


fid= fopen('Data_out.txt','w');
fid2= fopen('Data_TempK_PresBar_in.txt');
ncomp=fscanf(fid2,'%u \n',[1,1]);

for n=1:ncomp;
    data_comp=[0,0];
    compx=0;
    nt=0;

    data_comp=fscanf(fid2,'%u %u\n',[2,1]);
    compx=data_comp(1);
    nt=data_comp(2);

    !Find the component in DB:
    Found=0;
    ip=1;
    idb=ip;
    while (Found==0) && (ip<=np_db);
        if compx==nC_db(ip);
```

```
            idb=ip;
            Found=1;
        else
            ip=ip+1;
        end
    end
    if Found~=1;
        str=fprintf('ERROR - Component %u not found. \n',compx);
        fclose(fid);
        fclose(fid2);
        break;
    end;
    Cn=compx;

    %Initialise input variables
    rho = zeros(1,nt);

    %Step 2: Get the pressures (atm) and temperatures (K) of the required
viscosity

    T=fscanf(fid2,'%f \n',[nt,1])
    Pref=fscanf(fid2,'%f \n',[nt,1])

    str=fprintf('Comp %u \n',compx);
    str=fprintf('Temp %f \n',T);
    str=fprintf('Pres %f \n',Pref);

    %Pressure in Pa for FreeVol:
    P= Pref* 101325.01;
    %Pressure in MPa for densities:
    Pp = P/1000000;

    a0=0;

   %Calculated densities at (P,T) for comp:

   %Calculate the a0 coeff (Ciotta+extrapolation) of the Tait Eq:
   a0_coeff=[1.116758250843757e-008,-2.824192288915558e-
006,2.925519725620931e-004,-1.605374683250970e-002,0.5045346728241398,-
9.183416382219926,94.40973035167316,544.7115794363783];

   for i =0:7
       a0=a0+a0_coeff(8-i)*Cn^i;
   end;

   str=fprintf('Comp %u, a0 %f \n',compx,a0);

   %Calc densities at each temp:
   for it=1:nt;
    %Calc B as in modified Tait eq (Ciotta 2010):
    B(it)=b0 + (b1*T(it)) + (b2*T(it)^2);

    %Determine atmospheric densities rho0 (Ciotta, 2010) in kg/m3:
    rho0(it)=a0 + (a1*T(it)) + (a2*(T(it)^2));

    %Tait eq => Assael 2009, eq 1, giving densities (kg/m3) at all T
```

```
    %and Pp(MPa). P0 (MPa) taken as atmospheric
    rho(it) =rho0(it)/(1-(C*log10((B(it)+Pp(it))/(B(it)+P0))));
   end;

   fprintf(fid,' Component: %d\r\n',compx);
   fprintf(fid,' Mw: %12.3f \r\n', M_db(idb));
   fprintf(fid,'Calculated Densities (kg/m3): \r\n')
   fprintf(fid,'%f\r\n',rho);



%=========================================================================
=========================================================================
===

    disp 'Free Volume Model'
    %FreeVolume Model:
    %Table 4, Paper(1)
    %Pressure in MPa

    %lm in Angstrom (10^-10 metre)
    %lm_db interpolated+extrapolated up to C64


lm_db=[0.912704,1.4695864,0.842437,0.882164,0.8440835,0.7907931,0.7103977
,0.6169677,0.6363625,0.4959059,0.411636516,0.3692642,0.369757196,0.372467
2,0.337234786,0.304272,0.288085,0.273875,0.261336,0.250217,0.240315,0.231
463,0.223522,0.216375,0.209925,0.204089,0.198797,0.192988,0.189612,0.1856
23,0.181982,0.179656,0.175616,0.172835,0.17029,0.166962,0.165832,0.163885
,0.162106,0.160483,0.159004,0.157659,0.156438,0.155334,0.154338,0.14896,0
.14971];
    %E0 in J/mole = kg.m2/s2
    %E0_db interpolated+extrapolated up to C64

E0_db=[7075.999,8623.474,24577.727,23615.299,32747.847,41979.528,56508.03
6,59565.14643,64586.668,86965.542,103967.678,116003.825,131164.6254,14188
5.634,160153.9534,165980.3,178304.3946,194050.7683,210559.5693,227725.838
,245244.9665,263512.6582,282124.8938,301577.9023,321168.1359,341492.2481,
362347.0757,384429.6213,405637.0399,428066.6252,451015.7992,473982.1012,4
98463.1798,522956.7839,547960.7563,574073.0265,599491.6052,626014.5787,65
3040.1041,680566.405,708591.7672,737114.535,766133.1079,797445.9373,82565
1.5238,1333970, 1487672.6];
    %B dimensionless
    %B_db interpolated+extrapolated up to C64

B_db=[0.1255726,0.1364979,0.0589878,0.0944296,0.0627691,0.0492035,0.03527
72,0.040578507,0.0412388,0.0295993,0.026763934,0.0239963,0.022636616,0.01
958,0.019602257,0.018124,0.017195,0.015287,0.014087,0.012748,0.012035,0.0
10905,0.010356,0.00957,0.008969,0.008364,0.007811,0.007130786,0.006838,0.
00641,0.006015,0.0054292,0.005313,0.005001,0.004711,0.00431648,0.004193,0
.00396,0.003744,0.003542,0.003353,0.003177,0.003012,0.002838,0.002713,0.0
0133,0.00112];


    mu_fv = zeros(1,nt);
    mu_cP = zeros(1,nt);
    %Paper(1) eq(6):
```

```
    for i=1:nt;
        term1=E0_db(idb)+(P(i)*M_db(idb)/rho(i));
        term2= sqrt(3*R*T(i)*M_db(idb));
        term3=(rho(i)*lm_db(idb)*10^(-10)*term1)/term2;
        term4=(term1/(2*R*T(i)))^(3/2);
        term5=B_db(idb)*term4;
        term6=2.71828182845905^(term5);
        mu_fv(i)=term3*term6;
        mu_cP(i)=mu_fv(i)*1000;
    %
mu(i)=(rho(i)*lm_db(idb)*(E0_db(idb)+(P*M_db(idb)/rho(i)))/(sqrt(3*R*T(i)
*M_db(idb))))*exp(B_db(idb)*((E0_db(idb)+(P*M_db(idb)/rho(i)))/(2*R*T(i))
)^(3/2))
    end
    format long

    fprintf(fid,' Ref P(atm):   \r\n');
    fprintf(fid,' %12.3f   \r\n', Pref);
    fprintf(fid,' Temp(K):  \r\n');
    fprintf(fid,' %12.3f \r\n', T);

    fprintf(fid,'FreeVolume Model: \n');

    fprintf(fid,' FV Visc(cP):');
    fprintf(fid,' %f\r\n', mu_cP);

%=========================================================================
=========================================================================
===

    disp 'Assael-Dymond Hard Sphere Model, with Sun-Teja variation'
    %Database of constants and critical properties (Assael 1994 + Assael
2009)
    %a-eta_i from Assael 1992 IntJThermoPhysV13 no2 p269 and
    %Sun-Tejal, 2009 eq(1).
    a_mu=[1.09450,-9.26324,71.03850,-301.90120,797.69,-
1221.977,987.5574,-319.46360];

    V=zeros(1,nt);
    V0_ST = zeros(1,nt);
    VR_ST = zeros(1,nt);

    mu_HS = zeros(1,nt);
    mu_star =zeros(1,nt);
    V0_C = zeros(1,nt);
    VR_C = zeros(1,nt);

    mu_Ciotta = zeros(1,nt);
    mu_star_C =zeros(1,nt);


    %Eq 11 from Sun-Tejal 2009, Rmu generalised:
    Rmu_ST=1.0055+0.0472*Cn;
    Rmu_C=1.82;

    %Volume at (P,T) in m3/mol (kg/mol / kg/m3)
```

```
    V=M_db(idb)./rho;

    %V01 in 10^(-5)m3 for viscosity, from Sun-Tejal 2009, eq 12:
    for it=1:nt

V0_ST(it)=(((0.85501+0.39526*Cn)+(3.162*(Cn^1.17694))/(T(it)^0.3)))/(10^5
);

      %Reduced volume from calculated densities:
      VR_ST(it)=V(it)/V0_ST(it);

    end;

     %Calculate the viscosities
    for it=1:nt;
      logmu_star=0;

      %reduced viscosity from Sun-Tejal 2009 eq (1); Assael 2009 eq (6):
      for ip=1:8;
          i=ip-1;
          logmu_star=logmu_star + a_mu(ip)*(1/VR_ST(it))^i;
      end

      mu_star(it)=(10^logmu_star);

      %Viscosity from Assael 2009 eq(4), and Sun-Tejal 2009 eq (3):

mu_HS(it)=mu_star(it)*Rmu_ST*(sqrt(M_db(idb)*R*T(it)))/((6.035*(10^8))*(V
(it)^(2/3)));

    end

     fprintf(fid,' mu_HS(cP)from calculated densities: \n');
    fprintf(fid,' %f\r\n', mu_HS*1000);

 end

fclose(fid);
fclose(fid2);
type Data_out.txt
```

Appendix C: Heavy Pseudo-Component Viscosity using a Colloidal Systems Approach

Various different scientists (Storm and Sheu, 1993; Argillier *et al*., 2002; Luo and Gu, 2007) developed methods of incorporating the proven viscosity dependency on asphaltene content in oil systems, when calculating the viscosity of oil systems. They mainly used colloidal dispersion theories such as

$$\mu_r = \frac{\mu_{disp}}{\mu_{maltene}} = 1 + [\mu]\phi + K_1\phi^2 + K_2\phi^3 + ... \tag{C.1}$$

Where μ_r is the relative viscosity between those of the dispersion (maltenes+asphaltenes) and the maltenes. $[\mu]$ is the intrinsic viscosity of the asphaltene particles and depends on the particle shapes (shape factor ν) and salvation constant (K) in the following way:

$$[\mu] = K\nu \tag{C.2}$$

K_1 to K_n are coefficients based on the salvation constant K.

In the case of lower concentrations of asphaltene (in heavy oil the asphaltene concentration is in the order of 15 wt.%, while in bitumen it is around 20 wt.%) and higher temperatures it can be assumed that the higher order terms, which models asphaltene particle interactions and flocculation/precipitation at high concentrations and low temps, can be ignored. This is applicable in subsurface numerical simulation where temperatures are above 35 °C.

Luo and Gu (2007)'s intrinsic viscosity findings on Lloydminster (Canada) crude oil were used in this study to relate the very heavy pseudo-component viscosity to that of the light pseudo-component (saturates and aromatics) of which the viscosity was calculated with the Free Volume model as described in the thesis. Since the current study is focussed on sub-surface reservoir simulation of heavy oil (thus excluding oil sands), it would be correct to assume that the temperature would normally be above 40 deg C and that the behaviours

observed by Luo and Gu would be appropriate for a test of the grouping scheme in the current research. This assumes non-spherical particles, poly-dispersed, with little interaction between them. The weight percentage of the asphaltenes are assumed to be less than 20% , with molecular weights around twice that of the average molecular weight of the de-asphaltened oil (Storm *et al*., 1991).

Luo and Gu had used 60 different data points, consisting of ten oil samples with different asphaltene weight percentages, ranging from zero to 16.01 wt.%, with six measurements per sample at different temperatures, ranging from 20 to 60 °C. They used non-linear regression to calculate the intrinsic viscosities as a function of temperature, seen in Figure C.0.1. Using the linear regression least squares method to determine the trend of these vs temperature, the following linear correlation applies:

$$[\mu] = -0.1231T(\mathrm{K}) + 53.483 \tag{C.3}$$

So that the relative viscosity would be:

$$\mu_r = \frac{\mu_{disp}}{\mu_{maltene}} = 1 + \phi(-0.1231T + 53.483). \tag{C.4}$$

Where ϕ is the dry volume fraction of the asphaltenes in the sample (maltenes+asphaltenes) and related to the weight percentage as follows (Luo and Gu, 2007):

$$\phi = \frac{\rho_{sample} wt_{sample}}{\rho_{asphaltenes}}, \tag{C.5}$$

With

$$\rho_{asp} = \frac{wt_{asp}}{\frac{1}{\rho_{sample}} - \frac{1 - wt_{asp}}{\rho_{maltenes}}} \tag{C.6}$$

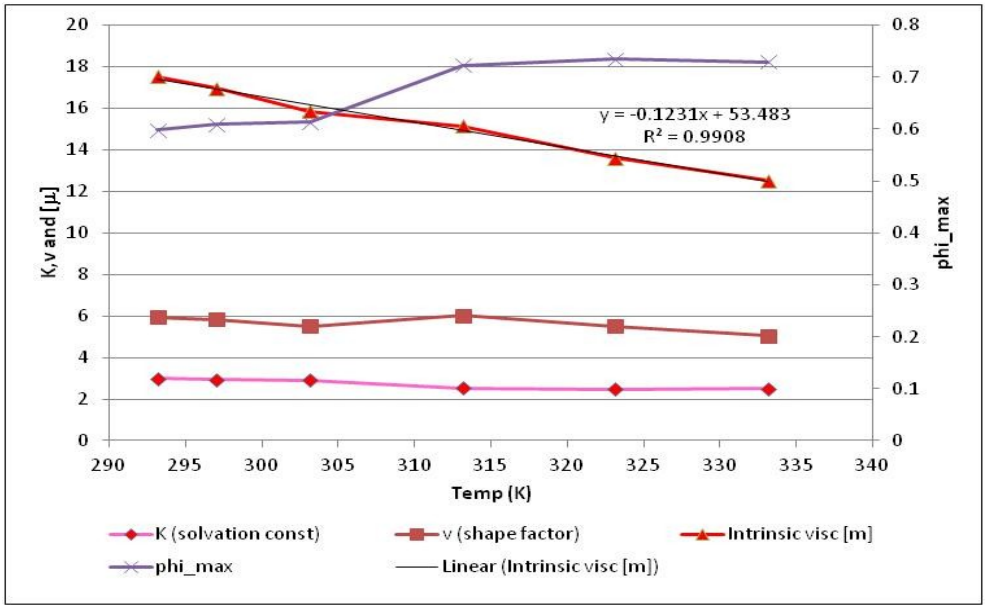


Figure C.0.1. Relative viscosity parameters *vs* temperature.

Nomenclature

AAD	=	Average Absolute Deviation
CWE	=	Cold Water Equivalent
ECN	=	Equivalent Carbon nNumber
FGPR	=	Field Gas Rate
FGPT	=	Total Field Gas Production
FOIP	=	Field Oil In Place
FOPR	=	Field Oil Production Rate
FOPT	=	Total Field Oil Production
FPR	=	Average Field Pressure
FWIT	=	Total Field Steam Injection (CWE)
FWPT	=	Total Field Water Production
MAD	=	Maximum absolute deviation
MF	=	Molecular Fraction
MW	=	Molecular Weight
RMS	=	Root mean square
SAGD	=	Steam assisted gravity drainage
SARA	=	Saturates, Aromatics, Resins and Asphaltenes
SLD	=	Steam line drive
WGOR	=	Well gas-oil ratio
WSTPR	=	Well Steam Production Rate
WGPR	=	Well Gas Production Rate
WOPR	=	Well Oil Production Rate
XMFi	=	Mole fraction of component *i* in oil phase
YMFi	=	Mole fraction of component *i* in gas phase
ZMFi	=	Total molefraction of component *i* in oil and gas phases

Symbols		Multiply Imperial Unit	By	To convert to SI Unit
A	Area	ft^2		m^2
b	Molar density	Dimensionless		
B	Fitting parameter in Free Volume model, associated with volume overlap	Dimensionless		
Cn	Number of Carbon atoms	Dimensionless		
C_p	Heat capacity	$BTU/ft^3/degF$		J/Kg/K
E	Energy	Btu	1.0543E+03	J
E_0	Energy of activation in Free Volume model.			J
f	Fraction	Dimensionless		
G	Activation energy	Btu	1.0543E+03	J
H	Height; Thickness	ft		m
H_p	Molar enthalpy	Dimensionless		$/m^3$
K	Permeability	mD		m^2
K	Thermal conductivity	BTU/ft/day/°F	0.072083	J.s/m.K (or Watts/m.K)
k	Effective permeability to oil	mD		m^2
k_r	Relative permeability	Dimensionless		
L	Length	ft		m
l_m	Characteristic length of molecule in Free Volume model			Å
M	Mobility	/cP		$/m^2$
M_w,				
MW	Molecular weight			g/mole
P	Pressure	psia	6,894.76	Pa
Q	Rate	stb/d	58.03036	m^3/s
q	Flux	ft^2/d		m^2/s
r	Radius	ft		m
S	Saturation, or Sensitivity	Dimensionless		
T	Temperature	°F	273.15+((T-32)*5/9))	K
u	Velocity	ft/s		m/s
V	Volume; Molar volume	ft^3	0.02832	m^3

v	Molar volume (in Free Volume model)		m^3/mole
x	Mole fraction in liquid phase; distance in x direction	Dimensionless	
y	Mole fraction in gas phase; distance in y direction	Dimensionless	
z	Total mole fraction; distance in z direction	Dimensionless	

Greek symbols		**Multiply Imperial Unit**	**By**	**To convert to SI Unit**
η, μ	dynamic (shear) viscosity	cP		m^2/s
ν	kinematic viscosity	cS		
ρ	density	lb/ft^3	16.0185	Kg/m3
Δ	delta (difference)	Dimensionless		
τ	shear stress	psi	6,894.76	Pa
λ	Thermal conductivity	BTU/ft/day/°F		J.s/m.K
α	Thermal diffusivity	ft^2/s		m^2/s
ϕ	porosity	Dimensionless		
ξ	friction coefficient	Dimensionless		

Constants

h	Planck's constant	6.626E-34 J s
R	Universal gas constant	8.3145 J/mol K
k_B	Boltzman's constant	1.3806503 × 10-23 m^2 kg /s^2 K
N_a	Avogrado's number	6.02214E+23

Subscripts

s	steam-oil interface; stiffness (in dumbess model)
c	critical, or component
0	zero-density, internal (in case of energy)
mix	mixture
g	gas
o	oil (relating phases); outer (relating radius)
pc	pseudo-component
$hvpc$	extra-heavy pseudo-component
e	effective

w	well
R	reservoir
p	phase
r	reduced
f	free

For P, T, V, MW, ρ :

*	Ratio to reference component (superscript)
r	Ratio of component critical (subcript)

Mathematical symbols

$\prod$	Product
$\sum$	Summation
∞	Infinity
$\rightarrow$	Approach
Δ	Delta (difference)

Software used:

Computer Modelling Group WinProp 2010

MATLAB R2011a

Schlumberger Information Systems: ECLIPSE Thermal 2010

Schlumberger Information Systems: ECLIPSE Office 2010

Schlumberger Information Systems: PVTi 2010

Schlumberger Information Systems: PETREL 2010

RefProp 8, NIST Standard Reference DB 23

References

Aasberg-Petersen, K., Knudsen, K., Fredenslund, A. 1991. Prediction of Viscosities of Hydrocarbon Mixtures. *Fluid Phase Equilibria* **70**: 293-308.

Aasen, E., Rytter, E., Øye, HA., 1990. Viscosity of n-Hydrocarbons and Their Mixtures. *Indust. Eng. Chem. Res*. **29**: 1635-1640.

Allal, A., Montfort, J. P. and Marin, G. 1996. *Proc. XIIth Congr. Rheology*. Eds. Ait Kadi, A., Dealy, J. M., James, D. F., Williams, M. C. p. 317.

Allal, A., Moha-Ouchane, M., Boned, C. 2001a. A New Free Volume Model for Dynamic Viscosity and Density of Dense Fluids versus Pressure and Temperature. *Phys Chem. Liquids*. **39**: 1-30.

Allal, A., Boned, C., Baylaucq, A. 2001b. Free-volume viscosity model for fluids in the dense and gaseous states. *Phy. Rev. E* **64**: 011203-1 – 011203-10.

Allen, R., Deo, M.D., Isaacson, A.E., Keiter, R.B., Kessler, C., Levey, R., Seok Oh, K., Smith, P.J., Spinti, J.P., Uchitel, K. 2007. A Technical, Economic, and Legal Assessment of North American Heavy Oil, Oil Sands, and Oil Shale Resources. Utah Heavy Oil Program. http://www.fossil.energy.gov/programs/oilgas/publications/ oilshale/ HeavyOilLowRes.pdf

Archer, J.S., Wall, C.G. 1999. *Petroleum Engineering: Principles and Practice.* Kluwer Academic Publishers, Dordrecht/Boston.

Argillier J-F., Coustet, C. Hénaut, I. 2002. Heavy Oil Rheology as a Function of Asphaltene and Resin Content and Temperature. Paper *SPE 79496*, presented at 2002 SPE International Thermal Operations and Heavy Oil Symposium and International Horizontal Well Technology Conference, Calgary, Alberta, Canada, 4-7 Nov. 2002.

Arrhenius, S. 1887. Über die innere Reibung verdünnter wässeriger Lösungen. *Zeitschrift fur Physikalische Chemie* **1**: 285-298.

Assael, M.J., Dymond, J.H. Tselekidou, V. 1990. Correlation of High-Pressure Thermal Conductivity, Viscosity and Diffusion Coefficients for n-Alkanes. *Int. J. Thermophys.* **11**(5): 863-873.

Assael, M. J., Charitidou, E., Dymond, J. H., Papadaki, M. 1992a. Viscosity and Thermal Conductivity of Binary n-Heptane + n-Alkane Mixtures. *Int. J. Thermophys.* **13**(2): 237-249.

Assael, M.J., Dymond, J.H., Papadaki, M., Patterson, P.M. 1992b. Correlation and Prediction of Dense Fluid Transport-Coefficients .1. Normal-Alkanes. *Int. J. Thermophys.* **13**(2): 269-281.

Assael, M. J., Dymond, J. H., Exadaktilou, D. 1994. An Improved Representation for n-Alkane Liquid Densities. *Int. J. Thermophys.* **15**(1): 155-164.

Assael, M.J., Kalyva, A.E., Kakosimos, K.E., Antoniadis, K.D. 2009. Correlation and Prediction of Dense Fluid Transport Coefficients. VIII. Mixtures of Alkyl Benzenes with other Hydrocarbons. *Int. J. Thermophys.* **30**: 1733–1747.

Attanasi, E.D., Meyer, R.F., 2007. *Natural Bitumen and Extra-Heavy Oil*. 2007 Survey of Energy Resources, World Energy Council. http://energy.cr.usgs.gov/oilgas/addoilgas/WEC07NBEHO.pdf.

Aucejo, A., Burget, M.C., Muñoz, R., Marques, J.L. 1995. Densities, Viscosities, and Refractive Indices of some n-Alkane Binary Liquid Systems at 298.15 K. *J. Chem. Eng. Data* **40**: 141-147.

Audonnet, F., Pádua, A.A.H. 2004. Viscosity and Density of Mixtures of Methane and n-Decane from 298 to 393 K and up to 75 MPa. *Fluid Phase Equilibria* **216**: 235-244.

Aziz, K., Ramesh, A.B., Woo, P.T. 1987. Fourth SPE Comparative Solution Project: Comparison of Steam Injection Simulators. Paper *SPE 13510*; *J. Pet. Tech*. **39**(12): 1576-1584.

Badre, S., Goncalves, C.C., Norinaga,K., Gustavson, G., Mullins, O.C. 2006. Molecular Size and Weight of Asphaltene and Asphaltene Solubility Fractions from Coals, Crude Oils and Bitumen. *Fuel* **85**:1-11.

Barrufet, M.A., Salem, S.K.E., Tantawy, M., Iglesias-Silva, G.A. 1996. Liquid Viscosities of Carbon Dioxide + Hydrocarbons from 310 K to 403 K. *J. Chem. Eng. Data* **41**: 436-439.

Barrufet, M.A., Hall, K.R., Estrada-Baltazar, A., Iglesias-Silva, G.A. 1999. Liquid Viscosity of Octane and Pentane + Octane Mixtures from 298.15 K to 373.15 K up to 25 MPa. *J. Chem. Eng. Data* **44**: 1310–1314.

Beggs, H.D., Robinson, J.R. 1975. Estimating the Viscosity of Crude Oil Systems. *J. Petrol. Tech.* **27**(9):1140-1141.

Boned. C., Allal, A., Baylaucq, A., Zéberg-Mikkelsen, C.K., Bessieres, D., Quiñones-Cisneros, S.E. 2004. Simultaneous free-volume modeling of the self-diffusion coefficient and dynamic viscosity at high pressure. *Phys. Rev. E* **69**: 031203-1-5.

Butler, R.M., McNab, G.S., Lo, H.Y. 1981. Theoretical Studies on the Gravity Drainage of Heavy Oil During In-Situ Steam Heating. *Can. J. Chem. Eng.* **59**:455-460.

Butler, R.M. 1985. A new approach to the modelling of steam-assisted gravity drainage. *J. Canad. Petrol. Tech.* **24**(3): 42-51.

Butler, R.M. 1994. Steam-assisted Gravity Drainage: Concept, Development, Performance and Future. *J. Canad. Petrol. Tech.* **33**(2):44-50.

Caudwell, D.R., Trusler, J.P.M., Vesovic, V., W.A. Wakeham. 2004. The Viscosity and Density of n-Dodecane and n-Octadecane at Pressures up to 200 MPa and Temperatures up to 473 K. *Int. J. Thermophys.* **25**: 1339-1352.

Chow, L., Butler, R.M. 1996. Numerical Simulation of the Steam-assisted Gravity Drainage Process (SAGD). *J. Canad. Petrol. Tech.* **35**(6): 55-62.

Ciotta, F. 2010. Viscosity of Asymmetric Liquids Mixtures under Extreme Conditions. *PhD thesis*, *Imperial College, London, UK*.

Chevalier J.L.E., Petrino, P.J., Gaston-Bonhomme Y.H. 1990. Viscosity and Density of Some Aliphatic, Cyclic, and Aromatic Hydrocarbons Binary Liquid Mixtures. *J. Chem. Eng. Data* 35: 206-212.

CMG WinProp User Manual V2010.

Cohen, M.H., Turnbull, D. 1959. Molecular Transport in Liquids and Glasses. *J. Chem. Phys*. **31**(5): 1164-1169.

Dealy JM. 1979. Rheological properties of oil sand bitumens. *Can. J. Chem. Eng.* **57**:677–683.

De Ghetto, G., Paone, F., Villa, M., 1995. Pressure-Volume-Temperature Correlations for Heavy and Extra Heavy Oils. Paper *SPE 30316*, presented at International Heavy Oil Symposium held in Calgary, Alberta, Canada, 19-21 Jun 1995.

De La Porte, J.J., Riesco, N., Vesovic, V. 2009. Prediction of Heavy Oil Viscosity in Current Reservoir Simulators. Paper *SPE 125500*, presented at the 2009 SPE/EAGE Reservoir Characterisation and Simulation Conference, Abu Dhabi, UAE, 19-21 Oct 2009.

De la Porte, J.J., Kossack, C.A., Vesovic, V. 2011. Heavy Oil Thermal Simulation with Single Heavy Oil Component: Magnitude of the Error and Proper Component Viscosity Estimation. Paper *WHOC11-354*, presented at World Heavy Oil Congress, Edmonton, Alberta, 14-17 Mar 2011.

Doolittle, A.K. 1951. Studies in Newtonian Flow. II. The Dependence of the Viscosity of Liquids on Free-Space. *J. Appl. Phys*. **22**(12):1471-1475.

Doolittle, A.K., Peterson, R.H. 1951. Preparation and Physical Properties of a Series of n-Alkanes, *J. American Chem. Soc.* **73:** 2145-2151**.**

Dusseault, M. 2002. *CHOPS: Cold Heavy Oil Production with Sand in the Canadian Heavy Oil Industry*. For Alberta Department of Energy. http://www.energy.gov.ab.ca/ OilSands.

Dymond, J.H., Young, K.J., Isdale, J.D. 1980. Transport Properties of Nonelectrolyte Liquid Mixtures—II. Viscosity Coefficients for the n-Hexane + n-Hexadecane System at Temperatures from 25 to 100°C at Pressures Up to the Freezing Pressure or 500 MPa. *Int. J. Thermophys*. **1**: 345-373.

Dymond, J.H., Robertson, J., Isdale, J.D. 1981. Transport Properties of Nonelectrolyte Liquid Mixtures—III. Viscosity Coefficients for n-Octane, n-Dodecane, And Equimolar Mixtures of n-Octane + n-Dodecane and n-Hexane + n-Dodecane From 25 to 100°C at Pressures Up to the Freezing Pressure or 500 MPa. *Int. J. Thermophys*. **2**: 133-154.

Dymond, J.H., Awan, M.A. 1989. Correlation of High-Pressure Diffusion and Viscosity Coefficients for n-Alkanes. *Int. J. Thermophys*. **10**(5): 941-951.

Dymond, J.H., Young, K.J. 1980a. Transport Properties of Nonelectrolyte Liquid Mixtures-I. Viscosity Coefficients for n-Alkane Mixtures at Saturation Pressure from 283 to 378 K. *Int. J. Thermophys*. **1**(4): 331-344.

Dymond, J.H., Young, K.J., Isdale, J.D. 1980b. Transport Properties of Nonelectrolyte Liquid Mixtures-II. Viscosity Coefficients for the n-Hexane + n-Hexadecane System at Temperatures from 25 to 100~ at Pressures Up to the Freezing Pressure or 500 MPa. *Int. J. Thermophys.*, **1**(4): 345–373.

Dymond, J.H., Robertson, J., Isdale, J. D. 1981. Transport Properties of Nonelectrolyte Liquid Mixtures-III. Viscosity Coefficients for n-Octane, n-Dodecane, and Equimolar Mixtures of n-Octane + n-Dodecane and n-Hexane + n-Dodecane from 25 to 100 deg C at Pressures Up to the Freezing Pressure or 500 MPa. *Int. J. Thermophys*. **2**(2):133-154.

Dymond, J.H., Malhotra, R. 1988. The Tait Equation: 100 Years On. *Int. J. Thermophys.* **9**(6): 941-951.

ECLIPSE Reference Manual, Version 2010, Schlumberger Information Systems.

ECLIPSE Technical Description, 2010.1, Schlumberger Information Systems.

Estrada-Baltazar, A., Alvarado, J.F.J., Iglesias-Silva, G.A., Barrufet, M.A. 1998a. Experimental Liquid Viscosities of Decane and Octane + Decane from 298.15 K to 373.15 K and up to 25 MPa. *J. Chem. Eng. Data* **43**: 441–446.

Estrada-Baltazar, A., Iglesias-Silva, G.A., Barrufet, M.A. 1998b. Liquid Viscosities of Pentane and Pentane + Decane from 298.15 K to 373.15 K and up to 25 MPa. *J. Chem. Eng. Data* **43**: 601–604.

Fenghour, A., Wakeham, W.A., Vesovic, V. 1998. The Viscosity of Carbon Dioxide. *J. Phys. Chem. Ref. Data* **27**: 31–44.

Galliéro, G., Boned, C., Baylaucq, A. 2005. Molecular Dynamics Study of the Lennard-Jones Fluid Viscosity: Application to Real Fluids. *Indust. Eng. Chem. Res*. **44**:6963-6972.

Giller, E.B., Drickamer, H.G. 1949. Viscosity of Normal Paraffins near the Freezing Point. *Indust. Eng. Chem.* **41**(9): 2067-2069.

Glasstone, S., Laidler, K.J., Eyring, H. 1941. *Theory of Rate Processes*. McGraw-Hill, New York.

Glasstone, S., Laidler, K.J., Eyring, H.J. 1941. *The Theory of Rate Processes.* New York City: McGraw-Hill.

Groenzin, H., Oliver C. Mullins, O.C. 2000. Molecular Size and Structure of Asphaltenes from Various Sources. *Energy & Fuels* **14**: 677-684.

Grunberg, L., Nissan, A.H. 1949. Mixture Law for Viscosity. *Nature* **164:** 799–800.

Harriman, G. 2004. Waxes and Asphaltenes – Their Chemistry, Analysis and relevance to Production Problems. GHGeochemical Services, www.ghgeochem.com/documents/waxes_and_asphaltenes.pdf.

Hernandez, J.C. 2001. Sensitivity of Reservoir Simulations to Uncertainties in Viscosity. *MPhil Thesis*, Imperial College, London.

Hernandez, J. C., Vesovic, V., Carter, J.N., Lopez, E. 2002. Sensitivity of Reservoir Simulations to Uncertainties in Viscosity. Paper *SPE 75227*, presented at the 2002 SPE/DOE Improved Oil Recovery Symposium, Tulsa, Oklahoma, 13-17 April 2002.

Hiemenz P.C., Rajagopalan, R. 1997. *Principles of Colloid and Surface Chemistry*, 3rd Edition. CRC Press, Taylor and Francis Group, Boca Raton, FL.

Huber, M.L., Laesecke, A., Perkins, R. 2004. Transport Properties of n-Dodecane. *Energy & Fuels* **18**: 968–975.

Huber, M.L., Laesecke, A., Xiang, H.W. 2005. Viscosity Correlations for Minor Constituent Fluids in Natural Gas: n-Octane and n-Decane. *Fluid Phase Equilibria* **228-229**: 401–408.

Irving, J.B. 1977a. Viscosity of Binary Liquid Mixtures: A Survey of Mixture Equations, National Engineering Laboratory, Report No. 630, East Kilbride, Glasgow, Scotland.

Irving, J.B. 1977b. Viscosity of Binary Liquid Mixtures: The Effectiveness of Mixture Equations, National Engineering Laboratory, Report No. 631, East Kilbride, Glasgow, Scotland.

Jamaluddin, A.K.M., Nazarko, T.W. Sills, S., Fuhr, B.J. 1996. Deasphalted Oil: A Natural Asphaltene Solvent. *SPE Production & Facilities*, **11**(3):161-165 1996. Paper *SPE 28994*, presented at 1995 SPE Intl. Symp. on Oilfield Chemistry, held in San Antonio, 14-17 Feb 1995.

Jaffe, A.M., Medlock, K.B. Soligo, R. 2011. *The Status of World Reserves: Conventional and Unconventional Resources in the Future Supply Mix*. James A. Baker III Institute for Public Policy, Rice University, Texas, US.

Joergensen, M. Stenby, E.H. 1995. Optimization of Pseudo-component Selection for Compositional Studies of Reservoir Fluids. Paper *SPE 30789-MS*, presented at the 70th Annual Tehnical Conference and Exhibition, Dallas, Texas, 22-25 Oct 1995.

Katz, D.L., Firoozabadi, A. 1978. Predicting Phase Behavior of Condensate/Crude-Oil Systems Using Methane Interaction Coefficients. *J. Pet. Tech*. **30**: 1649-1655; paper

SPE 6721, presented at the SPE-AIME 52nd Annual Fall Technical Conference and Exhibition, Denver, Oct 9-12, 1977.

Khan, M.A.B., Mehrotra, A.K., Svrcek, W.Y. 1984. Viscosity Models for Gas-free Athabasca Bitumen. *J. Canad. Petrol. Tech.*, **23**(3): 47-53.

Kiran, E., Sen, Y.L. 1992. High-Pressure Viscosity and Density of *n*-Alkanes. *Int. J. Thermophys.* **13:** 411–442.

Krejbjerg, K., Pedersen, K.S., 2006. Controlling VLLE Equilibrium with a Cubic EoS in Heavy Oil Modelling. Paper 2006-052, presented at the 57th Annual Technical Meeting of the Petroleum Society (Canadian International Petroleum Conference), Calgary, June 13-15, 2006.

Lawal, K.A., Adenuga, A.O. 2010. Pseudo-components for Nigerian Heavy Oil and Bitumen. Paper *SPE 136954*, presented at the 34th Annual SPE Intl Conf and Exhibition,Tinapa – Calabar, Nigeria, 31 Jul - 7 Aug 2010.

Lawal, K.A. 2011. Validation of a Pseudocomponent Scheme for Nigerian Heavy Oil and Bitumen. Paper *SPE 150815*, presented at the Nigerian Annual Intl Conf and Exhibition, Abuja, Nigeria, 30 Jul – 3 Aug 2011.

Lemmon, E.W., Huber, M.L., McLinden, M.O. 2007. NIST Standard Reference Database 23: Reference Fluid Thermodynamic and Transport Properties-REFPROP, Version 8.0, National Institute of Standards and Technology, Standard Reference Data Program, Gaithersburg, MD.

Lindeloff, N., Pedersen, K.S., Rønningsen, H.P., Milter. J. 2004. The Corresponding States Viscosity Model Applied to Heavy Oil Systems. *J. Petrol. Tech.* **43**(9): 47-53.

Lohrenz, J., Bray, B.G., Clark, C.R. 1964. Calculating Viscosities of Reservoir Fluids from their Compositions. *J. Pet. Tech.* **16**: 1171–1176.

Lolley, C.S., Richardson, W.C. 1997. Compositional Input for Thermal Simulation of Heavy Oils with Application to the San Ardo Field. SPE 37538, presented at the 1997

SPE International Thermal Operations and Heavy Oil Symposium, Bakersfield, California, 10-12 Feb 1997.

Lolley, C.S., Richardson, W.C. 1998. Minimum Pseudocomponent Requirements for Compositional Thermal Simulation of Heavy Oil. Paper *SPE 39640* presented at SPE/DOE Improved Oil Recovery Symposium held in Tulsa, Oklahoma, 19-22 Apr 1998.

Luo, P., Gu, Y. 2007. Effects of asphaltene content on the heavy oil viscosity at different temperatures. *Fuel* **86**: 1069–1078.

Macedo, P.B., Litovitz, T.A. 1965. On the Relative Roles of Free Volume and Activation Energy in the Viscosity of Liquids. *J. Chem. Phys*. **42**(1): 245-256.

Mack, C. 1938. Colloid Chemistry of Asphalts. *J. Phys. Chem*. **36**(12): 2901-2914.

Mago, A.L., Barrufet, M.A., Nogueria, M.C. 2005. Assessing the Impact of Oil Viscosity Mixing Rules in Cyclic Steam Stimulation of Extra-Heavy Oils. Paper *SPE 95643* presented at the SPE Annual Technical Conference and Exhibition, Dallas, Texas, 9-12 October 2005.

Marcano, E. 2013. Chávez: Oil Production at Orinoca Belt amounts to One Million Bpd. *El Universal* 13 January 2012.

Meyer, R.F., Attanasi, E.D. 2003. *Heavy Oil and Natural Bitumen – Strategic Petroleum Resources*. U.S. Geological Survey, Fact Sheet 70-03. http://pubs.usgs.gov/fs/fs070-03/ fs070-03.html.

Meyer, R.F., Attanasi, E.D., Freeman, P.A. 2007. *Heavy Oil and Natural Bitumen Resources in Geological Basins of the World*. U.S. Geological Survey, Open-File Report 2007-1084. http://pubs.usgs.gov/of/2007/1084/.

Monnery, W.D., Svrcek, W.Y., Mehrotra, A.K. 1995. Viscosity: A Critical Review of Practical Predictive and Correlative Methods. *Canad. J. Chem. Eng.* **73**: 3–40.

Nechitailo, V.S. 1991. Theory of Free Volume in Polymers. *Russian J. Phys. Chem.* **65**(7): 1052-1055.

Pedersen, S.K., Fredenslund, A., Christensen, P.L., Thomassen, P. 1984. Viscosity of Crude Oils. *Chem. Eng. Sci.* **39**(6): 1011-1016.

Pedersen, S.K., Fredenslund, A. 1987. An improved corresponding states model for the prediction of oil and gas viscosities and thermal conductivities. *Chem. Eng. Sci.* **42**(1): 182-186.

Pedersen, S.K., Christensen, P.L. 2007. *Phase Behaviour of Petroleum Reservoir Fluids*. CRC Press, Taylor & Francis Group, Florida.

Polikar, M., Farouq Ali, S.M., Puttagunta, V.R. 1990. High-Temperature Relative Permeabilities for Athabasca Oil Sands. *SPE Reservoir Eng*. **5**: 25 – 32.

Poling, B.E., Prausnitz, J.M., O;Connell, J.P. 2000. *The Properties of Gases and Liquids,* 5th ed.. New York, McGraw-Hill.

Prats, M., Thermal Recovery. *SPE monograph, Vol. 7*, Society of Petroleum Engineers, Richardson, Texas, 1982.

PVTi Reference Manual, 2010.1. Schlumberger Information Solutions.

Queimada, J., Quiñones-Cisneros, S. E., Marrucho, I. M., Coutinho, J.A.P., Stenby, E.H. 2003. Viscosity and Liquid Density of Asymmetric Hydrocarbon Mixtures. *Int. J. Thermophys*. **24**(5): 1221-1239.

Queimada, J., Marrucho, I. M., Coutinho, J. A. P., Stenby, E. H. 2005. Viscosity and Liquid Density of Asymmetric *n*-Alkane Mixtures: Measurement and Modeling. *Int. J. Thermophy*. **26**(1); 47-61.

Reid, R.C., Prausnitz, J.M., Poling, B.E. 1987. *The Properties of Gases and Liquids*, 4th Ed. McGraw-Hill, New York.

Ried, T.B. 1996. *Feasibility Study of Heavy Oil Recovery in the United States*. U.S. Department of Energy. http://www.netl.doe.gov/kmd/cds/disk27/niperbdm-0225.PDF

Rønningsen, H.P. 1993. Prediction of Viscosity and Surface Tension of North Sea Petroleum Fluids by Using the Average Molecular Weight. *Energy & Fuels* **7**:565-573.

Royal D.D., Vesovic V., Trusler J.P.M., Wakeham, W.A. 2003. Prediction of the viscosity of dense fluid mixtures. *Molec. Phys.* **101**(3): 339-278.

Schenk, C.J., Cook, T.A., Charpentier, R.R., Pollastro, R.M., Klett, T.R., Tennyson, M.E., Kirschbaum, M.A., Brownfield, M.E., Pitman, J.K. 2009. *An Estimate of Recoverable Heavy Oil Resources of the Orinoco Oil Belt, Venezuela*. U.S. Geological Survey, Fact Sheet FS09-3028. http://pubs.usgs.gov/fs/2009/3028/pdf/FS09-3028.pdf.

Sheu E.Y., Mullins, O.C. 1995. Asphaltenes: Fundamentals and Applications. Plenum Press, New York, 1995.

Shin, H., Polikar, M. 2005. Simple Thermal Efficiency Parameters as an Economic Indicator for SAGD Performance. Paper *SPE 94630* presented at SPE Hydrocarbon Economics and Evaluation Symposium held in Dallas, Texas, 3-5 Apr 2005.

Somerton, W.H. 1992. *Thermal Properties and Temperature-Related Behaviour of Rock/Fluid Systems*. Elsevier, New York.

Storm, D.A., Barresi, R.J., DeCanio, S.J. 1991. Colloidal Nature of Vacuum Residue. *Fuel* **70**: 779-782.

Storm, D.A., Sheu. E.Y. 1993. Rheological studies of Ratawi vacuum residue at 366K. *Fuel* **72**: 233-237.

Sun, T., Teja, A.S., 2009. Correlation and Prediction of the Viscosity and Thermal Conductivity of Dense Fluids. *J. Chem. Eng. Data* **54**: 2527-2531.

Touloukian, Y.S., Saxena, S.C., Hestermaus, P. 1975. Thermophysical Properties of Matter – TPRC Data Series Volume II Viscosity. Purdue Research Foundation.

Trevoy, D.J ., Drickamer, H. G., 1949. Viscosity of Liquid Hydrocarbon Mixtures. *J. Chem. Phys*.**17**(6): 582-583.

Vogel, E., Wilhelm, J., Küchenmeister, C. and Jaeschke, M. 2000. High-Precision Viscosity Measurements on Methane. *High Temperatures – High Pressures* **32**: 73–81.

Vogel, E., Küchenmeister, C., Bich, E., Laesecke, A. 1998. Reference Correlation of the Viscosity of Propane. *J. Phys. Chem. Ref. Data* **27**: 947–970.

Wakefield, D.L. and Marsh, K.N. 1987. Viscosities of Nonelectrolyte Liquid Mixtures. I. n-Hexadecane + n-Octane. *Int. J. Thermophys.* **8**: 649-662.

Wakefield, D.L., Marsh, K.N., Zwolinski, B.J. 1988a. Viscosities of Nonelectrolyte Liquid Mixtures. II. Binary and Quaternary Systems of Some n-Alkanes. *Int. J. Thermophys.* **9**(1): 47-59.

Wakefield, D.L. 1988b. Viscosities of Nonelectrolyte Liquid Mixtures. III. Selected Binary and Quaternary Mixtures. *Int. J. Thermophys.* **9**: 365-381.

Werner, A., de Hemptinne, J.C., Behar, F., Behar, E, Boned, C. 1998. A New Viscosity Model for Petroleum Fluids with High Asphaltenes Content. *Fluid Phase Equilibria* **147**: 319–341.

Whitson, C.H., Anderson, T.F., Søreide, I. 1989. C7+ Characterization of Related Equilibrium Fluid using the Gamma Distribution. *Advances In Thermodynamics*, **1,** G.A. Mansoori, ed. Taylor & Francis, New York, pp. 35-56.

Wilson, G. 1968. A Modified Redlich-Kwong Equation of State, Application to General Physical Data Calculations. Paper no 15C Ohio, presented at the AICHE 65th National Meeting, Cleveland, Ohio, May 1968.

WinProp User's Guide V 2010. Computer Modelling Group Ltd.

Wuttipittayamongkol, W. 2009. The Effective Grouping Strategies for Predicting the Viscosity of Oil. *MSc Thesis,* Imperial College, London.

Wu, J., Shan, Z. and Asfour, A-F.A. 1998. Viscometric Properties of Multicomponent Liquid n-Alkane Systems. *Fluid Phase Equilibria* **143**, 263-274.

Yen, T.F., Chilingarian, G.V. 1994. Asphaltenes and Asphalts, Vol. 1. Elsevier, Amsterdam.

Zéberg-Mikkelsen, C.K., Baylaucq. A., Barrouhou, M., Quiñones-Cisneros, S.E., Boned, C. 2004. Comparative study of viscosity models on the ternary system methylcyclohexane + cis-decalin + 2,2,4,4,6,8,8-heptamethylnonane up to 100 MPa. *Fluid Phase Equilibria* **222-223**:135-148.

Zéberg-Mikkelsen, C.K., Watson, G., Baylaucq, A., Galliero, G., Boned, C. 2006. Comparative experimental and modelling studies of the viscosity behaviour of Ethanol + C7 hydrocarbon mixtures versus pressure and temperature. *Fluid Phase Equilibria* **245**:6-19.